Antisense-mediated myostatin downregulation by destructive exon skipping using 2'O-methyl RNA and morpholino oligomers in skeletal muscle cells and animal models

Jagjeet Kaur Kang

A thesis submitted for the degree of

Doctor of Philosophy (PhD)

Centre for Biomedical science

School of Biological sciences

Royal Holloway, University of London

Egham, Surrey

United Kingdom

2012

Statement

The work presented in this thesis was mainly carried out at Centre for biomedical sciences, School of Biological sciences, Royal Holloway, University of London and some part of the B-PMO study detailed in chapter 5 was done at Department of physiology, anatomy and genetics, University of Oxford. All the *in vivo* experimentation was conducted under statutory Home Office recommendation, regulatory, ethical and licensing procedures and under the Animals (Scientific Procedures) Act 1986 (project licence PPL 70/7008). Unless otherwise stated in the text, all the work presented in thesis was conducted by Jagjeet Kaur Kang and has not been submitted for any other degree in this or any other university or institute.

Dedication

I would like to dedicate this work to patients suffering from muscle wasting disorders as it was an attempt to make some contribution in this area of research to help patients in future; also to my parents who always supported me with immense patience and always encouraged me throughout my PhD.

Acknowledgements

It is an honour to express my deepest gratitude to my supervisor Professor George Dickson for his invaluable support, guidance and constant encouragement throughout the course of this study. This research and thesis would not have been possible without his patience and support.

I would always be grateful to Dr Ian Graham for being a great teacher to me. His advice and support helped me in improving my technical skills and developing advanced understanding of molecular biology.

I am equally thankful to Dr Linda Popplewell for her constant encouragement and help with the experiments as well as for her invaluable suggestions and proof-reading of this thesis. Dr Alberto Malerba deserves special thanks for all the support in animal studies and for being a constant source of inspiration.

I am also immensely indebted to all the other members of Prof Dickson's lab for their guidance and support.

I thank all my family and friends from the bottom of my heart for being patient and instilling confidence and optimism in me through all the lows and highs. Finally, very special thanks to my loving parents and my best friend, Jaskanwar Pabla for being by my side and keeping my morale high through thick and thin.

ABSTRACT

Myostatin is a negative regulator of muscle mass, and several strategies are being developed to knock down the expression of the myostatin gene as a means to bring about improvements in muscle wasting conditions, including Duchenne muscular dystrophy (DMD). Improved muscle regeneration in the absence of myostatin has been demonstrated in *mdx* mice by crossing them with myostatin null mice. Increased muscle strength and improved dystrophic pathophysiology has been found in the *mdx* mice treated with myostatin antibodies, purified myostatin propeptide (natural binding partner of myostatin) with a mouse fusion protein and AAV-mediated transfer of propeptide. Virus-based strategies have the major drawbacks of uncontrolled insertion into the target genome and undesirable immune response; whereas, injecting binding partners to the target tissue might have low sustainability over a longer period of time.

In this study the design and use of antisense oligonucleotides (AOs) to manipulate myostatin pre-mRNA splicing and knockdown myostatin has been described. AOs of both 2'O-methyl RNA (2'OMePS-with a phosphorothioate backbone) and phosphorodiamidate morpholino (PMO) chemistries were designed using different bioinformatics algorithms. Efficiency of destructive myostatin exon skipping was then demonstrated and evaluated comparatively by oligomer transfection of cultured muscle cells, and RT-PCR and bioactivity analyses. Sustained and high levels of destructive exon skipping of the myostatin mRNA, and increases in skeletal muscle mass and fibre sizes was observed up to 2 months following a single injection of Vivo-PMO (PMO conjugated to a cell-penetrating octa-guanidine moiety) into the tibialis anterior muscle in normal mice. The efficiency of Vivo-PMO was also compared to a PMO conjugated to a cell penetrating peptide moiety (B-PMO) by single intra muscular treatment of wild type mice. Weekly intravenous injections of Vivo-PMO in normal mice also lead to myostatin exon skipping in selected skeletal muscles, and associated increases in tissue mass, cross-sectional area, and average fibre diameter. Dual exon skipping of myostatin and dystrophin was also carried out successfully in *mdx* mice. These studies indicate that (i) antisense-mediated destructive exon skipping can be induced in the myostatin RNA, (ii) antisense AO treatment reduces myostatin bioactivity and enhances muscle mass in vivo, and (iii) AO-induced myostatin exon-skipping may be a potential therapeutic strategy to counter muscular dystrophy, muscular atrophy, cachexia and sarcopenia.

TABLE OF CONTENTS

List of Tables

List of Figures

ABBREVIATIONS

AOs: Antisense Oligonucleotides

ATP: Adenosine triphosphate

BMD: Becker's muscular dystrophy

BMP1: Bone morphogenetic protein 1

COPD: Chronic obstructive pulmonary disease

CPP: Cell penetrating peptides

CSA: Cross-sectional area

DAPC: Dystrophin-associated protein complex

DMD: Duchenne Muscular Dystrophy

DMEM: Dulbecco's Modified Eagle Medium

DMSO: Dimethyl Sulphoxide

ECM: Extracellular matrix

EDL: Extensor digitorum longus

EDTA: Ethylenediaminetetraacetic acid

ENA: Ethylene bridged nucleic acid

ESE: Exonic splicing enhancer

ESS: Exon splicing suppressor

FCS: Fetal calf serum

GDF: Growth and differentiation Factor

H&E: Haematoxylin and eosin

IGF-1: Insulin-like Growth factor-1

IM: Intramuscular

IP: Intraperitoneal

LF 2000: Lipofectamine™ 2000

LNA: Locked nucleic acid

MDSC: Muscle derived stem cells

MEF2: Myocyte enhancer factor 2

nNOS : neuronal Nitric oxide synthase

OCT: Optimal cutting temperature

OTC: Ornithine transcarbamylase

PAH: Phenylalanine hydroxylase

PBS: Phosphate buffered saline

PKU: Phenylketonurea

PMO: Phosphorodiamidate morpholino oligomer

PNA: Peptide nucleic acid

PPMO: Peptide-linked PMO

RISC: RNA-induced silencing complex

RLU: Relative light units

RNA: Ribonucleic Acid

RT-PCR: Reverse transcriptase-Polymerase Chain Reaction

shRNA: short hairpin RNA

siRNA: Small interfering RNAs

TA: Tibialis Anterior

TBE: Tris/Borate/EDTA

TGF-β: Transforming growth factor β

2'OMePS: 2'O-methyl phosphorothionate

CHAPTER 1
INTRODUCTION

1.1 General structure and physiology of skeletal muscle

Skeletal muscle carries out all the voluntary movements of the body. Differentiated skeletal muscle cells, or myofibres are multinucleated cells formed as a result of fusion of various uninucleate cells called myoblasts. Depending upon the whole length of the muscle, individual myofibres vary in length ranging from a few mm to over 10 cm (Davies *et al*., 2001). The diameter of myofibres also varies ranging from 10-100µm. Each myofibre is composed of myofibrils which are the contractile functional units of striated muscle. Myofibrils are surrounded by cytoplasm known as sarcoplasm. Myofibres are surrounded by a cell membrane called the sarcolemma to which a layer of external connective tissue called the endomysium is attached. Bundles of myofibres are further surrounded by another connective tissue layer called the perimysium. The whole muscle tissue composed of a series of myofibre bundles is covered by a tougher connective tissue layer known as the epimysium (Keynes & Aidley, 2001; Marieb, 2009). These connective tissues structures continue beyond the length of the muscle tissue and culminate into a tendon which attaches to cartilage or a bone as shown in **Figure 1.1**.

Skeletal myofibres are striated due to specific arrangement of contractile proteins present in myofibrils such as actin and myosin that give them an alternate light and dark banded appearance. The so-called A-bands are highly refractile and appear dark, whereas I-bands are less refractile and appear lighter. In the middle of the I-band there is a dark line called the Z-line (or disc) and in the middle of the dark A-band there is a lighter zone called the H-zone with a central darker line called the M-line. The unit of length between two Z-lines is called a sarcomere. From either side of the Z-line, the I-band extends to the beginning of A-band which is made up of thick myosin filaments as shown in **Figure 1.1**. Myosin filaments are surrounded by actin filaments outside the H-zone and these are held in place by the M-line (Davson *et al*., 1970). The myofibrils have been demonstrated to be arranged in groups from four fibrils to twenty fibrils or more. These 'muscle columns' are separated by a 0.2µm-0.5µm sarcoplasmic layer. The cross-linking connections between actin and myosin filaments are called crossbridges (Davson *et al*., 1970).

The A-band does not undergo any change in length either during muscle stretching or shortening. The contraction is brought about by sliding of thin filaments (actin-based) between the thick filaments (myosin-based). A series of reactions between active sites on actin filaments and projections on myosin filaments take place. The projections on myosin filaments attach themselves with actin filaments to form a cross bridge and then pull on them, eventually releasing them and moving back to attach to another site further along the actin filament (Green, 1968).

The myosin filaments are composed of around 100 myosin molecules that have a golf club like appearance with double heads. Half of these heads point in one direction while the rest in opposite direction. These heads have ATPase activity that can release energy from ATP and facilitate binding to the actin molecule's active site. Between two actin strands are laid two strands of tropomyosin that controls the binding of actin strands to myosin. The tropomyosin strands alternate with molecules of troponin. At rest, tropomyosin and calcium-binding troponin prevent contact between actin and myosin filaments. When stimulation takes place, calcium is released that activates troponin and leads to comformational changes in tropomyosin facilitating interaction between actin and myosin. This results in ATP hydrolysis by myosin heads giving energy to myosin to attach to and push along actin filaments. Actin and myosin filaments come apart when ADP is re-substituted for ATP (Keynes & Aidley, 2001)

Figure 1.1

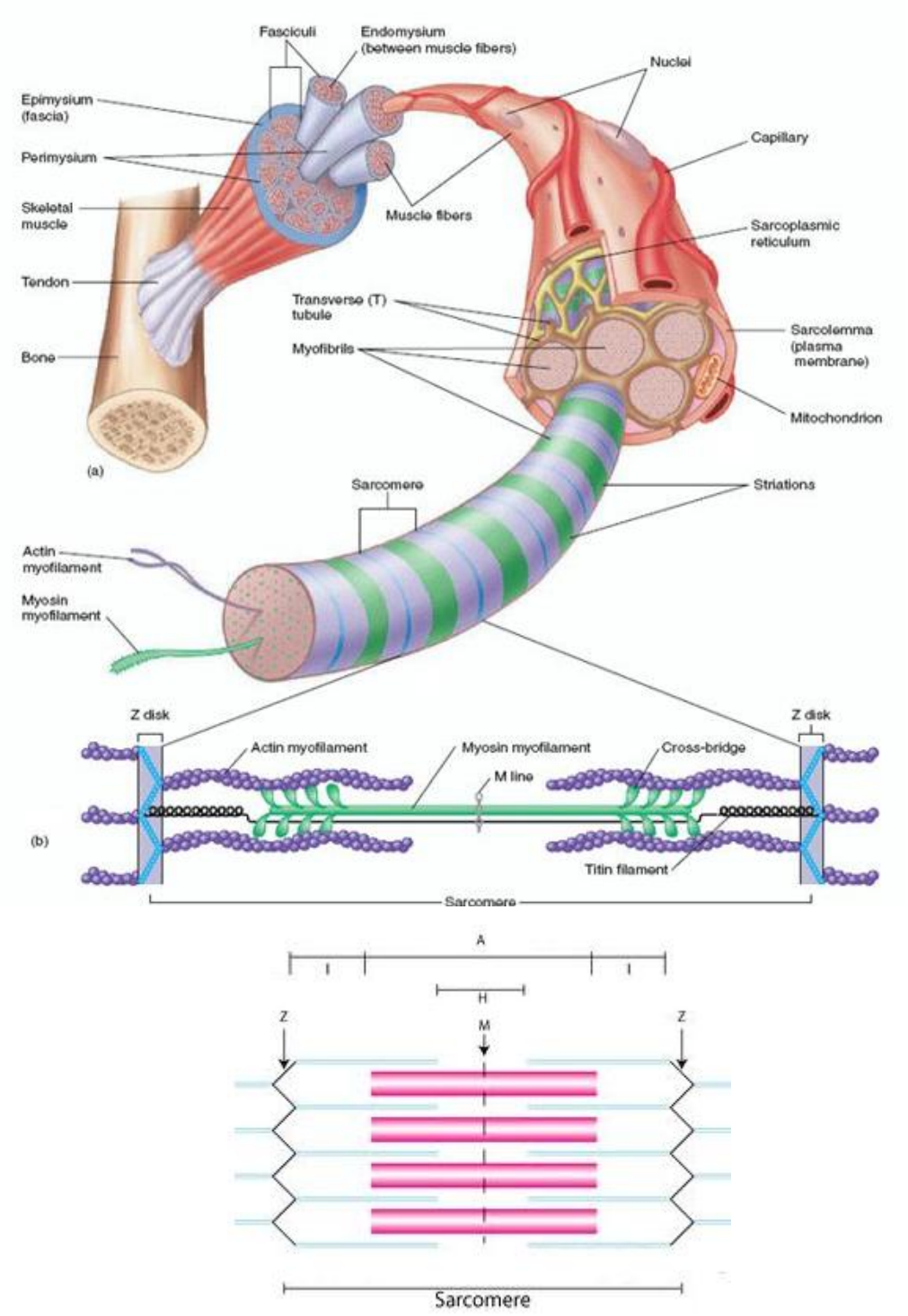

Figure 1.1: Diagrammatic representation of the framework of skeletal muscle showing (a) various connective tissue layers surrounding the muscle and myofibres within a muscle and (b) structure of a myofibril with myosin and actin filaments (Reprinted from Seeley *et al.*, 2006).

1.2 Control of skeletal muscle mass in health and disease

As skeletal muscle is the most abundant tissue in human body, maintenance of its mass is very important for strength, posture balance and some very basic and vital functions like locomotion and respiration. Muscle fibres are responsible for generating mechanical strength. Following an inflammatory, degenerative or traumatic injury, muscle progenitor cells transform into active myoblasts which proliferate and fuse into myotubes. These myotubes further differentiate into mature muscle myofibres (Wiendl *et al.*, 2005).

Sarcopenia is an unintentional degenerative loss of muscle mass and strength related to ageing. Histologically, sarcopenia is characterized by a decrease in myofibre number and size (Carmeli *et al.*, 2002). Cachexia, on the other hand, is a metabolic syndrome characterized by loss of muscle mass associated with underlying chronic diseases such as cancer, heart failure, kidney failure, AIDS and chronic obstructive pulmonary disease (COPD) etc (Evans *et al.*, 2008; Matsakas *et al.*, 2009). There is a very tightly regulated balance between skeletal muscle protein breakdown and synthesis via a network of signalling pathways. In case of sarcopenia, cachexia and several inherited and inflammatory myopathies, this balance between protein synthesis and breakdown is disturbed.

Factors leading to loss of muscle mass and function in sarcopenia have not been precisely understood (Cruz-Jentoft *et al.*, 2010). It has been shown by dual-emission X-ray absorptiometry that the incidence of sarcopenia in humans aged 65-69 years is 14% and in those aged 80 years or above is more than 50% (Baumgartner *et al.*, 1998). In case of limb muscles, the extent of muscle mass loss may reach up to about 20-30% and for the trunk muscles; it may reach up to nearly 40% between the age of 68 and 100 years (Baumgartner *et al.*, 1998). Key features of age-related skeletal muscle mass changes include myofibre atrophy, changes in extracellular matrix composition, disruption of contractile apparatus, and neuromuscular junction (NMJ) deterioration resulting in denervation of ageing muscle (Chai *et al.*, 2011). Neuromuscular changes (including loss or diminished function of neurons in brain and spinal cord, progressive degeneration of NMJs and demyelination of nerves) that contribute to denervation of myofibre take place within peripheral and central nervous system as well as within skeletal muscle (Flood & Coleman, 1988; Luff, 1998).

It has been reported that the following changes take place during ageing: (a) loss of number of motoneurons in the central nervous system (Tomlinson & Irving, 1977),

(b) axon demyelination (Knox *et al.*, 1989), (c) nerve terminal withdrawal from NMJs (Valdez *et al.*, 2010) and (d) re-innervation of denervated myofibres by the surviving motoneurons (Auld & Robitaille, 2003). It is however, not known if the initial myofibre denervation results from deleterious changes in neurons or muscle cells or both. It is likely that a healthy state of myofibres and motoneurons is the key in the maintenance of NMJs (McLennan & Koishi, 2002; Naguib *et al.*, 2002).

There are also a range of metabolic and signalling factors and pathways responsible for controlling skeletal muscle growth and accounting for muscle wasting which are described below.

1.2.1. Protein anabolism and catabolism

In the autophagic/lysosomal pathway, cell organelles and cytoplasm are sequestered into autophagosomes which then fuse with lysosomes, and proteins are digested (Lum *et al.*, 2005). Forkhead box O (FoxO) transcriptional factors normally inactivated by phosphorylation via PI3K/Akt (Phosphatidyl inositol-3 kinase/ protein kinase B, PKB or Akt) pathway (**Figure 1.2 (d))** (detailed later) translocate into nucleus and induce transcription of skeletal muscle-specific E3 ubiquitin ligases namely MuRF1 and MAFbx or atrogin 1 (Sandri *et al.*, 2004) as well as some autophagy-related genes, *LC3* and *Bnip3* (Mammucari et al., 2007). In contrast, insulin-like growth factor-1 (IGF-1) counteracts muscle atrophy by inhibiting autophagy and the ubiquitin-proteasome system (UPS) and also induces protein synthesis via the Akt-mTOR (mammalian target of rapamycin)-$p70^{S6K}$ (P70-S6k kinase) pathway (Glass, 2003).

There is conflicting data on the contribution to muscle wasting by the UPS in ageing (Bardag-Gorce *et al.*, 1999; Clavel *et al.*, 2006). Therefore, at least in sarcopenia, UPS may not be a major pathway leading to muscle loss. Involvement of calcium-dependent cysteine proteases, calpains, has been reported to be involved in muscle loss in ageing rats (Dargelos *et al.*, 2007). In transgenic mice over expressing IGF-1, it was evident that sarcopenia was partly prevented (Musaro *et al.*, 2001). Also, post-maturational ageing is associated with reduced concentration of serum IGF-1 (Dennis *et al.*, 2008). In case of cachexia however, UPS has been reported to be the major systemically-activated proteolytic machinery involved. The mRNA levels of ubiquitin were found to be two to four times higher in muscles from cancer patients than in muscles from control patients (Williams *et al.*, 1999).

When Foxo-1 was targeted and reduced in a cancer cachexia mouse model using an antisense oligonucleotide, there was also found to be an increase in levels of the muscle differentiation transcriptional regulator, MyoD, and a decrease in concentration of negative regulator of muscle mass, myostatin (Liu *et al.*, 2007). Besides increased catabolism, decreased anabolism has been shown by demonstrating downregulation of IGF-1 in animal models of cachexia (Costelli *et al.*, 2006).

1.2.2. Oxidative stress

In C2C12 cells, oxidative stress has been shown to induce expression of the E3 ubiquitin ligase (Li *et al.*, 2003) resulting in an increase in ubiquitin-conjugation and proteasome activity, and a decrease in myosin protein levels (Gomes-Marcondes & Tisdale, 2002). The chronic state of oxidative stress that exists even under normal conditions in muscle is increased with ageing because of an imbalance between generation and detoxification of reactive oxygen species (Sohal & Weindruch, 1996). Reactive oxygen species are regarded as a crucial factor increasing muscle protein catabolism by stimulation of UPS in both cachexia and sarcopenia (Gomes-Marcondes & Tisdale, 2002). Also, in both conditions there is an increase in reactive oxygen species due to lower activity of antioxidant enzymes (Mantovani *et al.*, 2003).

1.2.3. Regenerative capacity

Differentiation of myogenic cells is under the control of myogenic factors including MyoD, myogenin and Myf5 (Olson & Klein, 1994). When satellite cells are in their quiescent state, MyoD expression is absent but as soon as they become active, they start to proliferate and there are high levels of MyoD in their nucleus (Megeney *et al.*, 1996). MyoD is however ubiquitinated by atrophy-associated E3 ubiquitin ligase and thus degraded by the UPS (Tintignac *et al.*, 2005). In case of muscle atrophy along with MuRF1/MAFbx upregulation and increased oxidative stress, the regenerative capacity of satellite cells is also impaired (Zaccagnini *et al.*, 2007).

1.2.4. Steroids

Testosterone and its derivatives are steroid hormones that bind to cytosolic receptors and result in protein synthesis and increase in muscle mass (Bassel-Duby & Olson, 2006). This increase in muscle mass is hypertrophic as there is an increase in myofibre cross-sectional area of both type I and type II fibres but no change in number of fibres (Sinha-Hikim *et al.*, 2002). Ageing-related deficiency in anabolic hormones

promotes catabolism, occurring relatively abruptly in the case of estrogen in women at menopause, and relatively gradually in the case of testosterone in men. Hormone replacement therapy has been studied and resulted in conflicting outcomes for changes in lean mass and grip strength (Kenny *et al.*, 2001; Sih *et al.*, 1997). There is a relative deficiency of anabolic hormones in cachectic state. A reduced testosterone level might lead to reduced muscle strength and bone mass (Zitzmann & Nieschlag, 2000).

1.2.5. Inflammation

High levels of inflammatory markers are associated with physical decline in older persons (Schaap *et al.*, 2009) and induction of cancer-related muscle wasting (Argiles & Lopez-Soriano, 1999). Tumor necrosis factor-α (TNF-α) either in combination with other cytokines or on its own can induce mature myotube breakdown (Guttridge *et al.*, 2000). In cell culture, TNF-α has been shown to be a potent stimulator of MuRF1 and MAFbx expression (Adams *et al.*, 2007b; Li *et al.*, 2005). In some animal studies it has been shown that MuRF1 is essential for TNF-α induced reduction in muscle function (Adams *et al.*, 2008). When myocytes are exposed to TNF-α, it activates a transcription factor NF-κB (Nuclear factor 'kappa light chain enhancer' of activated B-cells) which in turn suppresses MyoD synthesis and inhibits muscle cell differentiation (Megeney *et al.*, 1996). Once activated, NF-κB also up-regulates cytokine synthesis which could result in further myofibre breakdown (Tisdale, 2000).

1.2.6. Genetic defect

Muscular dystrophies are a group of diseases with clinical and molecular heterogeneity characterized by skeletal muscle wasting that compromises the mobility of a patient. Mostly the mutations affecting the proteins that link the cytoskeleton to the basal lamina result in muscular dystrophies. Absence of such proteins cause disassembly of the entire multi protein complex and results in sarcolemma fragility in particular during intense contractile activity causing damage to the fibres (Blake *et al.*, 2002). The dystrophinopathies include muscle disease caused by mutations in dystrophin gene which links the muscle cytoskeleton with the extracellular matrix. The phenotype ranges from asymptomatic increase in serum creatine kinase level and muscle cramps to progressive muscle diseases including Duchenne or Becker muscular dystrophy (where skeletal muscle is primarily affected) and dystrophin-associated dilated cardiomyopathy (DCM), where heart is primarily affected. Whereas mutations in the dystrophin gene lead to Duchenne muscular dystrophy (DMD) and Becker muscular

dystrophy (BMD), mutations in the genes encoding sarcoglycan complex result in limb girdle muscular dystrophies (LGMD) (Swaggart *et al.*, 2011). LGMD patients generally show muscle weakness restricted to limb musculature (greater proximal than distal) (van der Kooi *et al.*, 1994). In congenital muscular dystrophy (CMD), there is severe muscle hypotonia at birth or within first few months of life. Symptoms also include generalised muscle weakness and contractures of variable severity. CMD is caused in approximately 50% of the cases by deficiency of an extracellular matrix protein, the α2 chain of laminin-2 (merosin). There are also other types of CMDs that are related to collagen VI or abnormal glycosylation of α-dystroglycan or integrin deficiency (Reed, 2009). Facioscapulohumeral muscular dystrophy (FSHD) is present typically before the age of 20 and results in marked weakness of facial muscles and stabilizers of scapula or dorsiflexors of foot. Weakness is slowly progressive and about 20% of the patients are restricted to wheelchair. In 95% of affected FSHD patients, a deletion of integral copies of 3.3kb DNA repeat motif called D4Z4 is detected. Oculopharyngeal muscular dystrophy (OPMD) usually has a late-onset (after the age of 45 years) and it is characterized by eyelid drooping and swallowing difficulties. As the disease progresses, limb and facial muscle weakness is also observed. It is caused by a defect in exon 1 of polyadenylate binding protein nuclear 1 (PABN1) encoding gene. PABN1 is responsible for efficient and progressive polymerisation and size control of poly (A) tails on the 3' ends of eukaryotic genes. A normal allele contains ten GCG trinucleotide repeats, whereas autosomal dominant allele ranges in size from 12-17 GCN repeats and autosomal recessive allele has eleven GCN repeats (Robinson *et al.*, 2006).

In DMD, weakness of respiratory and cardiac muscles due to lack of dystrophin protein causing respiratory or/and cardiac failure and subsequent premature death (Emery, 2002). Dystrophic satellite cells also have the same molecular defect and they produce fibres susceptible to degeneration. The satellite cell population is exhausted with time and there is progressive replacement of muscle tissue with adipose and connective tissue (Blake *et al.*, 2002).

Hereditary neuropathies are neurological conditions that are characterized by progressive loss of motor and/or sensory function and muscular atrophy. Motor axons are responsible for conduction of action potential from brain and spinal cord to skeletal muscles, whereas sensory axons conduct in the opposite direction. Peripheral nerves connect the brain and spinal cord to the rest of the body (Scherer, 2011). Functional damage to the peripheral nerves results in peripheral neuropathy. Hereditary peripheral

neuropathies are known as Charcot-Marie-Tooth (CMT) disease after the names of the physicians who described them first. The classification of CMT is based on severity of clinical symptoms and the type of primarily affected cells [myelin sheath (CMT1) or axon (CMT2)] (Vance, 1991). It is also classified based on whether sensory, motor and/or autonomic peripheral neurons are affected (Vance, 1991). In the case of inherited demyelinated neuropathies, although demyelination is a primary pathology, axon degeneration is a long-term consequence. Some patients have minimal symptoms while others may become wheelchair-dependent. In an inherited axonal neuropathy, demyelination takes place as a secondary symptom to axonal degeneration (Scherer & Wrabetz, 2008).

Familial amyotrophic lateral sclerosis (FALS), also known as Lou Gehrig's disease, is a fatal neurodegenerative disease of upper and lower motor neurons resulting in gradual degeneration and death of motor neurons (Siddique & Ajroud-Driss, 2011). Superoxide dismutase 1 (SOD1) is an enzyme that is responsible for destroying free superoxide radicals in the body. Mutations in this gene have been linked with FALS (Rosen, 1993). A4V (Alanine at codon 4 changed to valine) and H46R (Histidine at codon 46 changed to Arginine) mutations have been shown to be the most common FALS-causing mutations in American and Japanese population respectively. At least ten other genes have been linked to FALS (Cudkowicz *et al.*, 1997).

Spinal muscular atrophy (SMA) is an autosomal recessive neuromuscular disorder resulting from loss of function of *survival of motor neuron 1* gene (Lefebvre *et al.*, 1995). SMA is characterized by progressive loss of α-motor neurons in the anterior of the spinal cord resulting in trunk and limb paralysis along with atrophy of voluntary muscles (Munsat & Davies, 1992). Spinal and bulbar muscular atrophy (SBMA) or Kennedy's disease is an X-linked neurodegenerative disease caused by trinucleotide (CAG) repeat expansion in the androgen receptor gene resulting in toxic gain of function in mutant protein (Finsterer, 2009). SBMA pathology includes loss of primary motor neurons in the brain stem and spinal cord (Beitel *et al.*, 2005). Muscle cramps, arm and leg weakness, difficulty with swallowing and speech are some of the symptoms of SBMA apart from androgen sensitivity including reduced fertility and breast enlargement (Rhodes *et al.*, 2009). Huntington's disease is another inherited neurodegenerative disease in which there is a CAG repeat expansion which results in to a polyglutamine stretch translation in exon 1 of huntingtin gene. It affects muscle coordination and causes cognitive decline and dementia (Khoshnan & Patterson, 2011).

1.3 Negative growth regulation of skeletal muscle mass: Role of myostatin

Although there have been immense advances in the knowledge of various molecules and strategies that are active in cell proliferation and differentiation, a lot is still to be investigated regarding tissue size control. It was proposed decades ago that there exist certain negative growth regulators (or chalones) secreted by individual tissues which act to restrict the growth of the tissue that produces them (Bullough, 1962; 1965). Due to lack of sufficient evidence in support of the existence of such molecules with the characteristics of a 'negative growth regulator', this hypothesis was initially discarded. However, over the last decade or so, research in the field of skeletal muscle structure and function strongly suggests that this tissue does control its own mass through a regulatory mechanism that involves an endogenous negative muscle mass regulator called myostatin or GDF 8 (growth and differentiation factor 8) (Lee, 2004). In particular the study of natural and transgenic mutations in the myostatin gene have been shown to lead to major increases in muscle mass in cattle, mice and dogs as well as humans, and based on this various approaches have been explored to develop myostatin-targeted strategies that would lead to recovery of muscle mass and function in various muscle wasting conditions. Myostatin-null mice were also reported to have significantly lower fat accumulation and propensity to insulin resistance, suggesting that inhibiting the myostatin pathway could be a potential therapy for obesity as well as type II diabetes (Lin *et al.*, 2002; McPherron & Lee, 2002).

Initially myostatin was thought to be expressed predominantly in developing muscle. However, recent studies have demonstrated myostatin expression in adult tissue in different animal species (Ji *et al.*, 1998; Ostbye *et al.*, 2001; Rodgers *et al.*, 2001). Myostatin is first expressed in the myotome compartment of somites on 9.5^{th} day of embryonic development in mice. The expression is observed from there on throughout embryogenesis in skeletal muscles (Lee, 2004). Myostatin is expressed in adult tissue predominantly in skeletal muscles with adipose tissue also expressing detectable levels of myostatin RNA. The level of myostatin in different skeletal muscles varies from muscle to muscle (Lee, 2004).

The myostatin gene has a simple molecular arrangement. It has three exons separated by two intervening introns (Gonzalez-Cadavid *et al.*, 1998) as shown in **Figure 1.2**. The myostatin protein sequence has an N-terminal propeptide domain (~38kDa and also known as latency associated protein or LAP-fragment) with a small signal sequence, and a C-terminal receptor-binding domain (12kDa) that gives rise to

active peptide. Myostatin gene sequences are highly conserved among various mammalian species including humans, pigs, mice, rats as well as in chickens as determined by genomic southern analysis (Maccatrozzo *et al.*, 2001; McPherron *et al.*, 1997; Ostbye *et al.*, 2001; Rescan *et al.*, 2001; Roberts & Goetz, 2001). Myostatin sequence conservation in various species proposes that mutation of this gene would also then have a similar effect on its function across these species. Mice with a deletion of a part of the myostatin gene encoding C-terminal domain have been demonstrated to have individual muscles weighing up to twice as much as the wild type mice as shown in **Figure 1.3** (McPherron *et al.*, 1997). This increase in muscle mass was attributed to both an increase in number (hyperplasia) as well as size (hypertrophy) of myofibres. Homozygous mutant mice weighed ~100% more, whereas the heterozygotes weighed ~25% more than their wild type counterparts (McPherron & Lee, 2002). A natural myostatin mutation has been identified in cattle, which is related to increased skeletal muscle mass (McPherron *et al.*, 1997). The myostatin sequence of a breed of cattle called the Belgian Blue has a deletion of 11 nucleotides in the third exon resulting in a frame shift mutation and eventual loss of the entire active mature region of the myostatin protein. Another cattle breed called Piedmontese carries a missense mutation in the third exon of myostatin (McPherron & Lee, 1997). A mutation in myostatin gene in whippet dogs has been described to result into double muscling, the phenotype being typically called 'bully' whippet (Mosher *et al.*, 2007) (**Figure 1.4 A**). In these dogs there is a 2bp deletion in the third exon of the myostatin gene that leads to a premature stop codon and thereby, removal of 63 amino acids from the C-terminal domain of the protein. Heterozygous"bully" whippets with one copy of the mutant gene have increased muscle size and enhanced athletic performance compared to the normal whippets. However, homozygous"bully" whippets with two copies of mutant allele have a double muscling phenotype similar to double-muscled cattle with myostatin deficiency (Mosher *et al.*, 2007). Schuelke *et al.* were the first to identify a natural myostatin mutation in a human child in 2004 (Schuelke *et al.*, 2004) (**Figure 1.4 B).** All the exons and flanking intron regions of the patient's and his mother's gene were sequenced. There was a g→a transition in intron 1 of both the alleles of the patient and in one allele of his mother. Two PCR products were detected from the RNA of mutant construct by an RT-PCR across the boundary between exon 1 and exon 2. One band was equivalent in size to the full length band obtained for wild type construct whereas the second band contained an insertion of 108 bp of intron 1 that resulted from

activation of a cryptic splice site within intron 1. Quantification of band intensities showed that nearly 68% of myostatin mRNA from the mutant construct was misspliced (Schuelke *et al.*, 2004).

Figure 1.2 (a)

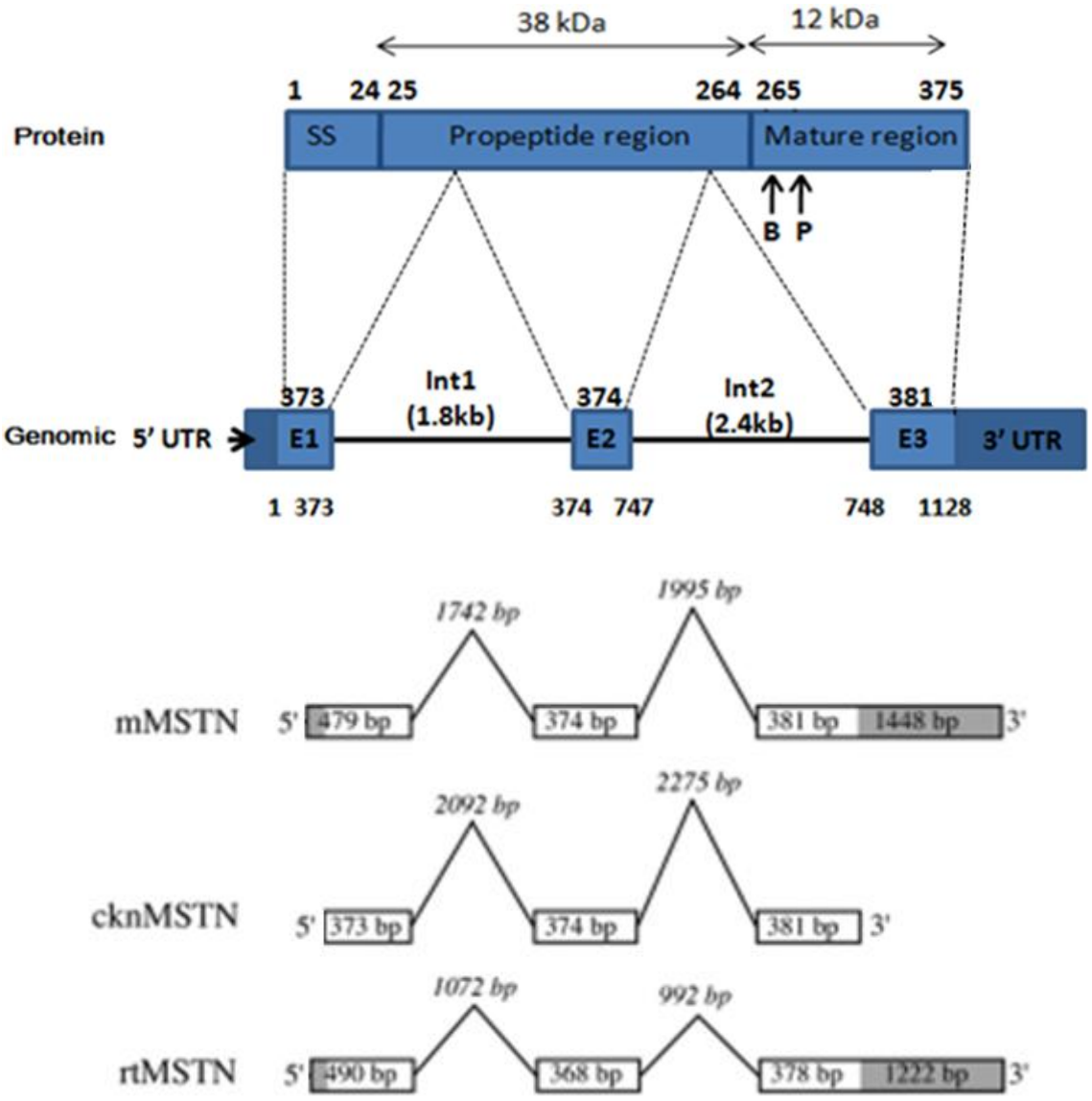

Figure 1.2 (a): Structural organization of myostatin gene. Myostatin gene is composed of 3 exons and two introns. Pre-mRNA splicing removes the intervening introns and translation takes place that results in the formation of latent myostatin that is attached to its natural binding partner called propeptide. The numbers above and below boxes in the figure indicate the amino acid residue positions in human gene. SS represent the signal sequence. Position of mutations in Belgium blue and Piedmontese cattle breed are roughly indicated by 'B' and 'P' respectively (Figure adapted from (Patel & Amthor, 2005)). At the bottom, an arrangement and sizes of exons and introns for other species (mouse, chicken and rat) are also shown for comparison (Figure adapted from (Rodgers & Garikipati, 2008)).

Figure 1.2 (b)

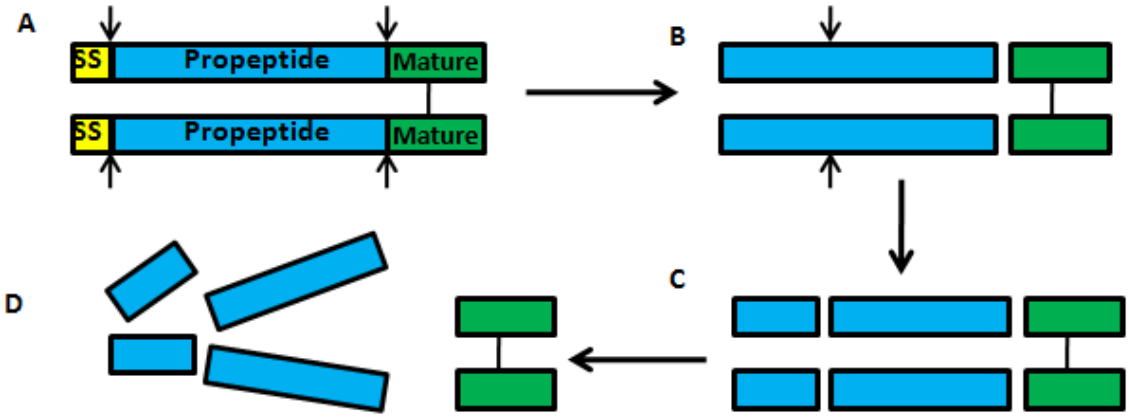

Figure 1.2 (b): Myostatin protein processing. Synthesized as a precursor, myostatin undergoes two proteolytic cleavage events. (A) One cleavage removes the N-terminal signal sequence and second cleavage generates a C-terminal fragment with receptor-binding activity. (B) Propeptide and C-terminal dimer remain non-covalently bound, until (C, D) myostatin is activated by cleavage of propeptide by BMP-1/tolloid family of metalloproteinases.Figure adapted from (Lee, 2004)

Figure 1.2 (c)

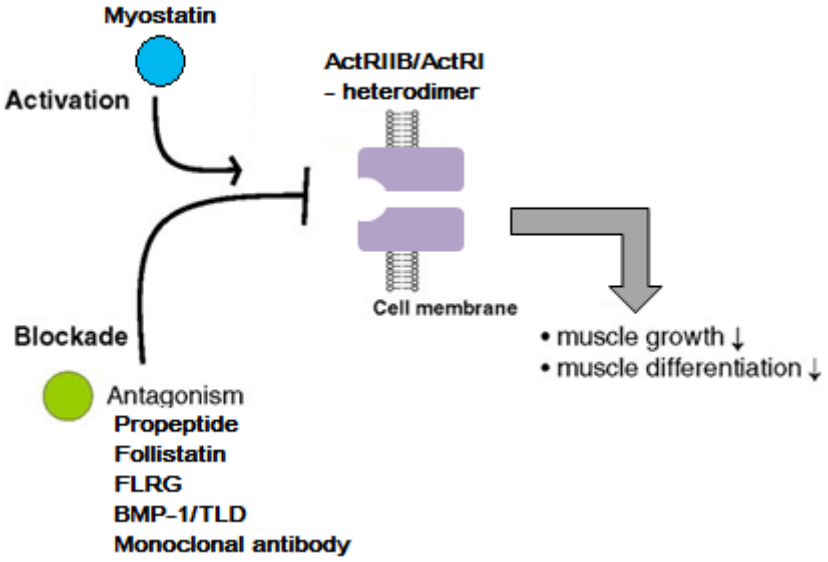

Figure 1.2 (c): A general overview of pathways activated by myostatin. Myostatin activates its receptors on binding them and results in decrease in muscle growth and differentiation. Various antagonists like propeptide, follistatin, FLRG etc. block myostatin activation and therefore inhibit its function (Figure adapted from (Elkina *et al.*, 2011)).

Figure 1.2 (d)

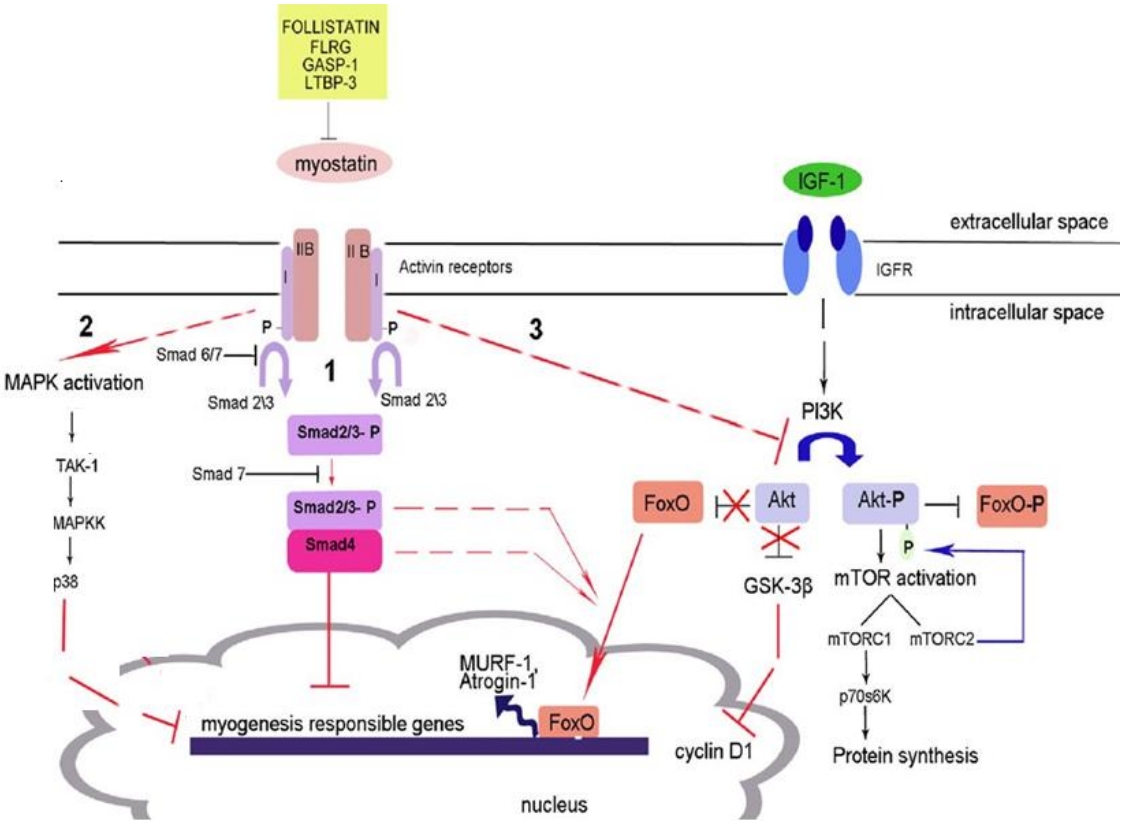

Figure 1.2 (d): Myostatin signalling pathway: In response to IGF signalling, Akt/mTOR pathway is activated and results in phosphorylation of Akt which further inhibits FOXO nuclear entry thereby preventing induction of gene expression of muscle atrophy mediators. Activated Akt is also responsible for increased protein synthesis resulting from activation of its downstream targets mTOR and $P70^{S6K}$. Mature myostatin binds to AcRII (type B to higher extent than type A) which activates AcRI. This further activates Smad 2/3 which form a complex with co-smad 4. This smad complex then translocates into the nucleus where it initiates the gene transcription. Myostatin inhibits Akt activation and therefore favours protein degradation. MAPK activation by myostatin results in blockade of genes responsible for myogenesis (Figure adapted from (Elkina *et al.*, 2011)).

Figure 1.3

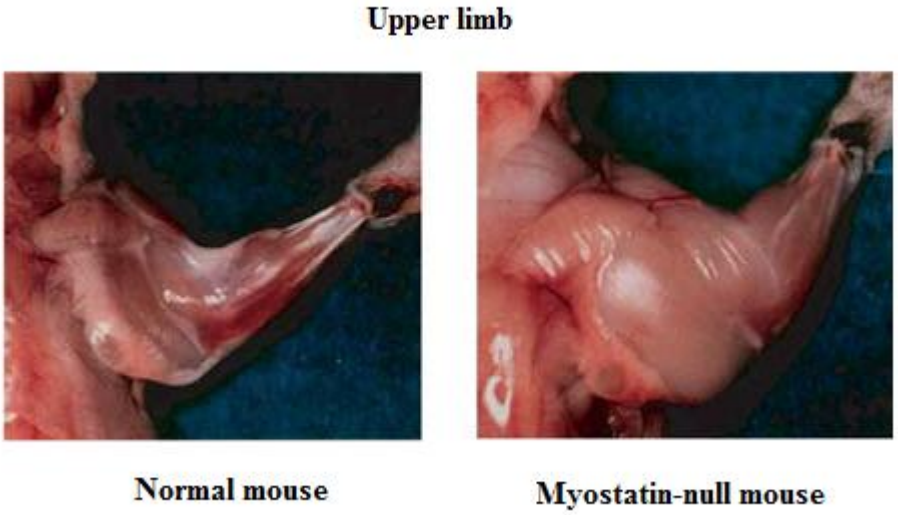

Figure 1.3: Myostatin null mice with increased muscle mass compared to normal mouse as shown in the upper limb (reprinted from McPherron *et al*., 1997)

Figure 1.4

(A)

(B)

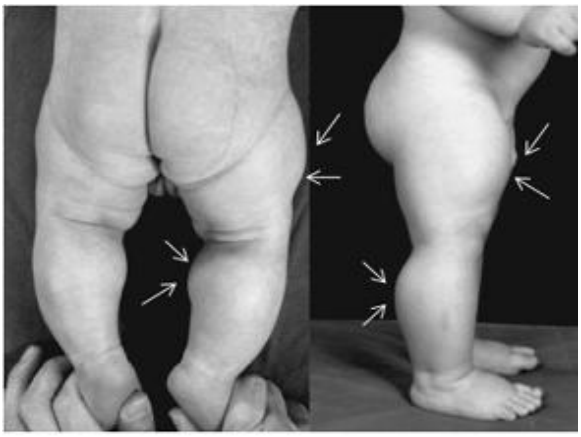

(C)

Pair wise comparison	Protein homology
Human vs. Mouse	96%
Human vs. Dog	95.7%
Human vs. Rat	94.9%
Human vs. Bovine	94.1%
Human vs. Chicken	92%

Figure 1.4: Natural Myostatin mutations in dog and a human child: (A). Comparative images of whippets with wild type genotype; with one normal and one mutant allele; and with two copies of mutant alleles. (B). A child pictured at 6 days and 7 months of age with a mutation in myostatin gene shown to have protruding calf and thigh muscles.(Reprinted (A): Mosher, 2007; (B): Schuelke, 2004). (C). Comparison of human myostatin protein sequence to other species for degree of conservation.

1.4 Myostatin signalling pathway

Myostatin is synthesized as a pre-propeptide that undergoes proteolytic processing to produce biologically active myostatin. Depending upon post-translational modifications, myostatin can exist in either active or inactive states (Hill *et al.*, 2002; Thies *et al.*, 2001). Proteolytic processing involves removal of the N-terminal signal peptide and generation of mature domain capable of binding to its receptor (Wakefield *et al.*, 1989). After proteolytic processing, the propeptide and disulphide-linked C-terminal dimer remains bound to each other non-covalently. Further cleavage of propeptide by members of BMP1 (Bone morphogenetic protein 1)/Tolloid family of metalloproteinases is required to allow the dissociation of propeptide and mature region (McPherron *et al.*, 1997) (**Figure 1.2 (b)).** It has been shown that propeptide region of TGF-β family members can also form disulphide linkages with latent TGF-β proteins (LTBP), a class of polypeptides. These latent proteins are responsible for increasing the rate of TGF-β secretion. When the complex consisting of mature region, propeptide region and the LTBP is secreted, non-covalent links are formed by the LTBP with the extra cellular matrix (ECM) components allowing large quantities of TGF-β to be stored in the ECM in an inactive form (Taipale *et al.*, 1994). Myostatin is present in the serum in its inactive form (Hill *et al.*, 2002) but there is inconsistency in the data regarding active myostatin detection in serum (Gonzalez-Cadavid *et al.*, 1998; Zimmers *et al.*, 2002) which is likely to be due to different antibodies used for myostatin detection with different specificities.

A majority of TGF-β superfamily members induce a signalling cascade through heterodimeric complexes of serine/threonine kinase receptors of type I and type II (also known as activin receptors type I and II). The TGF-β members bind to the activin receptor II (ActRIIB to a greater extent than ActRIIA) first and then to the receptor I (ActRI) thereby leading to phosphorylation of type I receptor kinases by type II receptor kinases (Chen *et al.*, 1998). Type I receptor kinases then in turn phosphorylate and activate Smad proteins which are a cluster of transcription factor molecules downstream of the TGF-β receptors acting as signal transducers. Upon activation, Smad2 and Smad3 form heterodimers with co-Smad, Smad4. This activated complex then moves from cytoplasm to nucleus where the target gene transcription is regulated (Langley *et al.*, 2002a; Shi & Massague, 2003).

Double muscling cattle with natural myostatin mutation have increased formation of type IIB fibres (fast glycolytic fibres) in their biceps (Stavaux *et al.*, 1994).

Myostatin null mice have increased type IIB but decreased type I and type IIA fibres in tibialis anterior (TA) and biceps. A decrease in fatigue resistance of the myostatin null biceps demonstrated by functional electrical stimulation supports the increase in type IIB fibre content (Girgenrath *et al.*, 2005). Myocyte enhancer factor 2 (MEF2) has an important role in the formation of oxidative type I fibres and therefore myostatin null muscle has been reported to have reduced levels of MEF2 and that of downstream genes like calcineurin (Wu *et al.*, 2000). Fast fibres have high levels of early muscle differentiation marker, MyoD and therefore myostatin null muscle were revealed to have increased levels of MyoD (Hennebry *et al.*, 2009). Transcriptional regulators of myogenic cell proliferation, Pax-3 and Myf-5 and correspondingly MyoD are downregulated in response to myostatin (Devitt *et al.*, 1997).

Myoblast differentiation and myotube hypertrophy are known to be mediated by the Akt/mTOR/p70S6 pathway. Induction of hypertrophy in adult skeletal muscle has been shown to be accompanied by increase in level of IGF-1 (DeVol *et al.*, 1990). IGF-1 binds to its receptor and leads to activation of phosphatidyl-inositol-3-kinase (PI3K) along with various other intracellular kinases. A membrane phospholipid, phosphatidyl-inositol-4,5-bisphosphate is then phosphorylated by PI3K into phosphatidyl-inositol-3,4,5-trisphosphate, which results in creation of a lipid-binding site for Akt on cell membrane. This in turn facilitates phosphorylation and activation of Akt by a kinase called PDK-1 (Vivanco & Sawyers, 2002). Various downstream targets of Akt include key regulatory proteins like mTOR and $p70^{S6K}$ involved in protein synthesis and translation (Cross *et al.*, 1995; Nave *et al.*, 1999). Myostatin has been shown to inhibit the IGF-1/PI3K/Akt pathway by mediating hypophosphorylation of Akt and thus reduces the muscle growth (Trendelenburg *et al.*, 2009). Hypophosphorylation of Akt leads to reduced levels of phosphorylation of FoxO1 and therefore an increase in levels of the atrophy mediator, atrogin-1 or MaFbx which activates ubiquitin E3 ligase (Langley *et al.*, 2002a). Therefore, myostatin is understood to inhibit the myotube hypertrophy which is induced by IGF-I and the activation of Akt (Morissette *et al.*, 2009) (See Figure 1.2 (d)).

Myostatin has been shown to mediate polyubiquitination of cyclin D1, thereby inhibiting G1 to S phase progression (Yang *et al.*, 2007). Myostatin also activates TGF-β-activated kinase 1 (TAK-1) which further activates p38 mitogen-activated protein kinase (MAPK). This is followed by an increase in levels of cyclin dependent kinase

inhibitor, p21 and thereby, a change in retinoblastoma protein phosphorylation status which blocks the G1 to S-phase progression (Philip *et al.*, 2005).

Myostatin has been demonstrated to also have a key regulatory role in skeletal muscle fibrosis. Expression of myostatin and its receptor ActRIIB on muscle fibroblasts and induction of fibroblast proliferation along with ECM protein synthesis has been reported both *in vitro* and *in vivo*. This muscle fibroblast proliferation involves the Smad, p38 MAPK and PI3K/Akt/mTOR signalling pathways (Li *et al.*, 2008).

1.5 Natural and therapeutic mechanisms of myostatin inhibition

The following strategies have been studied with an aim to inhibit the expression of myostatin gene.

1.5.1. Myostatin propeptide

Regulation of myostatin signalling has been extensively studied by recognizing various different inhibitors of myostatin that could be important in muscle growth promotion. Studies have shown that if myostatin is bound to its natural binding partner, the myostatin propeptide, it leads to myostatin inhibition due to its unavailability to bind to ActRIIB. Systemic administration of Adeno-associated virus-8 (AAV8) vector expressing mutated myostatin propeptide (AAV8ProMyo) to healthy mice led to myofibre hypertrophy which resulted in increase in muscle mass of the TA, extensor digitorum longus (EDL), gastrocnemius and rectus femoris muscles (Matsakas *et al.*, 2009). Another interesting study on systemic administration of AAV8ProMyo has shown that an increase in slow (soleus) muscle mass resulted in increased force output but the same was not observed in the fast (EDL) muscle mass. Therefore, it has been suggested that myostatin inhibition might have muscle- or fibre-type specific effects in terms of remodelling muscle mass and strength (Foster *et al.*, 2009).

A dominant negative myostatin transgene (dnMstat) has been reportedly synthesized by deleting C-terminal region of isolated myostatin gene and introducing a mutation to produce a peptide that is resistant to proteolytic activation (Morine *et al.*, 2010). This transgene was cloned into an AAV vector along with a liver specific promoter and then injected into *mdx* mice. This treatment resulted in increased skeletal muscle mass which was comparable to the increase obtained with other approaches such as use of myostatin propeptide and neutralizing antibodies to knockdown myostatin (Morine *et al.*, 2010).

1.5.2. Follistatin and related proteins

First isolated from the ovary, follistatin suppresses the follicle stimulating hormone (FSH). However, follistatin has also been shown to be a myostatin antagonist that binds to myostatin and blocks its association with the ActRIIB. Therefore, follistatin can lead to inhibition of myostatin activity, but as a potential therapeutic approach invokes serious concerns about adverse effects on reproductive capabilities (Lee *et al.*, 2004). However, a strategy using AAV based delivery system to deliver a form of alternatively spliced follistatin has been reported to increase muscle mass and size, largely bypassing adverse off-target side-effects (Rodino-Klapac *et al.*, 2009). Follistatin-related gene (FLRG) and growth and differentiation factor association protein (GASP-1) are two other proteins that are found associated with mature myostatin in human as well as mouse blood. They both bind to the C-terminal dimers and have been shown to inhibit the activity of myostatin in signalling assays (Hill *et al.*, 2002; Hill *et al.*, 2003).

1.5.3. Activin Receptor type IIB (ActRIIB)

Transgenic mice have been produced overexpressing a truncated form of the ActRIIB receptor, as the dominant negative form, capable of binding and sequestering myostatin but unable to initiate the signalling pathway. In these animals muscle hyperplasia as well as hypertrophy leads to significant increases in muscle mass (Lee & McPherron, 2001). Furthermore as a potential recombinant therapeutic protein, an ActRIIB-Fc fusion protein has been generated by fusing the human IgG1 Fc domain to the extracellular domain of ActRIIB lacking the intracellular kinase domain (Lee *et al.*, 2005). The extracellular domain is responsible for the TGF-β binding whereas the Fc domain of human IgG1 helps in homodimer formation which allows high receptor affinity for myostatin. The ActRIIB-Fc fusion protein was shown to inhibit myostatin signalling in A204 cells via a pGL3-$(CAGA)_{12}$-luciferase reporter system (Lee *et al.*, 2005). The ActRIIB-Fc fusion protein was also tested in mice that were treated with intraperitoneal injections leading to 30-60% dose-dependent increases in body weight (Lee *et al.*, 2005).

Acceleron has reported a single-dose and repeated doses sub-cutaneous studies of ACE-031 (a soluble form of ActRIIB) in healthy volunteers (http://www.acceleronpharma.com/products/ace-031/). And a phase 2 study in patients with Duchenne muscular dystrophy (ACE-031) has been conducted in Canada. The

main purpose of the studies was to determine if ACE-031 is safe and well-tolerated in children with DMD. Another purpose of the study was to obtain preliminary information regarding the effects of ACE-031 on muscle size, strength and function in patients with DMD. In all of the clinical trials conducted to date, increases in muscle mass were reported with ACE-031 treatment. During the course of clinical trials in healthy adults and in DMD boys, some participants experienced minor nosebleeds, gum bleeding and/or small dilated blood vessels within the skin. The majority of these events resolved fully upon discontinuation of treatment. By themselves, the minor bleeding events and dilated blood vessels were not considered to be a serious safety concern for study subjects. However, based on review of these preliminary safety data with the FDA and Health Canada, Acceleron ended the DMD trial and the follow-on extension studies. Acceleron reports that they intend to resume studies of ACE 031 in DMD as soon as possible pending further analysis of safety data and following discussions with regulatory agencies.

1.5.4. BMP-1 (Bone morphogenetic protein-1)/Tolloid family of metalloproteins

BMP-1/Tolloid family of metalloproteins and related proteinases like mTLL-1, mTLL-2 and mTLD cleave and release the mature myostatin fragment from its natural binding partner (myostatin propeptide) and allow the activation of activin receptors (Wolfman *et al.*, 2003). Therefore, proteases that are modified structurally in such a way that despite being able to bind to myostatin, they are unable to cleave it from propeptide, can restrict the activation of ActRIIB and eventually the myostatin effect on the muscle function.

1.5.5. Antibodies against myostatin

The mouse anti-myostatin monoclonal blocking antibody, JA16 was raised against recombinant myostatin to inhibit myostatin binding to its receptor ActRIIB. Intraperitoneal injections of JA16 for twelve weeks have been reported to lead to an increase in body weight, muscle mass and absolute muscle strength along with decrease in levels of serum creatine kinase and muscle degeneration in *mdx* mouse, a model of Duchenne muscular dystrophy (Bogdanovich *et al.*, 2002). A phase I/II clinical safety trial conducted for another myostatin neutralizing antibody, MYO-029 showed good tolerability and safety profiles (Wagner *et al.*, 2008).

1.6 Other RNA-based therapy for gene expression modulation

Regulation of pre-mRNA processing in a specific and precise manner is very crucial in directing gene expression (Sharp, 2009). This process known as pre-mRNA splicing includes removal of the introns to produce a mature mRNA transcript containing a single open reading frame coding regions. This mature mRNA is then translated into a functional protein (Crick, 1979). Alternative splicing contributes to proteomic diversity (Schmucker & Flanagan, 2004) and defects in alternative splicing have been demonstrated to be the cause of various disorders (Licatalosi *et al.*, 2008).

1.6.1. Pre-mRNA splicing

The removal of introns in a precise fashion is a key event in the expression of genes. This RNA splicing machinery has a very crucial role in the recognition and elimination of introns, and the fusion of exons in a very specific manner. In the case of alternative splicing, different isoforms of proteins perhaps having diverse functions can be generated through regulated splicing mechanism and spice site and exon recognition (Collins & Guthrie, 2000). Splice sites are specific sequences that are present at intron/exon boundaries and play an important role in directing the omission of introns and fusion of exons in mRNA. The 5'-end of the intron has a 5'-splice site at the junction of intron and exon with consensus sequence and a GU dinucleotide at the intronic end. The 3' end of the intron also has a consensus 3'-splice site which is characterized by conserved sequences including a terminal AG right at the 3' end, a polypyrimidine tract in the middle, and a branch point (Black, 2003).

Five different small nuclear ribonucleoproteins (snRNPs) namely, U1, U2, U4, U5 and U6 along with several other non-snRNPs form the spliceosome complex as shown in **Figure 1.5** (Collins & Guthrie, 2000) which is responsible for specific recognition of exons and introns, and for carrying out the two transesterification steps involved in the splicing process. The snRNA of U1 snRNP base pairs with and binds to the 5'-splice site. SF1, a branch point binding protein, then binds the components of the 3'splice site. U2 auxillary factor (U2AF) is a dimer composed of two subunits that are 65kDa and 35kDA in size. The 65kDA subunit of U2AF binds to the polypyrimidine tract whereas in some cases the smaller subunit of U2AF binds to the terminal AG at 3' splice site. U1 and U2AF attached to either end of the intron constitute the early (E) spliceosome complex, also known as the commitment complex. U2 snRNA binds to this E-complex via base pairing with the branch point, thereby forming the A-complex. This

A-complex is then joined by U4/U5/U6 to form the B-complex which then undergoes reorganization to replace U1 snRNP with U6 snRNP and remove U1 and U4 snRNPs, and thus form a C-complex (Black, 2003; Nilsen, 1996; 2002). The C-complex then catalyzes the two chemical reactions of splicing (**Figure 1.6**).

First of all, the phosphate at the 5' splice site is attacked by the 2'-OH group of a specific branch point A residue. This results in cleavage of the exon at 5' end and fusion of 2'-OH group with the 5' end of the intron. Two intermediate products are formed as an outcome of this reaction which are, (i) the 5' exon released from the mRNA and (ii) a 5' intron and 3' exon fragment. This is followed by an attack by the 3'-OH of the released exon on the phosphate group at the 3' end of the intron resulting in fusion of the two exons and elimination of the intron which is in a lariat conformation (Black, 2003).

Figure 1.5

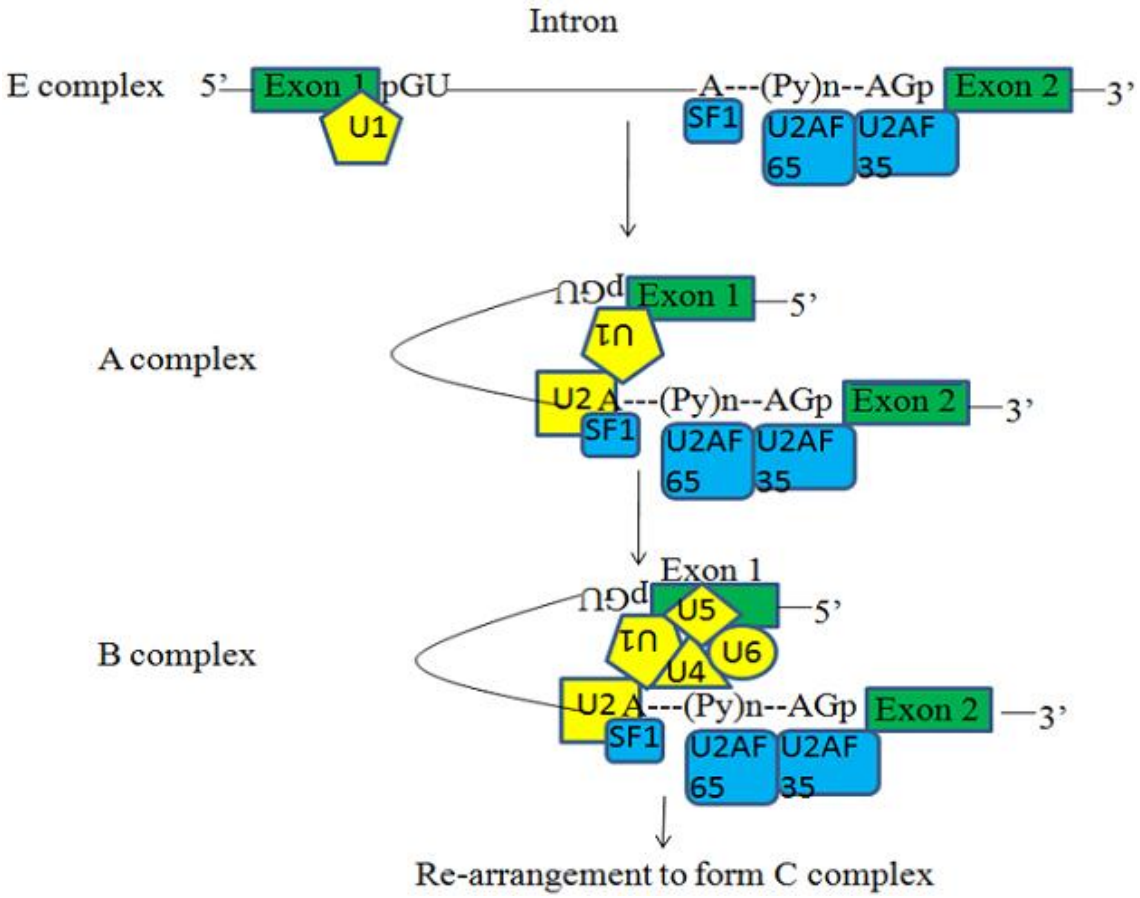

Figure 1.5: Spliceosomal assembly before transesterfication reactions for splicing. The small nuclear ribonucleoprotein (snRNP), U1 binds to the 5' splice site at the 5'end of the intron/exon boundary which is followed by SF1 binding to the 3' splice site and U2 auxillary factor (U2AF) binding to the 3' splice site of the intron. A 65kDa subunit of U2AF binds to the polypyrimidine tract in the middle, whereas a smaller subunit of U2AF binds to 3' terminal AG. Binding of these two snRNPs to the intron results in the formation of a complex namely E complex (or early complex). The E complex is then joined by U2 snRNA resulting in the formation of the A complex. This complex is then bound by U4/U5/U6 (forming B complex) which is followed by re-arrangement involving replacement of U1 with U6 and then removal of U1 and U4. The resulting complex is known as C complex. (Diagram modified from Black, 2003)

Figure 1.6

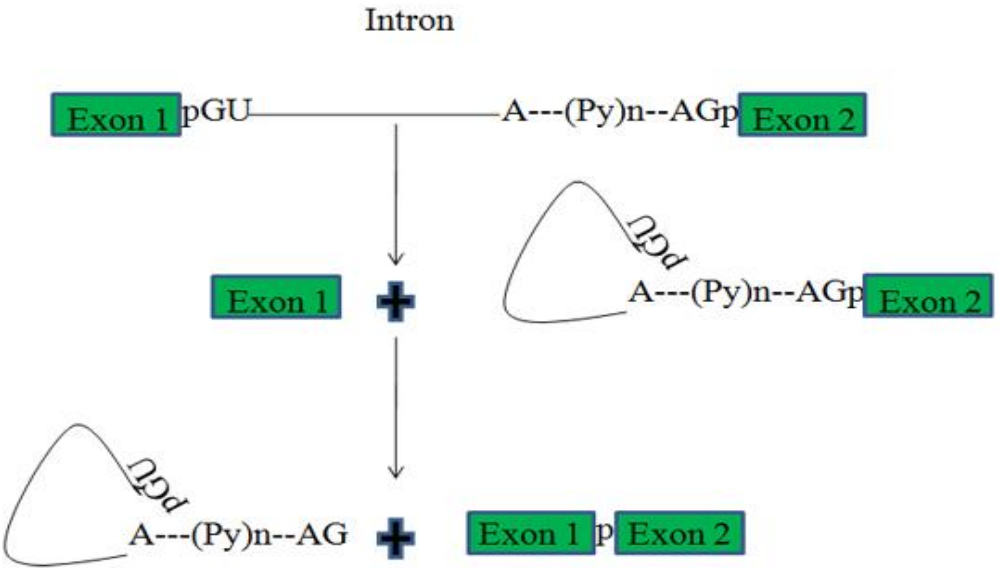

Figure 1.6: Transesterification reactions involved in splicing. A 2'-OH group on a specific A- residue at the branch point attacks the phosphate group at 5' splice site of the intron. This leads to release of exon at 5' end and fusion of 2'-OH group on the residue A to the 5' end of the intron. This is followed by an attack on the phosphate group of the 3' end of the intron by the 3'-OH of the released exon. The final product therefore is two exons fused together with the removal of intron in a lariat conformation. (Diagram modified from Black, 2003)

Targeting the defects in the pre-mRNA splicing as in the case of various genetic disorders by RNA modulation or splice correction overcomes the following flaws of conventional gene replacement therapies, (a) transgene size limitations, (b) low gene transfer efficiency, (c) insertion into the host genome and (d) immunological response to the vector components (Wood *et al.*, 2007). RNA modulation can therefore be used in removal of the target mRNA, mRNA repair or in alteration of the final mRNA product (Aartsma-Rus & van Ommen, 2007). Modulation of pre-mRNA splicing has been investigated as a potential treatment for various disease conditions.

1.6.2. RNA interference

RNA interference (RNAi) is a mechanism of double stranded RNA (dsRNA)-mediated mRNA silencing that can regulate endogenous gene expression. The double stranded RNA molecule is degraded by an endogenous ribonuclease (Dicer) into smaller fragments which are about 21-23 nucleotide long and are called small interfering RNAs (siRNAs) (Grishok *et al.*, 2000; Zamore *et al.*, 2000). A protein complex known as RNA-induced silencing complex (RISC) is then bound by the siRNAs. The RISC has a helicase as well as endonuclease activity. The two strands of the siRNA molecules are unwound by the helicase activity of RISC so that the antisense strands are facilitated to bind the targeted RNA molecule (Sharp & Zamore, 2000). The target RNA molecule is then hydrolyzed at the point of contact with the antisense strand by the endonuclease activity (Hutvagner & Zamore, 2002; Schwarz *et al.*, 2002). It is possible to induce RNAi exogenously by expression of duplexes of microRNA (miRNA) and short hairpin RNA (shRNA) with the viral vectors or by incorporating synthetic siRNA (de Fougerolles *et al.*, 2007; Liu *et al.*, 2008; Sledz & Williams, 2005).

Activation of exogenous siRNA-induced RNAi has a very promising therapeutic potential. Apart from knocking down the expression of genes that implicate a specific disease-related pathogenesis, RNAi has also been shown to allow specific knockdown of the alternatively spliced isoforms (Wood *et al.*, 2007). Almost 70% of the human genes with multiple exons are known to generate different transcripts through alternative splicing (Stamm *et al.*, 2005). Defects in this process can lead to various genetic disorders. RNAi targeted at specific sequences within or at the boundaries of the alternatively spliced exons can knockdown the expression of disease-related isoforms (Celotto & Graveley, 2002). However, the use of RNAi to target endogenous splicing factors needs to be monitored very precisely as it can possibly lead to substantial off-

target effects. Therefore, in the case of dominant genetic disorders where a mutant allele needs to be targeted but the normal allele has to stay intact as it might be crucial in certain important functions in the body, a very precise discrimination between the two alleles is required for RNAi applicability (Denovan-Wright & Davidson, 2006; Rodriguez-Lebron & Paulson, 2006). Some *in vitro* studies on allele-specific RNAi have been reported for spinocerebellar ataxia (Xia *et al.*, 2004), osteogenesis imperfecta (Millington-Ward *et al.*, 2004) and sickle cell anaemia (Dykxhoorn *et al.*, 2006). A combined study to inhibit myostatin using RNAi against ActRIIB and restore quasi dystrophin by U7 exon skipping has been reported recently to improve muscle physiology (Dumonceaux *et al.*, 2010).

Chemically synthesised siRNAs are short-lived and result in only transient inhibition of gene expression. Delivery of synthetic siRNAs requires a lot of emphasis on stabilization of the siRNAs as well as development of methods for targeting the siRNAs in an effective way. Viral vector based system has safety concerns. Although various viral vectors have been clinically tested in phase I safety trials, a complete assessment of efficacy, specificity and risks still needs to be done (Weinstein & Peer, 2010). Unmodified naked siRNAs when injected intravenously are recognized by Toll like receptors (TLRs) that stimulate the immune system and provoke an interferon response as well as cytokine induction and coagulation cascades (Szulc *et al.*, 2006). Another problem with RNAi lies in the off-target effects that are likely to be induced by this technology (Pei & Tuschl, 2006).

1.7. Some examples of disorders resulting from defective mRNA splicing

1.7.1. Phenylketonurea

Deficiency of phenylalanine hydroxylase (PAH) leads to an autosomal recessive genetic disorder, phenylketonurea (PKU) in humans. Human hepatic PAH is responsible for hydroxylation of phenylalanine to tyrosine, therefore its deficiency leads to abnormalities related to PAH metabolism that include severe brain damage (Scriver & Clow, 1980a; b). When a PKU carrier's PAH mutant cDNA clones were isolated, an internal deletion corresponding to exon 12 of the human PAH gene was revealed that resulted in production of a truncated protein. When the expression studies were carried out, it was found that this internal deletion led to termination of PAH activity resulting from instability of the protein (Woo *et al.*, 1986). Further investigation to find out about the molecular mechanism and basis of this activity demonstrated that there was a

GT→AT substitution at the donor splice site of intron 12 that consequently led to the skipping of exon 12 (DiLella *et al.*, 1986; Marvit *et al.*, 1987).

1.7.2. Ornithine transcarbamylase (OTC) deficiency

Deficiency of a liver specific X-linked enzyme, ornithine transcarbamylase (OTC) can lead to early death due to ammonia intoxication. OTC catalyzes the second step in urea cycle which involves production of citrulline by condensation of carbamyl phosphate and ornithine (Hata *et al.*, 1986; Horwich *et al.*, 1984). When cDNA samples from patients' liver were amplified using PCR, no full length product was observed, neither did western blot analysis of protein extracted from patient liver show any cross reacting material (Carstens *et al.*, 1991). Three of the seven samples showed PCR products smaller than the normal which upon sequencing revealed that two of the samples had no exon 7 of the gene and the third had a few base pairs of exon 5 missing. One of the mutants with missing exon 7 had a T→C substitution in the 5' splice donor site of intron 7 while the other one with missing exon 7 had an A→G substitution in the intron 7. An A→T change was found at the end of exon 4 in the 3' splice acceptor site of third mutant (Carstens *et al.*, 1991).

1.7.3. The Menkes disease

Defects in a copper-transporting ATPase gene (*ATP7A*) lead to a neurodegenerative disorder, the Menkes disease. In severe cases of Menkes disease, connective tissue abnormalities, distinctive 'kinky hair' and ultimate death in early childhood are observed. Approximately 22% of the *ATP7A* mutations are splice site mutations and over 60 splice mutations have been studied (Kaler *et al.*, 1996; Skjorringe *et al.*, 2011).

1.7.4. β-Thalassemia

β-Thalassemia is a serious genetic blood disorder in which production of a subunit of haemoglobin, β-globin is either partially or completely ablated by mutations in the β-globin gene. This defect results in decreased oxygen-carrying capacity of red blood cells causing compensatory bone marrow expansion and if untreated, fatal iron overload (Sazani & Kole, 2003). Splicing defect mutations are quite common in thalassemic patients. Mutations causing splicing defects, for instance, in intron 2 of β-globin gene lead to activation of a cryptic 3' splice site along with the production of an aberrant 5' splice site. This eventually leads to the inclusion of a part of the intron into

the spliced mRNA resulting in creation of an in-frame stop codon (Dominski & Kole, 1993; Lacerra *et al.*, 2000; Sazani & Kole, 2003; Suwanmanee *et al.*, 2002).

1.7.5. Cystic Fibrosis

Cystic fibrosis is a recessive genetic disease affecting lungs, pancreas, liver and intestine characterized by abnormal chloride and sodium transport across epithelium resulting in thick viscous secretions (Yankaskas *et al.*, 2004). About 14% of deleterious cystic fibrosis mutations result from defects in mRNA splicing of cystic fibrosis transmembrane conductance regulator (CFTR) gene. Nearly 2% of these mutations occur due to aberrant splicing resulting from a mutation in intron 19 of this gene that activates a cryptic 3' splice site and produces an aberrant 5' splice site (Friedman *et al.*, 1999; Tsui, 1992).

1.7.6. Cancer

In case of tumours that are noncompliant to apoptosis, maintenance of the correct ratio of antiapoptotic proteins to proapoptotic proteins is very crucial. The *bcl-x* gene can be spliced alternatively to result in the production of two isoforms that have proapoptotic function (bcl-xS) and antiapoptotic function (bcl-xL). Both the forms are required for normal functioning but in case of many cancers including prostate cancer, bcl-xL is over-represented (Krajewska *et al.*, 1996). Therefore, blocking the bcl-xL 5' splice site should increase the ratio of bcl-xS to bcl-xL, and simultaneously increase the proapoptotic signals and decrease the antiapoptotic signals, resulting in inhibition of growth or death of cancer cells.

1.7.7. Ataxia-Telangiectasia

A progressive autosomal recessive neurodegenerative disorder called ataxia-telangiectasia (A-T) is caused by a splicing mutation in *ataxia-telangiectasia mutated* (ATM) gene leading to activation of a cryptic 5' splice site; or a cryptic 3' splice site; or activation of a downstream 5' splice site leading to the inclusion of an intron within the spliced mRNA (Perlman *et al.*, 2003). PMO-based AOs targeted to these aberrant splice sites led to successful mRNA level restoration of normal splicing of ATM protein and also resulted in translation of full length product in three different cell lines for up to 84 hours (Du *et al.*, 2007).

1.7.8. Inflammatory diseases

Several proinflammatory factors are known to initiate signalling through myeloid differentiation factor 88 (MyD88) which further results in activation of Interleukin-1 receptor (IL-1R) -associated kinase known as IRAK-1. The activation of IRAK-1 via phosphorylation eventually leads to the activation of nuclear factor kappa-light-chain-enhancer of activated B-cells (NF-κB). There is a splice variant of MyD88, known as $MyD88_S$ which does not possess the capacity to bind to NF-κB (Janssens *et al.*, 2002). AOs of 2'OMePS chemistry, targeted at donor sites of MyD88 exon 3 resulted in an alteration of splicing ratio of MyD88 to $MyD88_S$, thereby leading to decreased proinflammatory signalling *in vitro* as well as *in vivo* (Vickers *et al.*, 2006).

1.8. Duchenne muscular dystrophy (DMD) and experimental treatment strategies

The largest gene of the human genome by far is the X-linked dystrophin gene which has 79 exons (Tennyson *et al.*, 1995). Dystrophin acts as a linker between muscle cytoskeleton and extracellular matrix via dystrophin-glycoprotein complex (DGC). There are four main domains of dystrophin protein, namely, the N-terminal region, a central domain (with spectrin-like repeats), a cysteine-rich domain and a C-terminal domain. The N-terminal region of dystrophin interacts with cytoskeletal actin. β-dystroglycan is bound by cysteine-rich domain of dystrophin protein. The C-terminal of dystrophin interacts with syntrophins and dystrobrevins as shown in **Figure 1.7**. Premature termination of the synthesis process of the dystrophin gene may occur as a result of certain mutations that disrupt the dystrophin transcript reading frame. Deficiency of dystrophin thus makes the myofibres more prone to damage resulting from mechanical contraction. This eventually leads to necrosis and failure of myofibre regeneration causing replacement of myofibres with fibrous and fatty connective tissue. This results in Duchenne muscular dystrophy (DMD) which is characterized by progressive muscle weakness and wasting (Whitehead *et al.*, 2006).

Frame shifting mutations in the *dystrophin* result in production of shortened products that are semi-functional because the open reading frame of the gene is still intact (Monaco *et al.*, 1988). The protein thus produced is internally truncated but is still partially functional and causes a less severe Becker muscular dystrophy (BMD) (Trollet *et al.*, 2009). Expression of small proportions of dystrophin-positive fibres known as 'revertant' fibres in DMD patients as well as in *mdx* mice (DMD mouse models that were derived from naturally occurring C57BL/10 mutants for *DMD* gene (Collins &

Morgan, 2003) that lack the complete *DMD* gene in both muscle and brain tissue (Vaillend *et al.*, 1995)), further provides evidence for the role of exon skipping as a mechanism for restoration of frame shift mutation (Sherratt *et al.*, 1993). A Japanese Duchene muscular dystrophy patient was demonstrated to have the dystrophin exon 19 shortened by 52 base pairs due to a deletion such that the pre-mRNA transcript had exon 19 missing and exon 18 was directly joined to exon 20 (Matsuo *et al.*, 1991).

Figure 1.7

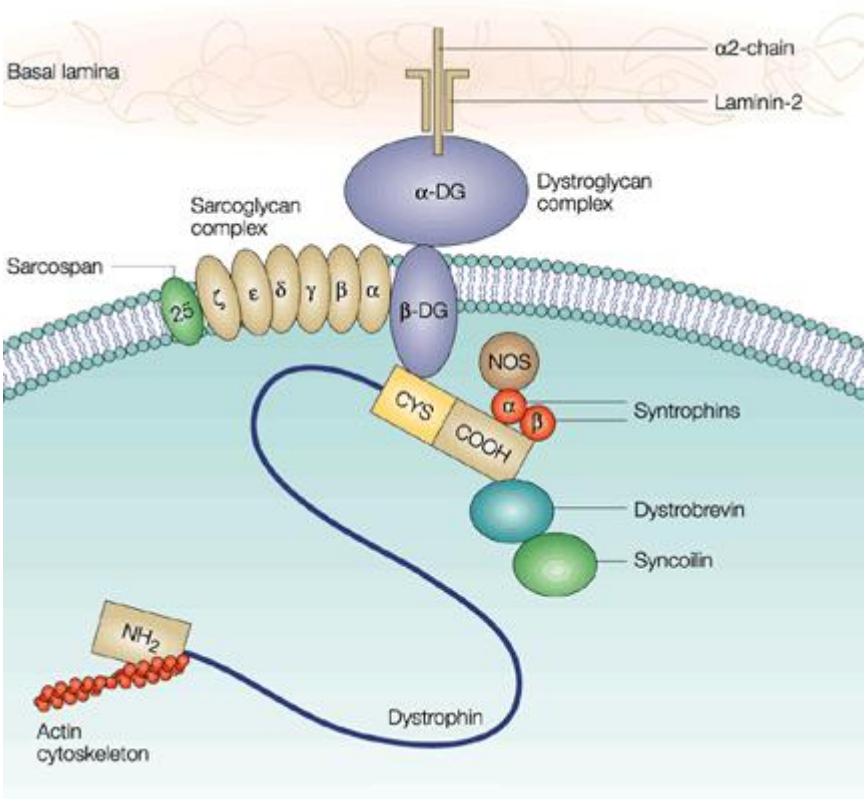

Figure 1.7: The dystrophin-glycoprotein (DGC) complex. A diagrammatic representation of the DGC complex showing dystrophin, dystroglycan complex, sarcoglycan complex, dystrobrevin, syntrophins and sarcospan. The extracellular ligand, laminin-2 binds to the α-dystroglycan which is further linked to a member of sarcolemmal glycoprotein complex, β-dystroglycan. β -dystroglycan is linked to dystrophin via its cysteine-rich domain. The N-terminal domain of dystrophin binds to the cytoskeletal actin and the carboxy terminal domain is linked to syntrophins. Figure adapted from (Khurana & Davies, 2003)

The following strategies have been investigated for their application in muscular dystrophy treatment:

1.8.1. Gene addition therapy

A number of conventional gene therapy strategies have been employed to correct the fatal mutations in dystrophin gene leading to DMD. Due to its large size (14 kb with 11.5kb coding sequence), replacement of the dystrophin gene with artificial cDNA constructs requires large capacity vectors. Adenoviral vectors are quite large in size that limits their diffusion into muscle tissue. Myofibre surface does not have many receptor molecules for the adenoviral vectors to come and adhere to. Also, the extra cellular matrix (ECM) surrounding the myofibres does not let the large sized vectors to cross it easily (Chen *et al.*, 1997a; Douglas, 2007). Immunogenicity is another disadvantage of adenovirus vectors for their proposed use in gene therapy (Douglas, 2007). Herpes simplex virus type I vectors have the capacity to carry large inserts but they offer limited persistence of gene expression owing to their cytotoxicity and immunogenicity (Akkaraju *et al.*, 1999; Huard *et al.*, 1997). Plasmid vectors being synthetic are relatively safe and flexible to carry large inserts. However, they need to be either tagged to certain lipid formulations for efficient delivery or have to be delivered by microtubules, electroporation or ultrasound.

Recombinant AAV (rAAV) vectors are smaller in size and have lower immunogenicity. However, due to their limited capacity, rAAV vectors are unable to accommodate full-sized dystrophin cDNA (Wang *et al.*, 2007) and are required in very high titers to achieve efficient systemic administration (Gregorevic *et al.*, 2004). Dystrophin minigenes with a lower number of centrally located spectrin-like domains (with preserved carboxy- and amino- terminal domains) when expressed as transgenes in *mdx* mice, substituted for the wild type gene (Deconinck *et al.*, 1997). As dystrophin-associated protein complex (DAPC) assembly takes place in the presence of dystrophin (Hoffman & Dressman, 2001) which is responsible for linking the extracellular matrix and cytoskeleton muscle fibres together (White *et al.*, 2002), microdystrophins delivered using AAV vectors have been shown to successfully restore DAPC expression as well as the strength and stability of sarcolemmal membrane which further prevents degeneration of muscle fibres (Athanasopoulos *et al.*, 2004; Gregorevic *et al.*, 2006; Wang *et al.*, 2000). AAV serotype 8 was found to be the most efficient to attain systemic transfer of dystrophin gene into skeletal as well as cardiac muscles in mice and

hamsters (Wang *et al.,* 2005). Microdystrophins were expressed in dystrophic mesoangioblasts of dogs and then transplanted into arterial circulation. This led to a widespread microdystrophin expression but there was no maintenance of force of contraction (Sampaolesi *et al.,* 2006). Progress in systemic delivery of rAAV microdystrophin vectors has been achieved using very high titers of rAAV using constitutive viral promoters driving gene expression. However, for clinical applicability, it is essential to develop rAAV vectors capable of achieving gene transfer efficiently at lower viral titers using a muscle specific promoter (Foster *et al.,* 2008).

Codon optimisation of microdystrophin can be achieved by inclusion of consensus Kozak sequence and codon usage optimisation for efficient translation (Garmory *et al.,* 2003; Kozak, 2005) and increased GC content to promote mRNA stability (Murray & Schoenberg, 2007). Codon optimisation of microdystrophin under the control of a muscle-restrictive promoter has been shown to significantly increase levels of microdystrophin mRNA and protein after intramuscular and systemic administration of plasmid DNA or (rAAV)2/8 in *mdx* mice as compared to the noncodon-optimized microdystrophins. This was also accompanied by significant improvement in specific force and protection from contraction-induced injury (Foster *et al.,* 2008). Nonhuman primate studies involving rhesus macaques using a fusion construct of AAV8 and FLAG-tagged microdystrophin have been reported (Rodino-Klapac *et al.,* 2010). Intramuscular injection of this microdystrophin construct into the tibialis anterior of macaques led to a 50-79% muscle transduction that persisted for a period of 5 months. Vascular delivery of this construct resulted in up to 80% gene expression in muscle fibres without any cellular immune responses (Rodino-Klapac *et al.*, 2010).

(AAV)2/8 vectors expressing mRNA sequence-optimised canine microdystrophin under the control of muscle-specific promoter have been generated. When these vectors were injected intramuscularly into canine X-linked muscular dystrophy (CXMDj) dog, stable and high levels of microdystrophin along with the association with DAPC was observed for at least eight weeks. The treated muscles were highly protected from dystrophic damage and there was no immune response (Koo *et al.*, 2011).

1.8.2. Utrophin

When dystrophin mRNA was examined in embryonic, newborn and adult mouse skeletal muscle, a discrete increase in mRNA size was observed between embryonic and adult stages that was nerve-independent. This indicated that a developmentally-regulated mRNA isoform switch occurs in the dystrophin gene expression in skeletal muscle (Dickson *et al.*, 1988). Utrophin is a homolog of dystrophin that maps to human chromosome 6 and was identified in 1989 (Love *et al.*, 1989). Utrophin and dystrophin show strong homology specifically in the N- and C-terminal ends (Pearce *et al.*, 1993). Utrophin is widely expressed in retinal glial cells, vascular endothelia, platelets, various kidney cells as well as in skeletal, smooth muscle and cardiac cells and in abundance at neuromuscular junctions (Love *et al.*, 1991; Ohlendieck *et al.*, 1991). Utrophin expression occurs before dystrophin in developing and regenerating muscle where it is detected along the muscle sarcolemma. Dystrophin replaces utrophin along the sarcolemma at birth or in mature muscle and therefore utrophin remains confined to neuromuscular junctions and vasculature (Ohlendieck *et al.*, 1991; Tinsley & Davies, 1993). Due to this utrophin has been considered as a foetal dystrophin homologue in developing muscle tissues suggesting common functions of the two proteins in muscle structure and physiology. A direct relationship between the utrophin expression level and the degree of improvement in muscle structure and function in dystrophic mice has been demonstrated (Tinsley *et al.*, 1998). In *mdx* mice, muscle necrosis occurs when utrophin expression falls down to adult level that is at the time it should be replaced by dystrophin (Khurana *et al.*, 1991). Exogenous expression of microutrophin using recombinant AAV vectors in *mdx* (Utr-/-) mice has been demonstrated to increase life span and improve muscle function but this strategy faces common gene therapy obstacles like vector delivery, stability of the construct, poor control of protein expression and immunogenicity (Odom *et al.*, 2008).

1.8.3. Muscle derived stem cells

Stem cells derived from blood vessels, bone marrow and muscle are capable of introducing dystrophin producing cells (Gussoni *et al.*, 1999). Muscle derived stem cells (MDSCs) are capable of self renewal as well as regeneration of other tissues. MDSCs that readily differentiate into muscle cells are known as CD45- whereas the ones that have lower myogenic potential are termed as CD45+ (Peng & Huard, 2004). Skeletal MDSCs that exhibit enhanced regeneration ability in different musculoskeletal system

tissues have been extensively isolated and characterized. A great focus has been laid on improving dystrophic muscle pathology based on investigations of high myogenic potential of the stem cells that have vascular or endothelial origin (Crisan *et al.*, 2008; Zheng *et al.*, 2007). Regeneration ability of adult skeletal muscle starts to diminish with age. Notch signalling is important in triggering satellite cells or muscle stem cells to induce muscle tissue regeneration; however, the activation of Notch is largely declined in ageing muscle tissue. It has been reported that regenerative capacity of muscle stem cells can be rejuvenated by forced activation of Notch (Collins & Partridge, 2005; Conboy *et al.*, 2003; Schultz & Lipton, 1982). When bone marrow mesenchymal stem cells (with otherwise low myogenic differentiation capacity) were engineered to produce higher levels of intracellular Notch protein and transplanted into *mdx* mice, they produced dystrophin in many fibres (Dezawa *et al.*, 2005). Although this approach is quite safe, it still requires immune suppression (Gussoni *et al.*, 1999; Sampaolesi *et al.*, 2003).

Transplantation of healthy myoblasts into affected muscles in order to provoke synthesis of new muscle fibres that have dystrophin expression has been achieved in *mdx* mice (Acsadi *et al.*, 1991; Hoffman *et al.*, 1987b). Implantation of exogenous myoblasts into the muscle for myofibre generation can however provoke immune response and has low efficiency due to limited cell migration and poor myoblast survival after transplantation (Gussoni *et al*. 1999).

1.8.4. Neuronal Nitric Oxide Synthase

Nitric oxide synthase (NOS) has three different isoforms namely: neuronal nitric oxide synthase (nNOS), inducible nitric oxide synthase (iNOS) and endothelial nitric oxide synthase (eNOS). nNOS occurs in a variety of cell types including skeletal muscle cells and neurons, and synthesizes nitric oxide (NO) which is responsible for a number of biological functions like neuromuscular transmission, regulation of sarcolemmal ionic pumps and calcium homeostasis among others (Kobzik *et al.*, 1994; Meszaros *et al.*, 1996). nNOS is restricted to cytosolic surface of the sarcolemma of fast twitch fibres. It is important that nNOS is correctly localized on the sarcolemmal membrane in order to prevent blood vessel constriction during muscular activity in order to enhance the blood circulation (Lai *et al.*, 2009). nNOS has been reported to be a component of dystrophin-associated glycoprotein complex (DGC) (Brenman *et al.*, 1995). In the absence of dystrophin, assembly of DGC at the sarcolemma fails and

therefore functional nNOS also gets displaced (Thomas *et al.,* 1998). nNOS-mediated vasodilation is thus hampered leading to necrosis and ischemia that causes very quick onset of fatigue in DMD patients (Sander *et al.,* 2000) (Kobayashi *et al.*, 2008). Reports suggest that spectrin repeats 16 and 17 (R16/17) on the dystrophin rod domain are very crucial in correctly locating nNOS to sarcolemma. When *mdx* mice were treated with mini- and microdystrophin genes containing R16/17, they proved as effective as previously reported mini and micro dystrophins in improving muscle pathology and also correctly positioned the nNOS on the sarcolemmal membrane which showed significant improvement in vasodilation during exercise leading to increase in blood supply (Lai *et al.*, 2009).

1.8.5. Insulin-like growth factor-1 (IGF-1)

Insulin-like growth factors are peptide hormones synthesized in the liver which are structurally homologous to proinsulin and are responsible for the growth and development of various types of cells. Mice carrying a mutation in IGF-1 gene showed extreme growth deficiency (Liu *et al.,* 1993). Cultured C2C12 cells when exposed to IGF-1 resulted in myotube hypertrophy due to a calcium signalling pathway initiated by IGF-1. Mice with continual IGF-1 expression also exhibit hypertrophy in muscles (Delaughter *et al.,* 1999; Semsarian *et al.,* 1999). Hypertrophy induced by elevated levels of IGF-1 produced as a result of over expression in transgenic mice leads to increased force production. When exogenous IGF-1 administration into *mdx* mice was carried out, it showed beneficial effects such as improved resistance to fatigue, increased muscle strength and elimination of age-related diaphragm fibrosis (Barton *et al.*, 2002; Gregorevic *et al.*, 2002; Schertzer *et al.*, 2006). In another study, when recombinant AAV vectors expressing microdystrophin (rAAV-muDys) were delivered into *mdx* muscles, there was an increase in resistance to mechanical injury but no increase in muscle mass. AAV vectors expressing muscle-specific IGF-1 (rAAV-mIgf-1) induced increase in muscle mass but no significant resistance to injury. Co-injection of rAAV-muDys and rAAV-mIgf-1 however, resulted in increased muscle mass as well as enhanced protection against injury induced by contraction (Abmayr *et al.*, 2005).

1. 8.6. Exon skipping

Exon skipping has been proposed as a method of treatment for DMD by using antisense oligonucleotides directed against the exons of mutant dystrophin to restore reading frame of the gene leading to a milder phenotype of BMD (Graham *et al.,* 2004a;

Matsuo, 1996; Popplewell *et al.,* 2009). Antisense oligonucleotides of 2'OMePS chemistry directed against 3' splice site of intron 22 and 5' splice site of intron 23 in primary *mdx* myotubes resulted in all the dystrophin pre-mRNA transcripts missing exon 23 after 24 hours of transfection (Wilton *et al.,* 1999). Further studies demonstrated effective dystrophin restoration by exon 46 skipping using AOs in DMD patient-derived muscle cells (van Deutekom *et al.,* 2001). An enhanced delivery of the AOs of 2'OMePS chemistry to the TA muscle of adult dystrophic mice resulted in dystrophin expression restoration in 20-30% of the fibres (Wells *et al.,* 2003).

Skipping of exon 51 particularly averts the onset of dystrophic phenotype in the vast majority of patient myoblasts (Aartsma-Rus & van Ommen, 2007; Arechavala-Gomeza *et al.,* 2007). A schematic diagram of exon 51 skipping is shown in **Figure 1.8**. A clinical trial using 2'OMePS to target exon 51 of dystrophin mRNA involved single intramuscular injection of 0.8mg AO into the tibialis anterior (TA) of four DMD patients and the biopsy was performed after 4 weeks. The treatment was well tolerated, exon skipping was induced and dystrophin expression was restored in 64-97% of the myofibres (van Deutekom *et al.,* 2007). In the first UK clinical trial for DMD, intramuscular injection of morpholino targeted against exon 51 of dystrophin mRNA (AVI-4658) into extensor digitorum brevis (EDB) of seven DMD patients was performed. Two patients were injected with 0.09 mg of the AO while the other five were injected with 0.9 mg of AO dissolved in 900 μL saline in each case. The muscles were biopsied between 3 to 4 weeks and the trial concluded with the results that the administration of AVI-4658 was safe and local restoration of dystrophin expression was observed in the 44-79% of the treated muscle (Kinali *et al.,* 2009).

Figure 1.8

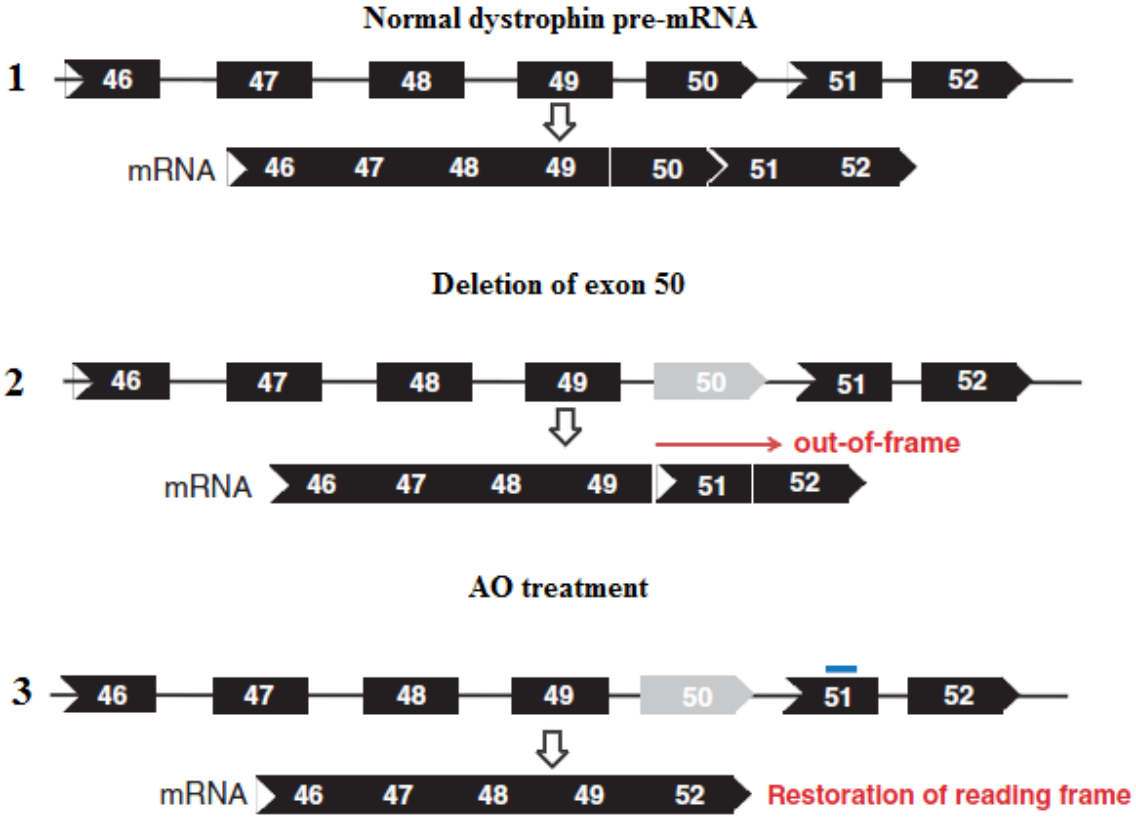

Figure 1.8: Illustration of exon 51 skipping therapy in DMD patients. Deletion of exon 50 from a normal dystrophin pre-mRNA results in disruption of open reading frame resulting in a pre-mature stop codon that eventually leads to an unstable and truncated protein. Use of antisense oligonucleotides targeted at exon 51 produces a truncated but functional protein (that lacks exon 50 and 51) by restoring the reading frame (Figure adapted from (Sugita & Takeda, 2010).

1.9 Therapeutic applications of exon skipping

Exon skipping applications include following mechanisms of action:

1.9.1. Exon exclusion/Reading frame restoration

AOs targeted at specific exons in dystrophin mRNA result in shorter dystrophin forms that are still functional. Exon skipping has also been explored as a therapeutic application in case of dystrophic epidermolysis bullosa (EB), which is a severe skin blistering condition resulting from mutations in type VII collagen, COL7A1 gene (Uitto *et al.*, 1995). Patients with in-frame exon skipping have milder symptoms indicating the possible use of AO-mediated reading frame restoration as a treatment (McGrath *et al.*, 1999). AOs targeted against exon 70 of COL7A1 mRNA resulted in exclusion of exon 70 and therefore resulted in a protein that was short of 16 amino acids encoded by exon 70. The shortened protein thus restored almost normal function (Goto *et al.*, 2006). Over 20% of recessive dystrophic EB patients have mutations in exon 70 making this approach quite significant for a large number of patients (Aartsma-Rus & van Ommen, 2007).

1.9.2. Exon inclusion

Exon skipping has also been used to induce inclusion of exons that have been skipped due to mutations disrupting exon splicing enhancers (ESEs). Spinal muscular atrophy (SMA) is caused due to a mutation in survival of motor neuron 1 (*SMN1*) gene (Munsat & Davies, 1992). *SMN2* is a paralogous gene which is almost the same as *SMN1* apart from a mutation in exon 7 which interrupts an SF2/ASF binding site and renders SMN2 transcript devoid of exon 7 (Cartegni & Krainer, 2002; Helmken *et al.*, 2003). Exon 7-specific AOs of 2'O-methoxy ethyl ribose either with a tail containing an ESE motif, or linked to serine-arginine peptide domain to recruit SF2/ASF to disrupted ESE, have been reported to promote exon 7 inclusion and an increase in full length SMN protein levels. Similar results were obtained with AOs targeting exon splicing silencers (ESSs) (Hua *et al.*, 2007; Skordis *et al.*, 2003).

1.9.3. Isoform switching

A striking example of use of exon skipping to change the levels of alternatively spliced genes is that of *Bcl-x* gene. The role of anti- and pro-apoptotic factors is extremely important in apoptosis. Defective splicing of these factors is one of the crucial reasons for development of cancer. *Bcl-x* gene has two isoforms namely Bcl-xS

and Bcl-xL. Bcl-xS is pro-apoptotic and sensitizes cells to chemotherapy whereas Bcl-xL is anti-apoptotic and induces resistance to chemotherapeutic agents and is over expressed in a number of cancers. These two isoforms result from two different 5' splice sites in exon 2 (Mercatante *et al.*, 2002). Antisense oligonucleotides of 2'OMePS chemistry targeted against the 5' splice site of bcl-x exon 2 in a lung carcinoma cells increased the bcl-xS to bcl-xL ratio which was not enough to induce apoptosis but it did result in sensitization of the cells to inducers of apoptosis like chemotherapy drugs or UVB radiation (Williams & Kole, 2006). Similar results have also been shown in the case of breast cancer and prostate cancer cell lines by the use of antisense oligonucleotides (Mercatante *et al.*, 2002). However systemic delivery of AOs targeting Bcl-x induced liver apoptosis in treated mice, thereby limiting the applicability of this approach.

Use of AOs has also been described for prostate-specific membrane antigen encoded by the *folate hydrolase* gene for isoform switching (Williams & Kole, 2006). One of the isoforms of the gene is expressed more than 100-fold higher in malignant than the normal prostate tissues and has an extracellular functional domain that regulates folate uptake (O'Keefe *et al.*, 2004). Three other prostate-specific membrane antigen isoforms exist. Two isoforms result from alternative splicing of exon 6 and 18 with no enzymatic domain at all or inactive domain respectively. Fourth isoform results from alternative donor splice site in first exon that lacks transmembrane domain. Individual AOs targeting exons 1, 6 and 18 were successful in inducing isoform switching along with lower levels of full length-isoform and decreased enzymatic activity (Williams & Kole, 2006).

1.9.4. Exon exclusion/Destructive exon skipping

Use of AOs for gene knockdown has been demonstrated by Apolipoprotein B (APOB) studies. There exist two isoforms of APOB, APOB100 and APOB48. APOB100 acts as a ligand for low density lipoprotein (LDL) receptor and plays central role in atherosclerosis (Soutar & Naoumova, 2007). APOB48 plays an important role in chylomicron assembly and intestinal fat transport. APOB48 arises from intestine tissue-specific RNA editing of a CAA into a UAA termination codon in exon 26 and lacks the LDL receptor-binding domain (Chester *et al.*, 2000). Due to the lack of this LDL receptor-binding domain in APOB48, chylomicrons are unable to bind via this receptor and are cleared by interaction between APOE and chylomicron remnant receptor. AOs

directed at exon 27 resulted in shortened and non-functional APOB100 protein ($APOB87_{SKIP27}$) (Khoo *et al.*, 2007). LDL particles containing $APOB87_{SKIP27}$ show greater fractional catabolic rates compared to those containing APOB100 due to greater affinity of APOB87-containing particles for LDL receptor and also appear to have dominant negative effect on secretion of APOB100. As RNA-editing signal for *APOB48* is located in exon 26, skipping of exon 27 will not affect this isoform. It will however disrupt the *APOB100* transcript's open reading frame resulting in lower amounts of APOB100 and a likely decrease in LDL and cholesterol levels (Khoo *et al.*, 2007). Gene knockdown by selective exon skipping therefore allows down regulation of the disadvantageous isoform of a gene while maintaining the normal levels of the desired isoform (Arechavala-Gomeza *et al.*, 2007).

1.10. Antisense oligonucleotides (AOs)

AOs are about 11-30 bp long chemically synthesized single stranded nucleic acid molecules that are complementary to a specific sequence of the target mRNA (Agrawal & Kandimalla, 2000). Based on the mechanism of action, the AOs function in the following ways: (i) RNAase H-mediated degradation of the target RNA by hydrolysis of RNA strand from the DNA/RNA duplex, (ii) Steric blocking of the target mRNA which physically inhibits the pre-mRNA splicing (Dias & Stein, 2002; Larrouy *et al.*, 1992). AOs are capable of hybridizing with the target sequence and blocking its splicing. They lead to steric hindrance and get in the way of certain proteins essential for pre-mRNA splicing and redirect the splicing process. Thus it leads to the formation of a truncated product and not the full length transcript This knocks down the expression of the gene from which the mRNA was transcribed (Adams *et al.*, 2007a). Due to the unstable nature of single stranded DNA molecules, it is important to modify the chemistries of AOs in order to provide them stability (Dean *et al.*, 1994; Minshull & Hunt, 1986).

One of the first ever uses of antisense technology was made in 1977 by Zamecnik and colleagues to block the circularization of proviral DNA of Rous sarcoma virus (RSV) 35S RNA in tissue cultured chick embryo fibroblasts (CEFs) infected with the virus (Schwartz *et al.*, 1977). Upon determination of the primary structure of RSV 35S RNA, a 21 nucleotide segment adjacent to the 3' poly-A tail was found to be identical to a 21 nucleotide sequence internal to the 5' cap in the same molecule (Haseltine *et al.*, 1977; Schwartz *et al.*, 1977). These reiterated sequences play a crucial

role in provirus DNA circularization prior to integration into cell genome. A deoxyribonucleotide complementary to the 13-nucleotide segment of the 21 nucleotide reiterated sequence was added to CEF cultures at the same time as RSV infection which led to inhibition of RSV production (Zamecnik & Stephenson, 1978).

Various chemistries of AOs have been developed so far. The mononucleotides generated as a result of nuclease degradation of AOs based on phosphodiester (PE) chemistry were reported to be cytotoxic and to exert a negative effect on proliferation of cells (Vaerman *et al.*, 1997). Methyl phosphonates are modified PE oligomers with the substitution of a methyl group for the non-bridging oxygen at each phosphate of the oligonucleotide chain. In spite of being very stable, these oligonucleotides have very low solubility owing to their uncharged nature (Miller *et al.*, 1981; Miller *et al.*, 1979). The phosphorothioate (PS) oligodeoxynucleotides (with a non-bridging oxygen atom of the phosphate group substituted with sulphur) were the first generation AOs with two important characteristics: resistance to nucleases and ability to direct RNase H-mediated degradation of the RNA part of RNA-DNA heteroduplexes. These properties made these AOs specifically capable of downregulating the expression of a gene (Crooke, 1998; Stein, 1998). Modification of the phosphate group of oligonucleotides can result in either negatively charged backbone (PS); or positively charged backbone (phosphorpiperazidate); or uncharged backbone (phosphormorpholidate; *N*-butyl-phosphoramidate). All of these modified compounds have been shown to be more effective than the parent phosphodiester compounds (Agrawal, 1996; Agrawal *et al.*, 1988). Fomivirsen (commercial name: Vitravene) was the first FDA-approved AO (phosphorothioate)-based drug for cytomegalovirus (CMV) retinitis that causes blindness in acquired immune deficiency syndrome (AIDS) patients. Although, Fomivirsen was able to effectively treat the infection, it had some adverse local ocular effects like inflammation (Grillone & Lanz, 2001).

Most of the newly developed AOs do not activate RNase H therefore preventing the destruction of pre-mRNA before its splicing, and this is of particular importance when using AOs to cause a shift in the aberrant or alternative splicing of the target pre-mRNA (Kole & Sazani, 2001; Mercatante *et al.*, 2001). For dystrophin skipping, it is highly important that the pre-mRNA is not destroyed before splicing so that the truncated product generated after splicing is still functional and thereby results in a milder Becker's muscular dystrophy phenotype rather than severe DMD symptoms.

A number of AO chemistries that have been most commonly used so far include 2'O-methyl phosphorothionate (2'O-MePS), peptide nucleic acid (PNA), locked nucleic acid (LNA), ethylene bridged nucleic acid (ENA), phosphorodiamidate morpholino oligomer (PMO or morpholino oligomer), peptide linked PMO (PPMO) (Karkare & Bhatnagar, 2006; Wilson & Keefe, 2006) and the recently developed dendrimeric octaguanidine-conjugated PMO (Vivo-PMO) (Morcos *et al.*, 2008) (**Figure 1.9**).

1.10.1. 2'O-methyl RNA (2'O-MePS)

The most frequently used second generation oligonucleotide chemistry *in vitro* is 2'O-MePS due to its high specificity and affinity to target mRNA, stability, nuclease resistance, safety and ease of synthesis. Methylation of the ribose ring of RNA at 2'-OH position results in 2'O-MePS generation. The additional methyl group at 2'-O- ribose position provides extra stability to the oligo making it resemble RNA rather than DNA (Agrawal & Zhao, 1998). Although 2'OMePS has various advantages, it cannot be used at high concentrations due to its low solubility (Lu *et al.*, 2005). Easy and cheaper synthesis however, does make 2'O-MePS a very suitable candidate for testing a particular AO sequence in tissue culture prior to *in vivo* studies (Baker *et al.*, 1997).

1.10.2. Peptide nucleic acids (PNAs)

PNAs consist of a polyamide backbone that is uncharged and contains repetitive N-(2-aminoethyl) glycine units to confer better stability. These repeating units have nucleobases linked to them by methylene carbonyl linkers. The stability of PNA is due to the lack of negative charge present in a regular phosphodiester linkage, which further results in absence of electrostatic repulsion (Jensen *et al.*, 1997; Nielsen *et al.*, 1991) (Hanvey *et al.*, 1992).

1.10.3. Ethylene bridged nucleic acids (ENAs)/Locked nucleic acids (LNAs)

If the ribose sugar moiety of nucleic acid is locked by an oxyethylene bridge that connects C-2' and C-4' atoms, it is termed as ethylene bridged nucleic acid (ENA), whereas if this linkage takes place by an oxymethylene bridge, it is termed a locked nucleic acid (LNA). This re-arrangement gives the ENAs or LNAs extremely high binding affinity due to a very stable conformation (Koshkin & Wengel, 1998; Kumar *et al.*, 1998; Morita *et al.*, 2001) making them a good candidate for antisense technology (Kumar *et al.*, 1998).

1.10.4. Phosphorodiamidate morpholino oligomers (PMOs)

In a PMO, the deoxyribose ring in DNA, or ribose ring in RNA, is replaced by a morpholine ring and different morpholine rings are linked together by phosphorodiamidate bonds. Due to the non-ionic nature of PMOs, non specific binding and protein interactions are reduced. PMOs are highly soluble so they can be used at higher dosages compared to 2'OMePSs (Nakamura & Takeda, 2009).

1.10.5. Peptide linked PMOs (PPMOs)

Different peptide-based transporter systems including penetratin, tat and polyarginine peptides have been shown to traverse cell membranes and have generated interest due to potential therapeutic applications. The limitations however are the expensive and laborious synthesis processes and mediocre efficacy (Ferrari *et al.*, 2003). Tat conjugated PMOs failed to be delivered efficiently across the cell membrane due to the prerequisite of protein folding and rearrangement during translocation (Ferrari *et al.*, 2003). Penetratin conjugated to PNA has been shown to penetrate the cell membrane and reach the cytosol but was not delivered to the nucleus (Richard *et al.*, 2003). Delivery across the cell membrane is mainly through endocytosis and the vesicles are then permeabilized to release the materials internally. However, it is the incapacity to permeabilize the vesicles that render the delivery of peptide conjugated AOs ineffective. Also, the lack of ability to get round the electrostatic interactions with the cellular heparan sulphates makes the delivery of molecules into the nucleus difficult (Richard *et al.*, 2003).

A peptide-conjugated PMO (PPMO) is a PMO conjugated to a cell penetrating peptide (CPP) containing arginine (R), 6-aminohexanoic acid (X), and/or β-alanine (B). Conjugation of CPPs to PMOs to form PPMOs has been used *in vitro* and *in vivo* for blocking the replication of harmful viruses like dengue (Kinney *et al.*, 2005), influenza (Ge *et al.*, 2006), SARS (Neuman *et al.*, 2006) and Ebola virus (Enterlein *et al.*, 2006). A delivery moiety with 6-9 arginine based peptide in a 6-aminohexanoic structure [(R-Ahx-R)$_4$] has been reported to deliver PMOs effectively to the cytosol and nucleus *in vitro* as well as *in vivo* (Wu *et al.*, 2007; Yuan *et al.*, 2006). PMO on its own need to be delivered in repeated large doses for measurable functional benefit (Alter *et al.*, 2006). PPMOs however are delivered much more effectively and uniformly to myocytes even at lower doses in DMD models with delivery to cardiomyocytes as well (Fletcher *et al.*, 2007; Goyenvalle *et al.*, 2010; Yin *et al.*, 2008). 2µg of PMO or a PPMO for dystrophin

exon 23 skipping injected locally into the TA of an *mdx* mice resulted in 14% and 85% restoration of dystrophin-positive fibres respectively (Wu *et al.*, 2008). When 12mg/Kg of a peptide conjugated PMO for dystrophin exon 23 skipping was injected into the tail vein of *mdx* mice, it resulted in restoration of dystrophin fibres in almost all the fibres as compared to only a small percentage of dystrophin restoration with a 400mg/Kg dose of naked PMO (Moulton *et al.*, 2009; Wu *et al.*, 2008).

P007-PMO is a PPMO that contains alternating non-natural 6-aminohexanoic acid and arginine [$(RXR)_4XB$] and B-PMO is another PPMO in which two 6-aminohexanoic acid residues were substituted with another non-natural amino acid, β-alanine [$(RXRRBR)_2XB$]. Both these PPMOs have been shown to restore dystrophin expression very effectively in skeletal muscle and cardiac tissue in *mdx* mice following single systemic administration (25mg/Kg body weight) (Jearawiriyapaisarn *et al.*, 2010; Yin *et al.*, 2008). AVI-5038 is a PPMO developed by AVIBiopharma to skip dystrophin exon 50. A PPMO dose of up to 9mg/Kg was well tolerated in pre-clinical studies. However a significant level of toxicology was observed in some groups from the preliminary data obtained from another pre-clinical study using 12mg/Kg PPMO following bolus intravenous injections (http://www.avibio.com/our-programs/rare-diseases/duchennemusculardystrophy/). A chimeric fusion peptide that consists of a muscle-targeting heptapeptide, apart from cell penetrating peptide conjugated PMO, has been demonstrated to restore high levels of uniform and widespread dystrophin protein expression at very low dose when administered systemically in *mdx* mice (Yin *et al.*, 2009). The effect was observed in multiple muscle groups and functional improvement was seen in dystrophic pathology without any toxicity or immune response (Yin *et al.*, 2010).

The toxicity of the PPMO chemistry is a challenge to overcome in order to develop a safe delivery moiety for clinical trials in humans. This is mainly predicted to be due to the cationic nature of the CPPs which further relies on the composition of the amino acids. Dose frequency also influences the level of toxicity conferred by the PPMOs with well spaced dosing regimen taken better by the animals than too frequent administration (Moulton & Moulton, 2010). Toxic effects of PPMOs include loss of weight and fatigue as well as degeneration of renal tubules (Amantana *et al.*, 2007; Moulton & Moulton, 2010). The toxic effects are observed at lower doses in monkeys, whereas mice seem to tolerate the same dose quite well so good pre-clinical studies are

vital to determine safety (Moulton & Moulton, 2010). Success with the PPMOs thus is likely to depend upon pre-clinical studies aimed at designing adequate dosing regimen, route of administration as well as frequency of dose in order to develop a safe efficiency/toxicity profile of the PPMO treatment across different species (Moulton & Moulton, 2010).

1.10.6. Dendrimeric octaguanidine-conjugated PMOs (Vivo-PMOs)

A newly developed dendritic transporter structure has a triazine core that acts as the centre for eight guanidinium heads arranged around it in such a manner that confers effective cell membrane penetration to the PMO that it is linked to. This octaguanidine transporter when linked to the PMO, the conjugated molecule is called Vivo-morpholino or Vivo-PMO (Morcos *et al.*, 2008). Eight guanidinium groups have been reported to have the optimal delivery efficiency (Futaki *et al.*, 2002). When eight guanidinium head groups were put together in an artificial scaffold and linked to flourescin in order to assess delivery efficacy, significantly enhanced delivery was observed compared to the arginine peptides (Rothbard *et al.*, 2004; Wender *et al.*, 2008; Wender *et al.*, 2005). The guanidinium head groups interact with the phospholipid phosphates through hydrogen bonding as well as through electrostatic interaction. Transgenic mice harbouring a β-globin splice mutation were injected with Vivo-PMO targeting the mutation site at a concentration of 12.5mg/Kg of the body weight for four consecutive days and sacrificed on the fifth day. Skeletal muscle, liver, colon and small intestine showed nearly complete splice correction as analyzed by RT-PCR. A very moderate delivery into the brain, heart, skin and lung was also observed (Roberts *et al.*, 2006). Aspartate aminotransferase (AST) and alanine aminotransferase (ALT) levels in the liver were also measured to assess the toxicity of the compound, but no significant change was recorded (Morcos *et al.*, 2008; Roberts *et al.*, 2006).

Vivo-PMO targeted against exon 23 of dystrophin at a concentration of 25mg/kg of the body weight of *mdx* mice injected systemically resulted in dystrophin expression being restored to normal levels (Morcos *et al.*, 2008). Another study using Vivo-PMO for dystrophin exon 23 skipping via intramuscular injections showed 62% to 95% increase in dystrophin-positive fibres in *mdx* mice at a dose of 2µg and 10µg respectively (Wu *et al.*, 2009). Vivo-PMO has been used in zebra fish to knockdown the level of αIIb involved in primary haemostasis (by complex formation with glycoprotein IIIa (gpIIIa) which is an essential step in blood clotting) following injury and thus

presents a potential strategy to study thrombocyte biochemistry (Kim *et al.*, 2010). The greater level of activity and effective delivery of Vivo-PMO into a broad range of tissues makes this chemistry a suitable candidate for our myostatin skipping study as well.

Figure 1.9

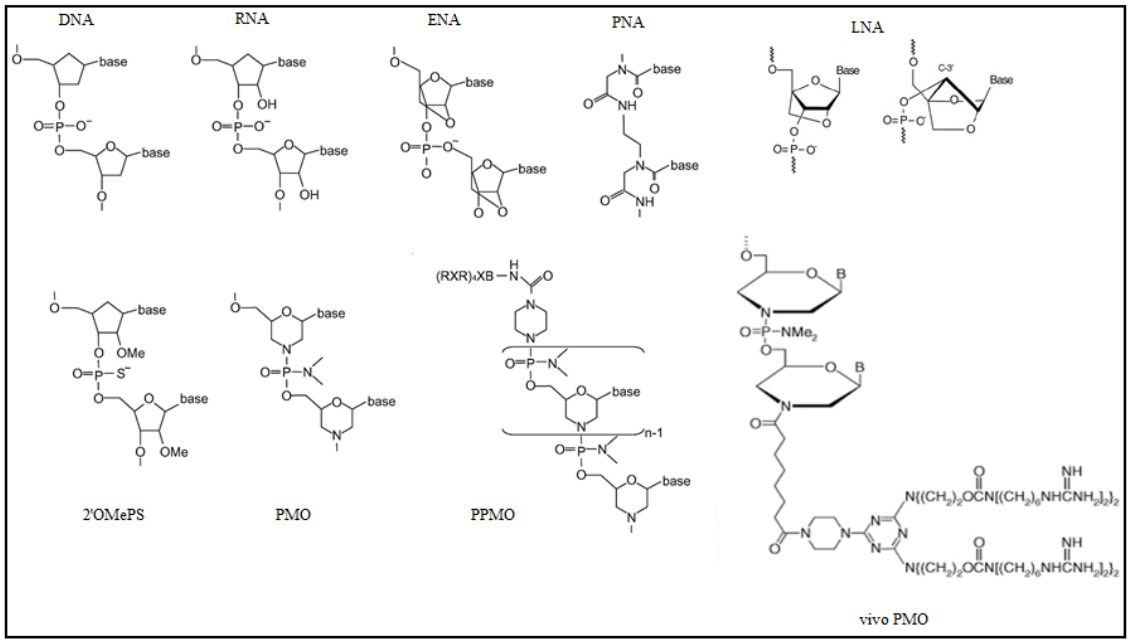

Figure 1.9: Different chemistries of antisense oligonucleotides: ENA with the ribose sugar moiety of nucleic acid locked by an oxyethylene bridge that connects C-2' and C-4' atoms; **PNA** with polyamine backbone instead of ribose-phosphate backbone; **LNA** with linkage through an oxymethylene bridge; **2'OMePS** with methylation of ribose ring of RNA at 2'-OH position of RNA; **PMO** with the deoxyribose ring in DNA or ribose ring in RNA replaced by a morpholine ring and different mopholine rings are linked together by phosphorodiamidate bonds; **PPMO** with PMOs linked to peptides that facilitate efficient delivery of the PMOs; **Vivo-PMO** with PMOs linked to dendrimeric octaguanidine moiety. (Image adapted from: (Moulton *et al.*, 2009; Sazani *et al.*, 2002b; Takeda, 2009; Wu *et al.*, 2009).

1.11. Exon skipping targets: Splicing enhancers and inhibitor elements

Apart from having a sequence encoding a specific protein, a gene also contains information about a number of other signals that affect the expression at the transcript level. The splicing information comes from the splicing code comprised of exon splicing enhancers (ESEs), exon splicing suppressors (ESSs), Intron splicing enhancers (ISE) and Intron splicing silencers (ISS) (Fu, 2004). Exon splicing enhancers (ESEs), also called exon recognition sequences are a heterogeneous group of various sequence motifs that precisely define exon for an efficient splicing process by acting as the sites for binding of Serine/Arginine-rich proteins (SR proteins), a family of conserved splicing factors (Liu *et al.*, 1998). A slight disruption in the ESE could lead to the entire exon exclusion, thereby resulting in a truncated product (Fairbrother *et al.*, 2004).

It has been proposed that the choice of target plays a crucial role in skipping specificity and efficacy. The acceptor splice site, donor splice site and branch point sequences have been demonstrated to successfully induce exon skipping (Dunckley *et al.*, 1998; Wilton & Fletcher, 2005b) but they have consensus sequences in common with various genes and therefore targeting them has a potential risk of off-target effects leading to skipping of exons of other genes (Aartsma-Rus & van Ommen, 2007; Sun & Chasin, 2000). ESE sites could therefore be relatively better and more specific skipping sites than the acceptor or donor splice sites (Aartsma-Rus *et al.*, 2002; van Deutekom *et al.*, 2001). For majority of exons, ESEs have been shown to be the optimal target site for precise recognition by the splicing machinery (Cartegni *et al.*, 2002). The RNA-binding domain of SR proteins binds to the ESEs and this leads to precise recognition of exons by recruitment of spliceosomal machinery (Fairbrother *et al.*, 2002; Graveley, 2000)

1.12 Aims and objectives of the study

Muscle mass loss resulting from cachexia, sarcopenia and obesity has a very high impact on public health. As myostatin is a negative regulator of muscle mass, strategies are being developed to knock down the expression of the myostatin gene in order to improve the condition of patients suffering from muscle wasting conditions.

RNA based modulation therapy has the potential to overcome difficulties encountered by conventional gene therapy methods. RNAi system faces a massive hurdle in terms of effective delivery of the RNAi molecules into the disease models for

clinical studies (Weinstein & Peer). In an alternative approach, antisense-mediated modulation of pre-mRNA splicing has been pioneered by Ryszard Kole (Dominski & Kole, 1993). The identification of exon/intron boundaries by the splicing machinery and therefore inclusion of the exons into the mRNA is extensively thought to depend on exonic splicing enhancer (ESE) motifs (Dunckley *et al.*, 1998). By masking these ESE sites with sequence-optimised AOs, the targeted exons are no longer recognised as exons, and are spliced out with neighbouring introns. Skipping of certain exons by AOs has been proposed to partly correct the mutated dystrophin and convert the severe DMD phenotype into a milder Becker muscular dystrophy (BMD) phenotype (Cartegni *et al.*, 2002). Clinical trials to determine the safety profile and the efficacy of single intramuscular doses of two different chemistries of AOs, 2'-O-methyl phosphorothioate (2'OMePS) and phosphorodiamidate morpholino oligomers (PMO) in DMD patients have been completed (Kinali *et al.*, 2009; van Deutekom *et al.*, 2007). The treatments were well tolerated by all the patients and the injection of AOs induced the production of dystrophin. When conjugated with a dendrimeric octaguanidine (Vivo-Morpholino), PMOs demonstrate a significantly increased delivery in the case of dystrophin skipping in animals (Gebski *et al.*, 2005; Wu *et al.*, 2009).

The focus of this study was to design specific AOs to utilize a destructive RNA exon skipping approach to target myostatin activity, and to investigate the outcome of myostatin mRNA disruption. Exon skipping of 374 bp long exon 2 of myostatin leads to an out-of-frame fusion of exons 1 and 3 and introduction of a premature stop codon due to disruption of the translational reading frame. The objective was to study whether an exon skipping approach allows myostatin activity levels to be reduced *in vitro* and *in vivo*. The study was also aimed at determining whether this antisense-based myostatin downregulation approach can be combined with dystrophin rescue by exon skipping without any interference, to inhibit myostatin expression and reframe dystrophin transcripts simultaneously. Another objective was to try and compare the efficacies of AOs when conjugated to cell penetrating peptide or octaguanidine moieties. This comparison was to investigate simultaneous exon skipping of myostatin and dystrophin to recognize a better chemistry that could be helpful in future experiments to develop an effective combination strategy for improvement in dystrophic pathology.

CHAPTER 2

MATERIALS AND METHODS

2.1. General reagents and buffers

Acetone (Sigma, 179124)

Ethylenediaminetetraacetic acid (EDTA) (Sigma, E5134)

Ethanol (Fischer Scientific, E/0650DF/17)

Isopentane (BDH, S-7653))

Isopropanol (VWR, 102246L)

Methanol (Fischer Scientific, M/4000/17)

PBS (Phosphate buffered saline) in water (PBS tablets- Oxoid, BR0014G)

PBST -1X PBS + 0.05% (v/v) Tween-20

PBS in 0.02% (w/v) EDTA

TBE (10X)-108g Tris Base, 55g Boric acid, 9.3g EDTA per litre of water

Trizma base (tris[hydroxymethyl]aminomethane)-(Sigma, T-1503)

Tween 20 (polyoxyethylenesorbitan monolaurate)-(Sigma, P-1379)

2.2. Bioinformatics analysis of the myostatin gene to design anti sense reagents

Three different bioinformatics algorithms namely ESE Finder, PESX and Rescue ESE were used to design antisense reagents. The query sequences were pasted in FASTA format in the query box of each program. Results from the three algorithms were merged to define exonic splicing enhancer (ESE) sites and used to identify the regions of the myostatin exon 2 which are expected to be optimal targets for exon skipping antisense reagents. A set of 12 antisense reagents of 2'O-methyl RNA (2'OMePS) chemistry were designed to target four different ESE-rich regions of exon 2 of myostatin.

2.3. Maintenance, subculture and transfection of C2C12 cells with the designed anti sense oligonucleotides

2.3.1. Materials

Cell line: C2C12, A204 (ATCC)

Dimethyl Sulphoxide (DMSO) (Sigma, D2650)

Growth medium:

(i) Antibiotics-100U/ml penicillin and 100µg/ml streptomycin (Sigma, A5955)

(ii) Dulbecco's Modified Eagle Medium (DMEM) (Sigma, D-5671),

(iii)10% Fetal Calf Serum (FCS) (Sigma, F7524),

(iv)1% Glutamine (Sigma, G7513)

Lipofectamine™ 2000 (Invitrogen, 11668-019): 1/400 dilution

Trypsin/EDTA (Sigma, T4049)

10X PBS (PBS tablets- Oxoid, BR0014G)

Nuclease-free water (Qiagen, 129114)

PMO stock (0.3mM) (Gene tools, Philomath)

2'OMePS stock (250µM) (Eurofins MWG Operon, Edersberg)

Leash stock (200µM) (Eurofins MWG Operon, Edersberg)

Agarose (Bioline, 41026)

1X TBE buffer

HyperLadder™ V (Bioline)

2.3.2. Methods

2.3.2.1. C2C12 cells- Maintenance and subculture

C2C12 mouse myoblasts were maintained in DMEM containing 10% fetal calf serum, 4mM L-glutamine, 100U/ml penicillin and 100µg/ml streptomycin at 37°C and 8% CO_2. Cells were split/24 hours to prevent differentiation and to maintain less than 70% confluence. In order to passage the cells, the dishes were given a wash with 1X PBS once followed by a wash with 1X PBS/EDTA. Cells were detached by incubating them with 0.15% trypsin-PBS for one minute at 37°C. 10ml of full growth medium was added to stop the action of trypsin. The cells were then pelleted by centrifugation at 1,000 rpm for 5 minutes at room temperature. The pellet was re-suspended in growth medium (composition as described above) and plated in a six well plate at a density of $1.5x10^5$cells/well. In order to freeze the cells, 10% DMSO and 9ml full growth medium was added to 1 ml of re-suspended cells in a vial.

2.3.2.2. Annealing of PMO to an oligonucleotide leash

PMOs were leashed to complementary stretches of negatively charged DNA (obtained from MWG) for efficient in vitro delivery (Gebski *et al.*, 2005), using Lipofectamine 2000 as transfection reagent. 50 µM stock of annealed PMO was prepared adding 12.5µl of 10X PBS, 16.65 µL water, 8.35 µL of 0.3 mM stock of PMO and 12.5 µl of 200 µM stock of leash and running the program described below. To 1µl of annealed PMO, 2µl of sterile PBS (10X) and 1µl water was added and the solution was incubated at 37ºC for 30 minutes. Following incubation, 1 µl of 5x loading buffer was added and the final solution was run on a 3% agarose gel in 1X TBE with HyperLadder™ V as the marker to confirm the annealing.

ANNEALING PROGRAM

1. 95ºC, 5 minutes
2. 85 ºC, 1 minute
3. 75 ºC, 1 minute
4. 65 ºC, 1 minute
5. 55 ºC, 1 minute
6. 45 ºC, 1 minute
7. 35 ºC, 5 minutes
8. 25 ºC, 1 minute
9. 15 ºC, 1 minute and then Hold at 4 ºC

2.3.2.3. C2C12 transfection with Antisense oligonucleotides (AOs)

The C2C12 cells were plated in 6-well dishes at a density of $1.5x10^5$cells/well and after about 48 hours, growth media was removed and replaced with 1600µl media that consisted of DMEM and L-Glutamine but no antibiotics and serum. Dilutions of Lipofectamine 2000 [5µl in 200µl (DMEM + 4mM L-Glutamine)] as well as 2'OMePS or PMOs (2µl (2'OMePS) or 10 µl (leashed PMO) in 200µl (DMEM + L-Glutamine) per 2ml transfection were prepared and allowed to stand at room temperature for 20 minutes. After 20 minutes of incubation, Lipofectamine 2000 and AO dilutions were mixed together and the total of 400µl was added to each well already containing 1600µl media making the total volume 2 ml (making final dilutions of 1/400 Lipofectamine and

1/1000 AOs), and the plates were incubated at 37ºC and 8% CO_2 for 4 hours. Then the transfection mixture was removed and replaced with 2ml of full growth medium with serum and antibiotics and cells were allowed to grow for 24 hours before RNA extraction. The transfections were performed in duplicates and the experiment repeated twice. Controls contained Lipofectamine 2000 but no antisense reagent.

2.4. RNA isolation

2.4.1. Materials

RNeasy Mini kit (Qiagen, 74104)

Qiashredder kit (Qiagen, 79654)

TRIzol reagent (Invitrogen, 15596-026)

Chloroform (Sigma, 472476)

Isopropanol (Sigma, 190764)

75% Ethanol (Absolute ethanol from Sigma, 459844)

2.4.2. Method

24 hours after AO transfection of C2C12 cells, RNA was extracted from each well using QIAshredder/RNeasy extraction kit. Cells were lysed by adding 350µl of lysis buffer to each well and cells scraped using a cell scraper. The cell lysate was then transferred to the QIAshredder column in a collection tube. The cell lysate was then homogenized through the column by centrifugation at 13,000 rpm for 2 minutes. The column was removed and after adding 350µl of 70% ethanol to the homogenized lysate, a total of 700µl lysate was transferred to the RNeasy column placed in a collection tube. The RNeasy columns were then centrifuged at 10,000 rpm for 15 seconds and the flow through was discarded. 700µl of buffer RWI was pipetted onto the column and centrifugation carried out at 10,000 rpm for 15 seconds. 500µl of buffer RPE (diluted with ethanol as directed by the supplier) was then added to the column and the column centrifuged at 10,000 rpm for 15 seconds. The same step was repeated with 500 µl of buffer RPE but tubes centrifuged at 10,000 rpm for 2 minutes in order to wash the column membrane to prevent ethanol carry over. The RNeasy columns were then placed on top of new 1.5 ml collection tubes, 30µl of RNase-free water added directly to the column membrane and centrifuged at 10,000 rpm for 1 minute to elute the RNA. The

concentration of the sample was then recorded spectrophotometrically using a nanodrop and samples stored at -80ºC.

For in vivo experiments RNA was extracted from tissue blocks using TRIzol reagent. 1ml TRIzol reagent was added to the tube containing 20µm tissue sections collected during cryosectioning. The tissue sections were shredded by syringing the TRIzol in and out using 19G as well as 26G needle. The homogenized samples were then incubated at room temperature for 5 minutes. 0.2 ml of chloroform was then added to each tube followed by vigorous shaking for 30 seconds and then incubation at room temperature for 5 minutes. The samples were then centrifuged at 12,000g for 15 minutes at 4ºC. The aqueous phase was then transferred to a new tube and RNA was precipitated by adding 0.5ml of isopropanol and mixing gently with a pipette. This was followed by 10 minutes incubation at room temperature. After 10 minutes, the samples were centrifuged at 12,000g for 10 minutes at 4ºC. The supernatant was then removed and pellet washed with 1ml of 75% ethanol for every 1ml of TRIzol reagent used and tubes gently flicked for mixing. This was followed by centrifugation at 7500g for 5 minutes. The supernatant was removed and pellet dissolved in 20µl of nuclease-free water.

2.5. Primers and AO sequences

The sequences of the primers obtained from Eurofins MWG Operon (Edergsberg) used for the RT-PCR (mystn_ex1F & mystn_skipR) and nested PCR (mystn_skipF, mystn_ex3R) are as following in Table 1.

Table 1: Sequence of primers used in myostatin nested-RT PCR

Name of the primer	Sequence of the primer
mystn_ex1F	5' GGAAGATGACGATTATCACGC 3'
mystn_skipR	5'GGGTGCGATAATCCAGTC 3'
mystn_skipF	5'CACGGAAACAATCATTACCAT 3'
mystn_ex3R	5'GCTTCAAAATCGACCGTGAG 3'

Antisense oligonucleotide sequences:

Antisense oligonucleotides- 2'OMePS (Eurofins MWG Operon, Edersberg) sequences are as following in Table 2

Table 2: Sequence of 2'O-methyl RNA oligonucleotides

Name of the 2'OMeOPS	Sequence
GDF8/A1	5' TCC ACA GTT GGG CTT TTA CT 3'
GDF8/A2	5' TCT GAG ATA TAT CCA CAG TT 3'
GDF8/A3	5' TCT TGA CGG GTC TGA GAT AT 3'
GDF8/B1	5' TGA TGA GTC TCA GGA TTT GC 3'
GDF8/B2	5' TTC ATG GGT TTG ATG AGT CT 3'
GDF8/B3	5' TTG TAC CGT CTT TCA TGG GT 3'
GDF8/C1	5' CAG AGA TCG GAT TCC AGT AT 3'
GDF8/C2	5' TGT CAA GTT TCA GAG ATC GG 3'
GDF8/C3	5' CCT GGG CTC ATG TCA AGT TT 3'
GDF8/D1	5' CTG GGA AGG TTA CAG CAA GA 3'
GDF8/D2	5' TCT CCT GGT CCT GGG AAG GT 3'
GDF8/D3	5' CAG CCC ATC TTC TCC TGG TC 3'

Antisense oligonucleotides- PMO (Gene tools, Philomath) sequences are as following:

Table 3: Sequence of morpholino (PMO) oligonucleotides

Name of the PMO	Sequence
Mst A	TCT TGA CGG GTC TGA GAT ATA TCC ACA GTT
Mst B	TTG TAC CGT CTT CAT GGG TTT GAT GAG TCT
Mst C	CCT GGG CTC ATG TCA AGT TTC AGA GAT CGG
Mst D	CAG CCC ATC TTC TCC TGG TCC TGG GAA GGT

Octaguanidine dendrimer-conjugated PMO or Vivo-PMO-D (Morcos *et al.*, 2008) (Gene tools, Philomath) sequence is as following:

AG CCC ATC TTC TCC TGG TCC TGG GAA GG

Peptide conjugated PMO or B-PMO-D (Yin *et al.*, 2008) (conjugated by Amer Saleh from Prof Mike Gait's group at MRC Laboratory of Molecular Biology, Cambridge) sequence is as following:

AG CCC ATC TTC TCC TGG TCC TGG GAA GG

2.6. RT-PCR

2.6.1. Materials

Gene script RT-PCR System (GeneSys Ltd., GS003)

2X Master Mix (Genesys Ltd., RM030)

HyperLadder™ IV (Bioline)

2.6.2. Method

1µg of RNA was reverse transcribed and resulting cDNA amplified using specific primers obtained from MWG, using the Genescript kit. The preparation of master mixes was done as follows:

Master Mix I (X1 reaction):

1. 2µl of 5mM dNTP mix
2. 1 µl of Primer Ex1F
3. 1 µl of Primer Skip R
4. 19µl of nuclease-free water*
5. 2µl of RNA*

* The volume of RNA and water varied depending upon the concentration of RNA.

Master Mix II (x1 reaction):

1. 10µl RT-PCR buffer
2. 0.5µl of enzyme mix
3. 14.5µl of nuclease-free water

To the RNA in PCR tubes, 23µl of Master Mix I and 25µl of Master Mix II was added, making a total volume of 50µl. The RT-PCR program was run as following:

2.6.3. RT-PCR Program

1. 45 ºC, 30 minutes
2. 92 ºC, 2 minutes
3. 92 ºC, 30 seconds
4. 54.5 ºC, 30 seconds
5. 68 ºC, 2 minutes
6. Go to step 3, 9 times
7. 92 ºC, 30 seconds
8. 54.5 ºC, 30 seconds
9. 68 ºC, 2 minutes, +5 seconds per cycle
10. Go to step 7, 24 times
11. 68 ºC, 10 minutes
12. END

2.7. Nested PCR and analysis of RNA by gel electrophoresis

2.7.1. Materials

2X Master Mix (Genesys Ltd., RM030)

HyperLadder™ IV (Bioline, BIO-33029)

Nuclease-free water (Qiagen, 129114)

Ethidium bromide solution (Sigma Aldrich, E1510)

SYBR® Safe DNA gel stain (S33102)

Agarose (Bioline, 41026)

2.7.2. Method

1µl of PCR products obtained was used as a template for carrying out nested PCR using 2X Master Mix. The master mix (X1 reaction) was prepared as following:

1. 12.5µl of 2X Master Mix
2. 1µl of Primer Skip F
3. 1µl of Primer Ex3R
4. 9.5µl of nuclease-free water

24µl of the above mixture was then added to 1µl of RT PCR products and the following program was run using MJ Research PTC-200 thermal cycler:

2.7.3. Nested PCR program

1. 92 ºC, 2 minutes

2. 92 ºC, 30 seconds

3. 56 ºC, 30 seconds

4. 68 ºC, 1 minute

5. Go to step 2, 29 times

6. 68 ºC, 10 minutes

7. END

The products from nested PCR were separated on 1.2% agarose gel with ethidium bromide or SYBR® Safe DNA gel stain (5µl for every 50µl of gel) in Tris-borate/EDTA buffer and HyperLadder™ IV was used as the marker. Densitometric

analysis of the agarose gels was carried out using Gene tools 3.05 (Syngene, MD, USA) and % skipping expressed as the amount of skipped product intensity relative to total PCR products detected.

2.8. Densitometry

2.8.1. Materials

Gene tools software by MW library

2.8.2. Method: Opened a new file in the software and clicked on spot blot for analysis type and chose rectangle as spot type. Image type was selected as fluorescence. Spots were created for manual positioning and the size of the rectangle adjusted as appropriate. In order to calculate the background, the rectangle was dragged to a position where there was no band and just uniform dark area. The table that opens up on starting the analysis shows the mean pixel values that were then exported to excel. Mean pixel value of the background spot was subtracted from the mean pixel value of the full length band and the skipped band to give the corrected full length and skipped band mean pixel values respectively. Mean pixel values of corrected full length (F) and corrected skipped bands (S) were added together (F+S) and percentage skipping was calculated by using the formula: Percentage skipping = [S/ (F+S)]*100.

2.9. Proliferation Assay

2.9.1. Materials

Cell proliferation assay: Cell Titer 96® Aqueous One Solution Cell Proliferation assay (Promega, G3582)

2.9.2. Method

A proliferation assay using Cell Titer 96® AQ_{ueous} One Solution Cell Proliferation assay was performed, as reported previously (Cory *et al.*, 1991). Assay reagent consists of two components: a tetrazolium compound, [3-(4,5-dimethylthiazol-2-yl)-5-(3-carboxymethoxyphenyl)-2-(4-sulfophenyl)-2H-tetrazolium; MTS] and phenazine ethosulphate (PES), an electron coupling reagent. A very high chemical stability of PES enables it to bind to MTS strongly. Bioreduction of the tetrazolium compound, MTS results in formation of a coloured product called formazan. This

product is soluble in the media the cells are grown in. Therefore, the amount of formazan produced and subsequently the absorbance recorded gives a measure of the number of viable cells present in each well of the 96-well culture plate.

C2C12 cells were seeded in full growth media at a density of $2.5x10^3$ cells per well of a 96 well plate and transfected with different 2'OMePS as described before. After 24 hours of transfecting the cells, the growth media was replaced with 75µl serum-free media and cells incubated at 37°C overnight. After 24 hrs, 15 µl of assay reagent was added to each well of the 96-well plate followed by incubation at 37ºC for four hours. Plates were read at 490nm after 4 hours. Statistical analysis on the data from the proliferation assay was performed using the individual t-test.

2.10. CAGA assay

2.10.1. Materials

pGL3-$(CAGA)_{12}$-luc plasmid (Wyeth pharmaceuticals)

Luria broth (Invitrogen, 12795-027)

LB-SOC (Invitrogen, 10855-021)

Lipofectamine™ 2000 (Invitrogen, 11668-019)

Agar (Invitrogen, 22700-025)

Ampicillin (Sigma, A0166-5G)

EndoFree Plasmid Maxi kit (Qiagen, 12362)

Luminometer (Bio-Rad laboratories)

QIAprep Spin Miniprep kit (Qiagen, 27104)

NEB 2 (Biolabs, B7002S)

Recombinant mouse GDF-8/Myostatin (rndsystems, 788/GD/CF)

Steady-Glo® Luciferase assay system (Promega, E2520)

2.10.2. Methods

2.10.2.1. E.coli transformation with pGL3$(CAGA)_{12}$

1ng plasmid pGL3$(CAGA)_{12}$ was added to 50µl of competent E.coli (Top10F', Invitrogen) on ice and incubated for 20 minutes on ice. The tube containing the plasmid and bacteria was then put on a heat block at 42ºC for 30 seconds, and then back on ice

for 2 minutes. 250 µl of LB-SOC was then added to the tube, the components transferred to a 20 ml centrifuge tube and left it on a shaker at 37 ºC for 1 hour. After the incubation 100 µl of cells were put on an LB/agar plate with Ampicillin (1ml/litre) and left overnight in a shaker at 37 ºC. Next day, the colonies were picked from the plate and inoculated into 6ml of LB with ampicillin in 8 separate centrifuge tubes. The tubes were loosely capped and left overnight in a shaker at 37ºC.

2.10.2.2. Mini prep

Tubes with 1.5 ml of the bacterial suspension were centrifuged at 13,000 rpm for 10 minutes. The pelleted bacterial cells were resuspended in 250µl of resuspension buffer P1 and vortexed until the pellet completely dissolved. 250 µl of lysis buffer P2 (NaOH/SDS) was added and the tube mixed by inverting until the cell suspension turned homogeneously blue. This was followed by addition of 350 µl of neutralization buffer N3 and mixing the suspension by inverting the tube 4-6 times and then centrifugation at 13,000 rpm for 10 minutes. The supernatant was then put into the QIA prep spin column which was then centrifuged at 13,000 rpm for 30-60 seconds. The flow through was discarded, the column was washed with 0.5 ml washing buffer PB (to remove endonucleases) and then centrifuged for 30-60 seconds at 13,000 rpm. The flow through was again discarded and the column washed with 0.75ml of buffer P1 followed by another centrifugation for 1 minute in order to remove residual buffer. The column was then placed in a clean 1.5 ml tube and 50µl of EB buffer (for elution of plasmid DNA from QIAprep column) was added to the column. The column was allowed to stand for 1 minute and then centrifuged for 1 minute.

2.10.2.3. Restriction digestion

For double digestion (10 reactions), a master mix containing 20 µl of 10x NEB 2, 5µl Hind III, 5µl Xbal, 20µl of 10x BSA and 50µl of water was prepared. 10µl of this master mix was then added to 10µl of plasmid DNA in each of the 8 tubes. For linear digestion, 20 µl of 10x NEB 2, 5µl Hind III and 75µl water was used in the master mix and 10µl of this was added to another 10µl plasmid from each of the 8 replicates and incubated at 37ºC for one hour. The samples were then loaded on a 0.8% agarose gel and compared against Hyperladder I.

2.10.2.4. Maxi prep

Two clones were selected from mini prep and 1ml of each added to two separate conical flasks containing 200ml of LB with ampicillin. The flasks were incubated overnight in a shaker at 37ºC. The cells were centrifuged at 3750 rpm for 30 minutes and the pellet re-suspended in 10 ml of resuspension buffer P1 and vortexed to dissolve the pellet completely. 10ml of lysis buffer P2 was then added and tubes vigorously inverted and incubated at room temperature for 5 minutes. 10 ml of chilled neutralization buffer P3 was then added to the lysate and mixed by vigorous inverting of the tube. The cap of a QIA filter cartridge was screwed in and the cartridge placed on a falcon tube. The lysate was then loaded on the barrel of the cartridge followed by incubation at room temperature for 10 minutes. The cap of the cartridge nozzle was the removed and plunger was inserted into the QIA filter cartridge in order to filter the lysate into the falcon tube. 2.5 ml of elution buffer EB was added to the filtrate and tube inverted to mix well followed by incubation at room temperature for 30 minutes. The QIAGEN tip 500 was equilibrated by adding 10 ml of equilibration buffer QBT to it and allowing the column to empty by gravity flow. The lysate was then applied to the tip and allowed to pass through the resin by gravity flow. The column was then washed with 30 ml of washing buffer QC. The DNA was then eluted with 15 ml elution buffer QN. The eluate was recovered in a falcon and 10.5 ml isopropanol added to it to be followed by centrifugation at 15,000x*g* at 4ºC for 30 minutes. 5ml of endotoxin free 70% ethanol was then added and centrifugation carried out at 15,000g for 10 minutes. The supernatant was decanted off and pellet air-dried. The pellet was redissolved in 300µl TE buffer and stored overnight at 4ºC before recording the OD and storage at -20ºC.

2.10.2.5. Reporter assay for measuring the biological activity of the cells

pGl3 luciferase reporter vector backbone has a coding sequence for luciferase from a firefly (*Photinus pyralis*) and this sequence is optimized for transcriptional analysis of eukaryotic cells. pGL3 vector with twelve CAGA elements cloned into was used as a reporter system for assessing the changes in TGF-β-induced transcriptional activity of phosphorylated Smads. Luciferase is a popular choice in reporter assays due to rapid reaction and therefore production of functional enzyme immediately upon translation. The luciferase reaction involves mono-oxygenation of luciferin in the presence of Mg^{2+}, molecular oxygen and ATP, catalyzed by luciferase (Kricka, 1988).

ATP is used as a cofactor although most of the energy for photon production is provided by molecular oxygen (Marques & da Silva, 2008). The Steady-Glo™ luciferase assay has a very salient feature of high signal half-life which is about 5 hours in mostly used cell culture media giving this system high reproducibility under standard laboratory conditions (Kurata *et al.*, 2004; Rose *et al.*, 2005).

A204 cells were seeded in a 100mm plate at a density of $2.5x10^6$ cells in DMEM with L-Glutamine, FCS and antibiotics (100U/ml penicillin and 10µg/ml streptomycin). After 48 hours, cells were re-seeded in a 150 mm dish. 24-48 hours later, the cells were transfected with pGL3-$(CAGA)_{12}$-luc (at a concentration of 4µg plasmid for every 10mm growth area of the culture dish) using Lipofectamine™2000 (1/400) as the transfection reagent in DMEM and L-Glutamine and incubated at 37ºC and 5% CO_2. After 3-4 hours, the media was replaced with full growth media and culture dish put back to the 37ºC incubator with 5% CO_2 overnight. 24 hours later, the transfected A204 cells were seeded in a 96-well dish for 24 hours in DMEM and L-Glutamine. The cells were transfected in a bigger dish before seeding them in a 96-well plate in order to have a uniform plasmid transfection. Next day, the recombinant mouse GDF-8/Myostatin was added to the cells at the concentrations (ng/ml): 0, 2.5, 5, 10, 20, 40, 80 diluted in serum-free media and the plate incubated at 37 ºC for 4-6 hours. Post incubation, 100µl of Steady-Glo® Reagent was added to each well and the plate read in a luminometer after 5 minutes.

After obtaining the dose response curve for myostatin, the conditioned media from C2C12 cells transfected with leashed PMO-D was incubated with A204 cells transfected with pGl3-$(CAGA)_{12}$-luc (media in A204 cells was replaced with serum-free media 24 hours before addition of conditioned media from PMO-treated C2C12 cells) for 4-6 hours and signal induced on adding the assay reagent was read using a luminometer. The control in this case was the supernatant from C2C12 cells transfected with leash alone (without PMO) and Lipofectamine™2000.

2.11. In vivo study

2.11.1. Materials

Sterile 0.9% injectable sodium chloride solution (Sigma, S8776)

Hypnorm (VetaPharma, Vm21757/4000)

Hypnovel (Roche, AUST R 46348)

OCT (Thermo scientific, LAMB-OCT)

Mice used were: C57BL/10, *mdx*

For all the in vivo experiments, animals were bought from Harlan (UK) and in-house maintained, and in vivo experimentation conducted under statutory Home Office recommendation, regulatory, ethical and licensing procedures and under the Animals (Scientific Procedures) Act 1986 (project licence PPL 70/7008).

2.11.2. Methods

The desired dilutions of the AOs were prepared in sterile injectable saline. For intramuscular injections, animals were anaesthetised via intraperitoneal injection of 3µl/g body weight of 25% (v/v) fentanyl/fluanisone (Hypnorm) and 25% (v/v) midazolam (Hypnovel) in sterile saline and injections carried out into each of the tibialis anterior (TA) muscle using 0.5ml insulin syringe with a 28G x 13mm needle. Animals were injected with a desired dilution of the AO in sterile saline (25µl) into the TA muscle. During recovery, the animals were placed on a heating pad and monitored hourly for about 4 hours. Whole body weights were recorded weekly. TAs of treated and control mice were excised post mortem and weights were recorded. For intravenous injections, animals were placed in a heat chamber at 40ºC for 10 minutes and then injected with a desired dilution of the AO in sterile saline (200µl) via the tail vein using a 29G needle. Whole body weights were measured weekly and individual muscles were weighed on excising the muscles after sacrificing the animals. The muscles were embedded in OCT embedding medium and frozen in iso-pentane cooled with liquid nitrogen. Cryosectioning was performed with OTF 5000 cryostat and 10µm transverse sections of each muscle were cut at up to 10 levels through the muscle length. The tissue cut in the intervening sections between the levels of a block was collected in pre-cooled 1.5 ml eppendorf tubes for protein and RNA extraction and stored at -80ºC.

2.12. Immunofluorescence and histological staining

2.12.1. Materials

Anti-Laminin (Sigma, L9393): 1/1000 dilution

Alexa fluor® 568 goat anti-rabbit (Invitrogen, A-11011): 1/200 dilution

H12 polyclonal rabbit antibody (Sherratt *et al.*, 1992): 1/400 dilution

Avidin/Biotin blocking kit (Vector labs, SP-2001)

Cryostat (Bright, OTF 5000)

DAB kit (Vector labs, SK-4100)

DakoCymation pen (Dako, S2002)

DPX mountant (BDH, 360294H)

Eosin Y (BDH, 34221HD)

Ethanol: 50%; 80%; 100%

Haematoxylin (Sigma, MHS16)

Dry skimmed milk

M.O.M kit (Vector labs, PK-2200)

Mouse IgG Vectastain ABC kit (Vector labs, PK-6102)

OCT (Optimal cutting temperature) compound (Raymond A Lamb-Labs, Lamb/OCT)

Rabbit anti mouse kit (Vecor labs, PK-6101)

Sreptavidin, Alexa fluor® 568 (Invitrogen, S-11226): 1/100 dilution

Superfrost Plus microslides (VWR, 48311-703)

Vectashield hard set mounting medium with DAPI (Vecor labs, H-1500)

Xylene (BDH, 102936H)

2.12.2 Methods

2.12.2.1. Haematoxylin and Eosin staining

10µm thick sections were cut from OCT-embedded muscle blocks using Bright OTF 5000 cryostat. Sections were placed on superfrost plus microslides and left outside to air dry before storing them at -80ºC. Fifteen slides with up to 7-8 levels of muscle sections were prepared for each block. For staining, the slides were taken out of the -80ºC freezer and left on the bench for about 10 minutes to let them completely dry. The slides were then put in ice cold methanol and left in the fridge for 10 minutes. After taking the slides out of the fridge they were left to dry on the bench. The slides were then put in a coplin jar containing haematoxylin for 10 minutes followed by a quick wash in tap water. After the wash, slides were put in a coplin jar containing eosin for 5 minutes. This was followed by two quick washes in distilled water and then putting the slides in

50% Ethanol for 3 minutes; 80% ethanol for 4 minutes; 100% ethanol for 5 minutes and finally in fresh 100% ethanol again for 5 minutes. The slides were then put in xylene for 10 minutes and mounted in DPX.

2.12.2.2. Laminin and Dystrophin staining

Slides were taken out of the -80C and left on the bench for about 10 minutes to let them completely dry. The slides were fixed with ice cold acetone at 4ºC for 5 minutes. The slides were then taken out and left to dry. An outline was drawn with a liquid blocker pen, DakoCymation pen in order to contain the reagents on the sections during treatment. The slides were then put in a humid chamber and blocked with 5% marvel (dry skimmed milk) in PBST for one hour at room temperature. Following incubation, the slides were given a quick wash in a PBST containing coplin jar. 2-3 drops of Avidin were then put on the slides for 15 minutes. The Avidin was then drained on a tissue paper and slides quickly given a rinse in PBST. 2-3 drops of Biotin were then put on the slides for 15 minutes followed by quick rinse in PBST. Primary antibody solution (1/1000) was prepared by adding 2µl of anti-laminin rat antibody to 2ml of 2.5% marvel. The required amount of the antibody solution was then put on each slide and the slide incubated at room temperature for one hour. Three washes for 5 minutes each were then given to the slides with PBST. Secondary antibody solution was prepared using vectashield rabbit anti rat mouse kit. To 10 ml of PBST, 3 drops of serum and 1 drop of anti-rat IgG (biotinylated) were added and the solution mixed well by inverting the tube. Equal amount of secondary antibody solution was then put on each slide and incubation at room temperature carried out for one hour. The slides were then washed thrice in PBST for 5 minutes each time. Tertiary treatment with 2µl Alexafluor® Sreptavidin-568 (1/100) in 2ml of PBST was done for 6-7 minutes. Again three washes with PBST for 5 minutes each was done. The slides were then mounted in vectashield, hard-set mounting medium for fluorescence with DAPI. For Dystrophin staining the same protocol was followed but the primary antibody used was H12 Polyclonal rabbit antibody (1/400) and the secondary antibody used was Alexafluor goat anti-rabbit-568 (1/200).

2.13. Microscopy

The images of stained tissue sections were captured using Leica application suite (Leica Microsystems, Germany). For fibre cross-sectional area analysis, the whole tissue

section was scanned and different regions were captured at 20X covering the entire tissue section making sure no overlaps took place. For the cross sectional area of the entire tissue section, images were captured at 5X. The images were recorded and processed using identical parameters of exposure, saturation, and gamma between differentially treated and untreated specimens. Analysis was performed using SigmaScan Pro 5 software as detailed in the next section.

2.14. Sigma scan analysis

For fibre cross sectional area analysis, the tissue section with the greatest cross sectional area was determined by eye. An image file was opened in SigmaScan Pro 5. F6 was then pressed to set intensity threshold (from which the software identifies the areas of interest and calls them objects (See the following screen shot representation). Then F2 was pressed to confirm that 'Area' is highlighted. In case of missing boundaries of the individual fibre, click on MODE on the main menu and then highlight 'Overlay draw mode' and using right click and moving the pointer along the boundary of the individual fibres, define the object. Then press F12 to count and identify each object. All the counted objects have an individual identifying number and the area represented by the number of pixels is determined. This information is saved automatically into a separate spreadsheet. Identify the smallest and the biggest fibre and from the individual numbers for these fibres, look for the area in pixels against these numbers in the spread sheet. One can now disregard all objects that are larger than the largest identified fibre and smaller than the identified smallest fibre.

To calculate the entire tissue area, after opening the image in SigmaScan, click on MODE on the menu bar, highlight 'Trace measurement mode' and use a series of left clicks to define the internal edge of the entire tissue and finally a right click when close to the starting point to close the area. Press F12 and the program will calculate the number of pixels for the gross tissue area. The data in Excel was arranged in descending order to eliminate all the values beyond smallest and largest values as determined by SigmaScan. The values of area measurement were converted from pixels to μm^2 depending on objective used. The fibre CSA values for all treated muscles and all control muscles were put together in one column each and frequency distribution was calculated using GraphPad Prism software. Statistical analysis was done using Chi-squared analysis.

Representation of SigmaScan analysis (for fibre cross sectional area)

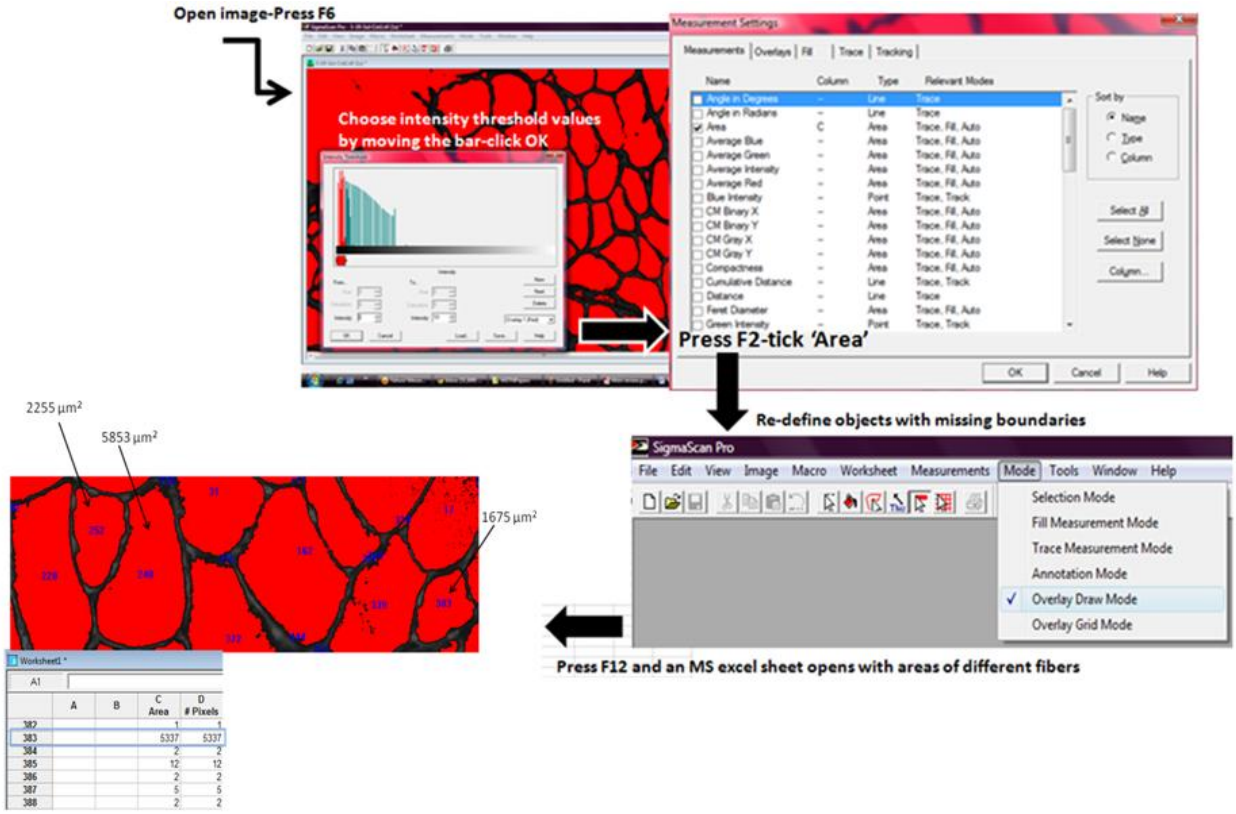

Area (pixel^2) * conversion factor of the microscope (for given magnification) to calculate µm^2

2.15. Statistical analysis

All the in vitro assay data (Proliferation assay and CAGA assay) and the animal tissue and gross body weight data was analyzed using two-tailed t-test (with standard error of mean). Standard deviation was calculated for percentage skipping of all treatment groups (Mean±SD). RT-PCR was performed on individually-treated-tissue bands unless otherwise stated that the tissues were pooled together. Densitometric analysis was followed by calculation of mean percent skipping and standard deviation. Fibre CSA was determined using chi-square test for frequency distributions.

CHAPTER 3

DESIGN OF ANTISENSE OLIGONUCLEOTIDES TO INDUCE SKIPPING OF MOUSE MYOSTATIN EXON 2 AND CELL CULTURE STUDIES OF THEIR EFFICACY

3.1 Introduction

3.1.1. Bioinformatics analysis of myostatin exon 2 to predict AO target sites

The first step to study AO-based exon skipping as a means of downregulating myostatin expression was to select the most amenable splicing motifs as the targets for AOs to skip the specific exons (Errington *et al.*, 2003; Popplewell *et al.*, 2009). In the case of DMD, different AOs targeted at specific exon(s) of dystrophin mRNA lead to restoration of reading frame and the resultant shortened but functional protein due to skipping of target exons (Aartsma-Rus *et al.*, 2002; Dickson *et al.*, 2002; Sherratt *et al.*, 1993). However, targeting one of the three exons of myostatin mRNA would disrupt the reading frame and result in downregulation of myostatin expression. It is quite difficult to precisely predict potential target ESE sites for AOs, therefore, three different computational methods namely, ESE Finder, Rescue ESE and PESX were used in conjunction in this study as discussed in the following sections.

3.1.1.1 ESE prediction using ESE-Finder software

Nearly 50% of point mutations causing genetic disorders result from aberrant splicing which further results either from blockade or creation of a splice site; or cryptic site activation; or intervention with splicing regulators (Cartegni *et al.*, 2002). The SR protein domain responsible for RNA-binding attaches to the ESEs and further employs spliceosomal complex components which eventually leads to precise identification of exon boundaries (Fairbrother *et al.*, 2002). An approach called systematic evolution of ligands by exponential enrichment (SELEX) has been used to predict putative ESE motifs of SR proteins that would bind to an ESE (Cartegni *et al.*, 2002). ESE finder is a user-friendly www interface (http://rulai.cshl.edu/cgi-bin/tools/ESE3/esefinder.cgi?process=home) that recognizes 6-8 nucleotide long possible ESE binding sites for SR proteins SC35, SF2/ASF, BRCA1, SRp40 and SRp55. ESE finder searches for the possible ESE sites in a given nucleotide sequence

based on the matrices relative to different SR protein motifs (Liu *et al.*, 2000; Liu *et al.*, 1998). The software allows a sequence to be either pasted directly into the query box or be uploaded from a file in FASTA format (preceded by '<') (Cartegni *et al.*, 2003). Multiple sequences can also be analyzed at the same time by separating the two sequences by a description for the following sequence in FASTA format. The sequence in question should however be in standard DNA notation. All the characters other than A, C, G and T will be ignored. Based on the matrices selected by the user, the program raises a series of scores. Initially only high score values for each matrix are displayed that correspond to the values greater than threshold value which is set in the input page. Default threshold values are the median of each sequence's highest score. For an easier and standardized representation of the results, a graphical output is generated that has the exonic sequence on the X-axis. Colour coded bars indicate the scores of different motifs above the selected threshold values. The breadth of the bars indicate the position and length along X-axis of the motifs whereas, the height represents the motif score (Cartegni *et al.*, 2003). It has been demonstrated by using ESE finder matrices that interruption of ESEs identified by different SR proteins is capable of inducing exon skipping (Caputi *et al.*, 2002; Cartegni & Krainer, 2002; Fackenthal *et al.*, 2002; Smith *et al.*, 2002). Importantly, the ESEs predicted using ESE finder, have been shown to be gathered in the regions where ESEs have been experimentally positioned (Liu *et al.*, 1998). Also the frequency of these putative ESEs is higher in exons than in introns (Liu *et al.*, 2000; Liu *et al.*, 1998). At least one of the predicted ESEs was shown to be either deleted or diminished in 50 point mutations causing exon skipping in humans (Dance *et al.*, 2002). In another bioinformatics tool, RESCUE ESE (http://genes.mit.edu/burgelab/rescue-ese/), the potential motifs of ESE are determined by frequencies of exon hexamers bound by weak or strong splice sites (Fairbrother *et al.*, 2002). Hexamers with weaker splice sites are expected to depend more on the ESEs for splicing (Fairbrother *et al.*, 2002) and some outputs from the RESCUE ESE and those from ESE Finder have shown overlaps. It is however important to note that ESE activity and the numerical scores cannot be strictly correlated. This is due to a number of variable factors including the presence of silencer elements or/and splice-site strengths. Therefore, the presence of a high score motif does not always mean that there is an ESE located at that position and also conversely, absence of a high score does not necessarily mean there is no ESE present at that site. This could also be due in part to certain redundant ESEs present near the actual ones that do not let the mutation of the

actual ESE to exert a significant effect (Cartegni *et al.*, 2003). As these matrices were developed in mammalian system, the sequence precision in human SR proteins is depicted and the application to other species will depend upon the degree of conservation of a particular SR protein across various species (Cartegni *et al.*, 2003).

3.1.1.2. ESE predictions using the RESCUE ESE (relative enhancer and silencer classification by unanimous enrichment) software

Another computational method to predict ESE activity called RESCUE ESE (http://genes.mit.edu/burgelab/rescue-ese/) has been developed. ESEs are recognized using this approach by looking up for hexanucleotides that fitted in to the following criteria: the hexanucleotides that were significantly more enriched in exons than in introns; that are present in exons with non consensus (weak) splice sites at a significantly higher rate than in exons with strong (consensus) splice sites. Point mutations of these predicted hexanucleotides resulted in more than two folds reduction in exon inclusion in 90% of the cases (Fairbrother *et al.*, 2002). Weak exons that have nonconsensus splice sites have greater selective pressure to have ESEs as compared to the stronger exons, thereby increasing the occurrence of ESEs in weak exons (Graveley, 2000). The sequence in question is either pasted directly or uploaded in multi-FASTA format. Once a vertebrate choice is made and the exon sequence is pasted in the query box preceded by "<" symbol, the output is shown in another section at the bottom of the page showing all the possible ESE positions along the sequence of the exon being investigated.

3.1.1.3. ESE and ESS predictions using PESX (putative exonic splicing enhancers/silencers) software

PESX (http://cubweb.biology.columbia.edu/pesx/) is an algorithm that focuses more on the information from non-protein coding exons. Comparative study of the real and pseudo exons (intronic regions that are similar to exons due to being bound by 3' and 5' splice sites and also because of being of same size as a typical exon) helps in understanding the distinctive sequence information used by the cellular machinery for precise splicing. This splicing information comes from the splicing code comprised of exon splicing enhancers (ESEs), exon splicing suppressors (ESSs), Intron splicing enhancers (ISE) and Intron splicing silencers (ISS) (Fu, 2004). The focus of this algorithm is on ESEs and ESSs. The exons with weak splice sites are expected to have

high ESE content for recognition compared to the exons with strong splice sites (Fairbrother *et al.*, 2002). Therefore an exon with no protein-coding information would have more ESEs than the ESSs. This tool compares the 8-mer (allowing one mismatch) frequencies in non-protein-coding exons with those in 5'untranslated regions (5'UTRs) of intronless genes and pseudo exons. Pseudo exons and 5'UTRs should therefore have more ESSs than the ESEs. The more frequently occurring sequences in non coding regions are nominated as alleged ESEs and the ones occurring less frequently are termed as putative ESSs (Zhang & Chasin, 2004).

3.1.2. Assessment of the activity of the designed AOs with C2C12 cells in culture

C2C12 cell line is an established murine pure myogenic cell line derived from C3H mice by injuring the muscle. Due to their proliferative and differentiation activity in cell culture, C2C12 cells have been widely used to study skeletal muscle cell growth and development, protein expression as well as in various exon skipping studies (Wilton *et al.*, 1999; Yaffe & Saxel, 1977). Myogenesis of C2C12 cells has been shown to be regulated by myostatin (Rios *et al.*, 2001; Taylor *et al.*, 2001). In order to test the efficacy of the AOs designed using different software described above, transfection of the C2C12 cells with these AOs was carried out. The transfections were carried out in serum-free media to avoid any interference in the results from myostatin present in media. The transfection reagent used was Lipofectamine™ 2000 as it is a standard transfection reagent for DNA or small RNA-based molecules like siRNA. 2'OMePS were used at 250nM concentration because this concentration has been previously reported as minimal effective dose for 2'OMePS (Graham *et al.*, 2004a)

3.1.3. Assay for assessment of proliferation of C2C12 cells followed by transfection with AOs

To verify the biological effect of myostatin exon skipping, a proliferation assay based on dehydrogenase activity of metabolically-active cells was performed. Cell Titer 96® AQ_{ueous} One Solution Cell Proliferation assay kit allows the colorimetric quantification of the viable number of cells. The direct relationship between the absorbance and number of cells is explained on the basis of dehydrogenase activity of the biologically active cells that results in production of NADPH or NADP which are responsible for MTS to formazan conversion (Berridge & Tan, 1993; Cory *et al.*, 1991).

3.1.4. Delivery of PMOs based on 2'OMePS sequences to induce myostatin exon 2 skipping in C2C12 cells

The PMO chemistry has been shown to have high nucleic acid binding, nuclease-resistance and high solubility in aqueous solutions (Alter *et al.*, 2006; Summerton & Weller, 1997). PMOs have been reported to exhibit higher efficiency and better restoration of dystrophin expression in *mdx* mice (Alter *et al.*, 2006) as well as in dystrophic dogs across various skeletal muscles in the body compared to other chemistries (Yokota *et al.*, 2009). However, PMOs being neutral in charge are incapable of diffusion across the membrane of the cell and therefore need to be administered at a much higher concentration to see a reasonable effect (Sazani *et al.*, 2001; Suwanmanee *et al.*, 2002). Standard cationic transfection reagents are therefore not sufficient on their own for PMO delivery in cell culture. In the case of mouse dystrophin exon 23 skipping, PMOs were conjugated to different complementary DNA or RNA sequences in order to surmount this problem and these sequences were termed 'leashes' (Morcos, 2001). When PMOs were delivered complexed with a leash in the presence of a standard transfection reagent to induce dystrophin exon 23 skipping in mdx cells, they were effective at much lower concentrations as compared to the unconjugated PMO (Sazani *et al.*, 2001). Conjugation to a leash has led to effective delivery and nuclear uptake of PMO (Popplewell *et al.*, 2010).

3.1.5. Reporter assay for determining the modulation of myostatin pathway by PMO-mediated exon skipping in C2C12 cells

It has been demonstrated that Smad 2 and Smad 3 are involved in TGF- β and activin signalling however Smad1, Smad5 and Smad9 are responsible for bone morphogenetic protein (BMP) signalling (Chen *et al.*, 1997b; Liu *et al.*, 1996; Suzuki *et al.*, 1997). These pathway-restricted Smad 2 and Smad3 form a heteromeric complex with Smad 4 which is a common component of TGF-β, activin and BMP signalling. The complexed Smads then move to the nucleus and regulate the transcription of various genes (Meersseman *et al.*, 1997). Smad 6 and Smad 7 have been shown to have an inhibitory effect on the phosphorylation of Smad 3 and Smad 4 (Hata *et al.*, 1998; Hayashi *et al.*, 1997). Several genes responsible for cell cycle regulation like Cyclin Dependent Kinase inhibitors (p21, p15) (Elbendary *et al.*, 1994) and also for the formation of extra cellular matrix, like Plasminogen activator inhibitor 1 (PAI-1),

fibronectin and procollagen are known to be activated by TGF-β (Inagaki *et al.*, 1994; Westerhausen *et al.*, 1991). Certain regions in the PAI-1 gene promoter have been reported to be responsive to TGF-β as the PAI-1 gene is strongly induced by TGF-β (Macias-Silva *et al.*, 1996). A combined over expression of Smad 2, Smad 3 and Smad 4 resulted in induction of endogenous PAI-1 promoter (Macias-Silva *et al.*, 1996). Short repetitive DNA elements in PAI-1 gene have been reported to be responsible for TGF- β responsiveness (Dennler *et al.*, 1998). When studies were carried out to identify these elements in the TGF-β responsive region of human PAI-1 promoter, three copies of the sequence AG(C/A)CAGACA were found at three different positions (Dennler *et al.*, 1998). The sequence was named as CAGA box and cloned into a transcriptional reporter system in order to analyze its role in the induction of PAI-1 by TGF-β.

When one of the three CAGA sequences was mutated by insertion of a mutant sequence (that was not induced by TGF-β), TGF-β induction was reduced compared to the wild type promoter. This response was more pronounced with mutations in two CAGA sites and PAI-1 promoter almost completely failed to respond to the TGF-β when all three sites were mutated. The CAGA elements have been shown to be specifically responsive to TGF-β and not to BMP (Dennler *et al.*, 1998). Myostatin propeptide has been shown to decrease the transcriptional activity of endogenous Smad proteins and therefore reduced TGF-β responsiveness to CAGA elements (Thies *et al.*, 2001; Whittemore *et al.*, 2003). CAGA assay has also been used to demonstrate neutralizing activity of the monoclonal antibody JA16 (Whittemore *et al.*, 2003). In another study, the CAGA elements were inserted into a promoter that controls the expression of Green fluorescence protein (GFP) in order to show a reduction in the transcriptional activity of endogenous Smad 2 in human myoblasts which expressed dominant negative form of ActRIIB (Fakhfakh *et al.*, 2011).

3.2. Aims of the chapter

In this chapter, design of various AOs targeted at mouse myostatin exon 2 using different bioinformatics algorithms has been described. The aim was to validate the use of different bioinformatics programs to design various AO sequences followed by testing their efficacy to downregulate myostatin mRNA by inducing exon skipping in skeletal muscle cell line C2C12. This involved optimising the transfection conditions,

testing various different primers and validating the PCR program for amplification of mRNA from the treated and control cells.

The study was also aimed at assessing any changes in the myostatin bioactivity following antisense-treatment.

PMO is one of the desirable chemistries for clinical applications. Use of the best 2'OMePS AO sequences to design PMO reagents and testing their efficacy in cell culture was another aim of the study in this chapter.

3.3. Results

3.3.1. Prediction of exon splicing enhancers (ESEs) and suppressors (ESSs) in exon 2 of mouse myostatin gene

The myostatin exon 2 pre-mRNA sequence was pasted into the query box of ESE Finder software in FASTA format and the output generated showed different coloured bars representing different SR protein motifs. This indicates the probability of presence of that motif in a particular position. **Figure 3.1** shows the result from ESE Finder for the myostatin exon 2 mRNA for putative ESEs. An output of the results obtained from pasting the myostatin exon 2 pre-mRNA sequence (in FASTA format) in the query box of RESCUE ESE and PESX is shown in **Figure 3.2** and **Figure 3.3** respectively.

Having analysed mouse myostatin pre-mRNA using different individual bioinformatics tools to predict ESE sites as potential targets of exon skipping, the results from all the three tools were combined. The predicted sequences which showed overlaps using all the three tools were taken into account and 20-mer AO sequences were designed around these sites. Four main sites in the whole exonic sequence were selected (based on coinciding ESE sites as predicted by at least two algorithms) and a set of three overlapping AOs were designed in each of these four regions (a total of 12 AOs) as shown in **Figure 3.4**. The three 20-mer AO sequences in every set were designed such that the last ten bases of AO-1 and first 10 bases of AO-2 overlapped, and so did the last ten bases of AO-2 and first ten bases of AO-3. Therefore, a total of twelve 2'OMePS AOs were designed for testing their exon skipping efficacy *in vitro* as well as *in vivo*. Sequences and positions of 2'OMePS and PMO AOs are shown in **Figure3.5**.

Figure 3.1

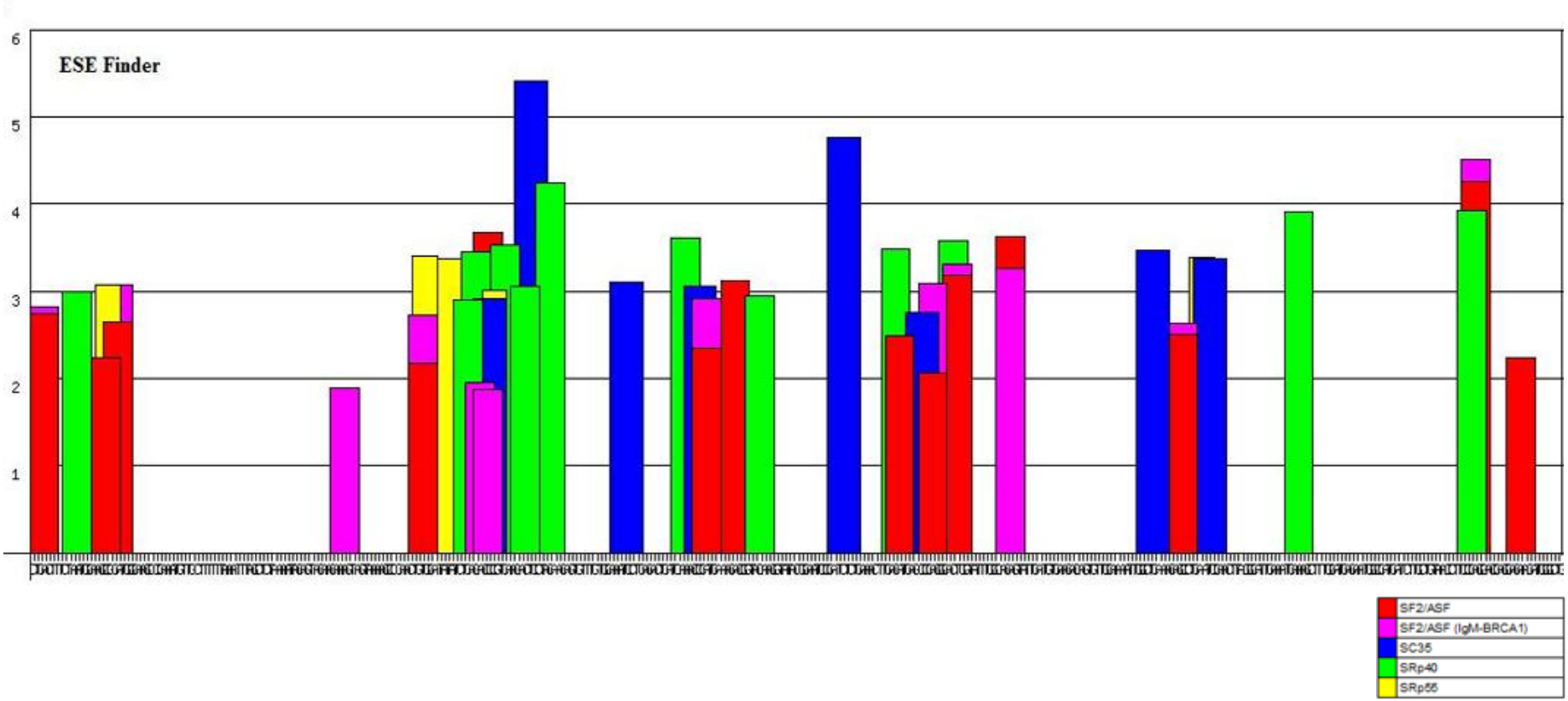

Figure 3.1. The ESE Finder output for myostatin exon 2: Different coloured bars represent different SR protein motifs as labelled in the panel below the figure. The width of each column represents the location and length across which a motif is possibly present and the height of each bar depicts the score for that particular motif above a set threshold value, which implies the probability of presence of that motif in a particular position.

Figure 3.2

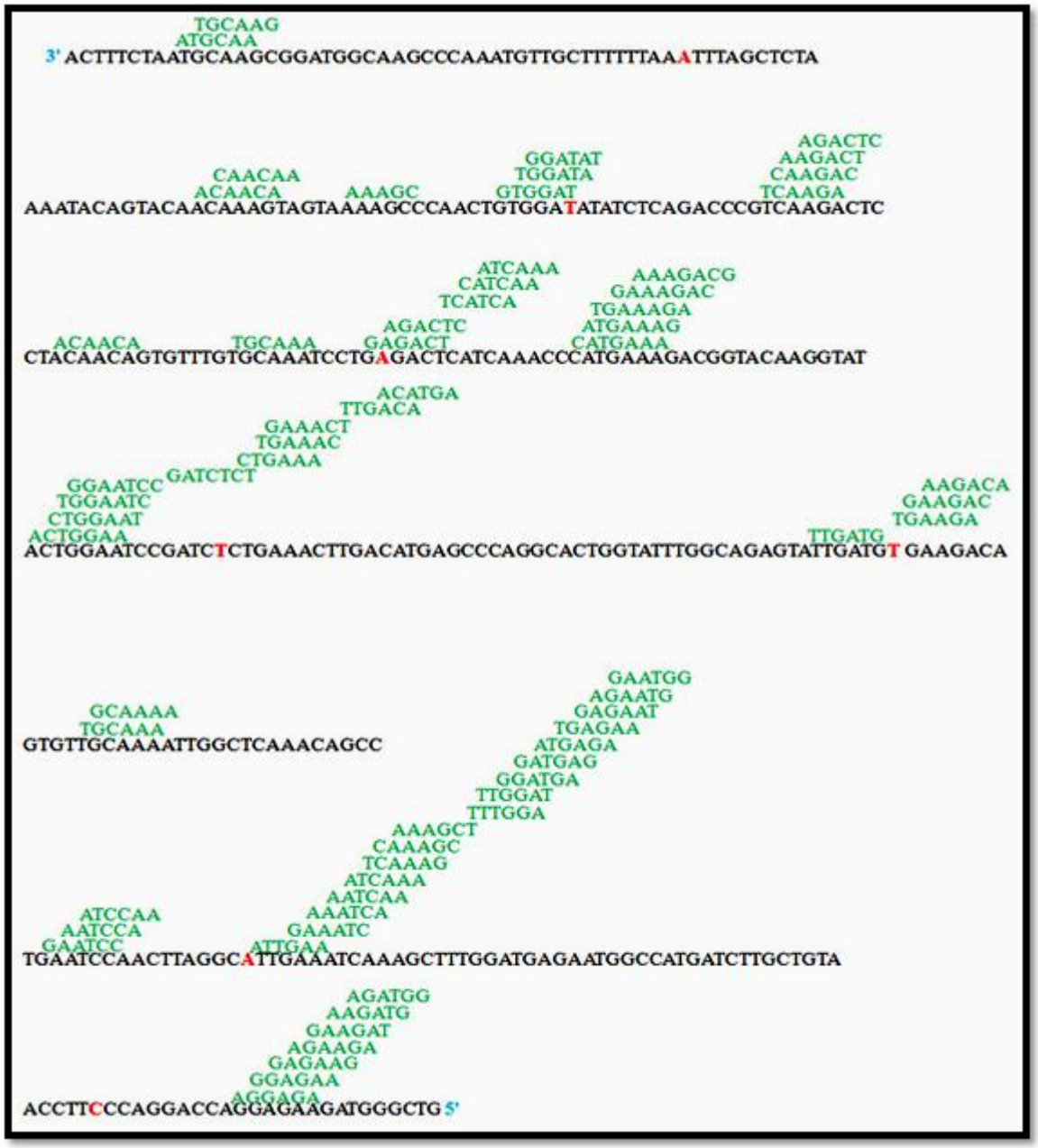

Figure 3.2: RESCUE ESE result for myostatin exon 2 mRNA analysis. Every 50th nucleotide is shown in red. Laddered green nucleotides are the putative ESEs as predicted by RESCUE ESE along the length of the exon sequence (shown in black).

Figure 3.3

CTGACTTTC**T**AATGCAAGCGGATGGCAAG**C**C**C**AAATGTTGC

TTTTTTAAATTTAGCTCTAAAATAC**A**GTA**C**AACAAAGTAGTAAAAGC
CCA

ACTGTGGATATATCTCAGA**C**CCGTCAAGACTCCTACAACAG**T**GTTTG
TGC

AA**A**TCCTGA**G**ACTCATCAAACCCATGAAAGACGGTAC**A**AGGTATACT
GGA

ATCCGATCTCTGAAACTTGACATGAGCCCAGGCACTGGTATTTGGCA
GAG

TATTGATG**T**GAAGACAGTGTTGCAAAATTGGCTCAAACAGCCTGAAT
CCA

AC**T**TAG**G**CATTGAAATC**A**AAGCTTTGGATGAGAA**T**GGCCATGATCTT
GCT

GTAACCTTCCC**A**GG**A**CC**AGGA**GAAGATGGGCTG

Figure 3.3: PESX analysis for myostatin exon 2 mRNA: The positions of predicted ESEs are shown in green and that of ESSs are shown in red. The first ESS/ESE bases are shown in bold letters and are underlined.

Figure 3.4: Joint representation of results from all the three different bioinformatics algorithms for designing AOs for mouse myostatin exon 2

Positions of twelve different 20-mer AOs designed relative to the exon 2 pre-mRNA of mouse myostatin obtained on combining the outputs of three different bioinformatics programs are shown. The *ESE Finder* analysis shows the location and values above threshold for SR protein binding motifs, SF2/ASF, SF2/ASF (BRCA 1), SC35, SRp40 and SRp55 which are shown as vertical bars above the sequence of exon 2. The *Rescue ESE* analysis shows the position of possible exonic splicing enhancer sites as black horizontal lines in a box parallel to the sequence of exon 2. The *PESX* analysis shows the location of ESEs as green horizontal lines, and exon splicing silencers (ESSs) as red horizontal lines in a different box below *Rescue ESE* output. The black horizontal laddered lines at the bottom represent the sequence of the 20-mer AOs which were obtained after aligning the outputs from the three algorithms.

Figure 3.4

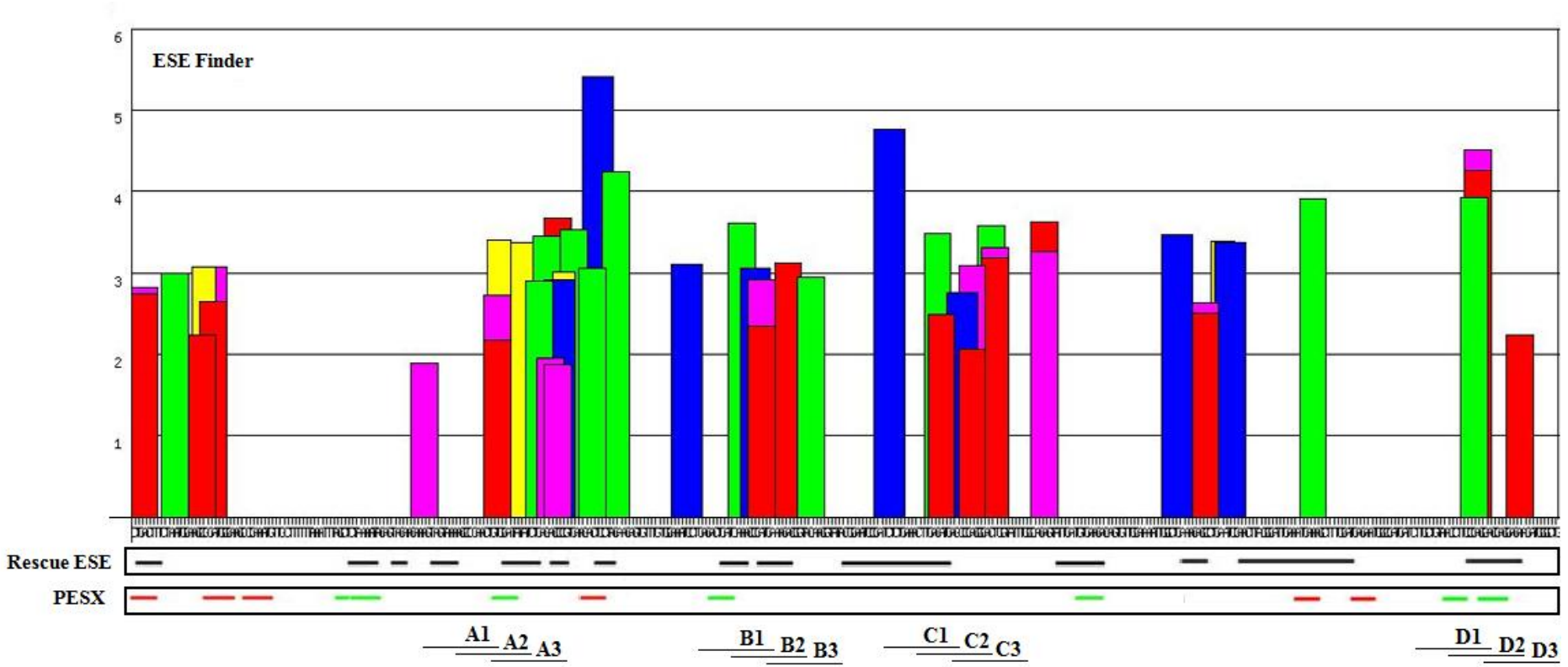
ESE Finder
6
5
4
3
2
1
Rescue ESE
PESX
A1
A2
A3
B1
B2
B3
C1
C2
C3
D1
D2
D3

Figure 3.5a

2'O-MePS	Sequence(5' to 3')	Position in myostatin mRNA(3'to 5')
GDF8/A1	TCCACAGTTGGGCTTTTACT	Exon 2: Nucleotides 80-99
GDF8/A2	TCTGAGATATATCCACAGTT	Exon 2: Nucleotides 91-110
GDF8/A3	TCTTGACGGGTCTGAGATAT	Exon 2: Nucleotides 101-120
GDF8/B1	TGATGAGTCTCAGGATTTGC	Exon 2: Nucleotides 140-159
GDF8/B2	TTCATGGGTTTGATGAGTCT	Exon 2: Nucleotides 151-170
GDF8/B3	TTGTACCGTCTT TCATGGGT	Exon 2: Nucleotides 161-180
GDF8/C1	CAGAGATCGGATTCCAGTAT	Exon 2: Nucleotides 184-203
GDF8/C2	TGTCAAGTTTCAGAGATCGG	Exon 2: Nucleotides 194-213
GDF8/C3	CCTGGGCTCATGTCAAGTTT	Exon 2: Nucleotides 204-223
GDF8/D1	CTGGGAAGGTTACAGCAAGA	Exon 2: Nucleotides 335-354
GDF8/D2	TCTCCTGGTCCTGGG AAGGT	Exon 2: Nucleotides 345-364
GDF8/D3	CAGCCCATCTTCTCCTGGTC	Exon 2: Nucleotides 355-374

Figure 3.5b

PMO	Sequence(5' to 3')	Position in myostatin mRNA 3'to 5'
Mstn A	TCTTGACGGGTCTGAGATATATCCACAGTT	Exon 2: Nucleotides 91-120
Mstn B	TTGTACCGTCTTTCATGGGTTTGATGAGTC	Exon 2: Nucleotides 151-180
Mstn C	CCTGGGCTCATGTCAAGTTTCAGAGATCGG	Exon 2: Nucleotides 194-223
Mstn D	CAGCCCATCTTCTCCTGGTCCTGGGAAGGT	Exon 2: Nucleotides 345-374

Human	ACC TTC CCA GGA CCA GGA GAA GAT GGG CTG
Mouse	ACC TTC CCA GGA CCA GGA GAA GAT GGG CTG
Rat	ACC TTC CCA GGA CCA GGA GAA GAT GGG CTG
Bovine	ACC TTC CCA GGA CCA GGA GAA GAT GGA CTG
Chicken	ACA TTC CCC AGG ACC GGG TGA AGA TGG TTG

Figure 3.5(a) Sequence of AOs targeted at mouse myostatin exon 2 designed using bioinformatics analysis. 20-mer Sequences of 2'OMePS AOs with their positions in the exon 2 of mouse myostatin. Each 2'OMePS AO-1 had an overlapping region of 10 bases to AO-2 and each AO-2 had an overlapping region of 10 bases to AO-3. **(b) Sequence of PMOs.** 30-mer AOs of PMO chemistry designed based on the sequences of 2'OMePSs. The 2'OMePS sequences of AO-2 and AO-3 of each of the four sets were merged together to make a 30-mer PMO sequence. Comparison of vertebrate myostatin mRNA sequence (3' to 5') against which AO-3 (used for all PMO experiments in vivo) was designed is also shown. Human, mouse and rat sequences have 100% homology for this AO whereas rat sequence has a mismatch of single base. Although PMO study is discussed later, the sequences are shown here for a better comparison and positioning relative to 2'OMePS sequences.

3.3.2. Myostatin exon 2 skipping in C2C12 cell culture following treatment with a range of AOs targeting ESEs

In order to verify the exon skipping potential of the designed AOs, C2C12 myoblast cultures were transfected (using Lipofectamine™ 2000) separately with all the twelve 2'OMePS (250nM) in serum-free media. After 4 hours of transfection, the media was replaced by full growth media containing 10% serum to let the cells proliferate under normal growth conditions. RNA was then extracted from the cells 24 hours after transfection and nested RT-PCR for skipping of myostatin performed on the RNA from transfected and control cells. The primers for the RT-PCR were designed to yield a full length product of 587 bps. Nested PCR primers were designed to give a full length product of 532 bps. Skipping of myostatin exon 2 (374 bps) results in the production of a product that is 158 bps long. A representative horizontal agarose gel (1.2%) electrophoresis separation of products obtained is shown in **Figure 3.6**. The level of skipping produced by each AO at 250nM was semi-quantified by densitometric analysis using the image analysis software, Gene Tools. All twelve 2'OMePSs induced myostatin exon 2 skipping to different levels. A2 and A3 induced almost complete skipping; B3, C3, and D3 induced 74%, 41% and 48% skipping. The nature of putative antisense-induced exon1-exon3 splicing product was confirmed by sequencing the products.

Figure 3.6

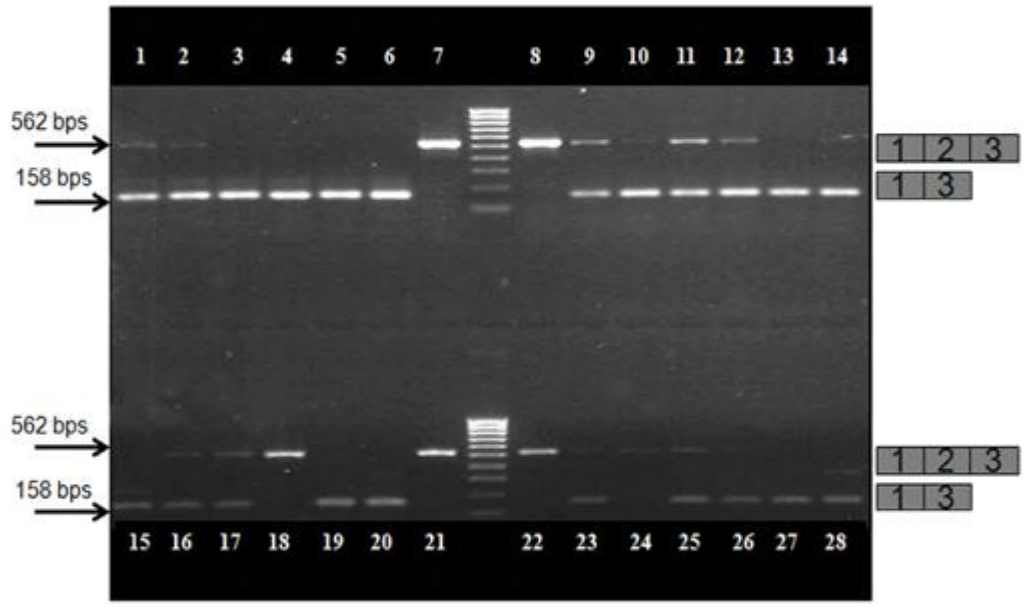

Figure 3.6: Comparison of efficacy of different 2'OMePS AOs to induce myostatin exon 2 skipping in C2C12 cell cultures. RT PCR was performed on 1µg mRNA from C2C12 cells treated with twelve different 2'OMePS AOs at 250nM concentration. Transfections were performed in duplicates and the nested RT PCR products were loaded on 1.2% agarose gel as follows: Tracks 1 and 2: oligomer A1; Tracks 3 and 4: oligomer A2; Tracks 5 and 6: oligomer A3; tracks 9 and 10: oligomer B1; Tracks 11 and 12: oligomer B2; Tracks 13 and 14: oligomer B3; Tracks 15 and 16: oligomer C1; Tracks 17 and 18: oligomer C2; Tracks 19 and 20: oligomer C3; Tracks 23 and 24: oligomer D1; Tracks 25 and 26: oligomer D2; Tracks 27 and 38: oligomer D3; Tracks 7, 8, 21 and 22: controls with transfection reagent Lipofectamine 2000 alone, but no AO; Size Marker used was HyperLadder IV.

3.3.3. Assessment of level of proliferation of C2C12 cells transfected with myostatin exon-skipping 2'OMePS AOs

The assay reagent was added to the cultured C2C12 cells which were transfected with the AOs (A3, B3, C3 and D3; based on the best RT-PCR results) using Lipofectamine™ 2000 as well as to the control cells without any AOs in a 96-well plate. The plates were incubated at 37ºC for 4 hours. Following incubation the plate was read at 490nm. The results of the proliferation assay showed a significant difference in cell proliferation in transfected C2C12 cells, compared to the untreated control cells (**Figure 3.7**). Statistical analysis of the data using individual t-test showed that the 2'OMePS A3 ($p=0.0031$), B3 ($p=0.0055$) and D3 ($p=0.0115$), induced a significant increase in cell proliferation, as compared to untransfected control cells. C3 ($p=0.0534$) did not produce a statistically significant change. The experiment was done in six replicates per condition.

Figure 3.7

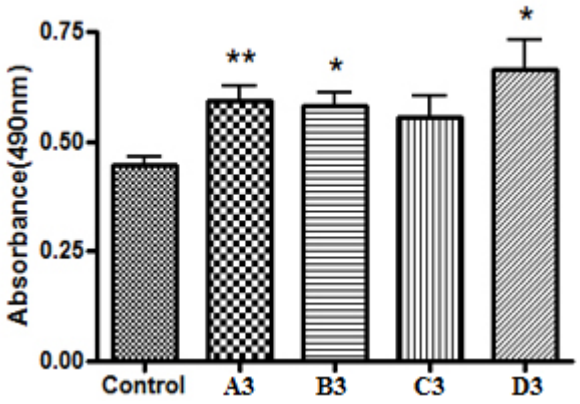

Figure 3.7: Proliferation assay for the C2C12 cells treated with myostatin exon skipping AOs. C2C12 cells were treated with four of 2'OMePS oligomers (A3, B3, C3 and D3) using Lipofectamine™ 2000 (LF2000), and assayed 24h later for determining the cell proliferation by lactic dehydrogenase assay. The transfections were performed in 6 replicates for each condition (6 wells transfected with each AO as well as controls, a total of 30 wells). t-test analysis with standard error of the mean,*: $p<0.05$; **: $p<0.01$.

3.3.4 Myostatin exon skipping efficacy of PMOs designed based on the most efficient 2'OMePS sequences in C2C12 cells

PMOs were designed on the basis of the sequences of the most efficient 2'OMePS AOs (A3, B3, C3 and D3) and initially tested in C2C12 cells after linking to a complementary stretch of DNA (leash) to improve delivery. The sequence and position of different leashes are shown in **Figure 3.8**. Nested RT PCR analysis of mRNA harvested from PMO-treated C2C12 cells demonstrated that exon skipping was induced by all the PMOs tested as shown in **Figure 3.9**.

3.3.5. Reporter assay for modulation of the myostatin signalling pathway in C2C12 cells by PMO-mediated exon skipping

The reporter vector used for the reporter assay was a modification of basic pGL3 luciferase vector which is highly flexible in allowing cloning of putative regulatory sequences due to the absence of promoter and enhancer sequences. pGL3 luciferase reporter vector backbone has a coding sequence for luciferase from a firefly (*Photinus pyralis*) and this sequence is optimized for transcriptional analysis of eukaryotic cells. Twelve CAGA elements were cloned into the pGL3 vector in order to develop a reporter system for assessing the changes in TGF-β-induced transcriptional activity of phosphorylated Smads (Diagrammatic representation **Figure 3.10**). Mini preps and maxi preps were carried out for pGL3$(CAGA)_{12}$-luc and the purified plasmid was used to transfect the human rhabdomyosarcoma A204 cells. **Figure 3.11** shows the products of restriction digestion using different restriction enzymes to confirm the structure of the plasmid.

Myostatin dose response curve was prepared by assaying different concentrations of myostatin onto the A204 cells transfected with pGL3-$(CAGA)_{12}$-luc. A204 cells were transfected with the plasmid pGL3-$(CAGA)_{12}$-luc in a 100mm dish first and 24 hours later seeded into 96-well dish in order to ensure uniform transfection in each well. Serum-free media was added to A204 cells 24 hours prior to adding myostatin dilutions to them. Dilutions of recombinant myostatin ranging from 2.5, 5, 10, 20, 40 and 80 ng/ml were assayed on to the transfected A204 cells and a standard curve obtained (as shown in **Figure 3.12**). The assay was performed in eight replicates per dose of treatment as well as for control.

Figure 3.8

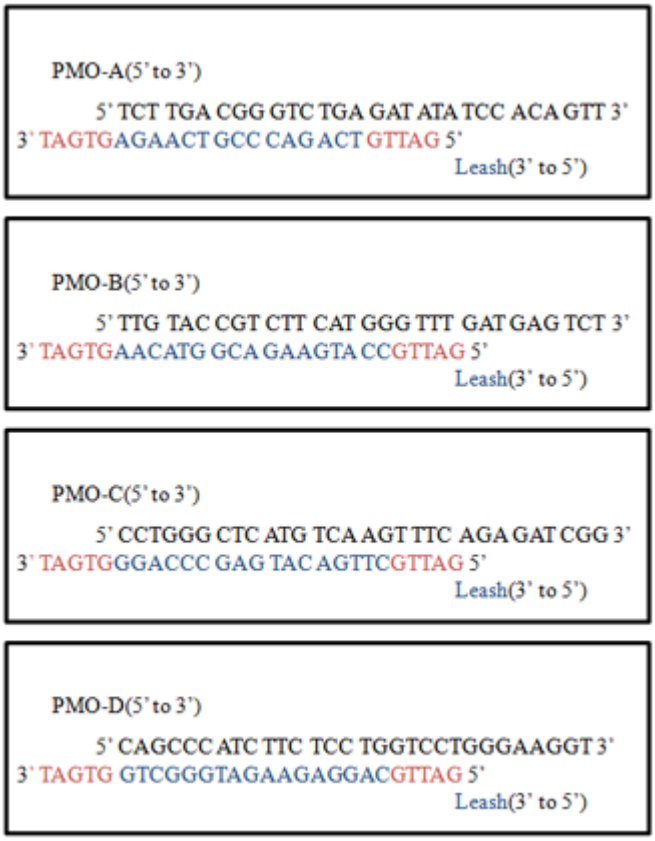

Figure 3.8: Position of the "leashes" relative to PMO sequence: The sequence of the PMO is shown in 5' to 3' orientation while leash sequence is shown in the complementary orientation. The complementary leash sequence is shown in blue while the non-complementary overhangs are shown in red colour.

Figure 3.9

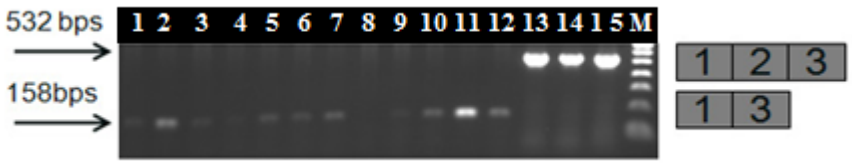

Figure 3.9: Demonstration of myostatin exon 2 skipping in C2C12 cell culture following treatment with a range of leashed PMO lipoplexes. C2C12 cell cultures treated with a range of leashed PMOs in lipoplex form with Lipofectamine™ 2000 exhibited skipping of exon 2 in myostatin mRNA. RT PCR was performed on 1µg mRNA from C2C12 cells treated with 250nM PMOs (designed on the basis of the most effective 2'OMePS sequences: A3, B3, C3 and D3) for a period of 24 hours. Transfections were performed in triplicate and RT PCR products were loaded on 1.2% agarose gel as follow: Tracks 1-3: PMO-A; Tracks 4-6: PMO-B; Tracks 7-9; PMO C; Tracks 10-12; PMO-D; Tracks 13-15 : Lipofectamine™ 2000-treated control; Track marked 'M': Size marker, HyperLadder IV

Figure 3.10

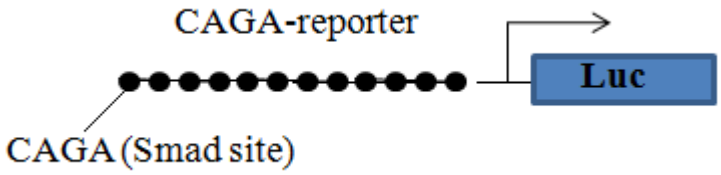

Figure 3.10: A diagrammatic representation of a Smad2 dependent reporter with a 12 times repetition of Samd2-binding site (CAGA) that further controls the expression of a firefly luciferase (Adapted from (Sartori *et al.*, 2009)).

Figure 3.11

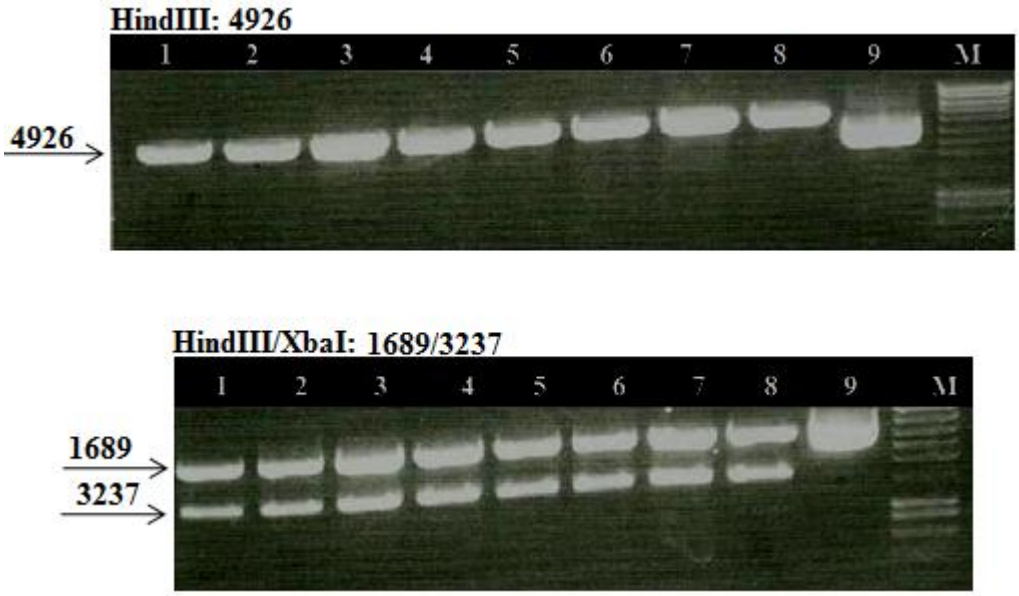

Figure 3.11: Restriction digestion for confirmation of CAGA plasmid structure. For purification of pGL3 plasmid DNA containing $(CAGA)_{12}$-luc, E.coli transfections were carried out with the reporter plasmid and ampicillin selection was performed. The competent colonies were then picked and a mini prep carried out for the same. In order to verify plasmid structure, restriction digestion was performed. For linear digestion only Xba1 was used whereas for double digestion, HindIII and Xba1 were used. The expected length of the PCR product for linear digestion with Hind III was 4926 bps and that for double digestion were 3237 bps and 1689 bps. Wells 1 to 8 in both the cases were loaded with eight different clones whereas ninth well was loaded with the uncut plasmid. Marker used was HyperLadder I.

C2C12 cells were treated with leashed PMO-D in serum-free media and incubated at 37ºC for 24 hours and 48 hours in different 6-well culture dishes. As controls, C2C12 cells were treated with just the leash in the presence of Lipofectamine™ 2000. The conditioned media from the cells was harvested after 24 hours and 48 hours. A204 cells were transfected with pGL3-$(CAGA)_{12}$-luc and after 48 hours were plated in opaque 96-well plates compatible for luminometer. Conditioned media from treated and control C2C12 cells was added to the pGL3-$(CAGA)_{12}$-luc-transfected A204 cells and plates incubated for 4-6 hours at 37ºC. After the incubation, the assay reagent from the Steady-Glo™ luciferase kit was added to the cells and plates read in a luminometer. The results depicted no significant change in the biological activity of the treated cells compared to the control cells after 24 hours measured as the Relative Light Units (RLU) although there was a trend towards decrease in luciferase signal in case of PMO-treated cells compared to the control cells. After 48 hours, the luciferase expression was significantly decreased for treated cells ($p=0.0111$) compared to the control cells as shown in **Figure 3.13**. Therefore, myostatin exon skipping in a mouse muscle cell line resulted in reduced biological activity of the treated cells compared to the control cells as shown by lower luciferase expression due to decrease in the TGF-β responsiveness.

The amount of myostatin present in the cells after PMO-treatment compared to the control cells was calculated from the myostatin standard curve (**Figure 3.14**). The PMO sequence used for this study (PMO-D) induced efficient skipping *in vitro* and also resulted in a significant increase in proliferation of treated cells. It also maps in a region totally conserved between mouse and human myostatin. The mean value of Relative light units (RLUs) obtained for PMO-D-treated cells was 289 and for control cells was 453. From the standard curve equation ($y = 18.62x + 215.2$), the amount of myostatin for PMO-treated cells was calculated to be 3.96 ng/ml and for control cells was calculated to be 12.77 ng/ml. Therefore, the AO-treated cells showed a 68.9% decrease in the biological activity dependent upon TGF-β signalling pathway after AO-induced exon skipping of myostatin. Controls had no myostatin treatment and the mean RLU values from controls were subtracted from the mean RLU values of treated cells.

Figure 3.12

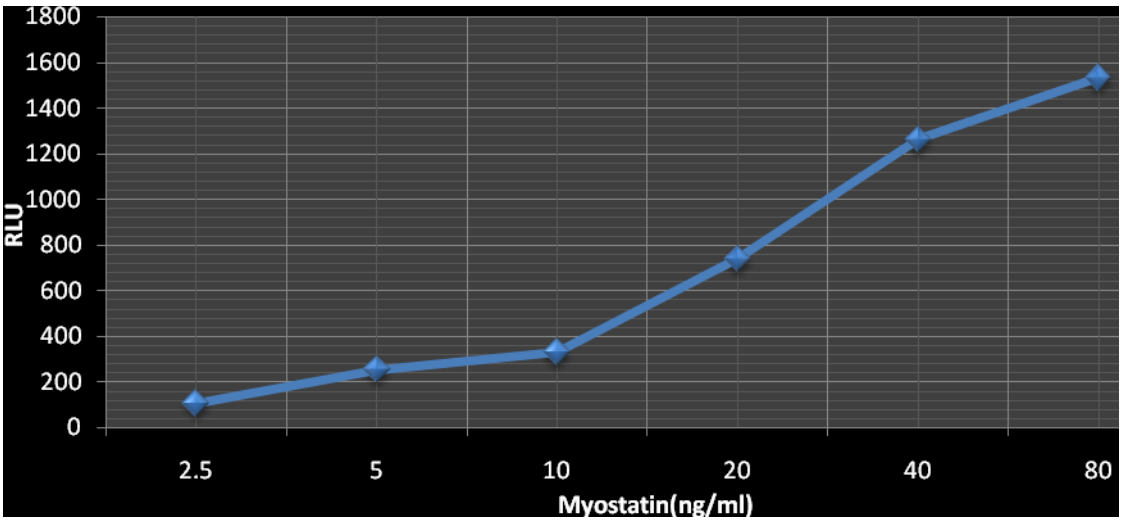

Figure 3.12: Myostatin dose response curve: A204 cells were transfected with pGL3-$(CAGA)_{12}$-luc and put in serum-free media 24 hours prior to the addition of myostatin. Transfected A204 cells were incubated with different myostatin dilutions (2.5 ng/ml; 5 ng/ml; 10ng/ml; 20 ng/ml; 40 ng/ml and 80 ng/ml) for 4 hours in serum-free media. After 4 incubation, luciferase assay was performed using Steady-Glo luciferase kit by adding 100µL of assay reagent to each well including the controls with no myostatin. After five minutes following the addition of assay reagent, the plate was read using a luminometer and mean of the background from the wells without any myostatin was subtracted from the mean of luminescence from different myostatin dilution replicates. A standard curve after subtracting background was then plotted for relative light units (RLU) against myostatin concentration. The assay was done in eight replicates for each myostatin dilution.

Figure 3.13

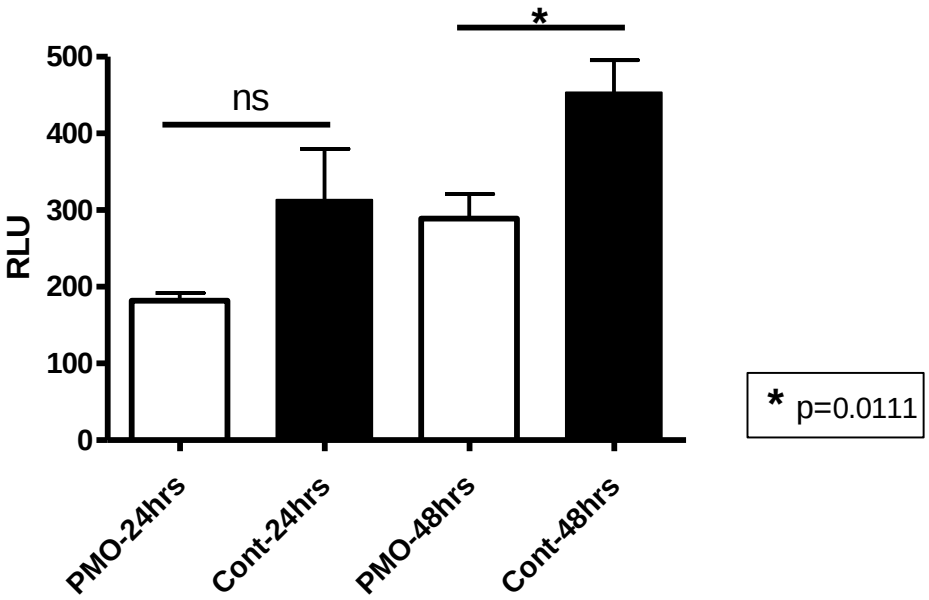

Figure 3.13: Reporter assay for estimation of biological activity of C2C12 cells after treatment with leashed-PMO-D to skip myostatin exon 2. C2C12 cells were transfected with leashed PMO-D and the conditioned C2C12 media was assayed on pGL3-$(CAGA)_{12}$-luc-transfected A204 cells after 24 hours and 48 hours of transfection. Each transfection was done in eight replicates; p=0.0111; *two-tailed t-test* with standard error of mean.

Figure 3.14

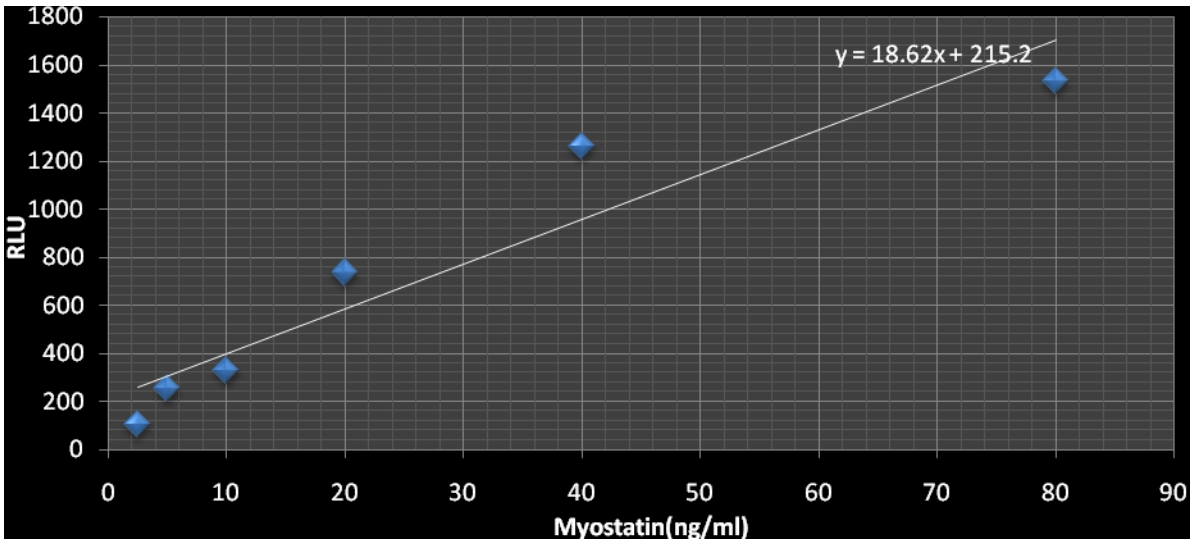

Figure 3.14: Estimation of the reduction in the amount of myostatin following PMO treatment. The mean RLU values for conditioned media from PMO-D-treated and control C2C12 cells (for the 48 hours time point) assayed on the reporter plasmid-transfected A204 cells were substituted in the equation obtained from the myostatin standard curve and amount of change in myostatin concentration was calculated.

3.4. Discussion

This part of the study was aimed at designing antisense oligonucleotides targeting myostatin exon 2 and verification of the feasibility of this approach to downregulate the expression of myostatin mRNA in cell culture. Although targeting donor splice site, acceptor splice sites and branch point sequences has successfully led to exon exclusion including DMD exon skipping (Graham *et al.*, 2004b; Wilton & Fletcher, 2005a; Wilton *et al.*, 2002), some studies have suggested that targeting splice sites does not always induce exon skipping (Wilton *et al.*, 2006). These contain some consensus sequences common to many other genes; therefore there lies a possible risk of disrupting the splicing of non-specific genes (Aartsma-Rus *et al.*, 2009). Exon splicing enhancers (ESEs) motifs form the binding sites for SR-protein RNA domains and thus help the splicing machinery in exon recognition (Stojdl & Bell, 1999). As SR protein binding to ESEs is very crucial for exon inclusion, blocking the ESEs with antisense oligonucleotides is expected to result in exon skipping. Different software including RESCUE ESE (Burge *et al.*, 2002; Burge *et al.*, 2004), ESEFinder (Krainer *et al.*, 2003) and PESX (Chasin & Zhang, 2004) have been widely used to predict possible ESE sites for different SR domains in order to assist in designing AOs (Aartsma-Rus *et al.*, 2004a; van Deutekom *et al.*, 2002; van Deutekom *et al.*, 2003) and therefore the same programs were used for this study.

The results predicting the presence of ESEs and ESSs along the myostatin exon-2 pre-mRNA using the above mentioned three bioinformatics programs were aligned together. ESE finder generates different coloured bars based on the probability of presence of different SR protein domains in a particular region defining its location and score. An emphasis was laid on regions with clusters of various SR binding domains rather than isolated higher peaks. The regions picked up by ESE finder, Rescue ESE and PESX were overlapped to narrow down and identify common regions of ESE sites as predicted by each program. Therefore, four different regions were chosen in exon 2 mRNA of myostatin where there was a coincidence of overlapping output from all the three programs avoiding the areas of putative ESS as predicted by PESX. A set of three overlapping AOs in each of these four regions were designed.

2'OMePS chemistry was used for the preliminary tissue culture studies because of the advantages of cheap and easy synthesis and ease of use due to charged backbone

over the uncharged PMO chemistry (Agrawal, 1999; Sazani *et al.*, 2002b). RNA from all the C2C12 cells transfected with twelve different 2'OMePS AO sequences showed skipped myostatin exon 2 as demonstrated by RT-PCR (Figure 3.6) along with the full length product. A study to test the AO sequences which seem to have weaker or no biological activity at all from these algorithm predictions would be able to validate further the integrity of our method of AO sequence selection. As myostatin has been established to be a negative regulator of muscle mass growth and differentiation (Grobet *et al.*, 1997; McPherron *et al.*, 1997; Szabo *et al.*, 1998), a decrease in its level is expected to result in enhanced proliferative capacity of muscle cells (Thomas *et al.*, 2000; Zhu *et al.*, 2000). Therefore, a colorimetric proliferation assay based on the principle of bioreduction of a tetrazolium compound by viable cells gives a quantitative measure of living cells present in a system (Berridge & Tan, 1993). On performing this assay on cells treated with four different AOs (one from each of the four sets based on RT PCR results), it was observed that the cells treated with AO-A3 showed increased proliferation compared to control cells ($p<0.01$), treatment with AOs B3 and D3 also showed an increased cell proliferation ($p<0.05$), whereas AO-C3 did not lead to a significant increase in level of proliferation compared to the control cells.

Exon skipping is dependent upon the AO's ability to reach nucleus and interfere with the spliceosome machinery. PMO chemistry has high nuclease resistance (Summerton & Weller, 1997) but due to uncharged background they cannot be delivered efficiently across cells using cationic liposomes. Therefore, they need to be used at very high concentrations (Sazani *et al.*, 2001; Suwanmanee *et al.*, 2002). Thus, an anionic single-stranded nucleic acid molecule called 'leash' was annealed to the PMO in order to mediate complex formation of PMO with the cationic transfection reagent. Various parameters including length of the annealing leash, extent and position of non-complementary overhangs and chemistry have been studied by other researchers. It is important for the leash to have enough stability to be delivered to the nucleus and also to retain some nuclease liability to liberate PMO from PMO: leash duplex. In order to maintain a balance between resistance and susceptibility to degradation, various chemistries have been studied (Gebski *et al.*, 2003). Presence of non-complementary overhangs particularly at 5'end has been shown to increase accessibility of nucleases which liberate the PMO from the leash (Morcos, 2001). Out of all the different leashes tested, the one with phosphodiester complementary region and phosphorothioate

overhangs performed much better than the others to induce exon skipping. Therefore, we used the same leash chemistry in our studies. Four different 20-mer 2'OMePS AO sequences were used as the basis for design and synthesis of four PMO sequences. All the PMOs linked to their respective leashes resulted in induction of exon 2 skipping of myostatin mRNA and therefore showed the feasibility of the approach with two different AO chemistries.

A luciferase reporter assay has been used to study the myostatin inhibition effect of myostatin propeptide as well as that of myostatin neutralizing antibody JA16 in terms of a decrease in Smad binding to TGF-β responsive elements called CAGA boxes (Dennler *et al.*, 1998); (Thies *et al.*, 2001; Whittemore *et al.*, 2003). A dose-response curve was prepared using different dilutions of recombinant mouse myostatin using human rhabdomyosarcoma cell line, A204 transfected with pGL3-$(CAGA)_{12}$-luc. When conditioned media from C2C12 cells treated with PMO-D was assayed on the A204 cells transfected with reporter plasmid containing Smad-binding site (CAGA) and luminescence was recorded, there was found to be a significant decrease ($p=0.011$) in the luciferase read out after 48 hours in case of medium from treated C2C12 cells compared to the control cells. This indicates a decrease in the transcriptional activity of endogenous Smad proteins which are crucial for TGF-β-mediated signal transduction (Dennler *et al.*, 1998). Therefore, inhibition of myostatin by exon skipping results in reduced biological activity related to modulation of myostatin pathway. This study thus confirms the reported results for myostatin blockade using dominant negative ActRIIB in human myoblasts (Fakhfakh *et al.*, 2011), myostatin-neutralizing antibody, JA16 (Whittemore *et al.*, 2003) and myostatin propeptide (Thies *et al.*, 2001) showing a decrease in Smad2 transcriptional activity and thus antagonizing biological activity. When the mean RLU values from the reporter assay for PMO-D treated cells were substituted in the myostatin standard curve equation, there was found to be a decrease in myostatin concentration in treated samples relative to the control cells by 68.9%. All these results were evident of skipping of myostatin exon 2 *in vitro* using two different chemistries along with modulation of proliferative capacity as well as alteration of myostatin signalling pathway of AO-treated cells. These results paved a path for the progression of this study *in vivo* in order to confirm the applicability of antisense-mediated exon skipping of myostatin in animals and for studying various aspects that

would determine the use of this strategy for therapeutic use in human musculoskeletal disorders.

CHAPTER 4

ANTISENSE OLIGONUCLEOTIDE-MEDIATED MYOSTATIN EXON SKIPPING IN WILD TYPE MICE

4.1. Introduction

Having demonstrated the capability of the designed AOs to induce myostatin exon 2 skipping in cell culture, it was important to investigate and establish their efficacy *in vivo* to determine their therapeutic potential. As an *in vivo* proof-of-concept study, intramuscular injection of 2'OMePS AOs targeting exon 23 mutation in *mdx* mouse (dystrophin-deficient mouse with a nonsense mutation in exon 23) resulted in dystrophin expression restoration for three months along with restoration of dystrophin-associated proteins and improvement in function of the treated muscle (Gebski *et al.*, 2003).

Selecting two AOs from *in vitro* studies based on efficacy and availability, an experiment was set up to test these sequences for their potential to induce myostatin exon skipping in wild type mice and to demonstrate the feasibility of this approach *in vivo*. PMOs have been proposed to have better stability in biological systems along with efficient exhibition of exon skipping (Hudziak *et al.*, 1996; Summerton *et al.*, 1997) but in their unmodified form, have not been very successfully delivered into normal muscle but only into damaged leaky muscle (Alter *et al.*, 2006). As discussed before, the delivery of naked PMO in a tissue culture system requires the use of complementary charged sequences and specific low-serum growth conditions (Morcos, 2007). Among several issues that pose difficulty in using unconjugated PMOs in an animal disease model is the inability of the PMOs to enter the cells and therefore they are rapidly eliminated from the circulation by the kidneys (Alter *et al.*, 2006). In a 7-week Dystrophin PMO study in mice, 100mg/Kg per week yielded only a restricted improvement in muscle function (Liang *et al.*, 2004). The doses required were even more for functional improvement as well as for the restoration of dystrophin to wild type levels in case of another study in dogs (Yokota *et al.*, 2009). Therefore, repeated large dose life-long treatment would be required for a therapeutic benefit. Variable exon skipping in different muscles and inconsistent dystrophin restoration from one section to the other of a muscle and also within the same section leads to a prediction that PMO is

taken up by leaky muscles only (Alter *et al.*, 2006; Wu *et al.*, 2008). Therefore, it becomes a necessity to look at a delivery system that along with being effective and safe also eliminates the need of high levels of dose and frequency. The conjugation of PMO with a dendrimeric octaguanidine (Vivo-PMO) significantly increases its delivery and efficiency compared to unmodified PMO (Morcos *et al.*, 2008);(Wu *et al.*, 2009). Restoration of dystrophin reading frame and expression of the protein in skeletal and cardiac muscles has been reported in *mdx* mice using Vivo-PMOs (Wu *et al.*, 2009).

When Vivo-PMO designed to correct the β-globin splice mutation was assessed for cytosolic and nuclear delivery efficiency, it was found that an intravenous dose of 12.5mg/Kg of body weight for four consecutive days in transgenic mice followed by sacrifice on fifth day led to almost complete splice correction in various tissues including skeletal muscle, diaphragm, liver and small intestine without any liver toxicity (Morcos *et al.*, 2008). Use of Vivo-PMO for dystrophin exon 23 skipping for a single intravenous injection at a dose of 6mg/Kg of the body weight resulted in higher level of dystrophin expression restoration compared to the same treatment with 300mg/Kg of body weight of unmodified PMO in *mdx* mice (Wu *et al.*, 2009). The same study showed that there was no toxicity conferred with the dosing regimen used.

In a repeated dose systemic study for dystrophin exon 23 skipping, 6mg/Kg of body weight of Vivo-PMO for exon 23 was injected intravenously into *mdx* mice for five times at biweekly intervals and muscles were harvested two weeks after last injection (Morcos *et al.*, 2008). Level of dystrophin expression was restored to normal levels in most of the fibres in skeletal muscle and about 40% restoration of dystrophin expression was also observed in cardiac muscle (Morcos *et al.*, 2008).

4.2 Aims of the chapter

The main aim of the study elaborated in this chapter was to determine the efficacy of designed and cell culture-tested AOs in animal system.

It was very crucial to investigate the time point at which the optimum effect of an antisense oligomer could be observed. Vivo-PMO was used with an aim of improving the delivery efficiency over unmodified PMO as previously reported (Morcos *et al.*, 2008; Wu *et al.*, 2009). Apart from looking at the optimum time point, it was also important to find out that once the Vivo-PMO has been administered at a

particular dose, how long does it take until any significant change is seen in the muscle weight and also to investigate how long does the effect last in terms of mRNA downregulation. This experiment was also aimed at determining the right dosing regimen to understand how frequently the Vivo-PMO needs to be administered in order to have a persistent effect.

Another objective of this study was to do a comparative analysis of the delivery efficiency of the recently developed PMO-conjugation systems with naked unconjugated PMO for targeting myostatin for exon skipping. Systemic delivery of conjugated myostatin PMO in wild type mice was another objective in this part of the study in order to treat the whole body rather than a specific muscle.

4.3. Results

4.3.1. Intramuscular treatment of wild type mice with the 2'OMePS AO effective in cell culture to induce myostatin exon skipping

On the basis of results obtained from the *in vitro* studies, two of the 2'OMePS (A2 and B3) were selected to verify their skipping efficacy *in vivo*. Each 2'OMePS was administered by single intramuscular injection (3nmol) into both tibialis anterior (TA) muscles of two 6 weeks old MF-1 mice (four muscles). As controls, normal saline was injected into both the TAs of two control animals. Two and four weeks after the single injections, TA muscles were recovered, pooled and analysed for the presence of myostatin exon 2 skipping in triplicates (of pooled RNA) by nested RT-PCR. RNA from control muscles was also pooled and nested RT-PCR was performed in duplicates. Both the 2'OMePS induced skipping after 2 weeks which persisted even after 4 weeks (**Figure 4.1**). A densitometric analysis of full-length and skipped products from nested RT-PCR analysis of RNA was performed to detect the efficacy of the tested 2'OMePS AOs. A2 produced 25.6% skipping and B3 showed 54.6% skipping after 2 weeks time point. However, after 4 weeks, A2 showed 48.6% skipping while B3 showed 24.5% skipping. From previous work on exon skipping for dystrophin, it is well established that the IM injections of AOs in undamaged muscles are not very efficient (Wu *et al.*, 2009). Although the skipping of myostatin exon 2 was evident, the effect was not sufficient to see any significant change in TA mass.

Figure 4.1

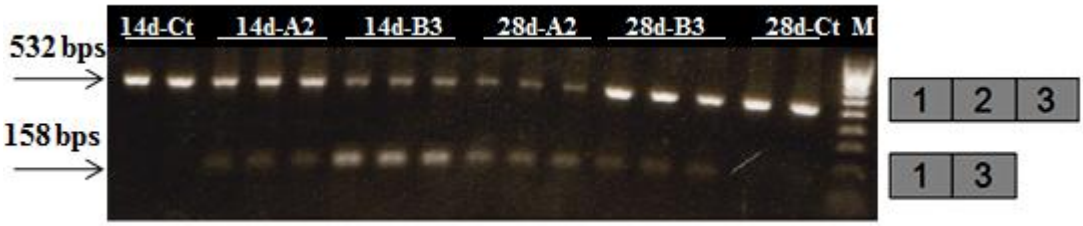

Figure 4.1: Exon skipping in mice following intramuscular injection of 2'OMePS AOs targeting myostatin exon 2. Oligomers A2 and B3 (3nmol) were administered by a single intramuscular injection into the tibialis anterior (TA) muscles of mice. Two and four weeks later, muscles were recovered, and RNA was extracted and analysed for the presence of myostatin exon 2 skipping by RT-PCR. Agarose ethidium bromide gel electrophoresis is shown for the products of RT PCR analysis. The upper and lower bands correspond to the normal full length product (532bp) and the exon 2 skipped product (158bp) respectively. Tracks 1 and 2: 14 days control (duplicates of two pooled samples); Tracks 3-5: 14 days A2-treated (triplicates of two pooled samples); Tracks 6-8: 14 days B3-treated (triplicates of two pooled samples); Tracks 9-11; 28 days A2-treated (triplicates of two pooled samples); Tracks 12-14: 28 days B3-treated (triplicates of two pooled samples); Tracks 15 and 16: 28 days control (duplicates of two pooled samples). The marker used is HyperLadder IV which was loaded in track marked 'M'.

4.3.2. Time course analysis for the treatment of wild type mice with octaguanidine linked PMOs (Vivo-PMO) for myostatin exon skipping by intramuscular injection

The aim of this experiment was to determine the level of myostatin mRNA down regulation at four different time points of one week, two weeks, four weeks and eight weeks (n=6 for treated and control mice for each time point). 6 weeks old wild type mice (C57BL/10) were injected into the TA with single intramuscular injection of 10µg (3nmol) of Vivo-PMO-D (PMO-D conjugated to octaguanidine dendrimer). Contralateral TA muscles were injected with same volume of normal saline as controls. Six mice were sacrificed after week 1, 2, 4 and 8 and both their TAs were weighed and embedded in OCT prior to being flash frozen in liquid nitrogen-cooled isopentane. Myostatin exon skipping was observed in the very first week which was still persistent after 8 weeks. There was no significant change in the weight of TA of treated and control muscles after week 1 and week 2. However, after 4 weeks, the treated muscles showed an increase in weight relative to the control muscle ($p=0.0404$). After 8 weeks as well there was a significant increase in the weight of treated TAs compared to the control TAs ($p=0.005$) as shown in **Figure 4.2**. In this figure, X-axis represents the time point, whereas, Y-axis represents the weight of TA muscles in milligrams. As each mouse had a contralateral control, normalizing the weight of treated as well as of control TA against the body weight would have given the same amount of change in muscle weight, so absolute muscle weights were used in the figure.

Myostatin skipping was observed in the very first week (**Figure 4.3**) which was still persistent after 8 weeks (**Figure 4.4 (a**). The level of skipping as quantified by densitometric analysis after week 1 was: 58.1% (±8.7 SD); week 2: 63.1% (±25.5 SD); week 4: 72.3% (±24.0 SD); week 8: 41% (±4.94 SD) (**Figure 4.4 (b**). Cross-sectional area (CSA) of the TA muscle fibres treated with Vivo-PMO-D and control muscles was calculated by staining tissue sections with laminin antibody and using SigmaScan Pro 5 software. Statistical analysis was performed using Chi-squared analysis for frequency distributions. No significant change in cross sectional area of the muscle fibres was observed (for week 4, $p>0.99$; week 8, $p>0.90$) (**Figure 4.5**). There was no significant change in the gross TA area of the treated and control muscles (two tailed t-test, for week 4, $p=0.124$; Week 8, $p=0.381$).

Figure 4.2

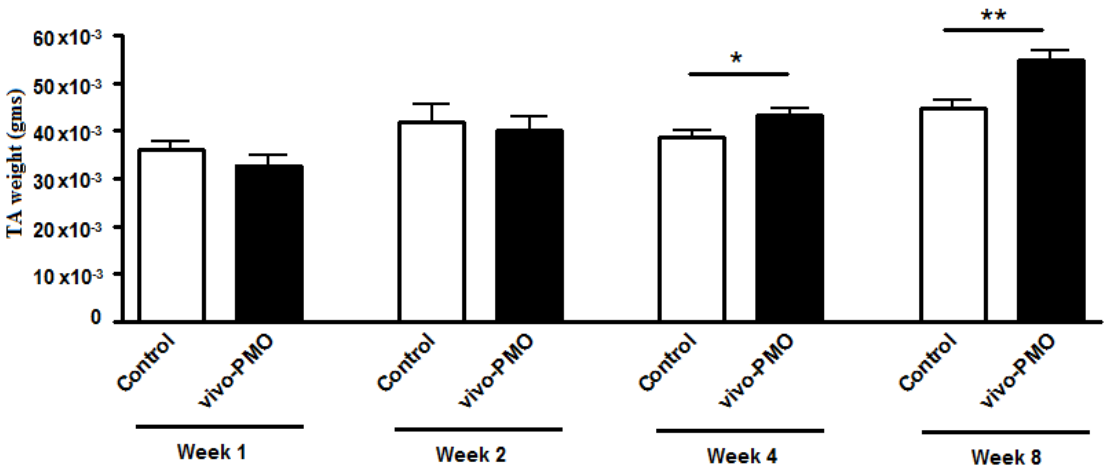

Figure 4.2: Change in the weight of TA muscles of wild type mice following single intramuscular injection of Vivo-PMO-D. Intramuscular injection of 10µg of Vivo-PMO-D was administered into the TA of four groups of six C57BL/10 mice each. The muscles were harvested after 1 week, 2 weeks, 4 weeks and 8 weeks. Contralateral control TA muscles were injected with same volume of normal saline. N=6 for control as well as for Vivo-PMO-D treatment. *p = 0.0404; **p = 0.005; two-tailed t-test with standard error of mean

Figure 4.3

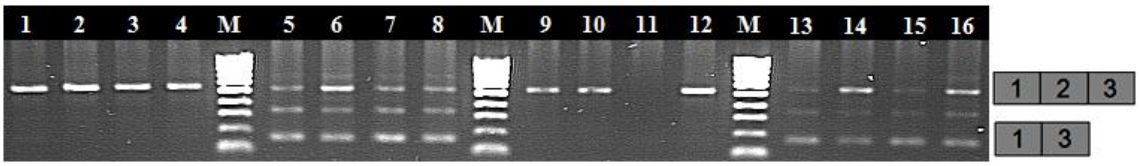

Figure 4.3: RT PCR analysis for time course study of intramuscular Vivo-PMO-D treatment in wild type mice for one and two weeks. Demonstration of myostatin exon 2 skipping following single intramuscular injection of 10µg of Vivo-PMO-D into the TA muscles of C57BL/10 mice. 6 mice were sacrificed after both week one and week two. A nested RT PCR was performed on 100ng mRNA from treated as well as control muscles (injected with normal saline) and the products were loaded on a 1.2% agarose gel. Different gel tracks were loaded with following samples: Tracks 1-4: Week 1 control TAs; Tracks 5-8: Week 1 Vivo-PMO-D treated TA; Tracks 9-12: Week 2 control TAs; Tracks 13-16: Week 2 Vivo-PMO-D treated TA. Tracks marked 'M' were loaded with the size marker HyperLadder IV. The faint shadow band of intermediate migration in some tracks was found upon sequencing to correspond to a product containing a partial sequence of exon 2 due to a cryptic 3' splice site downstream of the correct one. Percent skipping was calculated as Mean ± SD.

Figure 4.4 (a)

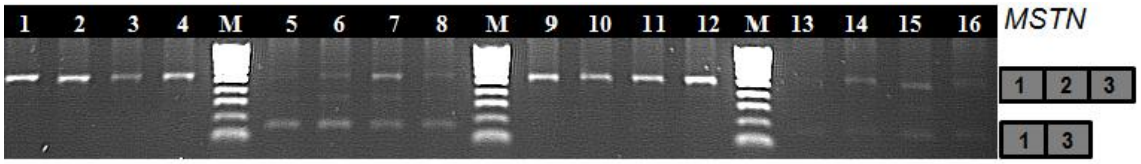

Figure 4.4 (a): RT PCR analysis for time course study of intramuscular Vivo-PMO-D treatment in wild type mice for four and eight weeks. The nested RT PCR products from mRNA of TA muscles treated with Vivo-PMO-D for four and eight weeks time points were loaded on a 1.2% agarose gel. The loading pattern of different samples was as following: Tracks 1-4: Week 4 control TAs; Tracks 5-8: Week 4 Vivo-PMO-D treated TAs; Tracks 9-12: Week 8 control TAs; Tracks 13-16: Week 8 Vivo-PMO-D treated TAs. Tracks marked 'M' were loaded with the size marker HyperLadder IV.

Figure 4.4 (b)

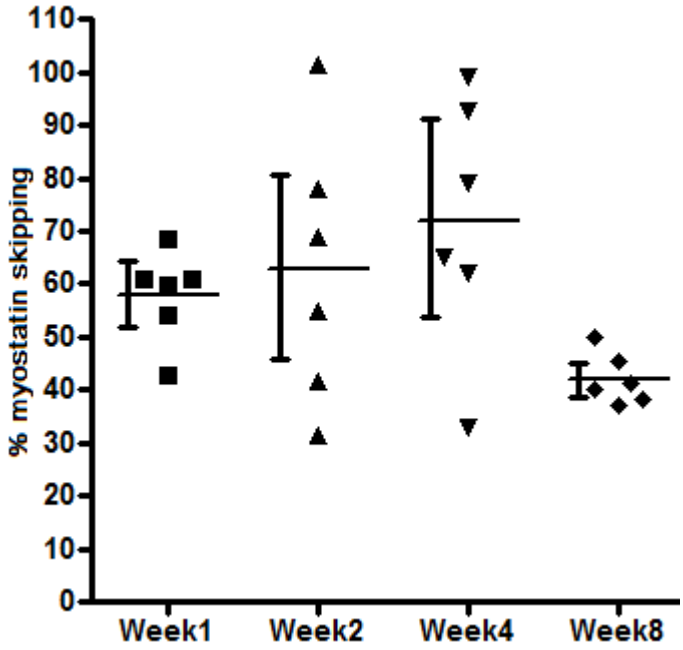

Figure 4.4(b): Scatter plot for time course study: Representation of level of myostatin exon skipping induced by Vivo-PMO in each mice of individual time point group (week1, week2, week4 and week8). Horizontal bars running through different ponts indicates mean values and the vertical bars represent mean±SD

Figure 4.5

Week 4

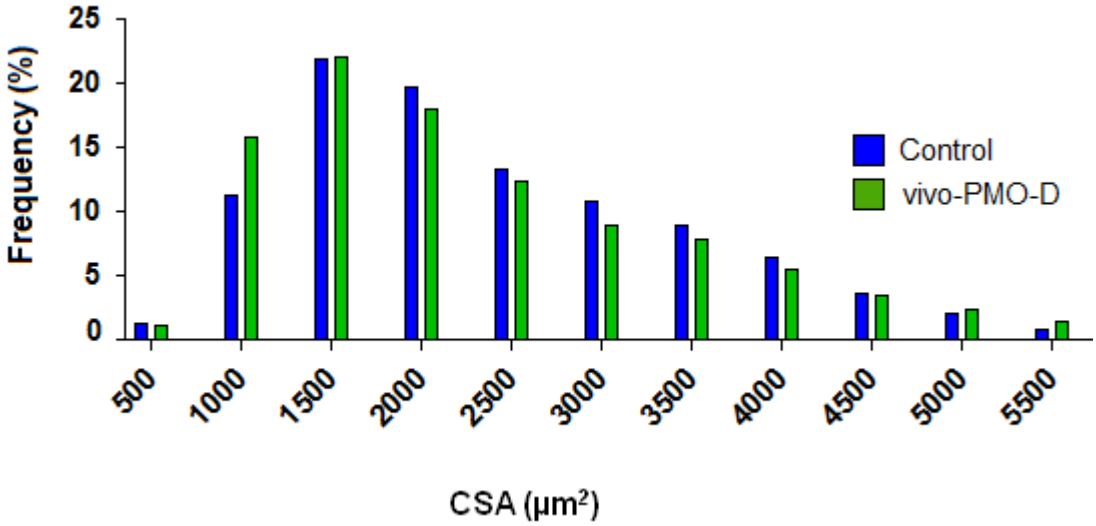

Week 8

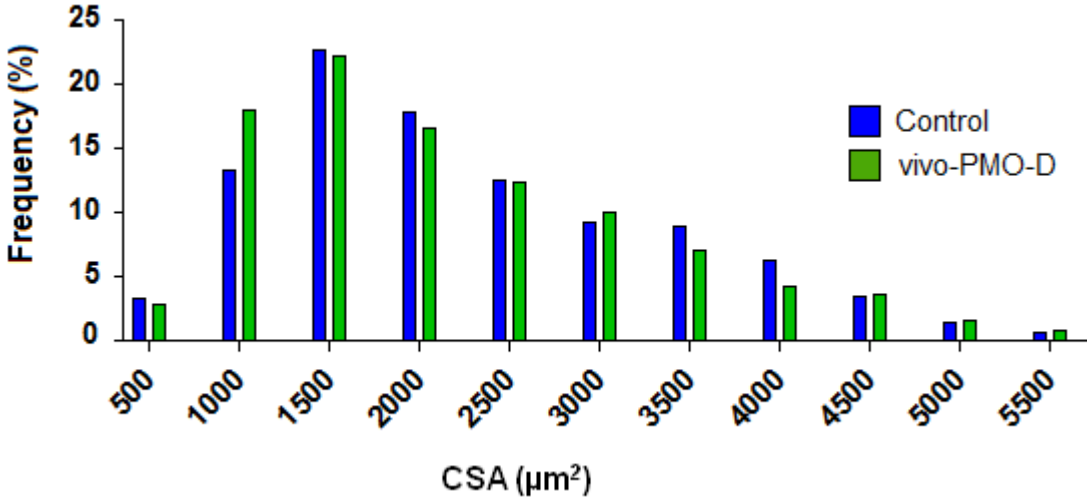

Figure 4.5: **Distribution of myofibre sizes in Vivo-PMO-D-treated TA muscles of wild type mice after four and eight weeks.** Cross-sectional area (CSA) of the TA muscle fibres treated with Vivo-PMO-D (Blue bars) and saline (Green bars) after 4 weeks and 8 weeks time points; n=6 for treated and control muscles.

4.3.3. Comparison of efficacies of myostatin exon 2 skipping induced by peptide conjugated PMOs (B-PMOs), Vivo-PMOs and unconjugated naked PMOs delivered by IM injection in wild type mice

The time-course study showed that a single intramuscular injection of Vivo-PMO-D into TA of wild type mice induced sustained myostatin exon 2 skipping from one week after the treatment up to the eighth week with a significant increase in muscle weight after four weeks. Therefore, a comparison of myostatin exon skipping efficacies of both arginine-rich cell penetrating peptide-conjugated PMO (B-PMO) which is abbreviated as $(RXRRBR)^2XB$-PMO; R= Arginine; X= 6-aminohexanoic acid; B= β-alanine (Yin *et al.*, 2009; Yin *et al.*, 2008) as well as dendrimeric octaguanidine conjugated morpholino (Vivo-PMO) (Wu *et al.*, 2009; Wu *et al.*, 2008) was done relative to the naked unconjugated PMO for a time point of eight weeks following single intramuscular injection.

Idividual TA muscles of twelve 6 weeks old wild type C57BL/10 mice were injected with saline (control) or with 3nmol (~10µg) of B-PMO-D, Vivo-PMO-D and unconjugated PMO-D, whereas the controls were treated with the same volume of normal saline into the TA muscle. Therefore, six muscles had each type of treatment Mice were weighed and sacrificed after eight weeks and TAs were weighed and embedded in OCT prior to being flash frozen in liquid nitrogen-cooled isopentane. Myostatin mRNA exon skipping was confirmed in the treated muscles by nested-RT-PCR. Densitometric analysis of the skipped and full length bands showed that there was 12.5% (±5.1 SD) myostatin exon 2 skipping in case of unconjugated PMO-D; 33.8% (±4.6 SD) exon skipping in case of Vivo-PMO-D and 43.5% (±9.5 SD) exon skipping in case of B-PMO-D (**Figure 4.6 (a)**). There was found to be a significant increase in the weights of TAs treated with B-PMO-D (p=0.04) compared to saline-treated controls. A significant increase in muscle weights was also recorded in case of Vivo-PMO-D treatment (p=0.01) compared to saline-treated controls as shown in **Figure 4.7**. However, unconjugated PMO-D did not lead to any significant change in the TA weight. The cross sectional area (CSA) of TA muscle fibres in Vivo-PMO-D-treated animals significantly increased ($0.04<p<0.05$) relative to the fibre CSA of control animals as shown in **Figure 4.8** (χ^2= 26.71; df =16). There was however no significant change in the fibre CSA of unconjugated PMO-D or B-PMO-D-treated muscles. Standard H&E (haematoxylin and eosin) staining was performed on transverse 10µm

sections of the muscles obtained using a cryostat. No changes in histology of control and treated muscles were revealed (**Figure 4.9**).

Figure 4.6 (a)

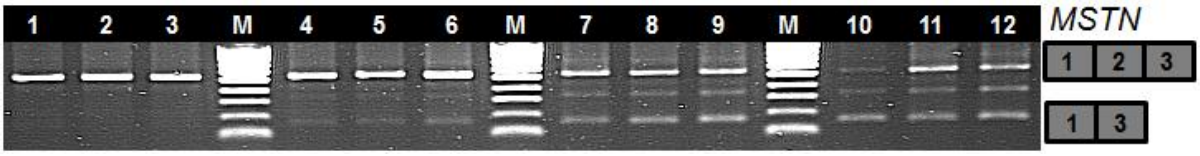

Figure 4.6 (a): Comparative analysis of myostatin exon 2 skipping efficacy of unconjugated PMO-D, Vivo-PMO-D and B-PMO-D. Different groups of C57BL/10 mice (three mice [six muscles] each group) were injected by an intramuscular injection of 3nmol of unconjugated PMO-D, Vivo-PMO-D and B-PMO-D into the TA muscles. Different treatment groups of mice were sacrificed after eight weeks time point and a nested RT PCR was performed on 100ng mRNA from treated as well as control muscles (injected with normal saline). The nested PCR products were loaded on a 1.2% agarose gel as following: Tracks 1-3: Control TAs; Tracks 4-6: Unconjugated PMO-D-treated TAs; Tracks 7-9: Vivo-PMO-D-treated TAs; Tracks 10-12: B-PMO-D-treated TAs. Tracks marked 'M' were loaded with the size marker HyperLadder IV. The faint shadow band of intermediate migration in some tracks was found upon sequencing to correspond to a product containing a partial sequence of exon 2 due to a cryptic 3' splice site downstream of the correct one. The figure shows some representative samples.

Figure 4.6(b)

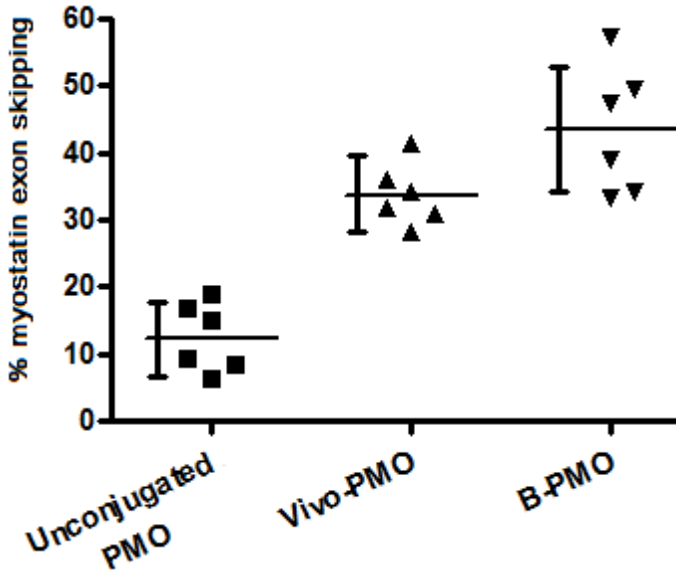

Figure 4.6 (b): Scatter plot for myostatin exon skipping analysis of unconjugated PMO, Vivo-PMO and B-PMO eight weeks following single IM injection (10µg each) into the TA of 6 weeks old C57BL/10 mice. Horizontal bars running through different ponts indicates mean values and the vertical bars represent mean±SD

Figure 4.7

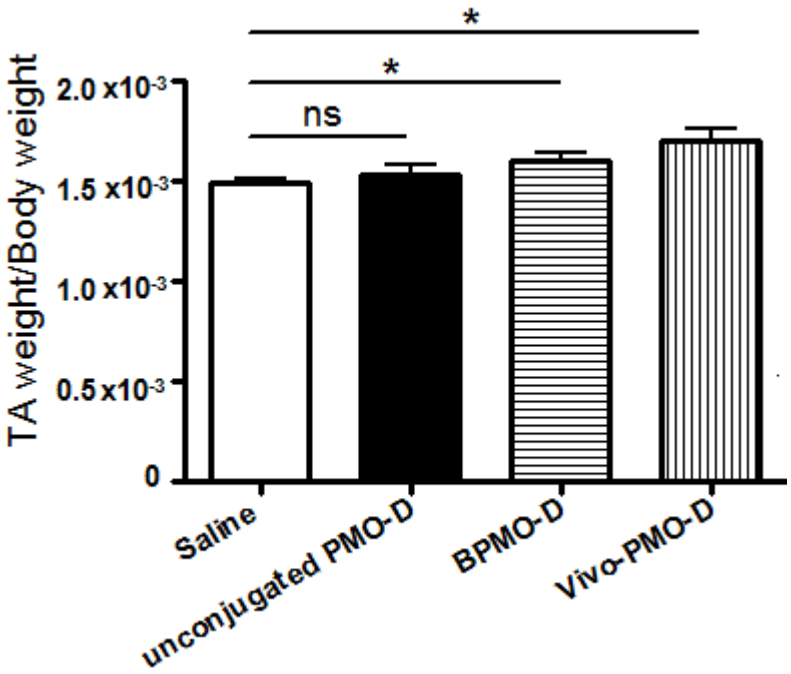

Figure 4.7: Effect of single intramuscular injection of unconjugated PMO-D, B-PMO-D or Vivo-PMO-D on the weight of the TA muscles in wild type mice. Single intramuscular injection of 3nmol (~10µg) of unconjugated PMO-D, B-PMO-D or Vivo-PMO-D was administered into the TA of C57BL10 mice and the mice were sacrificed after 8 weeks. Control TA muscles were injected with same volume of normal saline. N=6 for control as well as for treated muscles; ns= non significant change for Saline (Control) vs. Unconjugated PMO; *p for Saline (Control) vs. B-PMO-D = 0.04; *p for Saline (Control) vs. Vivo-PMO-D= 0.01. Two-tailed t-test was performed with standard error of mean.

Figure 4.8: Distribution of TA fibre diameter in wild type mice treated with unconjugated PMO-D, Vivo-PMO-D and B-PMO-D. The TA muscles of different groups of C57BL/10 mice were treated with 3nmol (~10µg) of unconjugated PMO-D, B-PMO-D and Vivo-PMO-D; Controls were treated with same volume of saline (n=6 for each treatment group) and mice were sacrificed after eight weeks. TA muscles were sectioned and immunostained with laminin in order to calculate fibre size distribution using SigmaScan Pro 5 software. In the top panel, green bars represent TA muscles treated with unconjugated PMO-D and blue bars represent TA muscles treated with normal saline; in the middle panel, red bars represent TA muscles treated with B-PMO-D and blue bars represent TA muscles treated with normal saline; in the bottom panel, yellow bars represent TA muscles treated with Vivo-PMO-D and the blue bars represent TA muscles treated with normal saline. p(unconjugated PMO-D vs. Saline) > 0.7; p(B-PMO-D vs. Saline) > 0.7; p(Vivo-PMO-D vs. Saline)<0.05

Figure 4.8

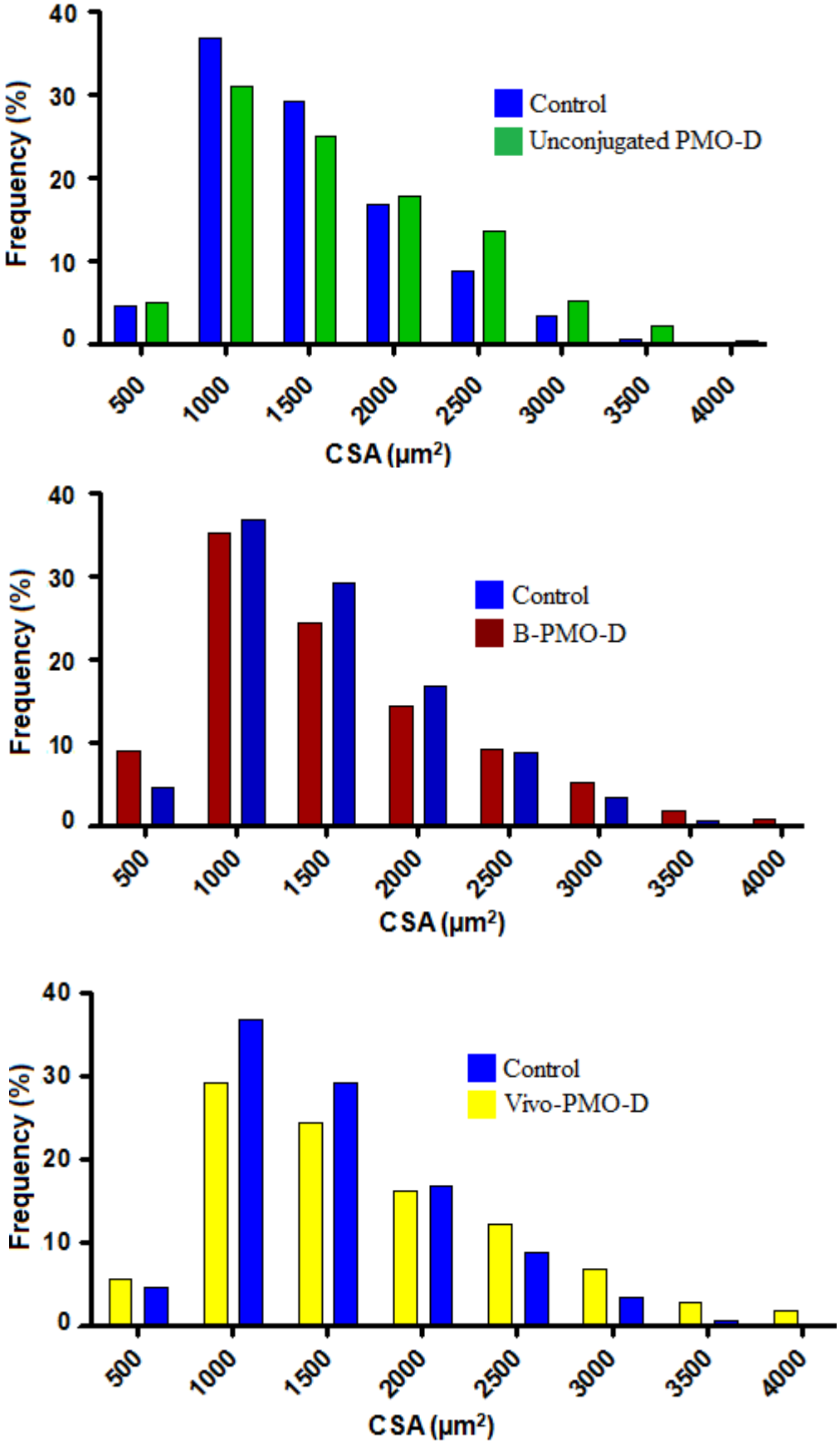
Frequency (%)
40
30
20
10
0
Control
Unconjugated PMO-D
500
1000
1500
2000
2500
3000
3500
4000
CSA (µm²)
Frequency (%)
Control
B-PMO-D
CSA (µm²)
Frequency (%)
Control
Vivo-PMO-D
CSA (µm²)

Figure 4.9: Histological staining of TA muscle cross sections from myostatin AO (Vivo-PMO-D, B-PMO-D and unconjugated PMO-D)-treated C57BL/10 mice. C57BL/10 mice injected with unconjugated PMO-D, B-PMO-D and Vivo-PMO-D were sacrificed after eight weeks and their TAs were cut into 10µm transverse sections using a cryostat. The slides with these sections were stained with haematoxylin and eosin. Scale bar represents 500µm.

Figure 4.9

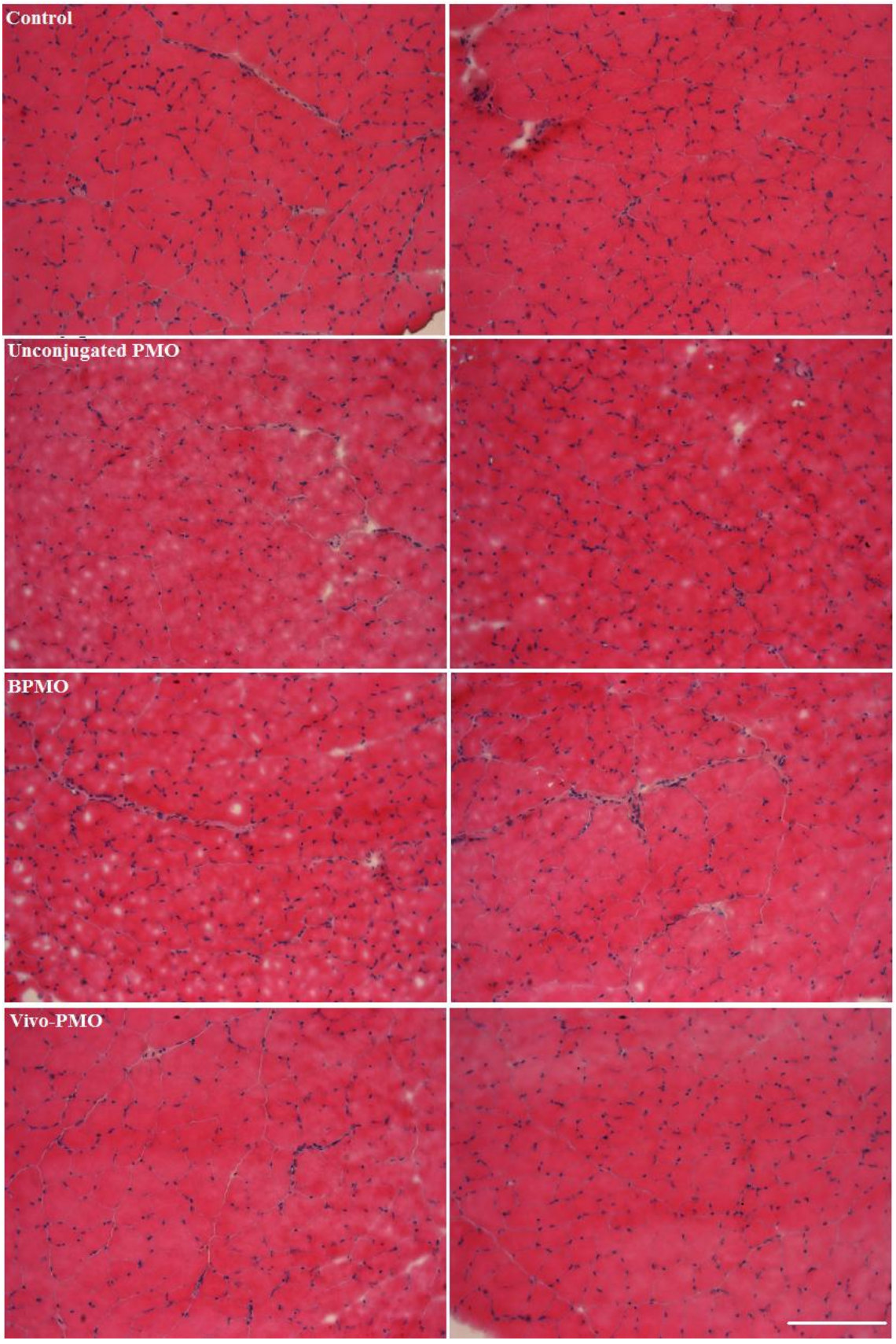

4.3.4. Systemic delivery of Vivo-PMO-D into wild type mice by IV injection

In order to determine the efficacy of Vivo-PMO-D by systemic delivery, weekly intravenous injections of Vivo-PMO-D for 5 weeks were administered into the tail vein of 6 weeks old C57BL/10 mice at 6mg/Kg of the body weight. The injections were performed by Dr Alberto Malerba. The whole body weight and weights of TA, Soleus and EDL were recorded 10 days after the last injection. Vivo-PMO-D induced 79.1% exon skipping of myostatin exon 2 in Soleus as determined by densitometric analysis on nested-RT PCR results of mRNA from treated muscle. A very low level of skipping was observed in EDL muscle (9%) (**Figure 4.10**). In accordance with the exon skipping data, treated soleus muscles showed a statistically significant increase in the weight ($p=0.0335$) as compared to the controls (**Figure 4.11**) whereas no significant change in weight of Vivo-PMO-D-treated EDL muscle was observed compared to the controls. The cross sectional area (CSA) of soleus muscle fibres in treated animals significantly increased ($p<0.0001$; with a significant shift on the distribution of CSA ($\chi^2= 38.34$; df =12) (**Figure 4.12** and **Figure 4.13**), while no change was observed in the fibre CSA of EDL muscle.

Figure 4.10

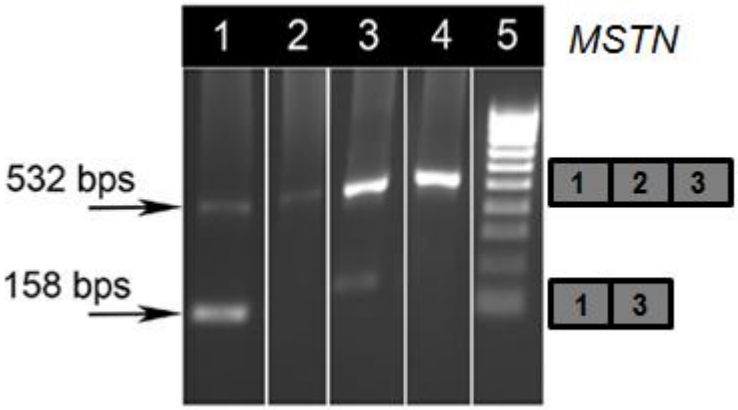

Figure 4.10: RT PCR analysis of mRNA from soleus and EDL muscles of wild type mice treated intravenously with Vivo-PMO-D. A nested RT-PCR was carried out on 1µg mRNA from soleus and EDL muscles of C57BL/10 mice treated intravenously with five weekly Vivo-PMO-D injections, and the products were resolved on a 1.2% agarose gel. Track 1: Vivo-PMO-D- treated soleus; Track 2: control soleus; Track 3: Vivo-PMO-D- treated EDL; Track 4: control EDL

Figure 4.11

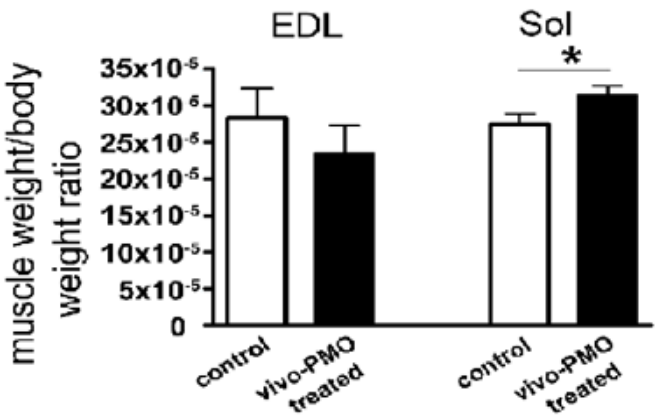

Figure 4.11: Effect of systemic delivery of Vivo-PMO-D on muscle mass of wild type mice. C57BL/10 mice were treated with 6mg/Kg of Vivo-PMO-D3 by five weekly intravenous injections and muscles were harvested for RNA extraction and immunohistology after 10 days of last injection. Weights of soleus muscles were significantly increased (p=0.034; n=6) whereas weights of EDL muscles showed no significant change.

Figure 4.12

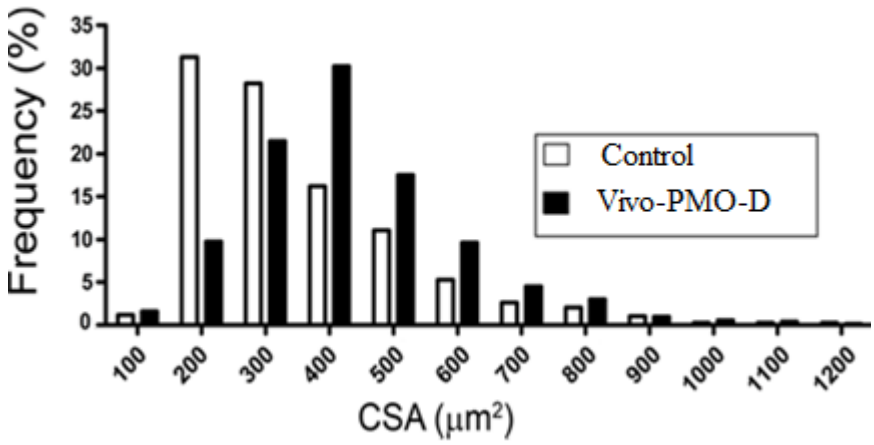

Figure 4.12: Distribution of myofibre sizes in soleus muscle of wild type mice treated intravenously with Vivo-PMO-D. Cross-sectional area (CSA) of the soleus muscle fibres of the C57BL/10 mice treated intravenously with Vivo-PMO (black bars) and control (open bars) was calculated by staining tissue sections with dystrophin antibody and using SigmaScan Pro 5 software. Statistical analysis was performed using Chi-squared analysis for frequency distributions.

Figure 4.13

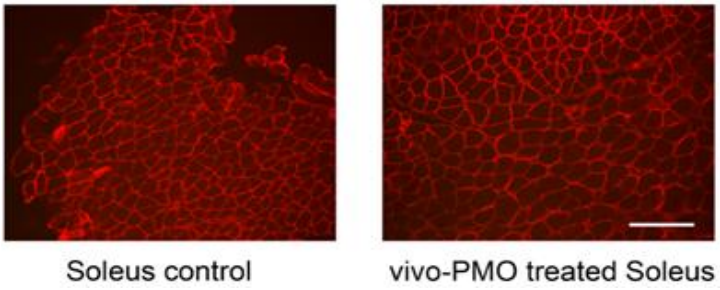

Figure 4.13: Immunohistological staining for soleus fibre cross sectional area analysis. Representative dystrophin immunohistology indicating increased myofibre CSA in Vivo-PMO-D-treated soleus muscle compared to control soleus muscle cryo-sections. Magnification bar represents 500 µm.

4.4. Discussion

With an aim of *in vivo* testing of the AO sequences successful in inducing myostatin exon 2 skipping in C2C12 cell culture, 2'OMePS AO were injected intramuscularly into the TAs of C57BL/10 mice. Although, 2'OMePS RNA sequences used were successful in bring about skipping of myostatin exon 2 in wild type mice, they did not have enough effect after four weeks following the single intramuscular injection into the TA of animals to result in any change in muscle mass. PMOs have been reported as more effective AO chemistry for exon skipping induction with longer lasting dystrophin expression restoration in *mdx* mice following intramuscular as well as intravenous administration compared to 2'OMePS chemistry (Fletcher *et al.*, 2006; Heemskerk *et al.*, 2009; Sazani *et al.*, 2002a). It is also reported in case of dystrophin exon skipping that intramuscular injections of unconjugated AOs are not quite efficient (Wu *et al.*, 2009). It has been shown that the level of dystrophin expression restoration and exon skipping induction in case of DMD by unconjugated AO chemistries is quite variable and therapeutic levels are attained only in skeletal muscle by the PMO chemistry (Alter *et al.*, 2006). Unconjugated PMO chemistry has not been able to induce effective dystrophin expression restoration in cardiac muscle, which has a massive direct impact in context of DMD due to death resulting mainly from cardiac and respiratory failure (Eagle *et al.*, 2007; Wagner *et al.*, 2007). Therefore, one of the most commonly used approach to enhance the effect of AOs and therefore the efficiency of exon skipping to have a reasonable therapeutic effect is to use certain delivery moieties which are capable of high charge-charge interactions with the membrane phospholipids (Futaki *et al.*, 2002; Wender *et al.*, 2000; Wu *et al.*, 2007).

Administration of a single intravenous injection of octaguanidine-linked morpholino oligomers (Vivo-PMO) targeting dystrophin exon 23 (VivoME23) led to a better expression restoration compared to the effect induced by unconjugated PMO (even at a concentration almost 50 times that of Vivo-PMO) in *mdx* mice (Wu *et al.*, 2009). In order to have a precise time line of efficient exon skipping induction a time course study was carried out to see how long does it actually take to induce a pronounced myostatin exon skipping following a single intramuscular Vivo PMO-D injection and for what duration does the effect of this single treatment persist. A 10µg injection of Vivo-PMO-D into the TA of C57BL/10 mice for a time course of one week, two weeks, four weeks and eight weeks was performed. The controls were treated with

an equal volume of normal saline. As shown by densitometric analysis, 58±8.7% myostatin exon 2 skipping was seen right after first week, followed by 63±25.5% skipping after two weeks, 72±24.0% skipping after four weeks and 41% skipping after eight weeks. There was however no change in the muscle weights after first and second week compared to the controls. A significant increase in TA weight was recorded after fourth week ($p=0.04$) and eighth week ($p=0.005$). When frequency distribution of TA fibre diameter was analyzed, there was no significant change in cross sectional area (CSA) of the fibres. Haematoxylin and Eosin staining was carried out to see if there was any influx of immune cells leading to inflammation resulting in an increase in Vivo-PMO-treated muscle weights. There was no significant change in the histology of treated as well as control muscles. Myostatin mRNA downregulation using antisense-mediated exon skipping in animals was demonstrated for the first time in these studies.

Out of the available PMO conjugation systems, Vivo-PMO and B-PMO both have been recently reported to have restored almost normal levels of dystrophin expression in skeletal muscle of *mdx* mice using different dosing regimens and routes of administration (Morcos *et al.*, 2008; Wu *et al.*, 2011; Yin *et al.*, 2008). It has been reported that B-PMO as well as Vivo-PMO have been used in repeated dose study for a period of three months without any obvious toxic effects (Wu *et al.*, 2009; Wu *et al.*, 2008; Yin *et al.*, 2008). Therefore, a comparative analysis of these two myostatin PMO-conjugations along with unmodified PMO was done as a key step for future myostatin exon skipping work. A single intramuscular injection of 10µg of Vivo-PMO-D, B-PMO-D and unconjugated naked PMO-D into the TA of different groups of C57BL/10 mice resulted in a significant increase in TA weights of the animals treated with B-PMO-D as well as with Vivo-PMO-D compared to controls following eight weeks of the treatment. Vivo-PMO-D treatment also resulted in a significant increase in the TA fibre diameter compared to the controls. There was, however, no change in the distribution of fibre CSA of muscles treated with B-PMO-D. H&E staining did not show any damage caused due to an immune response in the treated tissues by any of the treatments. It is likely that the dose used may have not been high enough to show a consistent significant effect in the case of unmodified PMO. These findings confirm better targeting and higher uptake of B-PMO and Vivo-PMO compared to unconjugated PMO.

A reported study of repeated biweekly injections of dystrophin exon 23-vivo-PMO (6mg/Kg of body weight) for five weeks resulted in dystrophin expression restoration to nearly normal levels with a pronounced effect in cardiac muscles as well (Morcos *et al.*, 2008). Based on these studies, a systemic study was undertaken with C57BL/10 mice using 6mg/Kg of body weight of Vivo-PMO-D targeted at myostatin exon 2 every week for five weeks. Conjugation of PMO to dendrimeric octaguanidine was successful in inducing exon skipping as well as in increasing the mass of Soleus muscle. This effect was however not seen in other muscles apart from EDL which showed a very low level of skipping and there was no change in the weight of the muscle. The reason for this could be anything ranging from dosing regimen, route of administration to time point at which the maximal effect can be seen. Perhaps it seems the dose and frequency of the Vivo-PMO for myostatin required to achieve significant level of change in weight of different muscles could probably be very different from dystrophin exon skipping system that was followed. Dystrophin is established to have longer half-life whereas myostatin seems to be more likely to need repeated dose of AOs to induce persistent exon skipping (Ghahramani Seno *et al.*, 2008). Also, the leaky muscles as in *mdx* mice would perhaps have a better effect compared to healthy muscle of wild type mice with a lack of porosity. Also, it has been proposed that a greater amount of ActRIIb are expressed on the surface of EDL muscle and that the intrinsic level of myostatin is greater in fast (myosin type IIb positive) myofibres (Foster *et al.*, 2009; Matsakas *et al.*, 2009).

A study has been reported to downregulate the expression of myostatin receptor AcRIIb using sh-RNA and restoration of quasi-dystrophin using a vectorized U7 exon skipping (U7-DYS). Co-expression of U7-DYS/sh-AcRIIb to restore quasi dystrophin expression and downregulate the expression of myostatin receptor in *mdx* mice showed force development comparable to C57BL/6 and much more enhanced as compared to U7-DYS or sh-AcRIIb expressed alone (Dumonceaux *et al.*, 2010). Therefore, it is quite crucial to determine the efficacy of a dual approach targeting myostatin and dystrophin to study the effects of myostatin inhibition and dystrophin restoration simultaneously in *mdx* mice from DMD point of view. U7-DYS/sh-AcRIIb study also suggests that in order to have a better understanding of how myostatin inhibition affects muscle force and strength, *in situ* contractile properties of the treated muscle need to be studied in future.

CHAPTER 5

ANTISENSE OLIGONUCLEOTIDE-MEDIATED MYOSTATIN AND DYSTROPHIN DUAL EXON SKIPPING IN *mdx* MICE

5.1. Introduction

As described before, *mdx* mice are murine models that have been widely used for DMD research (Coulton *et al.*, 1988; Hoffman *et al.*, 1987a; Morgan *et al.*, 1989). They were derived from C57BL10 colony resulting from spontaneous mutation leading to loss of dystrophin protein and very high levels of serum creatine kinase (Bulfield *et al.*, 1984). The use of AOs to induce exon skipping in dystrophin in order to restore its reading frame exhibited therapeutic potential of this approach for Duchenne muscular dystrophy *in vitro* (Aartsma-Rus *et al.*, 2002; Aartsma-Rus *et al.*, 2004b) as well as *in vivo* using *mdx* mice (Mann *et al.*, 2002). This led to subsequent clinical trials using 2'OMePS (van Deutekom *et al.*, 2007) and PMO (Kinali *et al.*, 2009) chemistries. However, due to severe DMD pathology including fibrosis and exhaustion of muscle regeneration capacity in DMD patients because of vigorous myoblast division in response to early degeneration of muscle cells (Blau *et al.*, 1985; Yoshida *et al.*, 1998), some sort of additional therapy is required along with dystrophin restoration. An example of such a combination therapy is the use of altered U7 snRNA for dystrophin restoration together with shRNA targeted against myostatin receptor, ActRIIb in AAV vector (Dumonceaux *et al.*, 2010). This study showed that there was an additional improvement in muscle physiology of *mdx* mice when myostatin pathway was inhibited along with restoration of dystrophin. However, there is the limitation of immune response related to viral vector system. Blocking myostatin signalling pathway with dominant negative ActRIIb (dnActRIIb), also added value to myoblast transplantation by increasing the proliferation of myoblasts and thus resulted in improvement of transplantation success (Fakhfakh *et al.*, 2011). AOs of 2'OMePS chemistry have recently been used to illustrate successful simultaneous induction of exon skipping of both myostatin and dystrophin (Kemaladewi *et al.*, 2011).

5.2 Aims of the chapter

In this chapter, simultaneous exon skipping of both myostatin and dystrophin was studied to determine the feasibility of this combination strategy to downregulate

myostatin expression and to correct dystrophin transcript in *mdx* mice. It is particularly important to use this combined approach because in DMD patients, severe muscle wasting and defective muscle regeneration can hamper the efficacy of dystrophin restoration on its own. Due to enormous muscle degeneration, myoblasts in DMD patients go through rigorous division in order to regenerate leading to saturation of muscle regeneration capacity (Blau *et al.*, 1985; Yoshida *et al.*, 1998). Different additional therapies have therefore been studied to accompany dystrophin expression restoration to surmount these issues. Myostatin inhibition being one of these strategies that can help reduce the muscle mass loss, an attempt was made to carry out dual exon skipping targeting dystrophin and myostatin genes at the same time. Two of the recently developed PMO conjugation systems namely B-PMO and Vivo-PMO were used and results were compared to see the effect in mouse model of DMD. A well established PMO sequence to target murine dystrophin exon 23 was used (Alter *et al.*, 2006; Fletcher *et al.*, 2006; Gebski *et al.*, 2003) along with PMO-D for myostatin exon 2 skipping, both in a B-PMO conjugation as well as in a Vivo-PMO complex.

5.3. Results

5.3.1. B-PMO-induced dual exon skipping of dystrophin and myostatin RNA in *mdx* mice following intramuscular injections of PMO combinations

Six weeks old *mdx* mice were treated with 3nmoles (~10µg) of single intramuscular injection of B-PMO-Dys (B-PMO for dystrophin exon 23 skipping) alone, B-PMO-D [named as B-PMO-Myo in this chapter to avoid confusion, so B-PMO-D and B-PMO-Myo are used interchangeably in this thesis for the same sequence of myostatin AO] alone and a cocktail of B-PMO-(Dys+Myo) (a total of 20µg) into the TA muscles. The control muscles were treated with the same volume of normal saline. There were six muscles per treatment and no contralateral controls. These injections were performed by Dr Graham McClorey at the Department of physiology, anatomy and genetics, University of Oxford. Mice were weighed and sacrificed after eight weeks and TAs were weighed and embedded in OCT prior to being flash frozen in liquid nitrogen-cooled isopentane. Efficiency of B-PMO AOs to induce exon skipping resulting in decrease in the level of myostatin expression at transcript level and reframing dystrophin was tested by RT-PCR. Myostatin exon skipping was confirmed in the treated muscles by nested-RT-PCR on the mRNA from treated samples as shown

in **Figure 5.1**. RT-PCR for dystrophin skipping induced by B-PMO-Dys is shown in **Figure 5.2**. Dual exon skipping induced by using a cocktail of both B-PMO-Myo and B-PMO-Dys is shown in **Figure 5.3 (a)**. Densitometric analysis of the skipped and full length bands showed that B-PMO-Myo alone induced 33% (±9.1 SD) skipping and B-PMO-Dys alone induced 56% (±14.4 SD) skipping. In case of animals treated with a cocktail of B-PMO-Myo and B-PMO-Dys, 65% (±11.3 SD) dystrophin skipping and 40% (± 6.0 SD) myostatin skipping was observed. These results showed the feasibility of the dual myostatin and dystrophin exon skipping mediated by B-PMO AOs without the possibility of interference with each other rather than their respective targets.

5.3.2. Effect of dystrophin and myostatin exon skipping induced by single intramuscular injection of B-PMOs on muscle weights of *mdx* mice

The muscle weights were normalized against the whole body weight for individual animals as there were no contralateral but separate controls. There was found to be a significant increase in the weights of TAs treated with B-PMO-Myo alone (p=0.03) compared to saline-treated controls as well as in the weights of TAs treated with a cocktail of B-PMO (Myo+Dys) (p=0.006) compared to saline-treated controls as shown in **Figure 5.4**, however, B-PMO-Dys on its own did not lead to any significant change in the TA weight.

Figure 5.1

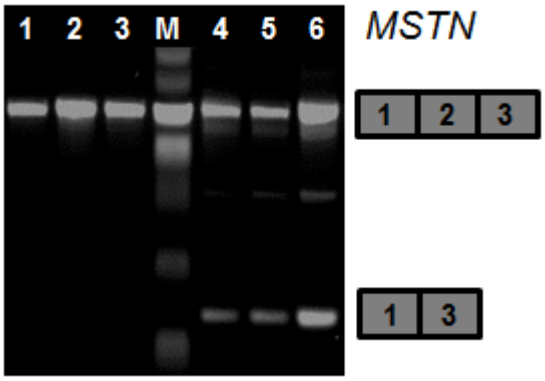

Figure 5.1: RT-PCR results from mRNA of B-PMO-treated TA muscle of *mdx* mice for myostatin exon skipping. Myostatin exon 2 skipping induced by B-PMO-Myo following single (10µg) intramuscular injection into the TA of *mdx* mice is shown. Mice were sacrificed after eight weeks and a nested RT PCR was performed on 100ng mRNA from treated as well as control muscles (injected with normal saline). The nested PCR products were loaded on a 1.2% agarose gel as following: Tracks 1-3: Control TAs; Tracks 4-6: B-PMO-Myo treated TAs. Tracks marked 'M' were loaded with the size marker HyperLadder IV. An intermediate faint band represents a cryptic 3' splice site downstream of the correct one as verified by sequencing. The figure shows some representative samples. Percent skipping was calculated as Mean±SD. *MSTN* represents myostatin.

Figure 5.2

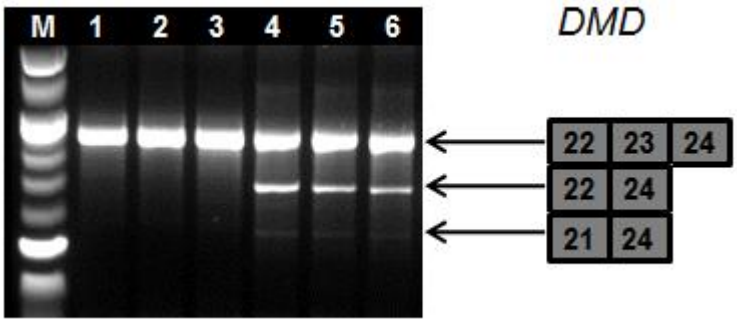

Figure 5.2: RT-PCR results from mRNA of B-PMO-treated TA muscle of *mdx* mice for dystrophin exon skipping. Dystrophin exon 23 skipping induced by B-PMO-Dys following a single (10µg) intramuscular injection into the TA of *mdx* mice is shown. Eight weeks post-injection, the mice were sacrificed and the TAs were harvested. The nested RT-PCR products were run on a 1.2% agarose gel as following: Tracks 1-3: Control TAs (injected with normal saline); Tracks 4-6: B-PMO-Dys-treated TAs. A shorter band apart from the exon 23-skipped band represents a transcript with exon 22/23 deletions as verified by sequencing. Pictures of gels with representative samples are shown. *DMD* represent dystrophin.

Figure 5.3 (a)

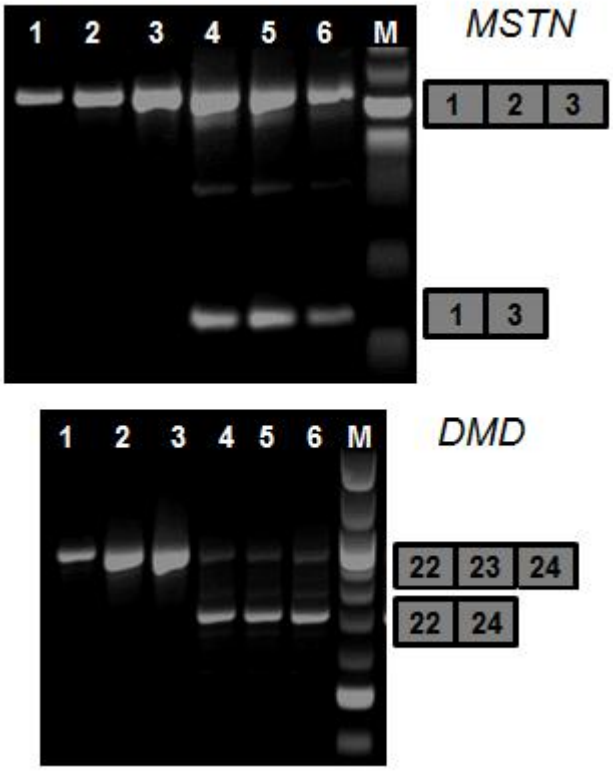

Figure 5.3 (a): Dual myostatin and dystrophin exon skipping in *mdx* mice. Myostatin exon 2 skipping and dystrophin exon 23 skipping induced by a cocktail of B-PMO-Myo (10µg) and B-PMO-Dys (10µg) following single intramuscular injection into the TA of *mdx* mice is shown. Mice were sacrificed after eight weeks and a nested RT PCR was performed on 100ng mRNA from treated as well as control muscles (injected with normal saline). The nested PCR products were loaded on a 1.2% agarose gel. In the top panel, Tracks 1-3: Controls; Tracks 4-6: B-PMO-Myo-treated TAs. In the bottom panel, Tracks 1-3: Controls; Tracks 4-6: B-PMO-Dys-treated TAs. Tracks marked 'M' were loaded with the size marker HyperLadder IV. The figure shows gels with representative samples; Densitometric analysis was performed on all the samples and average was calculated.

Figure 5.3 (b)

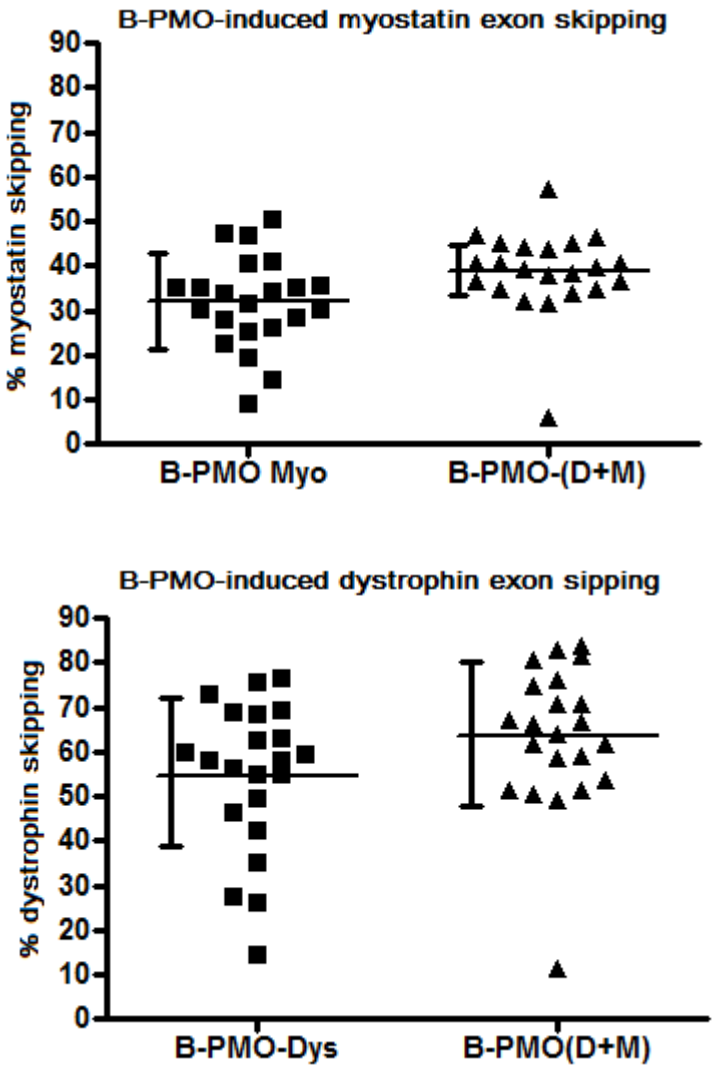

Figure 5.3 (b): Scatter plot for B-PMO-induced myostatin and dystrophin exon skipping levels eight weeks after single IM injections 3nmol (~10µg each) in the TA of mdx mice. A total of six muscles were treated per group. Multiple replicates (3-4) for each sample were loaded on the gel and then mean ± SD was calculated from the densitometric analysis. 'D+M' denotes cocktail of B-PMO-myostatin and B-PMO-dystrophin. Horizontal bars running through different ponts indicates mean values and the vertical bars represent mean±SD

Figure 5.4

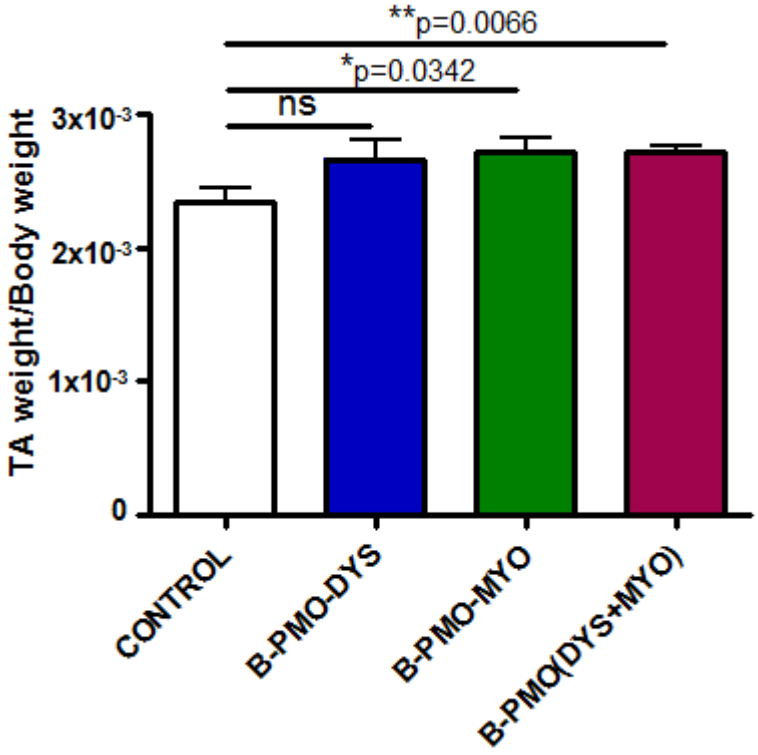

Figure 5.4: Effect of exon skipping induced by B-PMO-Myo and/or B-PMO-Dys on TA muscle weights of *mdx* mice following single intramuscular injection. Single intramuscular injection of 3nmol of each of B-PMO-Dys, B-PMO-Myo and B-PMO-(Dys+Myo) was administered into the TAs of different groups of *mdx* mice. Control TA muscles were injected with same volume of normal saline. Mice were sacrificed eight weeks after the injections were performed. N=6 for control as well as for treated muscles; ns= non significant change for Saline (Control) vs. B-PMO-Dys; **p* for Saline (Control) vs. B-PMO-Myo = 0.03; ***p* for Saline (Control) vs. B-PMO-(Dys+Myo) = 0.006. Two-tailed t-test was performed with standard error of mean.

5.3.3. Dystrophin expression restoration in *mdx* muscles following intramuscular B-PMO injections

Immunofluorescence staining of transverse TA muscle tissue sections was performed to detect the dystrophin protein expression and localization in *mdx* mice treated with B-PMO-Dys and a cocktail of B-PMO-Myo+Dys. Enhanced dystrophin expression detected by immunofluorescence in B-PMO-treated muscle sections compared to the control muscle sections can be seen as in **Figure 5.5**.

5.3.4. Effect of B-PMO induced myostatin and dystrophin dual exon skipping on size distribution of muscle fibres

The TA sections from each treatment group were stained with laminin and CSA of the fibres was calculated using SigmaScan Pro5 software followed by a chi-squared analysis on the data from different treatment groups. There was found to be no significant change in the TA fibre CSA distribution with either B-PMO-Myo or B-PMO-Dys or B-PMO-(Myo+Dys) (**Figure 5.6**); p (B-PMO-Dys vs. saline) >0.99; p (B-PMO-Myo vs. Saline) >0.99; p [B-PMO-(Dys+Myo) vs. Saline] >0.99.

5.3.5. Histological analysis of B-PMO-treated *mdx* muscles

Standard H&E (haematoxylin and eosin) staining was performed on transverse 10µm sections of the harvested muscles using a cryostat. The staining of the sections of tissue treated with B-PMO-Myo, B-PMO-Dys and a cocktail of B-PMO-Dys+Myo showed no damage to the muscle compared to untreated *mdx* mice (**Figure 5.7**).

Figure 5.5

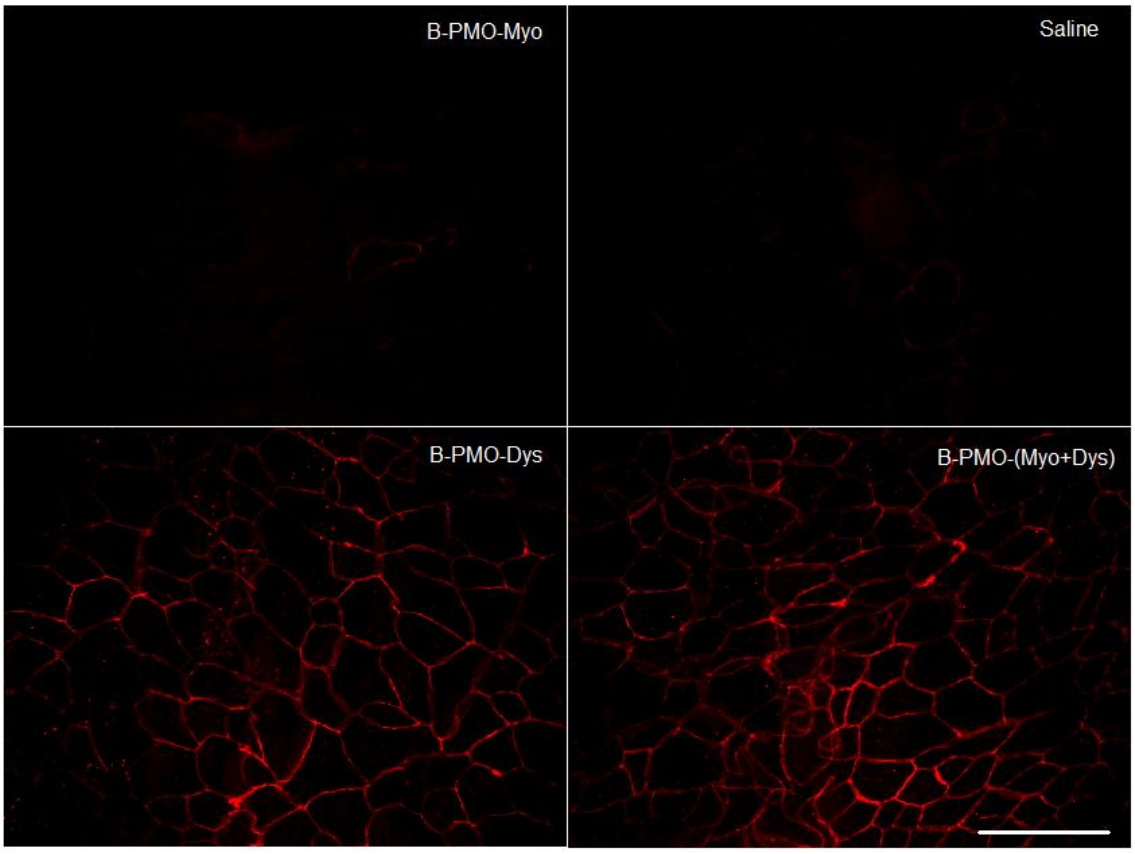

Figure 5.5: Dystrophin expression restoration in B-PMO-treated TA muscles of *mdx* mice. Immunohistochemical detection of dystrophin (red) in TA of the *mdx* mice treated with B-PMO-Dys and a cocktail of B-PMO-(Dys+Myo) is shown. *Mdx* mice treated with B-PMO-Myo alone and the ones with normal saline are the negative controls. Magnification bar represents 500µm.

Figure 5.6: TA fibre diameter distribution following B-PMO-Myo or/and B-PMO-Dys treatment in *mdx* mice. The TA muscles of *mdx* mice were treated with 3nmol (~10µg) of B-PMO-Myo; B-PMO-Dys; a cocktail of B-PMO-Dys+Myo (total 20µg); Controls were treated with same volume of saline and mice were sacrificed after eight weeks (n=6 each treatment). TA muscles were sectioned and immunostained with laminin in order to calculate fibre size distribution using SigmaScan Pro 5 software. In the top panel, green bars represent TA muscles treated with B-PMO-Myo and blue bars represent TA muscles treated with normal saline; in the middle panel, yellow bars represent TA muscles treated with B-PMO-Dys and blue bars represent TA muscles treated with normal saline; in the bottom panel, pink bars represent TA muscles treated with a cocktail of B-PMO-(Dys+Myo) and the blue bars represent TA muscles treated with normal saline. *p* (B-PMO-Dys vs. Saline) >0.99; *p* (B-PMO-Myo vs. Saline) >0.99; *p* [B-PMO-(Dys+Myo) vs. Saline] >0.99.

Figure 5.6

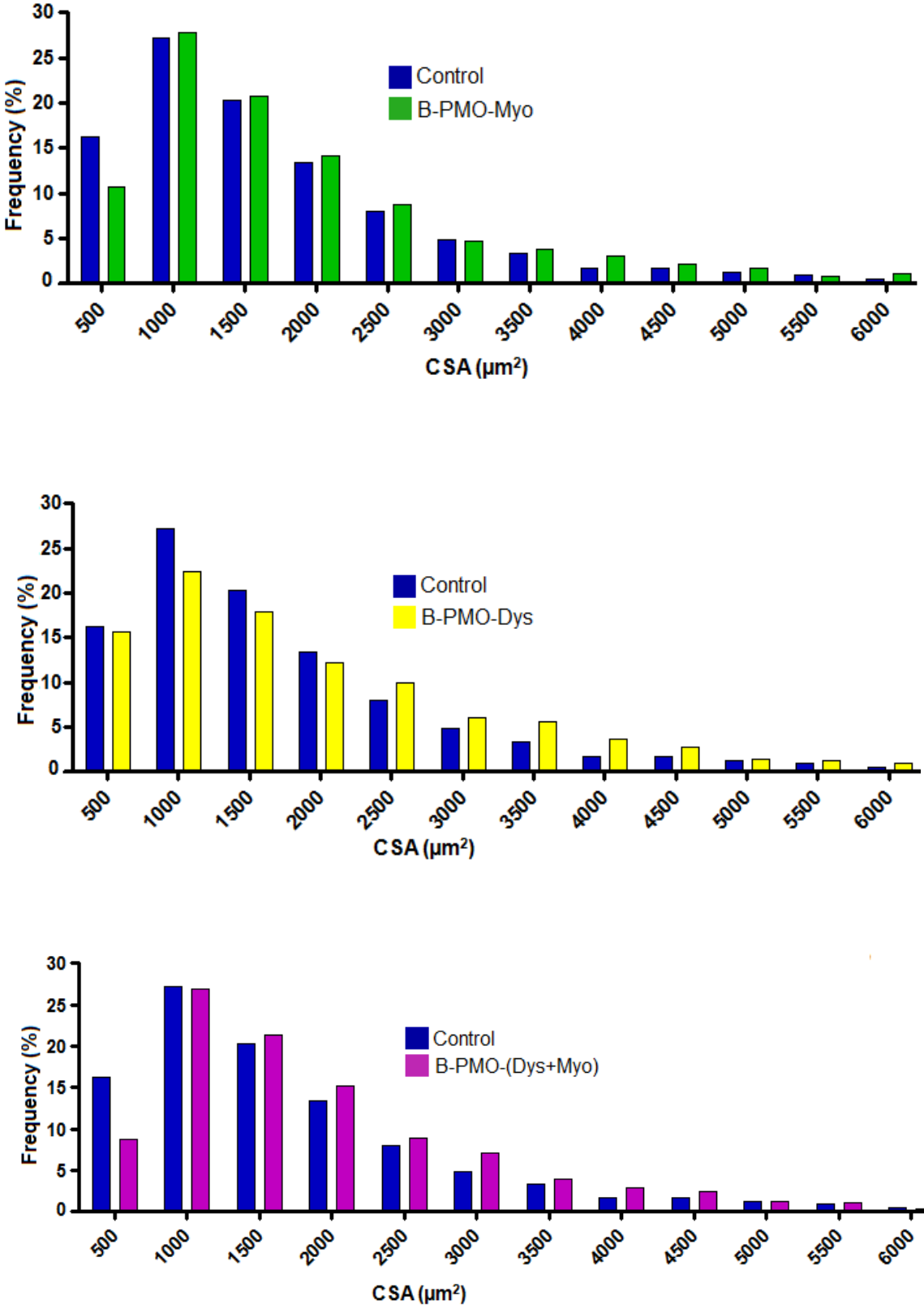
Frequency (%)
30
25
20
15
10
5
0
Control
B-PMO-Myo
500
1000
1500
2000
2500
3000
3500
4000
4500
5000
5500
6000
CSA (µm²)
Frequency (%)
Control
B-PMO-Dys
CSA (µm²)
Frequency (%)
Control
B-PMO-(Dys+Myo)
CSA (µm²)

Figure 5.7: **Histological analysis of B-PMO-treated and saline-treated TA muscle sections of *mdx* mice.** Haematoxylin and eosin staining of TA muscle transverse sections from *mdx* mice injected with B-PMO-Dys, B-PMO-Myo; a cocktail of B-PMO-(Dys+Myo) –a total of ~20 µg was performed. Representative pictures are shown. Magnification bar represents 500µm.

Figure 5.7

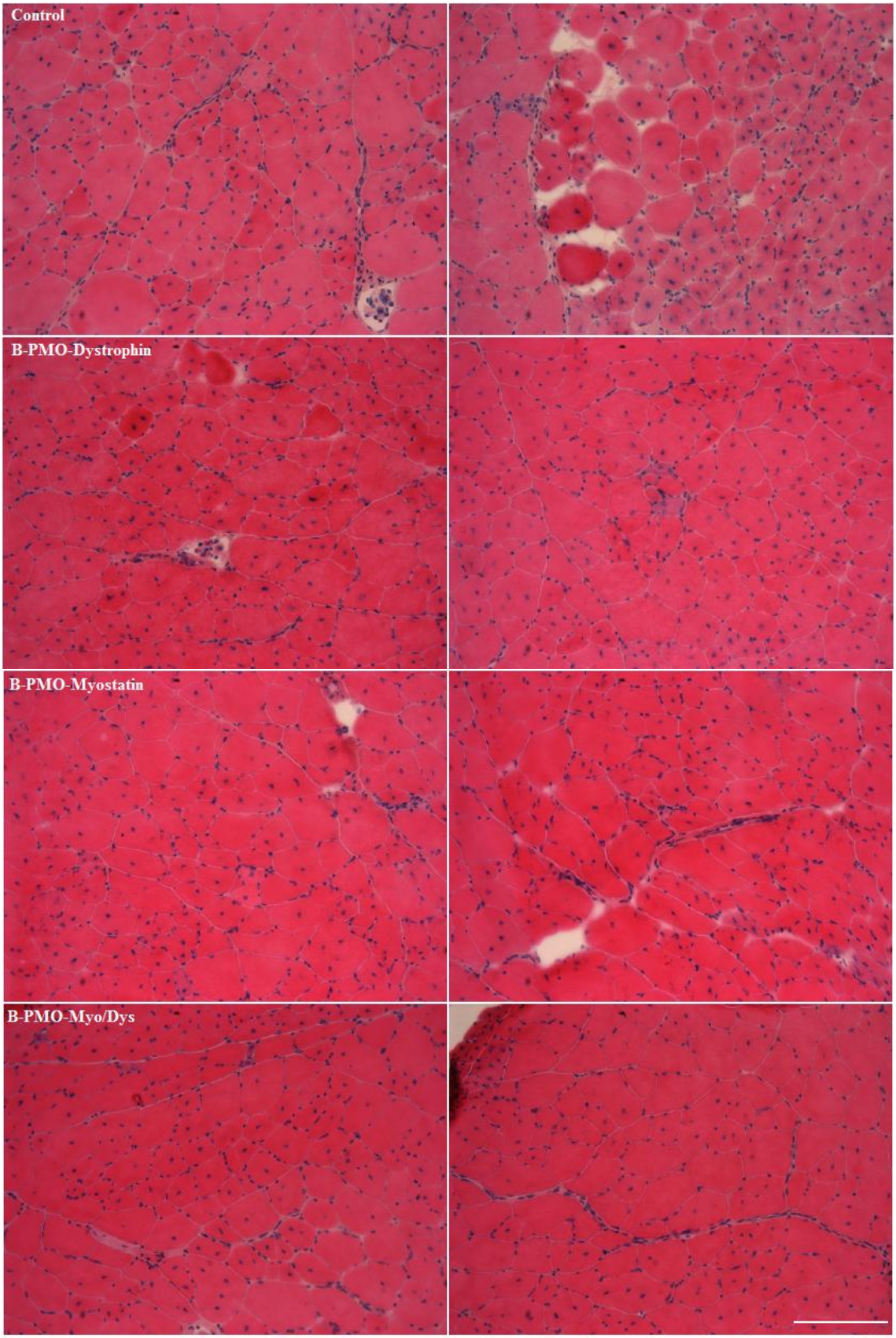

5.3.6. Vivo-PMO-induced dual exon skipping of dystrophin and myostatin RNA in *mdx* mice following intramuscular injections of PMO combinations

Single intramuscular injections of 3nmol (~10µg) of Vivo-PMO-Dys alone, Vivo-PMO-Myo alone and Vivo-PMO-(Myos+Dys) cocktail (a total of 20µg) were performed into the TAs of different groups of six weeks old *mdx* mice (no contralateral controls, 6 muscles per treatment). The controls were injected with the same volume of normal saline into the TA muscle. Mice were weighed and sacrificed after eight weeks and TAs were weighed and embedded in OCT prior to being flash frozen in liquid nitrogen-cooled isopentane. Myostatin exon skipping was confirmed at transcript level in the treated muscles by nested-RT-PCR as shown in **Figure 5.8**. RT-PCR for dystrophin skipping induced by Vivo-PMO-Dys is shown in **Figure 5.9 (a)**. Densitometric analysis of the skipped and full length bands showed that Vivo-PMO-Myo alone induced 46.9% (±28.3 SD) skipping and Vivo-PMO-Dys alone induced 37.4% (±7.2 SD) skipping. In case of animals treated with a cocktail of Vivo-PMO-(Myo+Dys), 30.6% (±3.5 SD) dystrophin skipping and 66.4% (±35.2 SD) myostatin skipping was observed. **Table 4** shows the percentage skipping induced by each treatment using both B-PMO as well as Vivo-PMO.

5.3.7. Effect of dystrophin and myostatin exon skipping induced by single intramuscular injection of Vivo-PMOs on muscle weights of *mdx* mice

The TA weights were normalized against body weight of the individual animals. Vivo-PMO-Dys led to a significant decrease in the muscle weight compared to saline treatment as did the cocktail of Vivo-PMO-(Dys+Myo) compared to saline control treatment. There was however no significant change in the weight of TAs treated with Vivo-PMO-Myo alone compared to saline-treated controls; as shown in **Figure 5.10**.

Figure 5.8

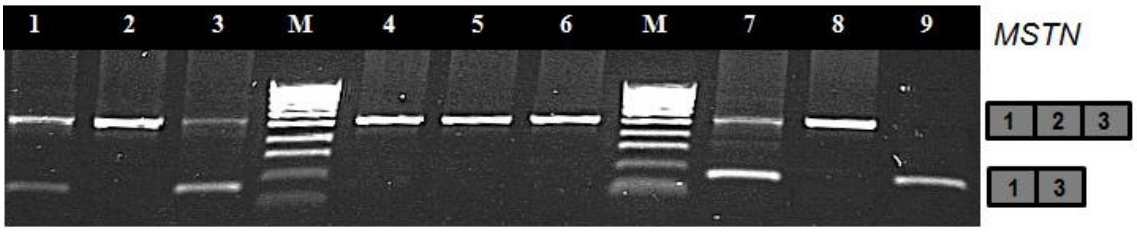

Figure 5.8: Myostatin exon skipping following Vivo-PMO-treatment in *mdx* mice. Myostatin exon 2 skipping induced by Vivo-PMO-Myo following single 3nmol intramuscular injection into the TA of six weeks old *mdx* mice is presented. Mice were sacrificed after eight weeks and a nested RT PCR was performed on 100ng mRNA from treated as well as control muscles (injected with normal saline). The nested PCR products were loaded on a 1.2% agarose gel. Different gel tracks were loaded with following samples: Tracks 1-3: TAs treated with Vivo-PMO-Myo alone; Tracks 4-6: TAs treated with saline; Tracks 7-9: TAs treated with a cocktail of Vivo-PMO-(Myo+Dys). Tracks marked 'M' were loaded with the size marker HyperLadder IV. Percent skipping was calculated as Mean±SD. The figure shows some representative samples.

Figure 5.9 (a)

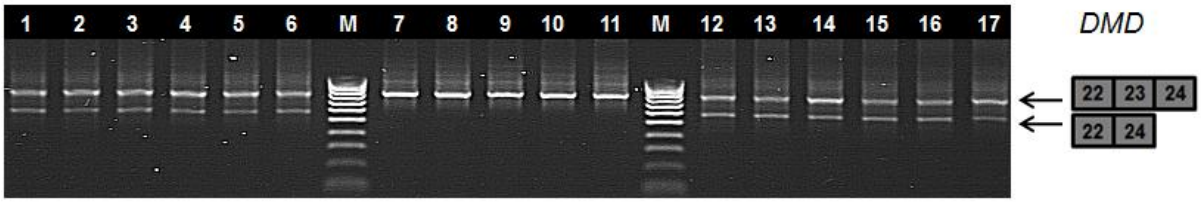

Figure 5.9 (a): Dystrophin exon 23 skipping in *mdx* mice induced by Vivo-PMO-Dys. Six weeks old *mdx* mice were treated with a single intramuscular injection of 3nmol of Vivo-PMO-Dys and a cocktail of Vivo-PMO (Dys+Myo) -a total of ~20µg. Controls were treated with same volume of normal saline. Mice were sacrificed after eight weeks and a nested RT-PCR was performed on 100ng mRNA from treated as well as control muscles. The nested PCR products were loaded on a 1.2% agarose gel. Tracks 1-6: TAs treated with a cocktail of Vivo-PMO-(Dys+Myo); Tracks 7-11: TAs treated with saline; Tracks 12-17: TAs treated with Vivo-PMO-Dys. Tracks marked 'M' were loaded with the size marker HyperLadder IV; n=6 for each group. The figure shows gel with representative samples; Densitometric analysis was performed on all the samples and average was calculated.

Figure 5.9 (b)

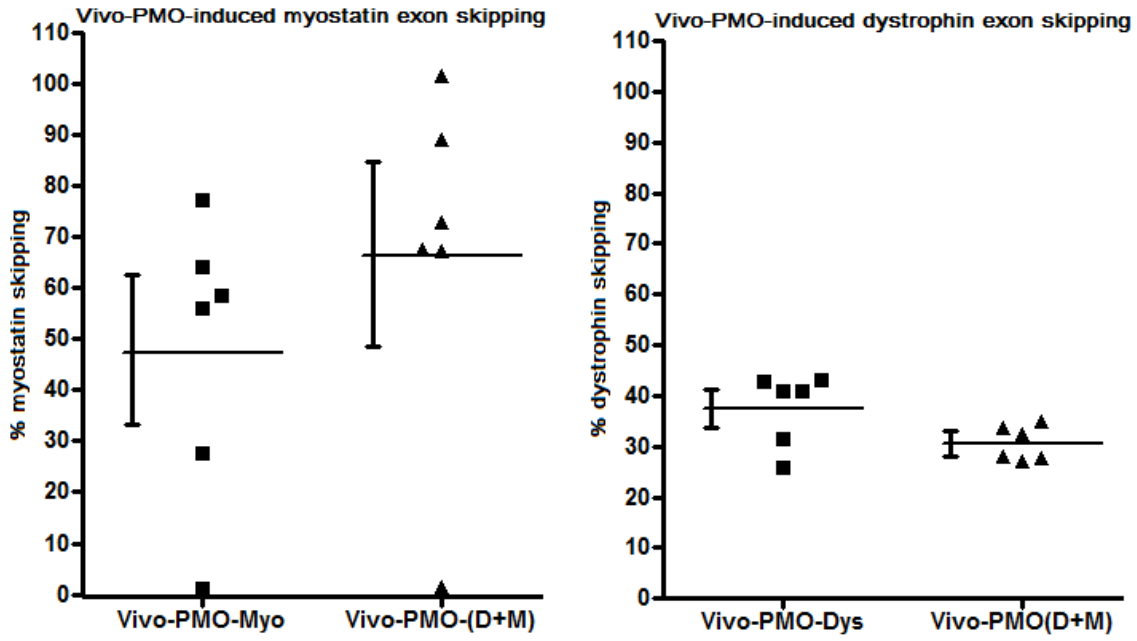

Figure 5.9 (b): Scatter plots for Vivo-PMO-induced myostatin and dystrophin exon skipping levels eight weeks after single IM injections (3nmol each) in the TA of mdx mice. Six muscles received each treatment. 'D+M' represents a cocktail of Vivo-PMO-myostatin and Vivo-PMO-dystrophin. Horizontal bars running through different ponts indicates mean values and the vertical bars represent mean±SD

Figure 5.10

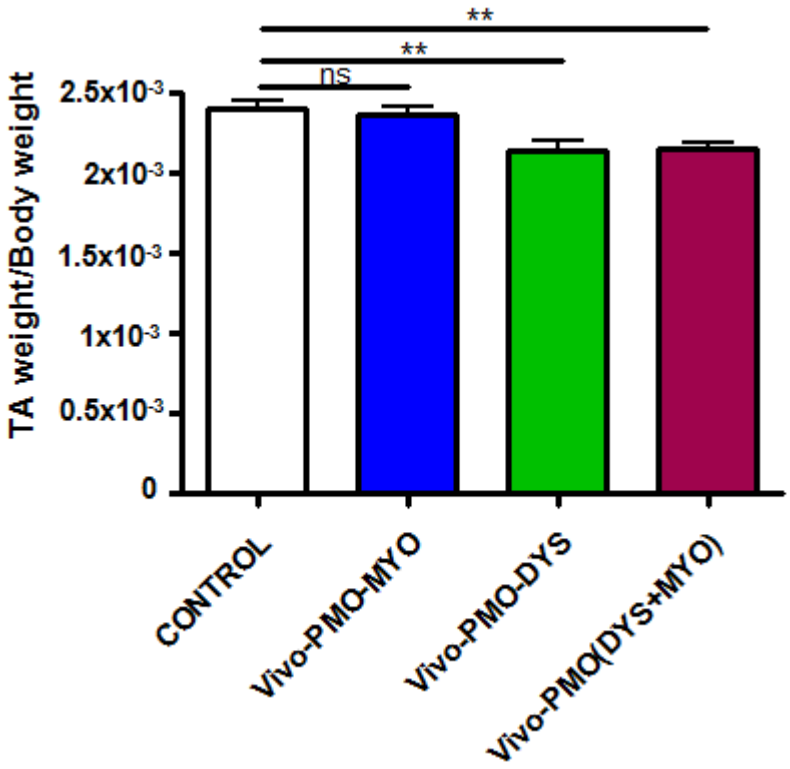

Figure 5.10: Change in weight of TA following single intramuscular Vivo-PMO treatment in *mdx*. Single intramuscular injections of 3nmol (~10µg) Vivo-PMO-Myo; Vivo-PMO-Dys; a cocktail of Vivo-PMO-(Dys+Myo) (total ~20µg) were administered into the TAs of six weeks old *mdx* mice. Controls were treated with same volume of normal saline. Mice were sacrificed and muscles harvested for RNA extraction and immunohistology after 8 weeks. Weights of TA muscles were normalized against whole body weight. There was no significant change in weights of Vivo-PMO-Myo-treated TAs compared to the controls. TAs treated with Vivo-PMO-Dys and with a cocktail of Vivo-PMO-(Dys+Myo) showed a significant decrease in weight compared to the controls. ***p*(Vivo-PMO-Dys vs. Control) = 0.009; ***p*(Vivo-PMO-(Dys+Myo) vs. Control) = 0.002; n=6 for each treatment; two-tailed t-test was performed with standard error of mean.

Table 4.

AO (10µg each)	Myostatin Skipping (%)	Dystrophin Skipping (%)	*p* value for weight change
B-PMO-Myostatin	33.0±9.1	----	0.03 (increase in weight)
B-PMO-Dystrophin	----	56.0±14.4	ns
B-PMO-Myo/Dys	40.0±6.0	65.0±11.3	0.006 (increase in weight)
Vivo-PMO-Myostatin	46.9±28.3	----	ns
Vivo-PMO-Dystrophin	----	37.4±7.2	0.009 (decrease in weight)
Vivo-PMO-Myo/Dys	66.4±35.2	30.6±3.5	0.002 (decrease in weight)

Table 4: Percentage skipping of myostatin exon 2 and dystrophin exon 23 and change in TA weight induced by B-PMO and Vivo-PMO in *mdx* mice. Table showing the percentage (Mean±SD) of myostatin exon 2 skipping induced by B-PMO as well as Vivo-PMO along with dystrophin exon 23 skipping induced by both the PMO conjugations in the TA muscle of dystrophic mice. Also shown are the values for percent exon skipping of myostatin and dystrophin when a dual treatment of PMOs for both myostatin and dystrophin using B-PMO as well as Vivo-PMO conjugations were administered intramuscularly.

5.3.8. Dystrophin expression restoration in *mdx* muscles following intramuscular Vivo-PMO injections

10µm transverse TA sections were stained with fluorescent dystrophin antibody and mounted in medium for fluorescence with DAPI. Restoration of dystrophin expression was evident from immunofluorescence detection of dystrophin on transverse TA sections as shown in **Figure 5.11**.

5.3.9. Effect of Vivo-PMO induced myostatin and dystrophin dual exon skipping on size distribution of muscle fibres in *mdx* mice

TA muscles of different treatment groups were cryosectioned and 10µm sections were stained with laminin antibody. Fibre cross sectional area was calculated using SigmaScan Pro5 software and chi squared analysis was performed on the data. There was no significant change in the fibre CSA with either of the treatment (trends of fibre CSA change shown in **Figure 5.12**), p (Vivo-PMO-Dys vs. Saline) >0.2; p (Vivo-PMO-Myo vs. Saline) >0.90; p [Vivo-PMO-(Dys+Myo) vs. Saline] >0.90.

5.3.10. Histological analysis of Vivo-PMO-treated *mdx* muscles

Standard H&E (haematoxylin and eosin) staining was performed on transverse 10µm sections of the muscles using a cryostat. There was no noticeable muscle damage caused by the treatment with either of the Vivo-PMO compared to untreated *mdx* mice (**Figure 5.13**).

Figure 5.11

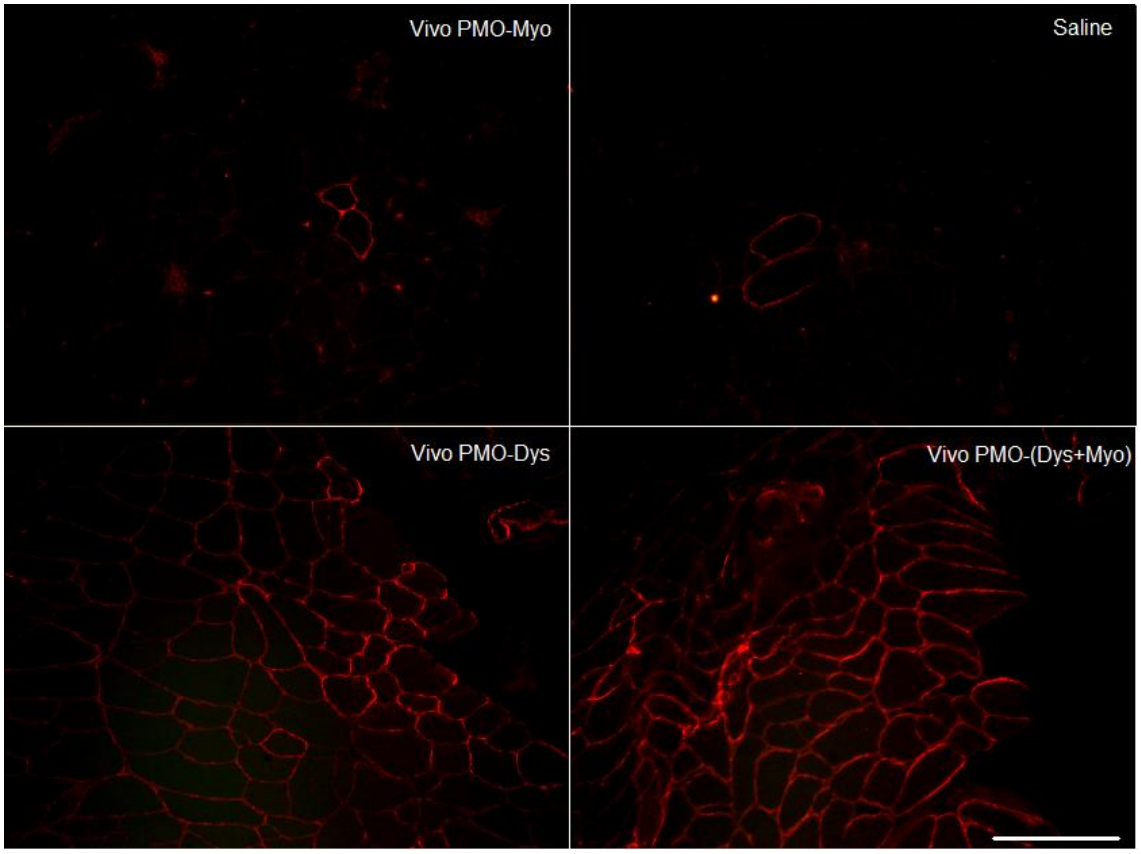

Figure 5.11: Immunohistochemical detection of dystrophin in TA sections of Vivo-PMO-treated *mdx* mice. Detection of dystrophin by immunohistochemical staining (red) in TA of the *mdx* mice treated with Vivo-PMO-Dys and a cocktail of Vivo-PMO-(Dys+Myo) is shown. *Mdx* mice treated with Vivo-PMO-Myo and the ones treated with normal saline are the negative controls. Dystrophin-positive fibres seen in the negative controls correspond to the revertant fibres. Magnification bar represents 500µm.

Figure 5.12: **Fibre diameter distribution in *mdx* TA muscles following different Vivo-PMO treatments**. The TA muscles of *mdx* mice were treated with 10µg of Vivo-PMO-Myo; Vivo-PMO-Dys; a cocktail of Vivo-PMO-Dys and Vivo-PMO-Myo (total 20µg); Controls were treated with same volume of saline and mice were sacrificed eight weeks post-injections. TA muscles were sectioned and immunostained with laminin and fibre size distribution was calculated using SigmaScan Pro 5 software. In the top panel, green bars represent TA muscles treated with Vivo-PMO-Myo and blue bars represent TA muscles treated with normal saline; in the middle panel, red bars represent TA muscles treated with Vivo-PMO-Dys and blue bars represent TA muscles treated with normal saline; in the bottom panel, yellow bars represent TA muscles treated with a cocktail of Vivo-PMO-(Dys+Myo) and the blue bars represent TA muscles treated with normal saline. For change in fibre CSA distribution, p (Vivo-PMO-dystrophin vs. Saline) > 0.2; p (Vivo-PMO-Myo vs. Saline) > 0.9; p [Vivo-PMO-(Dys+Myo) vs. Saline] > 0.9.

Figure 5.12

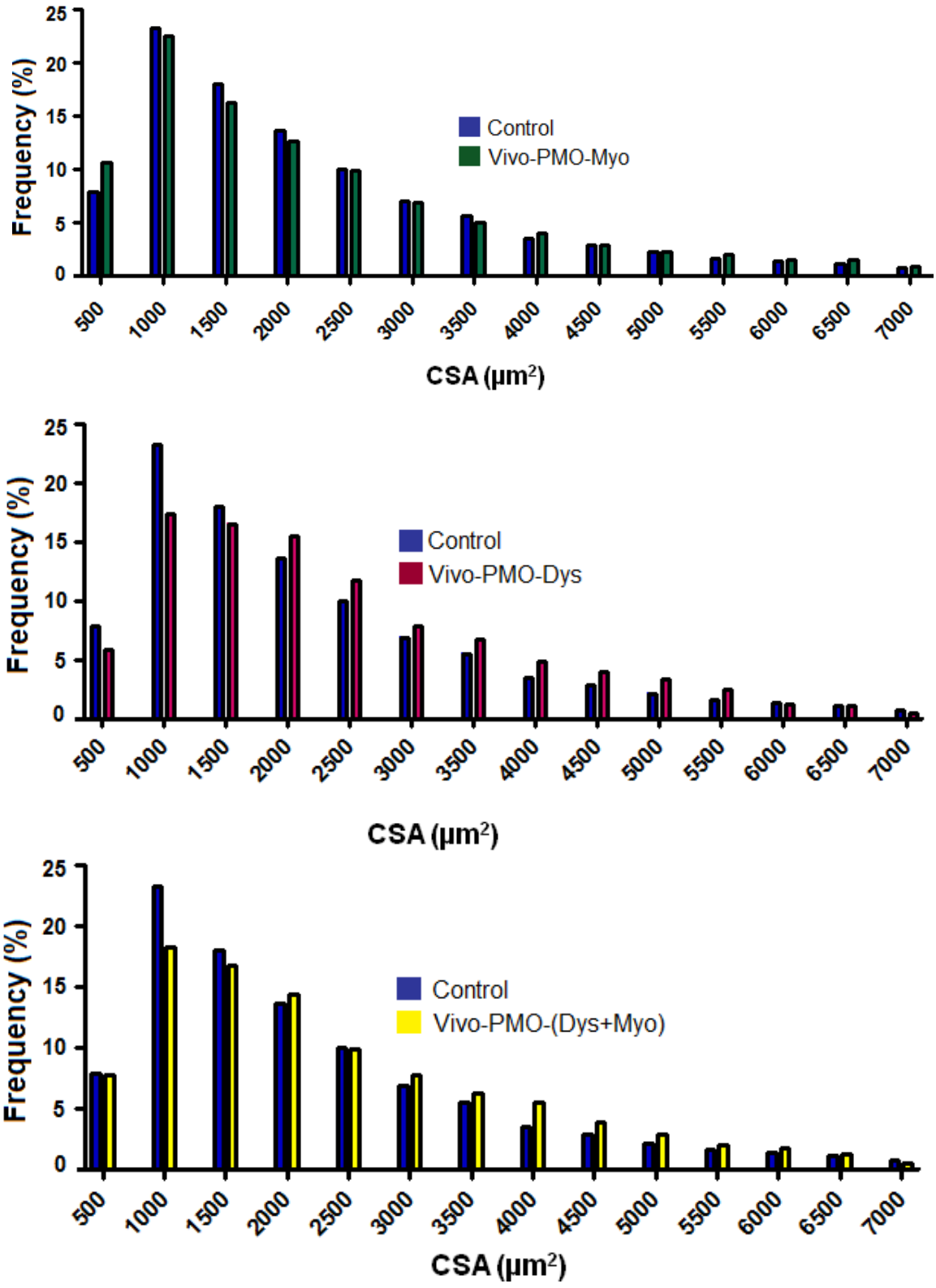
Frequency (%)
25
20
15
10
5
0
Control
Vivo-PMO-Myo
500
1000
1500
2000
2500
3000
3500
4000
4500
5000
5500
6000
6500
7000
CSA (µm²)
Frequency (%)
Control
Vivo-PMO-Dys
CSA (µm²)
Frequency (%)
Control
Vivo-PMO-(Dys+Myo)
CSA (µm²)

Figure 5.13: Histological staining of TA muscle of *mdx* mice treated with different Vivo-PMOs. Haematoxylin and eosin staining of TA muscle cross sections from *mdx* mice injected with 10µg Vivo-PMO-Dys, 10µg Vivo-PMO-Myo; a cocktail of Vivo-PMO-(Dys+Myo)- total of 20 µg. Animals were sacrificed after two months and their TAs were cut into 10µm transverse sections using a cryostat; n=6; representative pictures are shown. Magnification bar represents 500µm.

Figure 5.13

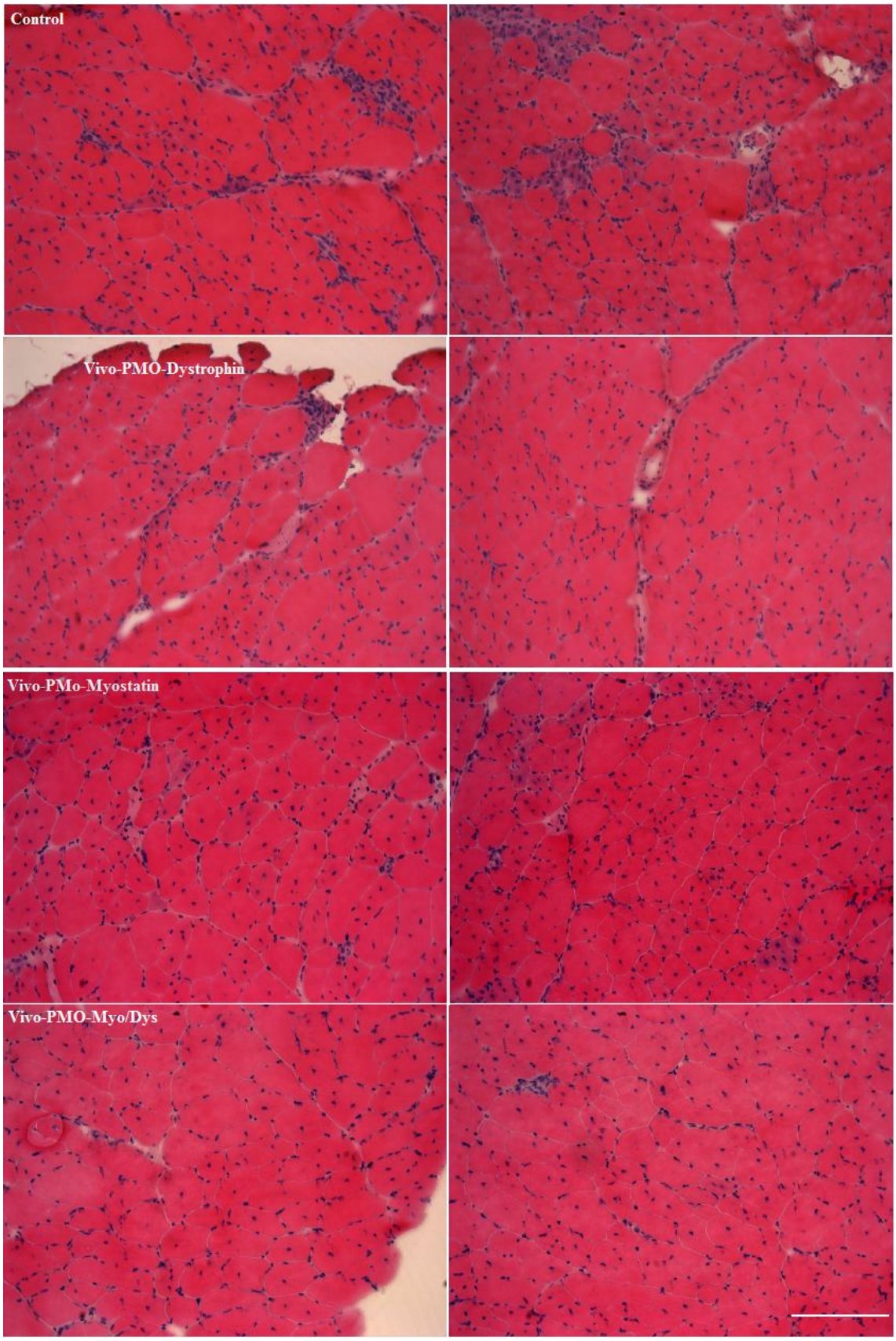
Control
Vivo-PMO-Dystrophin
Vivo-PMo-Myostatin
Vivo-PMO-Myo/Dys

5.4. Discussion

AO-mediated dystrophin exon skipping is potentially a very promising approach for correcting the underlying gene defect in DMD patients but it does not particularly aim at improvement in muscle regeneration and decreasing the level of fibrosis. In order to have an overall enhancement in the muscle development and function it is important to look at a combined therapy that along with restoring the expression of mutated gene, also addresses the issue of muscle loss. Therefore, in this study the aim was to investigate the potential of a combined approach of inhibiting the expression of myostatin, which is a negative regulator of muscle mass and at the same time reframing the dystrophin transcripts using antisense reagents.

A commonly used dystrophin AO sequence targeting exon 23 along with our myostatin exon 2 AO sequence linked to two different conjugations namely Vivo-PMO and B-PMO were used for the study in six weeks old *mdx* mice. Intramuscular B-PMO treatment targeted against myostatin alone resulted in a significant increase in muscle weight whereas B-PMO-dystrophin did not result in any significant change in muscle weight. A combination of both the AOs also resulted in an increase in muscle weight confirming the synergistic effect of both individual AOs. This has not been reported before although a 2'OMePS AO study has been conducted that showed induction of dual exon skipping of myostatin as well as dystrophin in *mdx* mice (Kemaladewi *et al.*, 2011) but there was no change in muscle weights. The studies reported in this chapter confirmed the previous results (Kemaladewi *et al.*, 2011) that myostatin and dystrophin AOs can be used simultaneously to induce exon skipping of pre-mRNAs of both the genes without any possible interference with each other. It was observed that B-PMO-Myo administration on its own induced exon skipping however when a combination of B-PMO-(Dys+Myo) was administered the level of myostatin exon skipping was higher as estimated by densitometric analysis. Similarly, dystrophin skipping level was enhanced when a cocktail of B-PMO-(Dys+Myo) was injected compared to B-PMO-Dys alone. An enhanced effect of a combination treatment of myostatin inhibition and dystrophin expression restoration on absolute and specific muscle maximal force compared to each treatment alone has been shown in a U7-DYS/shAcRIIb study to inhibit AcRIIb and skip dystrophin exon 23 (Dumonceaux *et al.,* 2010). These results suggest that myostatin inhibition and reframing dystrophin transcripts simultaneously could be crucial to have a better effect in terms of muscle weight and strength.

TA fibre diameter of the treated and control muscles was estimated to determine any change in the cross sectional area distribution of individual fibres of the tissue but there was no significant change with either of the treatment. Histological staining was performed on the tissue sections to see if there was any damage caused by the B-PMO treatment but it was observed that either of the treatment did not seemed to cause necrosis or infiltration of immune cells that could lead to inflammation. The treated tissue sections appeared normal thereby negating the possibility of inflamed muscles causing an increase in the weight. Dystrophin expression was checked by dystrophin immunostaining and dystrophin restoration was observed in case of B-PMO-Dys alone as well as in B-PMO-(Dys+Myo) cocktail. Overall, the increase in muscle weight and level of exon skipping seems to be more enhanced when the mRNA transcripts of both the genes are skipped simultaneously which could be due to restoration of fibre integrity resulting in protection from fibre damage.

A study for Vivo-PMO along the same lines as mentioned above was carried out for B-PMO. Six weeks old *mdx* mice were treated intramuscularly in the TA with a single 10µg injection of either Vivo-PMO-Myo alone or Vivo-PMO-Dys alone or with a cocktail of Vivo-PMO-(Myo+Dys) for eight weeks. Although an increased level of myostatin skipping induction was observed with the combined treatment of Vivo-PMO-(Dys+Myo) compared to Vivo-PMO-Myo alone, the percentage of dystrophin skipping with Vivo-PMO-(Dys+Myo) was found to be less than that observed with Vivo-PMO-Dys alone (**Table 4**). Contrary to the previous studies in wild type mice, Vivo-PMO alone did not lead to any increase in the muscle weight compared to the controls. However, a significant decrease in muscle weight was observed with the treatment of Vivo-PMO-Dys alone (p=0.009) and also with the Vivo-PMO cocktail (Myo+Dys) (p=0.002). This could be accounted for by the stabilization of muscle integrity because of a decrease in constant cycles of cell necrosis and renewal thereby, reversing the typical phenotype of 'pseudohypertrophy' in *mdx* muscles. As it has been shown in whippet dog breed, that dogs with one copy of two-base pair deletion in myostatin exon 3 are more muscular and faster than wild type as well as the ones with two copies of deletions, incomplete maintenance of the pathway could actually be more useful (Mosher *et al.*, 2007).

The analysis of fibre cross sectional area did not show any significant change despite a significant decrease in the weights of TAs treated with Vivo-PMO-Dys and

Vivo-PMO-(Dys+Myo). Therefore, the data on increase in muscle weight and its proportionality to hypertrophy following myostatin exon skipping treatment as observed in these intramuscular studies is not entirely consistent. It is likely that there are changes in the fibre diameter distribution of the treated muscles over the entire range of CSA values considered but it is distributed in such a way that it is well dispersed across the whole range of values that a significant change in any specific region is not observed. Increasing the number of animals used in future studies could possibly enhance the chances of producing a clearer and more precise trend of effects of myostatin exon skipping on muscle fibre CSA. Perhaps studies to determine the effect of myostatin exon skipping on muscle strength need to be done. The combined approach to downregulate the expression of myostatin receptor AcRIIb using sh-RNA and restoration of quasi-dystrophin using a vectorized U7 exon skipping (U7-DYS) showed that although no significant increase in muscle hypertrophy was observed with down regulation of AcRIIb although resulting in myostatin inhibition, a significantly enhanced muscle maximal strength was observed with the both the treatments together (Dumonceaux *et al.*, 2010).

H&E staining did not show any damage to the treated muscle compared to the control *mdx* muscles and dystrophin expression restoration was observed with Vivo-PMO-Dys as well as Vivo-PMO-(Dys+Myo) treatments by dystrophin immunohistological staining. Therefore, in order to have a better understanding of how a combination of myostatin inhibition and dystrophin expression restoration affects the strength, force and its functional properties, contractile properties of the muscle need to be analyzed. Thus from these studies so far, myostatin exon skipping does show a great potential to be a part of a combination therapy alongside dystrophin expression restoration. The next step from here would be to try different conjugation systems and carry on systemic studies to deliver the AOs to the entire body so that all the tissues can be treated. At the same time, it is very crucial to do some analysis of contractile properties of the muscle in order to understand how the treatment affects the absolute and specific muscle force as this will give important information for the studies to follow regarding different dosing regimens as well as routes of administration for a combined treatment with myostatin and dystrophin AOs.

CHAPTER 6

GENERAL DISCUSSION AND FUTURE WORK

Apart from being a characteristic feature of muscular disorders, skeletal muscle wasting also goes together with ageing-related immobility and cachexia resulting in fatal conditions like kidney failure and cardiac arrest. Therefore, treating the main causative agent of the muscular disorder along with the enhancement of muscle development could form a potent strategy to counter various muscle wasting conditions including Duchenne muscular dystrophy. It has been well established that myostatin is a negative regulator of skeletal muscle mass (Carnac *et al.*, 2006) and several approaches have been used to knock down this factor to induce an increase in skeletal muscle growth (Patel & Amthor, 2005). This could have important implications in disease conditions including cancer and HIV/AIDS which are accompanied by tremendous muscle mass loss. Sarcopenia, muscle atrophy, obesity-related metabolic disorders and insulin resistance can also be ameliorated by inducing myostatin inhibition. In context of Duchenne muscular dystrophy, although dystrophin restoration can be achieved using different approaches including over-expression of mini/microdystrophin and dystrophin exon skipping, it is likely to be less effective if the disease has already progressed to a state where there is tremendous muscle wasting and damage.

As myostatin has conserved function in humans there are immense expectations that muscle regeneration resulting from myostatin inhibition in animal models can be reproduced in humans. Inhibition of intracellular signal transduction, blockade of extracellular activity of myostatin and decrease in signalling of myostatin are various strategies that can be explored for inhibiting myostatin expression. Myostatin neutralizing antibody was prepared by immunizing myostatin-null mice with recombinant myostatin and its treatment resulted in improved muscle mass and function in pre-clinical studies (Enzmann *et al.*, 2003). Monoclonal neutralizing antibody to myostatin, MYO-029 was studied in a clinical trial which showed good safety but no improvement in muscle function of strength (Wagner *et al.*, 2008). A modified myostatin propeptide that is resistant to proteolytic cleavage has been shown to bind myostatin and inhibit its signal transduction that resulted in increase in skeletal muscle mass of adult mice (Wolfman *et al.*, 2003). Although follistatin, a secreted glycoprotein binds very strongly to myostatin, its inhibitory effects are not specific to myostatin

suggesting that it inhibits other TGF-β family members as well during muscle growth (Lee & McPherron, 2001). Myostatin inhibition by ACE-031, soluble form of activin receptor type IIB (AcRIIB) showed a significant increase in muscle mass independent of fibre type (Cadena *et al.*, 2010). A clinical trial to assess the safety profile of ACE-031 and for dose optimization was initiated in 2010 but was terminated in 2011 due to minor nosebleeds, gum bleeding and/or slightly dilated blood vessels in the skin of the patients under trial. All these issues were completely resolved on discontinuation of the treatment. Another trial by the same companies, Acceleron and Shire has been suspended and will start under extra safety monitoring to ensure patient safety in near future (http://www.muscular-dystrophy.org/research/news/3862).

The use of AOs to induce exon skipping and thereby downregulate the expression of myostatin presents several advantages over the other currently used gene therapy approaches. Firstly, there is no risk of uncontrolled insertion into the genome with AOs as in case of virus-mediated approaches (Amantana & Iversen, 2005). Moreover, with an appropriate dosing regimen, exon skipping levels can be regulated and, if necessary the treatment can be interrupted. Importantly AOs have not been reported to produce any toxic effects or immune response so far in animal models as well as when used in clinical application (Arora *et al.*, 2004).

In this study it is shown that AOs of 2'OMePS chemistry, designed using three bioinformatics algorithms (ESE Finder, PESX and Rescue ESE) resulted in a substantial level of myostatin exon 2 skipping *in vitro*. These bioinformatics programs have been successfully used in previous studies to design AOs for dystrophin exon skipping studies (Arechavala-Gomeza *et al.*, 2007; Popplewell *et al.*, 2009). The truncated transcript can be expected to undergo nonsense mediated decay but we observed a well defined skipped band that was sequenced and found to be of the right size. Although the shortened transcript is possibly stable but due to the lack of entire mature domain and a substantial segment of propeptide domain resultant of a premature stop codon, downstream signalling will eventually abolish. Myostatin being an inhibitor of myogenic differentiation controls the proliferation of myoblasts (Langley *et al.*, 2002b). Therefore, myostatin down regulation is expected to increase the cell proliferation. The AOs designed were biologically active and induced an increase in C2C12 cell proliferation. The efficacy of knock down by exon skipping *in vivo* has proved to be more challenging to establish than *in vitro*. The efficiency of myostatin skipping was

verified by injecting 2'OMePS intramuscularly, however, a significant change in muscle mass was not observed. Therefore it was necessary to carry out a time course analysis using single intramuscular administration of AO in wild type mice in order to have a clear time line that is needed to see an evident effect in the muscle weight. It was also important to estimate how long is the AO capable of inducing efficient exon skipping following single treatment of a specific dose. PMO chemistry was chosen for this experiment due to its better stability compared to the 2'OMePS and also because PMOs have been reported to have a longer effect *in vivo* (Iversen, 2001). This is particularly important for knocking down proteins with a very fast turnover like myostatin. The PMO sequence used for this study induced the most efficient skipping *in vitro*. It also maps in a region totally conserved between mouse and human myostatin paving the way to test the same PMO for clinical applications in humans.

In order to achieve a reasonable effect in undamaged muscles, a PMO conjugated to a delivery moiety has to be used (Morcos *et al.*, 2008). Vivo-PMO is commercially available and has been reported to be effective in normal healthy mice (Wu *et al.*, 2009). After four weeks of single treatment of Vivo-PMO-D in wild type mice, a significant increase in TA weight was observed and the effect was further evident after eight weeks as well. No histological signs of any damage to the tissue was observed neither was there any indication of general illness in the Vivo-PMO-treated mice during the experiment. Keeping this time frame in mind, a comparative study was done to see how efficiently a PMO targeted at myostatin is delivered when conjugated to delivery moieties like octaguanidine dendrimer (Vivo-PMO) and B-peptide (B-PMO) compared to a naked unconjugated PMO. As expected, a single intramuscular treatment of 10µg Vivo-PMO-D as well as B-PMO-D resulted in efficient skipping and a significant increase in TA muscle weight after four weeks and eight weeks whereas, unconjugated PMO did not lead to any significant change in TA weight.

Having tested the efficiency of these PMO conjugates, the aim of the study was to use these conjugation systems to target biologically active myostatin supplied to the injected muscle by the bloodstream. Moreover, in a hypothetical clinical approach, the whole body needs to be treated. Therefore, the next experiment was to administer wild type mice with AOs by systemic tail vein injections. By injecting Vivo-PMO-D, a significant increase in muscle size and the change of CSA fibre distribution has been obtained, but only in the soleus muscle. This was probably due to the lack of porosity of

vessels and fibres in the normal healthy mice used in this experiment. Also, the differential response in EDL and Soleus may be due in part to a greater amount of ActRIIb being expressed on the surface of EDL muscle, or because the intrinsic level of myostatin is greater in fast (myosin type IIb positive) myofibres (Foster *et al.*, 2009; Matsakas *et al.*, 2009). Alternatively, it can be speculated that the dosing regimen used which has been reported to be optimal for Vivo-PMO for exon skipping of dystrophin gene (Wu *et al.*, 2009), does not achieve sufficient skipping of myostatin gene. In the case of dystrophin skipping, the half life of dystrophin protein and mRNA is extremely long and therefore relatively smaller dosage of AO gives more sustained exon skipping (Ghahramani Seno *et al.*, 2008). However, in myostatin skipping, it is perhaps likely that more frequent re-dosing is required, to have a more sustained presence of AOs. This may explain the transient and weak effect in terms of whole body weight change observed *in vivo*. Differential effect seen if soleus and EDL is in compliance with some previously published data showing that soleus is the most affected muscle following a systemic approach to knock down myostatin (Foster *et al.*, 2009).

As discussed before in the case of DMD, along with dystrophin expression restoration, myostatin inhibition is equally important to take care of any muscle wasting and fibrosis that has already taken place. A study involving the use of U7-DYS/sh AcRIIb constructs to restore dystrophin expression as well as to inhibit myostatin receptor Activin receptor IIb (AcRIIb) simultaneously showed that downregulation of AcRIIb on its own was not sufficient to improve muscle strength of treated TA. Mdx mice were injected into their TAs with AAV vector carrying U7-DYS construct alone, shAcRIIb construct alone or the combination construct, U7-DYS/shAcRIIb. The controls were injected with either PBS or vector harbouring control sh-RNA. Animals were sacrificed after three months and the TA muscles were harvested and weighed followed by dystrophin expression analysis. The combined U7-DYS/shAcRIIb treatments led to a significant improvement in absolute and specific maximal muscle strength that was better than U7-DYS treatment on its own (Dumonceaux *et al.*, 2010). Another double strategy combining the dystrophin restoration and myostatin inhibition by exon skipping has been reported. 5-6 weeks old *mdx* mice (n=6) were injected into the gastrocnemius muscle with cocktails of 2'OMePS AOs (40μg each) for myostatin exon 2 and dystrophin exon 23 for four consecutive days with 48 hours resting time between second and third injection. The mice were sacrificed after 6 hours, one day and

two days of last injection (Kemaladewi *et al.*, 2011). Using 2'OMePS AOs for skipping dystrophin exon 23 and myostatin exon 2 concurrently, this study showed feasibility of inducing exon skipping using AOs for two different transcripts without any possible interference but the skipping levels were not quite high.

As a next step, the efficacy of simultaneous myostatin and dystrophin exon skipping induced by respective PMO sequences conjugated both as B-PMO as well as Vivo-PMO in mice with dystrophic pathology was studied. Single 10µg intramuscular B-PMO-myostatin administration to the *mdx* mice resulted in a significant increase in TA weight compared to control muscles as expected but when the same dose of B-PMO-dystrophin was administered, there was no significant change in the weights of the treated muscles. A combined B-PMO-myostatin/dystrophin treatment resulted in a significant increase in muscle weight and exon skipping was demonstrated by nested RT-PCR. It is likely that a higher dose of B-PMO-dystrophin is required to see a prominent effect. In the case of Vivo-PMO treatment, a significant decrease in the weight of TA muscle with Vivo-PMO-dystrophin treatment on its own was observed, whereas Vivo-PMO-myostatin did not cause any significant change in muscle weight. Vivo-PMO-myostatin/dystrophin treatment led to a significant decrease in muscle weight. The decrease in the muscle weight following Vivo-PMO-dystrophin can be described due to stoppage of degeneration/regeneration cycles in dystrophic muscle as a result of dystrophin restoration. As only a minimum standard dose was used, there is a likelihood of getting more pronounced effect in terms of change in muscle weight and dystrophin expression restoration if repeated injections are administered via systemic route for myostatin as well as dystrophin exon skipping together.

Future work needs to involve comparative studies of different systemic delivery routes. Direct evaluation of intravenous and intraperitoneal routes in *mdx* mice will be highly important in order to determine which method is more effective in better distribution of the AOs to the target tissues and therefore in inducing beneficial exon skipping. An optimal dosing regimen for myostatin exon skipping still needs to be determined. In one of our studies, five weekly intravenous injections of 6mg/Kg of body weight did not induce enough exon skipping in all the muscles of wild type mice except soleus but the weak effect could be due to intact healthy muscles of these animals compared to dystrophic animals. Consequently, a comparison of fortnightly and monthly dosing regimen needs to be studied over a longer time course. As it is clear

from the time course analysis in this study that once injected locally into the TAs of a wild type mice, PMO conjugated to octaguanidine dendrimer exhibited exon skipping until eight weeks. Therefore it may not be necessary to repeat the treatment as often as every week. Also in context of dystrophin/myostatin combination exon skipping approach, electrophysiological analyses would give an insight into how the muscle strength is affected by either myostatin skipping alone or dystrophin skipping alone or simultaneous dystrophin/myostatin skipping as it has been shown that dystrophin expression restoration and myostatin inhibition induced simultaneously have a better effect on improvement of maximal muscle strength (Dumonceaux *et al.*, 2010). Serum creatine kinase levels of *mdx* mice treated with PMO for dystrophin exon 23 skipping with seven intravenous treatments were reported to drop significantly compared to the controls (Alter *et al.*, 2006). Systemic studies to induce simultaneous dystrophin/myostatin exon skipping therefore need to be followed by an estimation of serum creatine kinase levels and examination of any immune response developed to the newly expressed dystrophin in treated and control *mdx* mice. Analysis of different markers from the serum including urea, alkaline phosphatase and aspartate transaminase can help to assess the toxicity level of the AOs used and is very important in a pre-clinical or clinical set up (Khajavi *et al.*, 2005).

A series of western blots were attempted during the course of this study to determine any changes in myostatin protein expression following AO-treatment using various antibodies but with no success. Rabbit anti-myostatin (GDF-8) polyclonal antibody (AB3139) by Chemicon International inc., rabbit anti-gdf8 polyclonal antibody by Bethyl laboratories (A300-401A) and a self-prepared monoclonal myostatin antibody from Markus Scheulke's lab in Berlin, were tested at different dilutions. Protein was extracted from cells and also conditioned media from cell culture were harvested for myostatin protein detection. The conditioned media were also concentrated using centrifugal filter units (Centricon® by Millipore) and conventional TCA (Trichloroacetic acid) method but still none of the antibodies showed a protein band for myostatin in the western blotting experiments. As a future study, a well-optimized qPCR study to quantify not only myostatin expression but also Smad2, Smad3, Smad7, myogenin, myoD etc following myostatin AO-treatment would give another very interesting insight into the modulation of signalling pathway resulting from myostatin inhibition.

This study represent a proof of principle that myostatin can be down regulated by skipping an exon from the transcript using antisense oligonucleotides. In case of DMD, development of an optimal strategy to counter muscle wasting requires correcting the genetic defect combined with enhanced muscle regeneration. Applications of dual myostatin/dystrophin exon skipping will depend upon further optimizations and investigations including different delivery routes, dosing regimens and electrophysiological studies to ensure effective *in vivo* knock down of myostatin expression and restoration of dystrophin expression for maximal therapeutic benefit. This work has the potential to be developed into part of an efficient treatment for age- and disease-related muscle wasting and various neuromuscular disorders including muscular dystrophies.

REFERENCES

Aartsma-Rus, A., Bremmer-Bout, M., Janson, A. A., den Dunnen, J. T., van Ommen, G. J. & van Deutekom, J. C. (2002). Targeted exon skipping as a potential gene correction therapy for Duchenne muscular dystrophy. *Neuromuscul Disord* **12 Suppl 1**, S71-77.

Aartsma-Rus, A., Heemskerk, H., de Winter, C., van Putten, M., Janson, A., Verschuuren, J., den Dunnen, J., van Deutekom, J. & van Ommen, G. J. (2009). Antisense-Mediated Exon Skipping for Duchenne Muscular Dystrophy. *Human Gene Therapy* **20**, 660-661.

Aartsma-Rus, A., Hoen, P. A. C., Kaman, W. E., Bremmer-Bout, M., Janson, A. M., den Dunnen, J. T., van Ommen, G. J. B. & van Deutekom, J. C. T. (2004a). Comparative analysis of antisense oligonucleotide analogs for targeted exon skipping in Duchenne muscular dystrophy. *Neuromuscular Disorders* **14**, 613-613.

Aartsma-Rus, A., Janson, A. A., Kaman, W. E., Bremmer-Bout, M., van Ommen, G. J., den Dunnen, J. T. & van Deutekom, J. C. (2004b). Antisense-induced multiexon skipping for Duchenne muscular dystrophy makes more sense. *Am J Hum Genet* **74**, 83-92.

Aartsma-Rus, A. & van Ommen, G. J. (2007). Antisense-mediated exon skipping: a versatile tool with therapeutic and research applications. *RNA* **13**, 1609-1624.

Abmayr, S., Gregorevic, P., Allen, J. M. & Chamberlain, J. S. (2005). Phenotypic improvement of dystrophic muscles by rAAV/microdystrophin vectors is augmented by Igf1 codelivery. *Mol Ther* **12**, 441-450.

Acsadi, G., Dickson, G., Love, D. R., Jani, A., Walsh, F. S., Gurusinghe, A., Wolff, J. A. & Davies, K. E. (1991). Human dystrophin expression in mdx mice after intramuscular injection of DNA constructs. *Nature* **352**, 815-818.

Adams, A. M., Harding, P. L., Iversen, P. L., Coleman, C., Fletcher, S. & Wilton, S. D. (2007a). Antisense oligonucleotide induced exon skipping and the dystrophin gene transcript: cocktails and chemistries. *BMC Mol Biol* **8**, 57.

Adams, V., Linke, A., Wisloff, U., Doring, C., Erbs, S., Krankel, N., Witt, C. C., Labeit, S., Muller-Werdan, U., Schuler, G. & Hambrecht, R. (2007b). Myocardial expression of Murf-1 and MAFbx after induction of chronic heart failure: Effect on myocardial contractility. *Cardiovasc Res* **73**, 120-129.

Adams, V., Mangner, N., Gasch, A., Krohne, C., Gielen, S., Hirner, S., Thierse, H. J., Witt, C. C., Linke, A., Schuler, G. & Labeit, S. (2008). Induction of MuRF1 is essential for TNF-alpha-induced loss of muscle function in mice. *J Mol Biol* **384**, 48-59.

Agrawal, S. (1996). Antisense oligonucleotides: towards clinical trials. *Trends Biotechnol* **14**, 376-387.

Agrawal, S. (1999). Importance of nucleotide sequence and chemical modifications of antisense oligonucleotides. *Biochim Biophys Acta* **1489**, 53-68.

Agrawal, S., Goodchild, J., Civeira, M. P., Thornton, A. H., Sarin, P. S. & Zamecnik, P. C. (1988). Oligodeoxynucleoside phosphoramidates and phosphorothioates as inhibitors of human immunodeficiency virus. *Proc Natl Acad Sci U S A* **85**, 7079-7083.

Agrawal, S. & Kandimalla, E. R. (2000). Antisense therapeutics: is it as simple as complementary base recognition? *Mol Med Today* **6**, 72-81.

Agrawal, S. & Zhao, Q. (1998). Antisense therapeutics. *Curr Opin Chem Biol* **2**, 519-528.

Akkaraju, G. R., Huard, J., Hoffman, E. P., Goins, W. F., Pruchnic, R., Watkins, S. C., Cohen, J. B. & Glorioso, J. C. (1999). Herpes simplex virus vector-mediated dystrophin gene transfer and expression in MDX mouse skeletal muscle. *J Gene Med* **1**, 280-289.

Alter, J., Lou, F., Rabinowitz, A., Yin, H., Rosenfeld, J., Wilton, S. D., Partridge, T. A. & Lu, Q. L. (2006). Systemic delivery of morpholino oligonucleotide restores dystrophin expression bodywide and improves dystrophic pathology. *Nat Med* **12**, 175-177.

Amantana, A. & Iversen, P. L. (2005). Pharmacokinetics and biodistribution of phosphorodiamidate morpholino antisense oligomers. *Curr Opin Pharmacol* **5**, 550-555.

Amantana, A., Moulton, H. M., Cate, M. L., Reddy, M. T., Whitehead, T., Hassinger, J. N., Youngblood, D. S. & Iversen, P. L. (2007). Pharmacokinetics, biodistribution, stability and toxicity of a cell-penetrating peptide-morpholino oligomer conjugate. *Bioconjug Chem* **18**, 1325-1331.

Arechavala-Gomeza, V., Graham, I. R., Popplewell, L. J., Adams, A. M., Aartsma-Rus, A., Kinali, M., Morgan, J. E., van Deutekom, J. C., Wilton, S. D., Dickson, G. & Muntoni, F. (2007). Comparative analysis of antisense oligonucleotide sequences for targeted skipping of exon 51 during dystrophin pre-mRNA splicing in human muscle. *Hum Gene Ther* **18**, 798-810.

Argiles, J. M. & Lopez-Soriano, F. J. (1999). The role of cytokines in cancer cachexia. *Med Res Rev* **19**, 223-248.

Arora, V., Devi, G. R. & Iversen, P. L. (2004). Neutrally charged phosphorodiamidate morpholino antisense oligomers: uptake, efficacy and pharmacokinetics. *Curr Pharm Biotechnol* **5**, 431-439.

Athanasopoulos, T., Graham, I. R., Foster, H. & Dickson, G. (2004). Recombinant adeno-associated viral (rAAV) vectors as therapeutic tools for Duchenne muscular dystrophy (DMD). *Gene Ther* **11 Suppl 1**, S109-121.

Auld, D. S. & Robitaille, R. (2003). Glial cells and neurotransmission: an inclusive view of synaptic function. *Neuron* **40**, 389-400.

Baker, B. F., Lot, S. S., Condon, T. P., Cheng-Flournoy, S., Lesnik, E. A., Sasmor, H. M. & Bennett, C. F. (1997). 2'-O-(2-Methoxy)ethyl-modified anti-intercellular adhesion molecule 1 (ICAM-1) oligonucleotides selectively increase the ICAM-1 mRNA level and inhibit formation of the ICAM-1 translation initiation complex in human umbilical vein endothelial cells. *J Biol Chem* **272**, 11994-12000.

Bardag-Gorce, F., Farout, L., Veyrat-Durebex, C., Briand, Y. & Briand, M. (1999). Changes in 20S proteasome activity during ageing of the LOU rat. *Mol Biol Rep* **26**, 89-93.

Barton, E. R., Morris, L., Musaro, A., Rosenthal, N. & Sweeney, H. L. (2002). Muscle-specific expression of insulin-like growth factor I counters muscle decline in mdx mice. *J Cell Biol* **157**, 137-148.

Bassel-Duby, R. & Olson, E. N. (2006). Signaling pathways in skeletal muscle remodeling. *Annu Rev Biochem* **75**, 19-37.

Baumgartner, R. N., Koehler, K. M., Gallagher, D., Romero, L., Heymsfield, S. B., Ross, R. R., Garry, P. J. & Lindeman, R. D. (1998). Epidemiology of sarcopenia among the elderly in New Mexico. *Am J Epidemiol* **147**, 755-763.

Beitel, L. K., Scanlon, T., Gottlieb, B. & Trifiro, M. A. (2005). Progress in Spinobulbar muscular atrophy research: insights into neuronal dysfunction caused by the polyglutamine-expanded androgen receptor. *Neurotox Res* **7**, 219-230.

Berridge, M. V. & Tan, A. S. (1993). Characterization of the cellular reduction of 3-(4,5-dimethylthiazol-2-yl)-2,5-diphenyltetrazolium bromide (MTT): subcellular localization, substrate dependence, and involvement of mitochondrial electron transport in MTT reduction. *Arch Biochem Biophys* **303**, 474-482.

Black, D. L. (2003). Mechanisms of alternative pre-messenger RNA splicing. *Annu Rev Biochem* **72**, 291-336.

Blake, D. J., Weir, A., Newey, S. E. & Davies, K. E. (2002). Function and genetics of dystrophin and dystrophin-related proteins in muscle. *Physiol Rev* **82**, 291-329.

Blau, H. M., Webster, C., Pavlath, G. K. & Chiu, C. P. (1985). Evidence for defective myoblasts in Duchenne muscular dystrophy. *Adv Exp Med Biol* **182**, 85-110.

Bogdanovich, S., Krag, T. O., Barton, E. R., Morris, L. D., Whittemore, L. A., Ahima, R. S. & Khurana, T. S. (2002). Functional improvement of dystrophic muscle by myostatin blockade. *Nature* **420**, 418-421.

Brenman, J. E., Chao, D. S., Xia, H., Aldape, K. & Bredt, D. S. (1995). Nitric oxide synthase complexed with dystrophin and absent from skeletal muscle sarcolemma in Duchenne muscular dystrophy. *Cell* **82**, 743-752.

Bulfield, G., Siller, W. G., Wight, P. A. & Moore, K. J. (1984). X chromosome-linked muscular dystrophy (mdx) in the mouse. *Proc Natl Acad Sci U S A* **81**, 1189-1192.

Bullough, W. S. (1962). The control of mitotic activity in adult mammalian tissues. *Biol Rev Camb Philos Soc* **37**, 307-342.

Bullough, W. S. (1965). Mitotic and functional homeostasis: a speculative review. *Cancer Res* **25**, 1683-1727.

Burge, C. B., Fairbrother, W. G., Yeh, R. F. & Sharp, P. A. (2002). Predictive identification of exonic splicing enhancers in human genes. *Science* **297**, 1007-1013.

Burge, C. B., Fairbrother, W. G., Yeo, G. W., Yeh, R., Goldstein, P., Mawson, M. & Sharp, P. A. (2004). RESCUE-ESE identifies candidate exonic splicing enhancers in vertebrate exons. *Nucleic Acids Research* **32**, W187-W190.

Cadena, S. M., Tomkinson, K. N., Monnell, T. E., Spaits, M. S., Kumar, R., Underwood, K. W., Pearsall, R. S. & Lachey, J. L. (2010). Administration of a soluble activin type IIB receptor promotes skeletal muscle growth independent of fiber type. *J Appl Physiol* **109**, 635-642.

Caputi, M., Kendzior, R. J., Jr. & Beemon, K. L. (2002). A nonsense mutation in the fibrillin-1 gene of a Marfan syndrome patient induces NMD and disrupts an exonic splicing enhancer. *Genes Dev* **16**, 1754-1759.

Carmeli, E., Coleman, R. & Reznick, A. Z. (2002). The biochemistry of aging muscle. *Exp Gerontol* **37**, 477-489.

Carnac, G., Ricaud, S., Vernus, B. & Bonnieu, A. (2006). Myostatin: biology and clinical relevance. *Mini Rev Med Chem* **6**, 765-770.

Carstens, R. P., Fenton, W. A. & Rosenberg, L. R. (1991). Identification of RNA splicing errors resulting in human ornithine transcarbamylase deficiency. *Am J Hum Genet* **48**, 1105-1114.

Cartegni, L., Chew, S. L. & Krainer, A. R. (2002). Listening to silence and understanding nonsense: exonic mutations that affect splicing. *Nat Rev Genet* **3**, 285-298.

Cartegni, L. & Krainer, A. R. (2002). Disruption of an SF2/ASF-dependent exonic splicing enhancer in SMN2 causes spinal muscular atrophy in the absence of SMN1. *Nat Genet* **30**, 377-384.

Cartegni, L., Wang, J., Zhu, Z., Zhang, M. Q. & Krainer, A. R. (2003). ESEfinder: A web resource to identify exonic splicing enhancers. *Nucleic Acids Res* **31**, 3568-3571.

Celotto, A. M. & Graveley, B. R. (2002). Exon-specific RNAi: a tool for dissecting the functional relevance of alternative splicing. *RNA* **8**, 718-724.

Chai, R. J., Vukovic, J., Dunlop, S., Grounds, M. D. & Shavlakadze, T. (2011). Striking denervation of neuromuscular junctions without lumbar motoneuron loss in geriatric mouse muscle. *PLoS One* **6**, e28090.

Chasin, L. A. & Zhang, X. H. F. (2004). Computational definition of sequence motifs governing constitutive exon splicing. *Genes & Development* **18**, 1241-1250.

Chen, H. H., Mack, L. M., Kelly, R., Ontell, M., Kochanek, S. & Clemens, P. R. (1997a). Persistence in muscle of an adenoviral vector that lacks all viral genes. *Proc Natl Acad Sci U S A* **94**, 1645-1650.

Chen, Y., Bhushan, A. & Vale, W. (1997b). Smad8 mediates the signaling of the ALK-2 [corrected] receptor serine kinase. *Proc Natl Acad Sci U S A* **94**, 12938-12943.

Chen, Y. G., Hata, A., Lo, R. S., Wotton, D., Shi, Y., Pavletich, N. & Massague, J. (1998). Determinants of specificity in TGF-beta signal transduction. *Genes Dev* **12**, 2144-2152.

Chester, A., Scott, J., Anant, S. & Navaratnam, N. (2000). RNA editing: cytidine to uridine conversion in apolipoprotein B mRNA. *Biochim Biophys Acta* **1494**, 1-13.

Clavel, S., Coldefy, A. S., Kurkdjian, E., Salles, J., Margaritis, I. & Derijard, B. (2006). Atrophy-related ubiquitin ligases, atrogin-1 and MuRF1 are up-regulated in aged rat Tibialis Anterior muscle. *Mech Ageing Dev* **127**, 794-801.

Collins, C. A. & Guthrie, C. (2000). The question remains: is the spliceosome a ribozyme? *Nat Struct Biol* **7**, 850-854.

Collins, C. A. & Morgan, J. E. (2003). Duchenne's muscular dystrophy: animal models used to investigate pathogenesis and develop therapeutic strategies. *Int J Exp Pathol* **84**, 165-172.

Collins, C. A. & Partridge, T. A. (2005). Self-renewal of the adult skeletal muscle satellite cell. *Cell Cycle* **4**, 1338-1341.

Conboy, I. M., Conboy, M. J., Smythe, G. M. & Rando, T. A. (2003). Notch-mediated restoration of regenerative potential to aged muscle. *Science* **302**, 1575-1577.

Cory, A. H., Owen, T. C., Barltrop, J. A. & Cory, J. G. (1991). Use of an aqueous soluble tetrazolium/formazan assay for cell growth assays in culture. *Cancer Commun* **3**, 207-212.

Costelli, P., Muscaritoli, M., Bossola, M., Penna, F., Reffo, P., Bonetto, A., Busquets, S., Bonelli, G., Lopez-Soriano, F. J., Doglietto, G. B., Argiles, J. M., Baccino, F. M. & Rossi Fanelli, F. (2006). IGF-1 is downregulated in experimental cancer cachexia. *Am J Physiol Regul Integr Comp Physiol* **291**, R674-683.

Coulton, G. R., Curtin, N. A., Morgan, J. E. & Partridge, T. A. (1988). The mdx mouse skeletal muscle myopathy: II. Contractile properties. *Neuropathol Appl Neurobiol* **14**, 299-314.

Crick, F. (1979). Split genes and RNA splicing. *Science* **204**, 264-271.

Crisan, M., Yap, S., Casteilla, L., Chen, C. W., Corselli, M., Park, T. S., Andriolo, G., Sun, B., Zheng, B., Zhang, L., Norotte, C., Teng, P. N., Traas, J., Schugar, R., Deasy, B. M., Badylak, S., Buhring, H. J., Giacobino, J. P., Lazzari, L., Huard, J. & Peault, B. (2008). A perivascular origin for mesenchymal stem cells in multiple human organs. *Cell Stem Cell* **3**, 301-313.

Crooke, S. T. (1998). Antisense therapeutics. *Biotechnol Genet Eng Rev* **15**, 121-157.

Cross, D. A., Alessi, D. R., Cohen, P., Andjelkovich, M. & Hemmings, B. A. (1995). Inhibition of glycogen synthase kinase-3 by insulin mediated by protein kinase B. *Nature* **378**, 785-789.

Cruz-Jentoft, A. J., Baeyens, J. P., Bauer, J. M., Boirie, Y., Cederholm, T., Landi, F., Martin, F. C., Michel, J. P., Rolland, Y., Schneider, S. M., Topinkova, E., Vandewoude, M. & Zamboni, M. (2010). Sarcopenia: European consensus on definition and diagnosis: Report of the European Working Group on Sarcopenia in Older People. *Age Ageing* **39**, 412-423.

Cudkowicz, M. E., McKenna-Yasek, D., Sapp, P. E., Chin, W., Geller, B., Hayden, D. L., Schoenfeld, D. A., Hosler, B. A., Horvitz, H. R. & Brown, R. H. (1997). Epidemiology of mutations in superoxide dismutase in amyotrophic lateral sclerosis. *Ann Neurol* **41**, 210-221.

Dance, G. S., Sowden, M. P., Cartegni, L., Cooper, E., Krainer, A. R. & Smith, H. C. (2002). Two proteins essential for apolipoprotein B mRNA editing are expressed from a single gene through alternative splicing. *J Biol Chem* **277**, 12703-12709.

Dargelos, E., Brule, C., Combaret, L., Hadj-Sassi, A., Dulong, S., Poussard, S. & Cottin, P. (2007). Involvement of the calcium-dependent proteolytic system in skeletal muscle aging. *Exp Gerontol* **42**, 1088-1098.

Davies, A., Kidd, C. & Blakeley, A.G.H. (2001). Human physiology. Churchill Livingstone, Edinburgh.

Davson H (1970). A textbook of general physiology (4th edition). Churchill, London

de Fougerolles, A., Vornlocher, H. P., Maraganore, J. & Lieberman, J. (2007). Interfering with disease: a progress report on siRNA-based therapeutics. *Nat Rev Drug Discov* **6**, 443-453.

Dean, N. M., McKay, R., Condon, T. P. & Bennett, C. F. (1994). Inhibition of protein kinase C-alpha expression in human A549 cells by antisense oligonucleotides inhibits induction of intercellular adhesion molecule 1 (ICAM-1) mRNA by phorbol esters. *J Biol Chem* **269**, 16416-16424.

Deconinck, N., Tinsley, J., De Backer, F., Fisher, R., Kahn, D., Phelps, S., Davies, K. & Gillis, J. M. (1997). Expression of truncated utrophin leads to major functional improvements in dystrophin-deficient muscles of mice. *Nat Med* **3**, 1216-1221.

Delaughter, M. C., Taffet, G. E., Fiorotto, M. L., Entman, M. L. & Schwartz, R. J. (1999). Local insulin-like growth factor I expression induces physiologic, then pathologic, cardiac hypertrophy in transgenic mice. *FASEB J* **13**, 1923-1929.

Dennis, R. A., Przybyla, B., Gurley, C., Kortebein, P. M., Simpson, P., Sullivan, D. H. & Peterson, C. A. (2008). Aging alters gene expression of growth and remodeling factors in human skeletal muscle both at rest and in response to acute resistance exercise. *Physiol Genomics* **32**, 393-400.

Dennler, S., Itoh, S., Vivien, D., ten Dijke, P., Huet, S. & Gauthier, J. M. (1998). Direct binding of Smad3 and Smad4 to critical TGF beta-inducible elements in the promoter of human plasminogen activator inhibitor-type 1 gene. *EMBO J* **17**, 3091-3100.

Denovan-Wright, E. M. & Davidson, B. L. (2006). RNAi: a potential therapy for the dominantly inherited nucleotide repeat diseases. *Gene Ther* **13**, 525-531.

Devitt, C. M., Seim, H. B., 3rd, Willer, R., McPherron, M. & Neely, M. (1997). Passive drainage versus primary closure after total ear canal ablation-lateral bulla osteotomy in dogs: 59 dogs (1985-1995). *Vet Surg* **26**, 210-216.

DeVol, D. L., Rotwein, P., Sadow, J. L., Novakofski, J. & Bechtel, P. J. (1990). Activation of insulin-like growth factor gene expression during work-induced skeletal muscle growth. *Am J Physiol* **259**, E89-95.

Dezawa, M., Ishikawa, H., Itokazu, Y., Yoshihara, T., Hoshino, M., Takeda, S., Ide, C. & Nabeshima, Y. (2005). Bone marrow stromal cells generate muscle cells and repair muscle degeneration. *Science* **309**, 314-317.

Dias, N. & Stein, C. A. (2002). Antisense oligonucleotides: basic concepts and mechanisms. *Mol Cancer Ther* **1**, 347-355.

Dickson, G., Hill, V. & Graham, I. R. (2002). Screening for antisense modulation of dystrophin pre-mRNA splicing. *Neuromuscul Disord* **12 Suppl 1**, S67-70.

Dickson, G., Pizzey, J. A., Elsom, V. E., Love, D., Davies, K. E. & Walsh, F. S. (1988). Distinct dystrophin mRNA species are expressed in embryonic and adult mouse skeletal muscle. *FEBS Lett* **242**, 47-52.

DiLella, A. G., Marvit, J., Lidsky, A. S., Guttler, F. & Woo, S. L. (1986). Tight linkage between a splicing mutation and a specific DNA haplotype in phenylketonuria. *Nature* **322**, 799-803.

Dominski, Z. & Kole, R. (1993). Restoration of correct splicing in thalassemic pre-mRNA by antisense oligonucleotides. *Proc Natl Acad Sci U S A* **90**, 8673-8677.

Douglas, J. T. (2007). Adenoviral vectors for gene therapy. *Mol Biotechnol* **36**, 71-80.

Du, L., Pollard, J. M. & Gatti, R. A. (2007). Correction of prototypic ATM splicing mutations and aberrant ATM function with antisense morpholino oligonucleotides. *Proc Natl Acad Sci U S A* **104**, 6007-6012.

Dumonceaux, J., Marie, S., Beley, C., Trollet, C., Vignaud, A., Ferry, A., Butler-Browne, G. & Garcia, L. (2010). Combination of myostatin pathway interference and dystrophin rescue enhances tetanic and specific force in dystrophic mdx mice. *Mol Ther* **18**, 881-887.

Dunckley, M. G., Manoharan, M., Villiet, P., Eperon, I. C. & Dickson, G. (1998). Modification of splicing in the dystrophin gene in cultured Mdx muscle cells by antisense oligoribonucleotides. *Hum Mol Genet* **7**, 1083-1090.

Dykxhoorn, D. M., Schlehuber, L. D., London, I. M. & Lieberman, J. (2006). Determinants of specific RNA interference-mediated silencing of human beta-globin alleles differing by a single nucleotide polymorphism. *Proc Natl Acad Sci U S A* **103**, 5953-5958.

Eagle, M., Bourke, J., Bullock, R., Gibson, M., Mehta, J., Giddings, D., Straub, V. & Bushby, K. (2007). Managing Duchenne muscular dystrophy--the additive effect of spinal surgery and home nocturnal ventilation in improving survival. *Neuromuscul Disord* **17**, 470-475.

Elbendary, A., Berchuck, A., Davis, P., Havrilesky, L., Bast, R. C., Jr., Iglehart, J. D. & Marks, J. R. (1994). Transforming growth factor beta 1 can induce CIP1/WAF1 expression independent of the p53 pathway in ovarian cancer cells. *Cell Growth Differ* **5**, 1301-1307.

Elkina, Y., von Haehling, S., Anker, S. D. & Springer, J. (2011). The role of myostatin in muscle wasting: an overview. *J Cachexia Sarcopenia Muscle* **2**, 143-151.

Emery, A. E. (2002). The muscular dystrophies. *Lancet* **359**, 687-695.

Enterlein, S., Warfield, K. L., Swenson, D. L., Stein, D. A., Smith, J. L., Gamble, C. S., Kroeker, A. D., Iversen, P. L., Bavari, S. & Muhlberger, E. (2006). VP35 knockdown inhibits Ebola virus amplification and protects against lethal infection in mice. *Antimicrob Agents Chemother* **50**, 984-993.

Enzmann, V., Howard, R. M., Yamauchi, Y., Whittemore, S. R. & Kaplan, H. J. (2003). Enhanced induction of RPE lineage markers in pluripotent neural stem cells engrafted into the adult rat subretinal space. *Invest Ophthalmol Vis Sci* **44**, 5417-5422.

Errington, S. J., Mann, C. J., Fletcher, S. & Wilton, S. D. (2003). Target selection for antisense oligonucleotide induced exon skipping in the dystrophin gene. *J Gene Med* **5**, 518-527.

Evans, W. J., Morley, J. E., Argiles, J., Bales, C., Baracos, V., Guttridge, D., Jatoi, A., Kalantar-Zadeh, K., Lochs, H., Mantovani, G., Marks, D., Mitch, W. E., Muscaritoli, M., Najand, A., Ponikowski, P., Rossi Fanelli, F., Schambelan, M., Schols, A., Schuster, M., Thomas, D., Wolfe, R. & Anker, S. D. (2008). Cachexia: a new definition. *Clin Nutr* **27**, 793-799.

Fackenthal, J. D., Cartegni, L., Krainer, A. R. & Olopade, O. I. (2002). BRCA2 T2722R is a deleterious allele that causes exon skipping. *Am J Hum Genet* **71**, 625-631.

Fairbrother, W. G., Yeh, R. F., Sharp, P. A. & Burge, C. B. (2002). Predictive identification of exonic splicing enhancers in human genes. *Science* **297**, 1007-1013.

Fairbrother, W. G., Yeo, G. W., Yeh, R., Goldstein, P., Mawson, M., Sharp, P. A. & Burge, C. B. (2004). RESCUE-ESE identifies candidate exonic splicing enhancers in vertebrate exons. *Nucleic Acids Res* **32**, W187-190.

Fakhfakh, R., Michaud, A. & Tremblay, J. P. (2011). Blocking the myostatin signal with a dominant negative receptor improves the success of human myoblast transplantation in dystrophic mice. *Mol Ther* **19**, 204-210.

Ferrari, A., Pellegrini, V., Arcangeli, C., Fittipaldi, A., Giacca, M. & Beltram, F. (2003). Caveolae-mediated internalization of extracellular HIV-1 tat fusion proteins visualized in real time. *Mol Ther* **8**, 284-294.

Finsterer, J. (2009). Bulbar and spinal muscular atrophy (Kennedy's disease): a review. *Eur J Neurol* **16**, 556-561.

Fletcher, S., Honeyman, K., Fall, A. M., Harding, P. L., Johnsen, R. D., Steinhaus, J. P., Moulton, H. M., Iversen, P. L. & Wilton, S. D. (2007). Morpholino oligomer-mediated exon skipping averts the onset of dystrophic pathology in the mdx mouse. *Mol Ther* **15**, 1587-1592.

Fletcher, S., Honeyman, K., Fall, A. M., Harding, P. L., Johnsen, R. D. & Wilton, S. D. (2006). Dystrophin expression in the mdx mouse after localised and systemic administration of a morpholino antisense oligonucleotide. *J Gene Med* **8**, 207-216.

Flood, D. G. & Coleman, P. D. (1988). Neuron numbers and sizes in aging brain: comparisons of human, monkey, and rodent data. *Neurobiol Aging* **9**, 453-463.

Foster, H., Sharp, P. S., Athanasopoulos, T., Trollet, C., Graham, I. R., Foster, K., Wells, D. J. & Dickson, G. (2008). Codon and mRNA sequence optimization of microdystrophin transgenes improves expression and physiological outcome in dystrophic mdx mice following AAV2/8 gene transfer. *Mol Ther* **16**, 1825-1832.

Foster, K., Graham, I. R., Otto, A., Foster, H., Trollet, C., Yaworsky, P. J., Walsh, F. S., Bickham, D., Curtin, N. A., Kawar, S. L., Patel, K. & Dickson, G. (2009). Adeno-associated virus-8-mediated intravenous transfer of myostatin propeptide leads to systemic functional improvements of slow but not fast muscle. *Rejuvenation Res* **12**, 85-94.

Friedman, K. J., Kole, J., Cohn, J. A., Knowles, M. R., Silverman, L. M. & Kole, R. (1999). Correction of aberrant splicing of the cystic fibrosis transmembrane conductance regulator (CFTR) gene by antisense oligonucleotides. *J Biol Chem* **274**, 36193-36199.

Fu, X. D. (2004). Towards a splicing code. *Cell* **119**, 736-738.

Futaki, S., Nakase, I., Suzuki, T., Youjun, Z. & Sugiura, Y. (2002). Translocation of branched-chain arginine peptides through cell membranes: flexibility in the spatial disposition of positive charges in membrane-permeable peptides. *Biochemistry* **41**, 7925-7930.

Garmory, H. S., Brown, K. A. & Titball, R. W. (2003). DNA vaccines: improving expression of antigens. *Genet Vaccines Ther* **1**, 2.

Ge, Q., Pastey, M., Kobasa, D., Puthavathana, P., Lupfer, C., Bestwick, R. K., Iversen, P. L., Chen, J. & Stein, D. A. (2006). Inhibition of multiple subtypes of influenza A virus in cell cultures with morpholino oligomers. *Antimicrob Agents Chemother* **50**, 3724-3733.

Gebski, B. L., Errington, S. J., Johnsen, R. D., Fletcher, S. & Wilton, S. D. (2005). Terminal antisense oligonucleotide modifications can enhance induced exon skipping. *Neuromuscul Disord* **15**, 622-629.

Gebski, B. L., Mann, C. J., Fletcher, S. & Wilton, S. D. (2003). Morpholino antisense oligonucleotide induced dystrophin exon 23 skipping in mdx mouse muscle. *Hum Mol Genet* **12**, 1801-1811.

Ghahramani Seno, M. M., Graham, I. R., Athanasopoulos, T., Trollet, C., Pohlschmidt, M., Crompton, M. R. & Dickson, G. (2008). RNAi-mediated knockdown of dystrophin expression in adult mice does not lead to overt muscular dystrophy pathology. *Hum Mol Genet* **17**, 2622-2632.

Girgenrath, S., Song, K. & Whittemore, L. A. (2005). Loss of myostatin expression alters fiber-type distribution and expression of myosin heavy chain isoforms in slow- and fast-type skeletal muscle. *Muscle Nerve* **31**, 34-40.

Glass, D. J. (2003). Signalling pathways that mediate skeletal muscle hypertrophy and atrophy. *Nat Cell Biol* **5**, 87-90.

Gomes-Marcondes, M. C. & Tisdale, M. J. (2002). Induction of protein catabolism and the ubiquitin-proteasome pathway by mild oxidative stress. *Cancer Lett* **180**, 69-74.

Gonzalez-Cadavid, N. F., Taylor, W. E., Yarasheski, K., Sinha-Hikim, I., Ma, K., Ezzat, S., Shen, R., Lalani, R., Asa, S., Mamita, M., Nair, G., Arver, S. & Bhasin, S. (1998). Organization of the human myostatin gene and expression in healthy men and HIV-infected men with muscle wasting. *Proc Natl Acad Sci U S A* **95**, 14938-14943.

Goto, M., Sawamura, D., Nishie, W., Sakai, K., McMillan, J. R., Akiyama, M. & Shimizu, H. (2006). Targeted skipping of a single exon harboring a premature termination codon mutation: implications and potential for gene correction therapy for selective dystrophic epidermolysis bullosa patients. *J Invest Dermatol* **126**, 2614-2620.

Goyenvalle, A., Babbs, A., Powell, D., Kole, R., Fletcher, S., Wilton, S. D. & Davies, K. E. (2010). Prevention of dystrophic pathology in severely affected dystrophin/utrophin-deficient mice by morpholino-oligomer-mediated exon-skipping. *Mol Ther* **18**, 198-205.

Graham, I. R., Hill, V. J., Manoharan, M., Inamati, G. B. & Dickson, G. (2004a). Towards a therapeutic inhibition of dystrophin exon 23 splicing in mdx mouse muscle induced by antisense oligoribonucleotides (splicomers): target sequence optimisation using oligonucleotide arrays. *J Gene Med* **6**, 1149-1158.

Graham, I. R., Hill, V. J., Manoharan, M., Inamati, G. B. & Dickson, G. (2004b). Towards a therapeutic inhibition of dystrophin exon 23 splicing in mdx mouse muscle induced by antisense oligoribonucleotides (splicomers): target sequence optimisation using oligonucleotide arrays. *Journal of Gene Medicine* **6**, 1149-1158.

Graveley, B. R. (2000). Sorting out the complexity of SR protein functions. *RNA* **6**, 1197-1211.

Gregorevic, P., Allen, J. M., Minami, E., Blankinship, M. J., Haraguchi, M., Meuse, L., Finn, E., Adams, M. E., Froehner, S. C., Murry, C. E. & Chamberlain, J. S. (2006). rAAV6-microdystrophin preserves muscle function and extends lifespan in severely dystrophic mice. *Nat Med* **12**, 787-789.

Gregorevic, P., Blankinship, M. J., Allen, J. M., Crawford, R. W., Meuse, L., Miller, D. G., Russell, D. W. & Chamberlain, J. S. (2004). Systemic delivery of genes to striated muscles using adeno-associated viral vectors. *Nat Med* **10**, 828-834.

Gregorevic, P., Plant, D. R., Leeding, K. S., Bach, L. A. & Lynch, G. S. (2002). Improved contractile function of the mdx dystrophic mouse diaphragm muscle after insulin-like growth factor-I administration. *Am J Pathol* **161**, 2263-2272.

Green, J. H. (1968). An introduction to Human physiology (2nd edition). Oxford University press, London.

Grillone, L. R. & Lanz, R. (2001). Fomivirsen. *Drugs Today (Barc)* **37**, 245-255.

Grishok, A., Tabara, H. & Mello, C. C. (2000). Genetic requirements for inheritance of RNAi in C. elegans. *Science* **287**, 2494-2497.

Grobet, L., Martin, L. J., Poncelet, D., Pirottin, D., Brouwers, B., Riquet, J., Schoeberlein, A., Dunner, S., Menissier, F., Massabanda, J., Fries, R., Hanset, R. & Georges, M. (1997). A deletion in the bovine myostatin gene causes the double-muscled phenotype in cattle. *Nat Genet* **17**, 71-74.

Gussoni, E., Soneoka, Y., Strickland, C. D., Buzney, E. A., Khan, M. K., Flint, A. F., Kunkel, L. M. & Mulligan, R. C. (1999). Dystrophin expression in the mdx mouse restored by stem cell transplantation. *Nature* **401**, 390-394.

Guttridge, D. C., Mayo, M. W., Madrid, L. V., Wang, C. Y. & Baldwin, A. S., Jr. (2000). NF-kappaB-induced loss of MyoD messenger RNA: possible role in muscle decay and cachexia. *Science* **289**, 2363-2366.

Hanvey, J. C., Peffer, N. J., Bisi, J. E., Thomson, S. A., Cadilla, R., Josey, J. A., Ricca, D. J., Hassman, C. F., Bonham, M. A., Au, K. G. & et al. (1992). Antisense and antigene properties of peptide nucleic acids. *Science* **258**, 1481-1485.

Haseltine, W. A., Maxam, A. M. & Gilbert, W. (1977). Rous sarcoma virus genome is terminally redundant: the 5' sequence. *Proc Natl Acad Sci U S A* **74**, 989-993.

Hata, A., Lagna, G., Massague, J. & Hemmati-Brivanlou, A. (1998). Smad6 inhibits BMP/Smad1 signaling by specifically competing with the Smad4 tumor suppressor. *Genes Dev* **12**, 186-197.

Hata, A., Tsuzuki, T., Shimada, K., Takiguchi, M., Mori, M. & Matsuda, I. (1986). Isolation and characterization of the human ornithine transcarbamylase gene: structure of the 5'-end region. *J Biochem* **100**, 717-725.

Hayashi, H., Abdollah, S., Qiu, Y., Cai, J., Xu, Y. Y., Grinnell, B. W., Richardson, M. A., Topper, J. N., Gimbrone, M. A., Jr., Wrana, J. L. & Falb, D. (1997). The MAD-related protein Smad7 associates with the TGFbeta receptor and functions as an antagonist of TGFbeta signaling. *Cell* **89**, 1165-1173.

Heemskerk, H. A., de Winter, C. L., de Kimpe, S. J., van Kuik-Romeijn, P., Heuvelmans, N., Platenburg, G. J., van Ommen, G. J., van Deutekom, J. C. & Aartsma-Rus, A. (2009). In vivo comparison of 2'-O-methyl phosphorothioate and morpholino antisense oligonucleotides for Duchenne muscular dystrophy exon skipping. *J Gene Med* **11**, 257-266.

Helmken, C., Hofmann, Y., Schoenen, F., Oprea, G., Raschke, H., Rudnik-Schoneborn, S., Zerres, K. & Wirth, B. (2003). Evidence for a modifying pathway in SMA discordant families: reduced SMN level decreases the amount of its interacting partners and Htra2-beta1. *Hum Genet* **114**, 11-21.

Hennebry, A., Berry, C., Siriett, V., O'Callaghan, P., Chau, L., Watson, T., Sharma, M. & Kambadur, R. (2009). Myostatin regulates fiber-type composition of skeletal muscle by regulating MEF2 and MyoD gene expression. *Am J Physiol Cell Physiol* **296**, C525-534.

Hill, J. J., Davies, M. V., Pearson, A. A., Wang, J. H., Hewick, R. M., Wolfman, N. M. & Qiu, Y. (2002). The myostatin propeptide and the follistatin-related gene are inhibitory binding proteins of myostatin in normal serum. *J Biol Chem* **277**, 40735-40741.

Hill, J. J., Qiu, Y., Hewick, R. M. & Wolfman, N. M. (2003). Regulation of myostatin in vivo by growth and differentiation factor-associated serum protein-1: a novel protein with protease inhibitor and follistatin domains. *Mol Endocrinol* **17**, 1144-1154.

Hoffman, E. P., Brown, R. H., Jr. & Kunkel, L. M. (1987a). Dystrophin: the protein product of the Duchenne muscular dystrophy locus. *Cell* **51**, 919-928.

Hoffman, E. P. & Dressman, D. (2001). Molecular pathophysiology and targeted therapeutics for muscular dystrophy. *Trends Pharmacol Sci* **22**, 465-470.

Hoffman, E. P., Monaco, A. P., Feener, C. C. & Kunkel, L. M. (1987b). Conservation of the Duchenne muscular dystrophy gene in mice and humans. *Science* **238**, 347-350.

Horwich, A. L., Fenton, W. A., Williams, K. R., Kalousek, F., Kraus, J. P., Doolittle, R. F., Konigsberg, W. & Rosenberg, L. E. (1984). Structure and expression of a complementary DNA for the nuclear coded precursor of human mitochondrial ornithine transcarbamylase. *Science* **224**, 1068-1074.

Hua, Y., Vickers, T. A., Baker, B. F., Bennett, C. F. & Krainer, A. R. (2007). Enhancement of SMN2 exon 7 inclusion by antisense oligonucleotides targeting the exon. *PLoS Biol* **5**, e73.

Huard, J., Krisky, D., Oligino, T., Marconi, P., Day, C. S., Watkins, S. C. & Glorioso, J. C. (1997). Gene transfer to muscle using herpes simplex virus-based vectors. *Neuromuscul Disord* **7**, 299-313.

Hudziak, R. M., Barofsky, E., Barofsky, D. F., Weller, D. L., Huang, S. B. & Weller, D. D. (1996). Resistance of morpholino phosphorodiamidate oligomers to enzymatic degradation. *Antisense Nucleic Acid Drug Dev* **6**, 267-272.

Hutvagner, G. & Zamore, P. D. (2002). RNAi: nature abhors a double-strand. *Curr Opin Genet Dev* **12**, 225-232.

Inagaki, Y., Truter, S. & Ramirez, F. (1994). Transforming growth factor-beta stimulates alpha 2(I) collagen gene expression through a cis-acting element that contains an Sp1-binding site. *J Biol Chem* **269**, 14828-14834.

Iversen, P. L. (2001). Phosphorodiamidate morpholino oligomers: favorable properties for sequence-specific gene inactivation. *Curr Opin Mol Ther* **3**, 235-238.

Janssens, S., Burns, K., Tschopp, J. & Beyaert, R. (2002). Regulation of interleukin-1- and lipopolysaccharide-induced NF-kappaB activation by alternative splicing of MyD88. *Curr Biol* **12**, 467-471.

Jearawiriyapaisarn, N., Moulton, H. M., Sazani, P., Kole, R. & Willis, M. S. (2010). Long-term improvement in mdx cardiomyopathy after therapy with peptide-conjugated morpholino oligomers. *Cardiovasc Res* **85**, 444-453.

Jensen, K. K., Orum, H., Nielsen, P. E. & Norden, B. (1997). Kinetics for hybridization of peptide nucleic acids (PNA) with DNA and RNA studied with the BIAcore technique. *Biochemistry* **36**, 5072-5077.

Ji, S., Losinski, R. L., Cornelius, S. G., Frank, G. R., Willis, G. M., Gerrard, D. E., Depreux, F. F. & Spurlock, M. E. (1998). Myostatin expression in porcine tissues: tissue specificity and developmental and postnatal regulation. *Am J Physiol* **275**, R1265-1273.

Kaler, S. G., Das, S., Levinson, B., Goldstein, D. S., Holmes, C. S., Patronas, N. J., Packman, S. & Gahl, W. A. (1996). Successful early copper therapy in Menkes disease associated with a mutant transcript containing a small In-frame deletion. *Biochem Mol Med* **57**, 37-46.

Karkare, S. & Bhatnagar, D. (2006). Promising nucleic acid analogs and mimics: characteristic features and applications of PNA, LNA, and morpholino. *Appl Microbiol Biotechnol* **71**, 575-586.

Kemaladewi, D. U., Hoogaars, W. M., van Heiningen, S. H., Terlouw, S., de Gorter, D. J., den Dunnen, J. T., van Ommen, G. J., Aartsma-Rus, A., ten Dijke, P. & t Hoen, P. A. (2011). Dual exon skipping in myostatin and dystrophin for Duchenne muscular dystrophy. *BMC Med Genomics* **4**, 36.

Kenny, A. M., Prestwood, K. M., Gruman, C. A., Marcello, K. M. & Raisz, L. G. (2001). Effects of transdermal testosterone on bone and muscle in older men with low bioavailable testosterone levels. *J Gerontol A Biol Sci Med Sci* **56**, M266-272.

Khajavi, M., Inoue, K., Wiszniewski, W., Ohyama, T., Snipes, G. J. & Lupski, J. R. (2005). Curcumin treatment abrogates endoplasmic reticulum retention and aggregation-induced apoptosis associated with neuropathy-causing myelin protein zero-truncating mutants. *Am J Hum Genet* **77**, 841-850.

Khoo, B., Roca, X., Chew, S. L. & Krainer, A. R. (2007). Antisense oligonucleotide-induced alternative splicing of the APOB mRNA generates a novel isoform of APOB. *BMC Mol Biol* **8**, 3.

Khoshnan, A. & Patterson, P. H. (2011). The role of IkappaB kinase complex in the neurobiology of Huntington's disease. *Neurobiol Dis* **43**, 305-311.

Khurana, T. S. & Davies, K. E. (2003). Pharmacological strategies for muscular dystrophy. *Nat Rev Drug Discov* **2**, 379-390.

Khurana, T. S., Watkins, S. C., Chafey, P., Chelly, J., Tome, F. M., Fardeau, M., Kaplan, J. C. & Kunkel, L. M. (1991). Immunolocalization and developmental expression of dystrophin related protein in skeletal muscle. *Neuromuscul Disord* **1**, 185-194.

Kim, S., Radhakrishnan, U. P., Rajpurohit, S. K., Kulkarni, V. & Jagadeeswaran, P. (2010). Vivo-Morpholino knockdown of alphaIIb: A novel approach to inhibit thrombocyte function in adult zebrafish. *Blood Cells Mol Dis* **44**, 169-174.

Kinali, M., Arechavala-Gomeza, V., Feng, L., Cirak, S., Hunt, D., Adkin, C., Guglieri, M., Ashton, E., Abbs, S., Nihoyannopoulos, P., Garralda, M. E., Rutherford, M., McCulley, C., Popplewell, L., Graham, I. R., Dickson, G., Wood, M. J., Wells, D. J., Wilton, S. D., Kole, R., Straub, V., Bushby, K., Sewry, C., Morgan, J. E. & Muntoni, F. (2009). Local restoration of dystrophin expression with the morpholino oligomer AVI-4658 in Duchenne muscular dystrophy: a single-blind, placebo-controlled, dose-escalation, proof-of-concept study. *Lancet Neurol* **8**, 918-928.

Kinney, R. M., Huang, C. Y., Rose, B. C., Kroeker, A. D., Dreher, T. W., Iversen, P. L. & Stein, D. A. (2005). Inhibition of dengue virus serotypes 1 to 4 in vero cell cultures with morpholino oligomers. *J Virol* **79**, 5116-5128.

Knox, C. A., Kokmen, E. & Dyck, P. J. (1989). Morphometric alteration of rat myelinated fibers with aging. *J Neuropathol Exp Neurol* **48**, 119-139.

Kobayashi, Y. M., Rader, E. P., Crawford, R. W., Iyengar, N. K., Thedens, D. R., Faulkner, J. A., Parikh, S. V., Weiss, R. M., Chamberlain, J. S., Moore, S. A. & Campbell, K. P. (2008).

Sarcolemma-localized nNOS is required to maintain activity after mild exercise. *Nature* **456**, 511-515.

Kobzik, L., Reid, M. B., Bredt, D. S. & Stamler, J. S. (1994). Nitric oxide in skeletal muscle. *Nature* **372**, 546-548.

Kole, R. & Sazani, P. (2001). Antisense effects in the cell nucleus: modification of splicing. *Curr Opin Mol Ther* **3**, 229-234.

Koo, T., Okada, T., Athanasopoulos, T., Foster, H., Takeda, S. & Dickson, G. (2011). Long-term functional adeno-associated virus-microdystrophin expression in the dystrophic CXMDj dog. *J Gene Med* **13**, 497-506.

Koshkin, A. A. & Wengel, J. (1998). Synthesis of Novel 2',3'-Linked Bicyclic Thymine Ribonucleosides. *J Org Chem* **63**, 2778-2781.

Kozak, M. (2005). Regulation of translation via mRNA structure in prokaryotes and eukaryotes. *Gene* **361**, 13-37.

Krainer, A. R., Cartegni, L., Wang, J. H., Zhu, Z. W. & Zhang, M. Q. (2003). ESEfinder: a web resource to identify exonic splicing enhancers. *Nucleic Acids Research* **31**, 3568-3571.

Krajewska, M., Krajewski, S., Epstein, J. I., Shabaik, A., Sauvageot, J., Song, K., Kitada, S. & Reed, J. C. (1996). Immunohistochemical analysis of bcl-2, bax, bcl-X, and mcl-1 expression in prostate cancers. *Am J Pathol* **148**, 1567-1576.

Kricka, L. J. (1988). Clinical and biochemical applications of luciferases and luciferins. *Anal Biochem* **175**, 14-21.

Kumar, R., Singh, S. K., Koshkin, A. A., Rajwanshi, V. K., Meldgaard, M. & Wengel, J. (1998). The first analogues of LNA (locked nucleic acids): phosphorothioate-LNA and 2'-thio-LNA. *Bioorg Med Chem Lett* **8**, 2219-2222.

Kurata, S., Okuyama, T., Osada, M., Watanabe, T., Tomimori, Y., Sato, S., Iwai, A., Tsuji, T., Ikawa, Y. & Katoh, I. (2004). p51/p63 Controls subunit alpha3 of the major epidermis integrin anchoring the stem cells to the niche. *J Biol Chem* **279**, 50069-50077.

Lacerra, G., Sierakowska, H., Carestia, C., Fucharoen, S., Summerton, J., Weller, D. & Kole, R. (2000). Restoration of hemoglobin A synthesis in erythroid cells from peripheral blood of thalassemic patients. *Proc Natl Acad Sci U S A* **97**, 9591-9596.

Lai, Y., Thomas, G. D., Yue, Y., Yang, H. T., Li, D., Long, C., Judge, L., Bostick, B., Chamberlain, J. S., Terjung, R. L. & Duan, D. (2009). Dystrophins carrying spectrin-like repeats 16 and 17 anchor nNOS to the sarcolemma and enhance exercise performance in a mouse model of muscular dystrophy. *J Clin Invest* **119**, 624-635.

Langley, B., Thomas, M., Bishop, A., Sharma, M., Gilmour, S. & Kambadur, R. (2002a). Myostatin inhibits myoblast differentiation by down-regulating MyoD expression. *J Biol Chem* **277**, 49831-49840.

Langley, B., Thomas, M., Bishop, A., Sharma, M., Gilmour, S. & Kambadur, R. (2002b). Myostatin inhibits myoblast differentiation by down-regulating MyoD expression. *J Biol Chem* **277**, 49831-49840.

Larrouy, B., Blonski, C., Boiziau, C., Stuer, M., Moreau, S., Shire, D. & Toulme, J. J. (1992). RNase H-mediated inhibition of translation by antisense oligodeoxyribonucleotides: use of backbone modification to improve specificity. *Gene* **121**, 189-194.

Lee, S. J. (2004). Regulation of muscle mass by myostatin. *Annu Rev Cell Dev Biol* **20**, 61-86.

Lee, S. J., Lee, K. W. & Lee, H. J. (2004). Abies nephrolepis leaf phenolics prevent the inhibition of gap junction intercellular communication by hydrogen peroxide in rat liver epithelial cells. *Biofactors* **21**, 357-360.

Lee, S. J. & McPherron, A. C. (2001). Regulation of myostatin activity and muscle growth. *Proc Natl Acad Sci U S A* **98**, 9306-9311.

Lee, S. J., Reed, L. A., Davies, M. V., Girgenrath, S., Goad, M. E., Tomkinson, K. N., Wright, J. F., Barker, C., Ehrmantraut, G., Holmstrom, J., Trowell, B., Gertz, B., Jiang, M. S., Sebald, S. M., Matzuk, M., Li, E., Liang, L. F., Quattlebaum, E., Stotish, R. L. &

Wolfman, N. M. (2005). Regulation of muscle growth by multiple ligands signaling through activin type II receptors. *Proc Natl Acad Sci U S A* **102**, 18117-18122.

Lefebvre, S., Burglen, L., Reboullet, S., Clermont, O., Burlet, P., Viollet, L., Benichou, B., Cruaud, C., Millasseau, P., Zeviani, M. & et al. (1995). Identification and characterization of a spinal muscular atrophy-determining gene. *Cell* **80**, 155-165.

Li, Y. P., Chen, Y., John, J., Moylan, J., Jin, B., Mann, D. L. & Reid, M. B. (2005). TNF-alpha acts via p38 MAPK to stimulate expression of the ubiquitin ligase atrogin1/MAFbx in skeletal muscle. *FASEB J* **19**, 362-370.

Li, Y. P., Chen, Y., Li, A. S. & Reid, M. B. (2003). Hydrogen peroxide stimulates ubiquitin-conjugating activity and expression of genes for specific E2 and E3 proteins in skeletal muscle myotubes. *Am J Physiol Cell Physiol* **285**, C806-812.

Li, Z. B., Kollias, H. D. & Wagner, K. R. (2008). Myostatin directly regulates skeletal muscle fibrosis. *J Biol Chem* **283**, 19371-19378.

Liang, K. W., Nishikawa, M., Liu, F., Sun, B., Ye, Q. & Huang, L. (2004). Restoration of dystrophin expression in mdx mice by intravascular injection of naked DNA containing full-length dystrophin cDNA. *Gene Ther* **11**, 901-908.

Licatalosi, D. D., Mele, A., Fak, J. J., Ule, J., Kayikci, M., Chi, S. W., Clark, T. A., Schweitzer, A. C., Blume, J. E., Wang, X., Darnell, J. C. & Darnell, R. B. (2008). HITS-CLIP yields genome-wide insights into brain alternative RNA processing. *Nature* **456**, 464-469.

Lin, J., Arnold, H. B., Della-Fera, M. A., Azain, M. J., Hartzell, D. L. & Baile, C. A. (2002). Myostatin knockout in mice increases myogenesis and decreases adipogenesis. *Biochem Biophys Res Commun* **291**, 701-706.

Liu, C. M., Yang, Z., Liu, C. W., Wang, R., Tien, P., Dale, R. & Sun, L. Q. (2007). Effect of RNA oligonucleotide targeting Foxo-1 on muscle growth in normal and cancer cachexia mice. *Cancer Gene Ther* **14**, 945-952.

Liu, F., Hata, A., Baker, J. C., Doody, J., Carcamo, J., Harland, R. M. & Massague, J. (1996). A human Mad protein acting as a BMP-regulated transcriptional activator. *Nature* **381**, 620-623.

Liu, H. X., Chew, S. L., Cartegni, L., Zhang, M. Q. & Krainer, A. R. (2000). Exonic splicing enhancer motif recognized by human SC35 under splicing conditions. *Mol Cell Biol* **20**, 1063-1071.

Liu, H. X., Zhang, M. & Krainer, A. R. (1998). Identification of functional exonic splicing enhancer motifs recognized by individual SR proteins. *Genes Dev* **12**, 1998-2012.

Liu, J. P., Baker, J., Perkins, A. S., Robertson, E. J. & Efstratiadis, A. (1993). Mice carrying null mutations of the genes encoding insulin-like growth factor I (Igf-1) and type 1 IGF receptor (Igf1r). *Cell* **75**, 59-72.

Liu, Z., Sall, A. & Yang, D. (2008). MicroRNA: An emerging therapeutic target and intervention tool. *Int J Mol Sci* **9**, 978-999.

Love, D. R., Hill, D. F., Dickson, G., Spurr, N. K., Byth, B. C., Marsden, R. F., Walsh, F. S., Edwards, Y. H. & Davies, K. E. (1989). An autosomal transcript in skeletal muscle with homology to dystrophin. *Nature* **339**, 55-58.

Love, D. R., Morris, G. E., Ellis, J. M., Fairbrother, U., Marsden, R. F., Bloomfield, J. F., Edwards, Y. H., Slater, C. P., Parry, D. J. & Davies, K. E. (1991). Tissue distribution of the dystrophin-related gene product and expression in the mdx and dy mouse. *Proc Natl Acad Sci U S A* **88**, 3243-3247.

Lu, Q. L., Rabinowitz, A., Chen, Y. C., Yokota, T., Yin, H., Alter, J., Jadoon, A., Bou-Gharios, G. & Partridge, T. (2005). Systemic delivery of antisense oligoribonucleotide restores dystrophin expression in body-wide skeletal muscles. *Proc Natl Acad Sci U S A* **102**, 198-203.

Luff, A. R. (1998). Age-associated changes in the innervation of muscle fibers and changes in the mechanical properties of motor units. *Ann N Y Acad Sci* **854**, 92-101.

Lum, J. J., DeBerardinis, R. J. & Thompson, C. B. (2005). Autophagy in metazoans: cell survival in the land of plenty. *Nat Rev Mol Cell Biol* **6**, 439-448.

Maccatrozzo, L., Bargelloni, L., Radaelli, G., Mascarello, F. & Patarnello, T. (2001). Characterization of the myostatin gene in the gilthead seabream (Sparus aurata): sequence, genomic structure, and expression pattern. *Mar Biotechnol (NY)* **3**, 224-230.

Macias-Silva, M., Abdollah, S., Hoodless, P. A., Pirone, R., Attisano, L. & Wrana, J. L. (1996). MADR2 is a substrate of the TGFbeta receptor and its phosphorylation is required for nuclear accumulation and signaling. *Cell* **87**, 1215-1224.

Mammucari, C., Milan, G., Romanello, V., Masiero, E., Rudolf, R., Del Piccolo, P., Burden, S. J., Di Lisi, R., Sandri, C., Zhao, J., Goldberg, A. L., Schiaffino, S. & Sandri, M. (2007). FoxO3 controls autophagy in skeletal muscle in vivo. *Cell Metab* **6**, 458-471.

Mann, C. J., Honeyman, K., McClorey, G., Fletcher, S. & Wilton, S. D. (2002). Improved antisense oligonucleotide induced exon skipping in the mdx mouse model of muscular dystrophy. *J Gene Med* **4**, 644-654.

Mantovani, G., Maccio, A., Madeddu, C., Mura, L., Gramignano, G., Lusso, M. R., Massa, E., Mocci, M. & Serpe, R. (2003). Antioxidant agents are effective in inducing lymphocyte progression through cell cycle in advanced cancer patients: assessment of the most important laboratory indexes of cachexia and oxidative stress. *J Mol Med (Berl)* **81**, 664-673.

Marieb, E. N. (2009). Essentials of human anatomy and physiology (9^{th} edition). Pearson/Benjamin Cummings, San Francisco, CA.

Marques, S. M. & da Silva, J. C. (2008). An optimized luciferase bioluminescent assay for coenzyme A. *Anal Bioanal Chem* **391**, 2161-2168.

Marvit, J., DiLella, A. G., Brayton, K., Ledley, F. D., Robson, K. J. & Woo, S. L. (1987). GT to AT transition at a splice donor site causes skipping of the preceding exon in phenylketonuria. *Nucleic Acids Res* **15**, 5613-5628.

Matsakas, A., Foster, K., Otto, A., Macharia, R., Elashry, M. I., Feist, S., Graham, I., Foster, H., Yaworsky, P., Walsh, F., Dickson, G. & Patel, K. (2009). Molecular, cellular and physiological investigation of myostatin propeptide-mediated muscle growth in adult mice. *Neuromuscul Disord* **19**, 489-499.

Matsuo, M. (1996). Duchenne/Becker muscular dystrophy: from molecular diagnosis to gene therapy. *Brain Dev* **18**, 167-172.

Matsuo, M., Masumura, T., Nishio, H., Nakajima, T., Kitoh, Y., Takumi, T., Koga, J. & Nakamura, H. (1991). Exon skipping during splicing of dystrophin mRNA precursor due to an intraexon deletion in the dystrophin gene of Duchenne muscular dystrophy kobe. *J Clin Invest* **87**, 2127-2131.

McGrath, J. A., Ashton, G. H., Mellerio, J. E., Salas-Alanis, J. C., Swensson, O., McMillan, J. R. & Eady, R. A. (1999). Moderation of phenotypic severity in dystrophic and junctional forms of epidermolysis bullosa through in-frame skipping of exons containing non-sense or frameshift mutations. *J Invest Dermatol* **113**, 314-321.

McLennan, I. S. & Koishi, K. (2002). The transforming growth factor-betas: multifaceted regulators of the development and maintenance of skeletal muscles, motoneurons and Schwann cells. *Int J Dev Biol* **46**, 559-567.

McPherron, A. C., Lawler, A. M. & Lee, S. J. (1997). Regulation of skeletal muscle mass in mice by a new TGF-beta superfamily member. *Nature* **387**, 83-90.

McPherron, A. C. & Lee, S. J. (1997). Double muscling in cattle due to mutations in the myostatin gene. *Proc Natl Acad Sci U S A* **94**, 12457-12461.

McPherron, A. C. & Lee, S. J. (2002). Suppression of body fat accumulation in myostatin-deficient mice. *J Clin Invest* **109**, 595-601.

Meersseman, G., Verschueren, K., Nelles, L., Blumenstock, C., Kraft, H., Wuytens, G., Remacle, J., Kozak, C. A., Tylzanowski, P., Niehrs, C. & Huylebroeck, D. (1997). The C-

terminal domain of Mad-like signal transducers is sufficient for biological activity in the Xenopus embryo and transcriptional activation. *Mech Dev* **61**, 127-140.

Megeney, L. A., Kablar, B., Garrett, K., Anderson, J. E. & Rudnicki, M. A. (1996). MyoD is required for myogenic stem cell function in adult skeletal muscle. *Genes Dev* **10**, 1173-1183.

Mercatante, D. R., Mohler, J. L. & Kole, R. (2002). Cellular response to an antisense-mediated shift of Bcl-x pre-mRNA splicing and antineoplastic agents. *J Biol Chem* **277**, 49374-49382.

Mercatante, D. R., Sazani, P. & Kole, R. (2001). Modification of alternative splicing by antisense oligonucleotides as a potential chemotherapy for cancer and other diseases. *Curr Cancer Drug Targets* **1**, 211-230.

Meszaros, L. G., Minarovic, I. & Zahradnikova, A. (1996). Inhibition of the skeletal muscle ryanodine receptor calcium release channel by nitric oxide. *FEBS Lett* **380**, 49-52.

Miller, P. S., McParland, K. B., Jayaraman, K. & Ts'o, P. O. (1981). Biochemical and biological effects of nonionic nucleic acid methylphosphonates. *Biochemistry* **20**, 1874-1880.

Miller, P. S., Yano, J., Yano, E., Carroll, C., Jayaraman, K. & Ts'o, P. O. (1979). Nonionic nucleic acid analogues. Synthesis and characterization of dideoxyribonucleoside methylphosphonates. *Biochemistry* **18**, 5134-5143.

Millington-Ward, S., McMahon, H. P., Allen, D., Tuohy, G., Kiang, A. S., Palfi, A., Kenna, P. F., Humphries, P. & Farrar, G. J. (2004). RNAi of COL1A1 in mesenchymal progenitor cells. *Eur J Hum Genet* **12**, 864-866.

Minshull, J. & Hunt, T. (1986). The use of single-stranded DNA and RNase H to promote quantitative 'hybrid arrest of translation' of mRNA/DNA hybrids in reticulocyte lysate cell-free translations. *Nucleic Acids Res* **14**, 6433-6451.

Monaco, A. P., Bertelson, C. J., Liechti-Gallati, S., Moser, H. & Kunkel, L. M. (1988). An explanation for the phenotypic differences between patients bearing partial deletions of the DMD locus. *Genomics* **2**, 90-95.

Morcos, P. A. (2001). Achieving efficient delivery of morpholino oligos in cultured cells. *Genesis* **30**, 94-102.

Morcos, P. A. (2007). Achieving targeted and quantifiable alteration of mRNA splicing with Morpholino oligos. *Biochem Biophys Res Commun* **358**, 521-527.

Morcos, P. A., Li, Y. & Jiang, S. (2008). Vivo-Morpholinos: a non-peptide transporter delivers Morpholinos into a wide array of mouse tissues. *Biotechniques* **45**, 613-614, 616, 618 passim.

Morgan, J. E., Coulton, G. R. & Partridge, T. A. (1989). Mdx muscle grafts retain the mdx phenotype in normal hosts. *Muscle Nerve* **12**, 401-409.

Morine, K. J., Bish, L. T., Pendrak, K., Sleeper, M. M., Barton, E. R. & Sweeney, H. L. (2010). Systemic myostatin inhibition via liver-targeted gene transfer in normal and dystrophic mice. *PLoS One* **5**, e9176.

Morissette, M. R., Cook, S. A., Buranasombati, C., Rosenberg, M. A. & Rosenzweig, A. (2009). Myostatin inhibits IGF-I-induced myotube hypertrophy through Akt. *Am J Physiol Cell Physiol* **297**, C1124-1132.

Morita, K., Hasegawa, C., Kaneko, M., Tsutsumi, S., Sone, J., Ishikawa, T., Imanishi, T. & Koizumi, M. (2001). 2'-O,4'-C-ethylene-bridged nucleic acids (ENA) with nuclease-resistance and high affinity for RNA. *Nucleic Acids Res Suppl*, 241-242.

Mosher, D. S., Quignon, P., Bustamante, C. D., Sutter, N. B., Mellersh, C. S., Parker, H. G. & Ostrander, E. A. (2007). A mutation in the myostatin gene increases muscle mass and enhances racing performance in heterozygote dogs. *PLoS Genet* **3**, e79.

Moulton, H. M. & Moulton, J. D. (2010). Morpholinos and their peptide conjugates: therapeutic promise and challenge for Duchenne muscular dystrophy. *Biochim Biophys Acta* **1798**, 2296-2303.

Moulton, H. M., Wu, B., Jearawiriyapaisarn, N., Sazani, P., Lu, Q. L. & Kole, R. (2009). Peptide-morpholino conjugate: a promising therapeutic for Duchenne muscular dystrophy. *Ann N Y Acad Sci* **1175**, 55-60.

Munsat, T. L. & Davies, K. E. (1992). International SMA consortium meeting. (26-28 June 1992, Bonn, Germany). *Neuromuscul Disord* **2**, 423-428.

Murray, E. L. & Schoenberg, D. R. (2007). A+U-rich instability elements differentially activate 5'-3' and 3'-5' mRNA decay. *Mol Cell Biol* **27**, 2791-2799.

Musaro, A., McCullagh, K., Paul, A., Houghton, L., Dobrowolny, G., Molinaro, M., Barton, E. R., Sweeney, H. L. & Rosenthal, N. (2001). Localized Igf-1 transgene expression sustains hypertrophy and regeneration in senescent skeletal muscle. *Nat Genet* **27**, 195-200.

Naguib, M., Flood, P., McArdle, J. J. & Brenner, H. R. (2002). Advances in neurobiology of the neuromuscular junction: implications for the anesthesiologist. *Anesthesiology* **96**, 202-231.

Nakamura, A. & Takeda, S. (2009). Exon-skipping therapy for Duchenne muscular dystrophy. *Neuropathology* **29**, 494-501.

Nave, B. T., Ouwens, M., Withers, D. J., Alessi, D. R. & Shepherd, P. R. (1999). Mammalian target of rapamycin is a direct target for protein kinase B: identification of a convergence point for opposing effects of insulin and amino-acid deficiency on protein translation. *Biochem J* **344 Pt 2**, 427-431.

Neuman, B. W., Stein, D. A., Kroeker, A. D., Moulton, H. M., Bestwick, R. K., Iversen, P. L. & Buchmeier, M. J. (2006). Inhibition and escape of SARS-CoV treated with antisense morpholino oligomers. *Adv Exp Med Biol* **581**, 567-571.

Nielsen, P. E., Egholm, M., Berg, R. H. & Buchardt, O. (1991). Sequence-selective recognition of DNA by strand displacement with a thymine-substituted polyamide. *Science* **254**, 1497-1500.

Nilsen, T. W. (1996). A parallel spliceosome. *Science* **273**, 1813.

Nilsen, T. W. (2002). The spliceosome: no assembly required? *Mol Cell* **9**, 8-9.

O'Keefe, D. S., Bacich, D. J. & Heston, W. D. (2004). Comparative analysis of prostate-specific membrane antigen (PSMA) versus a prostate-specific membrane antigen-like gene. *Prostate* **58**, 200-210.

Odom, G. L., Gregorevic, P., Allen, J. M., Finn, E. & Chamberlain, J. S. (2008). Microutrophin delivery through rAAV6 increases lifespan and improves muscle function in dystrophic dystrophin/utrophin-deficient mice. *Mol Ther* **16**, 1539-1545.

Ohlendieck, K., Ervasti, J. M., Matsumura, K., Kahl, S. D., Leveille, C. J. & Campbell, K. P. (1991). Dystrophin-related protein is localized to neuromuscular junctions of adult skeletal muscle. *Neuron* **7**, 499-508.

Olson, E. N. & Klein, W. H. (1994). bHLH factors in muscle development: dead lines and commitments, what to leave in and what to leave out. *Genes Dev* **8**, 1-8.

Ostbye, T. K., Galloway, T. F., Nielsen, C., Gabestad, I., Bardal, T. & Andersen, O. (2001). The two myostatin genes of Atlantic salmon (Salmo salar) are expressed in a variety of tissues. *Eur J Biochem* **268**, 5249-5257.

Patel, K. & Amthor, H. (2005). The function of Myostatin and strategies of Myostatin blockade-new hope for therapies aimed at promoting growth of skeletal muscle. *Neuromuscul Disord* **15**, 117-126.

Pearce, M., Blake, D. J., Tinsley, J. M., Byth, B. C., Campbell, L., Monaco, A. P. & Davies, K. E. (1993). The utrophin and dystrophin genes share similarities in genomic structure. *Hum Mol Genet* **2**, 1765-1772.

Pei, Y. & Tuschl, T. (2006). On the art of identifying effective and specific siRNAs. *Nat Methods* **3**, 670-676.

Peng, H. & Huard, J. (2004). Muscle-derived stem cells for musculoskeletal tissue regeneration and repair. *Transpl Immunol* **12**, 311-319.

Perlman, S., Becker-Catania, S. & Gatti, R. A. (2003). Ataxia-telangiectasia: diagnosis and treatment. *Semin Pediatr Neurol* **10**, 173-182.

Philip, B., Lu, Z. & Gao, Y. (2005). Regulation of GDF-8 signaling by the p38 MAPK. *Cell Signal* **17**, 365-375.

Popplewell, L. J., Adkin, C., Arechavala-Gomeza, V., Aartsma-Rus, A., de Winter, C. L., Wilton, S. D., Morgan, J. E., Muntoni, F., Graham, I. R. & Dickson, G. (2010). Comparative analysis of antisense oligonucleotide sequences targeting exon 53 of the human DMD gene: Implications for future clinical trials. *Neuromuscul Disord* **20**, 102-110.

Popplewell, L. J., Trollet, C., Dickson, G. & Graham, I. R. (2009). Design of Phosphorodiamidate Morpholino Oligomers (PMOs) for the Induction of Exon Skipping of the Human DMD Gene. *Mol Ther* **17**, 554-561.

Reed, U. C. (2009). Congenital muscular dystrophy. Part II: a review of pathogenesis and therapeutic perspectives. *Arq Neuropsiquiatr* **67**, 343-362.

Rescan, P. Y., Jutel, I. & Ralliere, C. (2001). Two myostatin genes are differentially expressed in myotomal muscles of the trout (Oncorhynchus mykiss). *J Exp Biol* **204**, 3523-3529.

Rhodes, L. E., Freeman, B. K., Auh, S., Kokkinis, A. D., La Pean, A., Chen, C., Lehky, T. J., Shrader, J. A., Levy, E. W., Harris-Love, M., Di Prospero, N. A. & Fischbeck, K. H. (2009). Clinical features of spinal and bulbar muscular atrophy. *Brain* **132**, 3242-3251.

Richard, J. P., Melikov, K., Vives, E., Ramos, C., Verbeure, B., Gait, M. J., Chernomordik, L. V. & Lebleu, B. (2003). Cell-penetrating peptides. A reevaluation of the mechanism of cellular uptake. *J Biol Chem* **278**, 585-590.

Rios, R., Carneiro, I., Arce, V. M. & Devesa, J. (2001). Myostatin regulates cell survival during C2C12 myogenesis. *Biochem Biophys Res Commun* **280**, 561-566.

Roberts, J., Palma, E., Sazani, P., Orum, H., Cho, M. & Kole, R. (2006). Efficient and persistent splice switching by systemically delivered LNA oligonucleotides in mice. *Mol Ther* **14**, 471-475.

Roberts, S. B. & Goetz, F. W. (2001). Differential skeletal muscle expression of myostatin across teleost species, and the isolation of multiple myostatin isoforms. *FEBS Lett* **491**, 212-216.

Robinson, D. O., Wills, A. J., Hammans, S. R., Read, S. P. & Sillibourne, J. (2006). Oculopharyngeal muscular dystrophy: a point mutation which mimics the effect of the PABPN1 gene triplet repeat expansion mutation. *J Med Genet* **43**, e23.

Rodgers, B. D. & Garikipati, D. K. (2008). Clinical, agricultural, and evolutionary biology of myostatin: a comparative review. *Endocr Rev* **29**, 513-534.

Rodgers, B. D., Weber, G. M., Sullivan, C. V. & Levine, M. A. (2001). Isolation and characterization of myostatin complementary deoxyribonucleic acid clones from two commercially important fish: Oreochromis mossambicus and Morone chrysops. *Endocrinology* **142**, 1412-1418.

Rodino-Klapac, L. R., Haidet, A. M., Kota, J., Handy, C., Kaspar, B. K. & Mendell, J. R. (2009). Inhibition of myostatin with emphasis on follistatin as a therapy for muscle disease. *Muscle Nerve* **39**, 283-296.

Rodino-Klapac, L. R., Montgomery, C. L., Bremer, W. G., Shontz, K. M., Malik, V., Davis, N., Sprinkle, S., Campbell, K. J., Sahenk, Z., Clark, K. R., Walker, C. M., Mendell, J. R. & Chicoine, L. G. (2010). Persistent expression of FLAG-tagged micro dystrophin in nonhuman primates following intramuscular and vascular delivery. *Mol Ther* **18**, 109-117.

Rodriguez-Lebron, E. & Paulson, H. L. (2006). Allele-specific RNA interference for neurological disease. *Gene Ther* **13**, 576-581.

Rose, S. D., Kim, D. H., Amarzguioui, M., Heidel, J. D., Collingwood, M. A., Davis, M. E., Rossi, J. J. & Behlke, M. A. (2005). Functional polarity is introduced by Dicer processing of short substrate RNAs. *Nucleic Acids Res* **33**, 4140-4156.

Rosen, D. R. (1993). Mutations in Cu/Zn superoxide dismutase gene are associated with familial amyotrophic lateral sclerosis. *Nature* **364**, 362.

Rothbard, J. B., Jessop, T. C., Lewis, R. S., Murray, B. A. & Wender, P. A. (2004). Role of membrane potential and hydrogen bonding in the mechanism of translocation of guanidinium-rich peptides into cells. *J Am Chem Soc* **126**, 9506-9507.

Sampaolesi, M., Blot, S., D'Antona, G., Granger, N., Tonlorenzi, R., Innocenzi, A., Mognol, P., Thibaud, J. L., Galvez, B. G., Barthelemy, I., Perani, L., Mantero, S., Guttinger, M., Pansarasa, O., Rinaldi, C., Cusella De Angelis, M. G., Torrente, Y., Bordignon, C., Bottinelli, R. & Cossu, G. (2006). Mesoangioblast stem cells ameliorate muscle function in dystrophic dogs. *Nature* **444**, 574-579.

Sampaolesi, M., Torrente, Y., Innocenzi, A., Tonlorenzi, R., D'Antona, G., Pellegrino, M. A., Barresi, R., Bresolin, N., De Angelis, M. G., Campbell, K. P., Bottinelli, R. & Cossu, G. (2003). Cell therapy of alpha-sarcoglycan null dystrophic mice through intra-arterial delivery of mesoangioblasts. *Science* **301**, 487-492.

Sander, M., Chavoshan, B., Harris, S. A., Iannaccone, S. T., Stull, J. T., Thomas, G. D. & Victor, R. G. (2000). Functional muscle ischemia in neuronal nitric oxide synthase-deficient skeletal muscle of children with Duchenne muscular dystrophy. *Proc Natl Acad Sci U S A* **97**, 13818-13823.

Sandri, M., Sandri, C., Gilbert, A., Skurk, C., Calabria, E., Picard, A., Walsh, K., Schiaffino, S., Lecker, S. H. & Goldberg, A. L. (2004). Foxo transcription factors induce the atrophy-related ubiquitin ligase atrogin-1 and cause skeletal muscle atrophy. *Cell* **117**, 399-412.

Sartori, R., Milan, G., Patron, M., Mammucari, C., Blaauw, B., Abraham, R. & Sandri, M. (2009). Smad2 and 3 transcription factors control muscle mass in adulthood. *Am J Physiol Cell Physiol* **296**, C1248-1257.

Sazani, P., Gemignani, F., Kang, S. H., Maier, M. A., Manoharan, M., Persmark, M., Bortner, D. & Kole, R. (2002a). Systemically delivered antisense oligomers upregulate gene expression in mouse tissues. *Nat Biotechnol* **20**, 1228-1233.

Sazani, P., Kang, S. H., Maier, M. A., Wei, C., Dillman, J., Summerton, J., Manoharan, M. & Kole, R. (2001). Nuclear antisense effects of neutral, anionic and cationic oligonucleotide analogs. *Nucleic Acids Res* **29**, 3965-3974.

Sazani, P. & Kole, R. (2003). Therapeutic potential of antisense oligonucleotides as modulators of alternative splicing. *J Clin Invest* **112**, 481-486.

Sazani, P., Vacek, M. M. & Kole, R. (2002b). Short-term and long-term modulation of gene expression by antisense therapeutics. *Curr Opin Biotechnol* **13**, 468-472.

Schaap, L. A., Pluijm, S. M., Deeg, D. J., Harris, T. B., Kritchevsky, S. B., Newman, A. B., Colbert, L. H., Pahor, M., Rubin, S. M., Tylavsky, F. A. & Visser, M. (2009). Higher inflammatory marker levels in older persons: associations with 5-year change in muscle mass and muscle strength. *J Gerontol A Biol Sci Med Sci* **64**, 1183-1189.

Scherer, S. S. (2011). The debut of a rational treatment for an inherited neuropathy? *J Clin Invest* **121**, 4624-4627.

Scherer, S. S. & Wrabetz, L. (2008). Molecular mechanisms of inherited demyelinating neuropathies. *Glia* **56**, 1578-1589.

Schertzer, J. D., Ryall, J. G. & Lynch, G. S. (2006). Systemic administration of IGF-I enhances oxidative status and reduces contraction-induced injury in skeletal muscles of mdx dystrophic mice. *Am J Physiol Endocrinol Metab* **291**, E499-505.

Schmucker, D. & Flanagan, J. G. (2004). Generation of recognition diversity in the nervous system. *Neuron* **44**, 219-222.

Schuelke, M., Wagner, K. R., Stolz, L. E., Hubner, C., Riebel, T., Komen, W., Braun, T., Tobin, J. F. & Lee, S. J. (2004). Myostatin mutation associated with gross muscle hypertrophy in a child. *N Engl J Med* **350**, 2682-2688.

Schultz, E. & Lipton, B. H. (1982). Skeletal muscle satellite cells: changes in proliferation potential as a function of age. *Mech Ageing Dev* **20**, 377-383.

Schwartz, D. E., Zamecnik, P. C. & Weith, H. L. (1977). Rous sarcoma virus genome is terminally redundant: the 3' sequence. *Proc Natl Acad Sci U S A* **74**, 994-998.

Schwarz, D. S., Hutvagner, G., Haley, B. & Zamore, P. D. (2002). Evidence that siRNAs function as guides, not primers, in the Drosophila and human RNAi pathways. *Mol Cell* **10**, 537-548.

Scriver, C. R. & Clow, C. L. (1980a). Phenylketonuria and other phenylalanine hydroxylation mutants in man. *Annu Rev Genet* **14**, 179-202.

Scriver, C. R. & Clow, C. L. (1980b). Phenylketonuria: epitome of human biochemical genetics (second of two parts). *N Engl J Med* **303**, 1394-1400.

Seeley, R.R., Stephens, T.D., Tate, P. (2006). Anatomy and physiology (7th edition). McGrawHill, Dubuque, IA.

Semsarian, C., Wu, M. J., Ju, Y. K., Marciniec, T., Yeoh, T., Allen, D. G., Harvey, R. P. & Graham, R. M. (1999). Skeletal muscle hypertrophy is mediated by a Ca2+-dependent calcineurin signalling pathway. *Nature* **400**, 576-581.

Sharp, P. A. (2009). The centrality of RNA. *Cell* **136**, 577-580.

Sharp, P. A. & Zamore, P. D. (2000). Molecular biology. RNA interference. *Science* **287**, 2431-2433.

Sherratt, T. G., Vulliamy, T., Dubowitz, V., Sewry, C. A. & Strong, P. N. (1993). Exon skipping and translation in patients with frameshift deletions in the dystrophin gene. *Am J Hum Genet* **53**, 1007-1015.

Sherratt, T. G., Vulliamy, T. & Strong, P. N. (1992). Evolutionary conservation of the dystrophin central rod domain. *Biochem J* **287 (Pt 3)**, 755-759.

Shi, Y. & Massague, J. (2003). Mechanisms of TGF-beta signaling from cell membrane to the nucleus. *Cell* **113**, 685-700.

Siddique, T. & Ajroud-Driss, S. (2011). Familial amyotrophic lateral sclerosis, a historical perspective. *Acta Myol* **30**, 117-120.

Sih, R., Morley, J. E., Kaiser, F. E., Perry, H. M., 3rd, Patrick, P. & Ross, C. (1997). Testosterone replacement in older hypogonadal men: a 12-month randomized controlled trial. *J Clin Endocrinol Metab* **82**, 1661-1667.

Sinha-Hikim, I., Artaza, J., Woodhouse, L., Gonzalez-Cadavid, N., Singh, A. B., Lee, M. I., Storer, T. W., Casaburi, R., Shen, R. & Bhasin, S. (2002). Testosterone-induced increase in muscle size in healthy young men is associated with muscle fiber hypertrophy. *Am J Physiol Endocrinol Metab* **283**, E154-164.

Skjorringe, T., Tumer, Z. & Moller, L. B. (2011). Splice site mutations in the ATP7A gene. *PLoS One* **6**, e18599.

Skordis, L. A., Dunckley, M. G., Yue, B., Eperon, I. C. & Muntoni, F. (2003). Bifunctional antisense oligonucleotides provide a trans-acting splicing enhancer that stimulates SMN2 gene expression in patient fibroblasts. *Proc Natl Acad Sci U S A* **100**, 4114-4119.

Sledz, C. A. & Williams, B. R. (2005). RNA interference in biology and disease. *Blood* **106**, 787-794.

Smith, P. J., Spurrell, E. L., Coakley, J., Hinds, C. J., Ross, R. J., Krainer, A. R. & Chew, S. L. (2002). An exonic splicing enhancer in human IGF-I pre-mRNA mediates recognition of alternative exon 5 by the serine-arginine protein splicing factor-2/alternative splicing factor. *Endocrinology* **143**, 146-154.

Sohal, R. S. & Weindruch, R. (1996). Oxidative stress, caloric restriction, and aging. *Science* **273**, 59-63.

Soutar, A. K. & Naoumova, R. P. (2007). Mechanisms of disease: genetic causes of familial hypercholesterolemia. *Nat Clin Pract Cardiovasc Med* **4**, 214-225.

Stamm, S., Ben-Ari, S., Rafalska, I., Tang, Y., Zhang, Z., Toiber, D., Thanaraj, T. A. & Soreq, H. (2005). Function of alternative splicing. *Gene* **344**, 1-20.

Stavaux, D., Art, T., McEntee, K., Reznick, M. & Lekeux, P. (1994). Muscle fibre type and size, and muscle capillary density in young double-muscled blue Belgian cattle. *Zentralbl Veterinarmed A* **41**, 229-236.

Stein, C. A. (1998). How to design an antisense oligodeoxynucleotide experiment: a consensus approach. *Antisense Nucleic Acid Drug Dev* **8**, 129-132.

Stojdl, D. F. & Bell, J. C. (1999). SR protein kinases: the splice of life. *Biochemistry and Cell Biology-Biochimie Et Biologie Cellulaire* **77**, 293-298.

Sugita, H. & Takeda, S. (2010). Progress in muscular dystrophy research with special emphasis on gene therapy. *Proc Jpn Acad Ser B Phys Biol Sci* **86**, 748-756.

Summerton, J., Stein, D., Huang, S. B., Matthews, P., Weller, D. & Partridge, M. (1997). Morpholino and phosphorothioate antisense oligomers compared in cell-free and in-cell systems. *Antisense Nucleic Acid Drug Dev* **7**, 63-70.

Summerton, J. & Weller, D. (1997). Morpholino antisense oligomers: design, preparation, and properties. *Antisense Nucleic Acid Drug Dev* **7**, 187-195.

Sun, H. & Chasin, L. A. (2000). Multiple splicing defects in an intronic false exon. *Mol Cell Biol* **20**, 6414-6425.

Suwanmanee, T., Sierakowska, H., Lacerra, G., Svasti, S., Kirby, S., Walsh, C. E., Fucharoen, S. & Kole, R. (2002). Restoration of human beta-globin gene expression in murine and human IVS2-654 thalassemic erythroid cells by free uptake of antisense oligonucleotides. *Mol Pharmacol* **62**, 545-553.

Suzuki, A., Chang, C., Yingling, J. M., Wang, X. F. & Hemmati-Brivanlou, A. (1997). Smad5 induces ventral fates in Xenopus embryo. *Dev Biol* **184**, 402-405.

Swaggart, K. A., Heydemann, A., Palmer, A. A. & McNally, E. M. (2011). Distinct genetic regions modify specific muscle groups in muscular dystrophy. *Physiol Genomics* **43**, 24-31.

Szabo, G., Dallmann, G., Muller, G., Patthy, L., Soller, M. & Varga, L. (1998). A deletion in the myostatin gene causes the compact (Cmpt) hypermuscular mutation in mice. *Mamm Genome* **9**, 671-672.

Szulc, J., Wiznerowicz, M., Sauvain, M. O., Trono, D. & Aebischer, P. (2006). A versatile tool for conditional gene expression and knockdown. *Nat Methods* **3**, 109-116.

Taipale, J., Miyazono, K., Heldin, C. H. & Keski-Oja, J. (1994). Latent transforming growth factor-beta 1 associates to fibroblast extracellular matrix via latent TGF-beta binding protein. *J Cell Biol* **124**, 171-181.

Takeda, S. (2009). [Exon skipping therapy for Duchenne muscular dystrophy by using antisense Morpholino]. *Rinsho Shinkeigaku* **49**, 856-858.

Taylor, W. E., Bhasin, S., Artaza, J., Byhower, F., Azam, M., Willard, D. H., Jr., Kull, F. C., Jr. & Gonzalez-Cadavid, N. (2001). Myostatin inhibits cell proliferation and protein synthesis in C2C12 muscle cells. *Am J Physiol Endocrinol Metab* **280**, E221-228.

Tennyson, C. N., Klamut, H. J. & Worton, R. G. (1995). The human dystrophin gene requires 16 hours to be transcribed and is cotranscriptionally spliced. *Nat Genet* **9**, 184-190.

Thies, R. S., Chen, T., Davies, M. V., Tomkinson, K. N., Pearson, A. A., Shakey, Q. A. & Wolfman, N. M. (2001). GDF-8 propeptide binds to GDF-8 and antagonizes biological activity by inhibiting GDF-8 receptor binding. *Growth Factors* **18**, 251-259.

Thomas, G. D., Sander, M., Lau, K. S., Huang, P. L., Stull, J. T. & Victor, R. G. (1998). Impaired metabolic modulation of alpha-adrenergic vasoconstriction in dystrophin-deficient skeletal muscle. *Proc Natl Acad Sci U S A* **95**, 15090-15095.

Thomas, M., Langley, B., Berry, C., Sharma, M., Kirk, S., Bass, J. & Kambadur, R. (2000). Myostatin, a negative regulator of muscle growth, functions by inhibiting myoblast proliferation. *J Biol Chem* **275**, 40235-40243.

Tinsley, J., Deconinck, N., Fisher, R., Kahn, D., Phelps, S., Gillis, J. M. & Davies, K. (1998). Expression of full-length utrophin prevents muscular dystrophy in mdx mice. *Nat Med* **4**, 1441-1444.

Tinsley, J. M. & Davies, K. E. (1993). Utrophin: a potential replacement for dystrophin? *Neuromuscul Disord* **3**, 537-539.

Tintignac, L. A., Lagirand, J., Batonnet, S., Sirri, V., Leibovitch, M. P. & Leibovitch, S. A. (2005). Degradation of MyoD mediated by the SCF (MAFbx) ubiquitin ligase. *J Biol Chem* **280**, 2847-2856.

Tisdale, M. J. (2000). Biomedicine. Protein loss in cancer cachexia. *Science* **289**, 2293-2294.

Tomlinson, B. E. & Irving, D. (1977). The numbers of limb motor neurons in the human lumbosacral cord throughout life. *J Neurol Sci* **34**, 213-219.

Trendelenburg, A. U., Meyer, A., Rohner, D., Boyle, J., Hatakeyama, S. & Glass, D. J. (2009). Myostatin reduces Akt/TORC1/p70S6K signaling, inhibiting myoblast differentiation and myotube size. *Am J Physiol Cell Physiol* **296**, C1258-1270.

Trollet, C., Athanasopoulos, T., Popplewell, L., Malerba, A. & Dickson, G. (2009). Gene therapy for muscular dystrophy: current progress and future prospects. *Expert Opin Biol Ther* **9**, 849-866.

Tsui, L. C. (1992). The spectrum of cystic fibrosis mutations. *Trends Genet* **8**, 392-398.

Uitto, J., Hovnanian, A. & Christiano, A. M. (1995). Premature termination codon mutations in the type VII collagen gene (COL7A1) underlie severe recessive dystrophic epidermolysis bullosa. *Proc Assoc Am Physicians* **107**, 245-252.

Vaerman, J. L., Moureau, P., Deldime, F., Lewalle, P., Lammineur, C., Morschhauser, F. & Martiat, P. (1997). Antisense oligodeoxyribonucleotides suppress hematologic cell growth through stepwise release of deoxyribonucleotides. *Blood* **90**, 331-339.

Vaillend, C., Rendon, A., Misslin, R. & Ungerer, A. (1995). Influence of dystrophin-gene mutation on mdx mouse behavior. I. Retention deficits at long delays in spontaneous alternation and bar-pressing tasks. *Behav Genet* **25**, 569-579.

Valdez, G., Tapia, J. C., Kang, H., Clemenson, G. D., Jr., Gage, F. H., Lichtman, J. W. & Sanes, J. R. (2010). Attenuation of age-related changes in mouse neuromuscular synapses by caloric restriction and exercise. *Proc Natl Acad Sci U S A* **107**, 14863-14868.

van der Kooi, A. J., de Visser, M. & Barth, P. G. (1994). Limb girdle muscular dystrophy: reappraisal of a rejected entity. *Clin Neurol Neurosurg* **96**, 209-218.

van Deutekom, J., Aartsma-Rus, A., Bremmer-Bout, M., Janson, A., den Dunnen, J. & van Ommen, G. J. (2002). Antisense-mediated exon skipping as a gene correction therapy for Duchenne muscular dystrophy. *Journal of the Neurological Sciences* **199**, S75-S76.

van Deutekom, J. C., Bremmer-Bout, M., Janson, A. A., Ginjaar, I. B., Baas, F., den Dunnen, J. T. & van Ommen, G. J. (2001). Antisense-induced exon skipping restores dystrophin expression in DMD patient derived muscle cells. *Hum Mol Genet* **10**, 1547-1554.

van Deutekom, J. C., Janson, A. A., Ginjaar, I. B., Frankhuizen, W. S., Aartsma-Rus, A., Bremmer-Bout, M., den Dunnen, J. T., Koop, K., van der Kooi, A. J., Goemans, N. M., de Kimpe, S. J., Ekhart, P. F., Venneker, E. H., Platenburg, G. J., Verschuuren, J. J. & van Ommen, G. J. (2007). Local dystrophin restoration with antisense oligonucleotide PRO051. *N Engl J Med* **357**, 2677-2686.

van Deutekom, J. C. T., Aartsma-Rus, A., Janson, A. A. M., Kaman, W. E., Bremmer-Bout, M., den Dunnen, J. T., Baas, F. & van Ommen, G. J. B. (2003). Therapeutic antisense-induced exon skipping in cultured muscle cells from six different DMD patients. *Human Molecular Genetics* **12**, 907-914.

Vance, J. M. (1991). Hereditary motor and sensory neuropathies. *J Med Genet* **28**, 1-5.

Vickers, T. A., Zhang, H., Graham, M. J., Lemonidis, K. M., Zhao, C. & Dean, N. M. (2006). Modification of MyD88 mRNA splicing and inhibition of IL-1beta signaling in cell culture and in mice with a 2'-O-methoxyethyl-modified oligonucleotide. *J Immunol* **176**, 3652-3661.

Vivanco, I. & Sawyers, C. L. (2002). The phosphatidylinositol 3-Kinase AKT pathway in human cancer. *Nat Rev Cancer* **2**, 489-501.

Wagner, K. R., Fleckenstein, J. L., Amato, A. A., Barohn, R. J., Bushby, K., Escolar, D. M., Flanigan, K. M., Pestronk, A., Tawil, R., Wolfe, G. I., Eagle, M., Florence, J. M., King, W. M., Pandya, S., Straub, V., Juneau, P., Meyers, K., Csimma, C., Araujo, T., Allen, R., Parsons, S. A., Wozney, J. M., Lavallie, E. R. & Mendell, J. R. (2008). A phase I/IItrial of MYO-029 in adult subjects with muscular dystrophy. *Ann Neurol* **63**, 561-571.

Wagner, K. R., Lechtzin, N. & Judge, D. P. (2007). Current treatment of adult Duchenne muscular dystrophy. *Biochim Biophys Acta* **1772**, 229-237.

Wakefield, L. M., Smith, D. M., Broz, S., Jackson, M., Levinson, A. D. & Sporn, M. B. (1989). Recombinant TGF-beta 1 is synthesized as a two-component latent complex that shares some structural features with the native platelet latent TGF-beta 1 complex. *Growth Factors* **1**, 203-218.

Wang, B., Li, J. & Xiao, X. (2000). Adeno-associated virus vector carrying human minidystrophin genes effectively ameliorates muscular dystrophy in mdx mouse model. *Proc Natl Acad Sci U S A* **97**, 13714-13719.

Wang, Z., Kuhr, C. S., Allen, J. M., Blankinship, M., Gregorevic, P., Chamberlain, J. S., Tapscott, S. J. & Storb, R. (2007). Sustained AAV-mediated dystrophin expression in a canine model of Duchenne muscular dystrophy with a brief course of immunosuppression. *Mol Ther* **15**, 1160-1166.

Wang, Z., Zhu, T., Qiao, C., Zhou, L., Wang, B., Zhang, J., Chen, C., Li, J. & Xiao, X. (2005). Adeno-associated virus serotype 8 efficiently delivers genes to muscle and heart. *Nat Biotechnol* **23**, 321-328.

Weinstein, S. & Peer, D. RNAi nanomedicines: challenges and opportunities within the immune system. *Nanotechnology* **21**, 232001.

Weinstein, S. & Peer, D. (2010). RNAi nanomedicines: challenges and opportunities within the immune system. *Nanotechnology* **21**, 232001.

Wells, K. E., Fletcher, S., Mann, C. J., Wilton, S. D. & Wells, D. J. (2003). Enhanced in vivo delivery of antisense oligonucleotides to restore dystrophin expression in adult mdx mouse muscle. *FEBS Lett* **552**, 145-149.

Wender, P. A., Galliher, W. C., Goun, E. A., Jones, L. R. & Pillow, T. H. (2008). The design of guanidinium-rich transporters and their internalization mechanisms. *Adv Drug Deliv Rev* **60**, 452-472.

Wender, P. A., Kreider, E., Pelkey, E. T., Rothbard, J. & Vandeusen, C. L. (2005). Dendrimeric molecular transporters: synthesis and evaluation of tunable polyguanidino dendrimers that facilitate cellular uptake. *Org Lett* **7**, 4815-4818.

Wender, P. A., Mitchell, D. J., Pattabiraman, K., Pelkey, E. T., Steinman, L. & Rothbard, J. B. (2000). The design, synthesis, and evaluation of molecules that enable or enhance cellular uptake: peptoid molecular transporters. *Proc Natl Acad Sci U S A* **97**, 13003-13008.

Westerhausen, D. R., Jr., Hopkins, W. E. & Billadello, J. J. (1991). Multiple transforming growth factor-beta-inducible elements regulate expression of the plasminogen activator inhibitor type-1 gene in Hep G2 cells. *J Biol Chem* **266**, 1092-1100.

White, S., Kalf, M., Liu, Q., Villerius, M., Engelsma, D., Kriek, M., Vollebregt, E., Bakker, B., van Ommen, G. J., Breuning, M. H. & den Dunnen, J. T. (2002). Comprehensive detection of genomic duplications and deletions in the DMD gene, by use of multiplex amplifiable probe hybridization. *Am J Hum Genet* **71**, 365-374.

Whitehead, N. P., Yeung, E. W. & Allen, D. G. (2006). Muscle damage in mdx (dystrophic) mice: role of calcium and reactive oxygen species. *Clin Exp Pharmacol Physiol* **33**, 657-662.

Whittemore, L. A., Song, K., Li, X., Aghajanian, J., Davies, M., Girgenrath, S., Hill, J. J., Jalenak, M., Kelley, P., Knight, A., Maylor, R., O'Hara, D., Pearson, A., Quazi, A., Ryerson, S., Tan, X. Y., Tomkinson, K. N., Veldman, G. M., Widom, A., Wright, J. F., Wudyka, S.,

Zhao, L. & Wolfman, N. M. (2003). Inhibition of myostatin in adult mice increases skeletal muscle mass and strength. *Biochem Biophys Res Commun* **300**, 965-971.

Wiendl, H., Hohlfeld, R. & Kieseier, B. C. (2005). Immunobiology of muscle: advances in understanding an immunological microenvironment. *Trends Immunol* **26**, 373-380.

Williams, A., Sun, X., Fischer, J. E. & Hasselgren, P. O. (1999). The expression of genes in the ubiquitin-proteasome proteolytic pathway is increased in skeletal muscle from patients with cancer. *Surgery* **126**, 744-749; discussion 749-750.

Williams, T. & Kole, R. (2006). Analysis of prostate-specific membrane antigen splice variants in LNCap cells. *Oligonucleotides* **16**, 186-195.

Wilson, C. & Keefe, A. D. (2006). Building oligonucleotide therapeutics using non-natural chemistries. *Curr Opin Chem Biol* **10**, 607-614.

Wilton, S. D. & Fletcher, S. (2005a). Antisense oligonucleotides in the treatment of Duchenne muscular dystrophy: Where are we now? *Neuromuscular Disorders* **15**, 399-402.

Wilton, S. D. & Fletcher, S. (2005b). Antisense oligonucleotides in the treatment of Duchenne muscular dystrophy: Where are we now? *Neuromuscul Disord* **15**, 399-402.

Wilton, S. D., Lloyd, F., Carville, K., Fletcher, S., Honeyman, K., Agrawal, S. & Kole, R. (1999). Specific removal of the nonsense mutation from the mdx dystrophin mRNA using antisense oligonucleotides. *Neuromuscul Disord* **9**, 330-338.

Wilton, S. D., Mann, C. J., Honeyman, K., McClorey, G. & Fletcher, S. (2002). Improved antisense oligonucleotide induced exon skipping in the mdx mouse model of muscular dystrophy. *Journal of Gene Medicine* **4**, 644-654.

Wilton, S. D., McClorey, G., Moulton, H. M., Iversen, P. L. & Fletcher, S. (2006). Antisense oligonucleotide-induced exon skipping restores dystrophin expression in vitro in a canine model of DMD. *Gene Therapy* **13**, 1373-1381.

Wolfman, N. M., McPherron, A. C., Pappano, W. N., Davies, M. V., Song, K., Tomkinson, K. N., Wright, J. F., Zhao, L., Sebald, S. M., Greenspan, D. S. & Lee, S. J. (2003). Activation of latent myostatin by the BMP-1/tolloid family of metalloproteinases. *Proc Natl Acad Sci U S A* **100**, 15842-15846.

Woo, S. L., DiLella, A. G., Marvit, J. & Ledley, F. D. (1986). Molecular basis of phenylketonuria and potential somatic gene therapy. *Cold Spring Harb Symp Quant Biol* **51 Pt 1**, 395-401.

Wood, M., Yin, H. & McClorey, G. (2007). Modulating the expression of disease genes with RNA-based therapy. *PLoS Genet* **3**, e109.

Wu, B., Benrashid, E., Lu, P., Cloer, C., Zillmer, A., Shaban, M. & Lu, Q. L. (2011). Targeted skipping of human dystrophin exons in transgenic mouse model systemically for antisense drug development. *PLoS One* **6**, e19906.

Wu, B., Li, Y., Morcos, P. A., Doran, T. J., Lu, P. & Lu, Q. L. (2009). Octa-guanidine morpholino restores dystrophin expression in cardiac and skeletal muscles and ameliorates pathology in dystrophic mdx mice. *Mol Ther* **17**, 864-871.

Wu, B., Moulton, H. M., Iversen, P. L., Jiang, J., Li, J., Spurney, C. F., Sali, A., Guerron, A. D., Nagaraju, K., Doran, T., Lu, P., Xiao, X. & Lu, Q. L. (2008). Effective rescue of dystrophin improves cardiac function in dystrophin-deficient mice by a modified morpholino oligomer. *Proc Natl Acad Sci U S A* **105**, 14814-14819.

Wu, H., Naya, F. J., McKinsey, T. A., Mercer, B., Shelton, J. M., Chin, E. R., Simard, A. R., Michel, R. N., Bassel-Duby, R., Olson, E. N. & Williams, R. S. (2000). MEF2 responds to multiple calcium-regulated signals in the control of skeletal muscle fiber type. *EMBO J* **19**, 1963-1973.

Wu, R. P., Youngblood, D. S., Hassinger, J. N., Lovejoy, C. E., Nelson, M. H., Iversen, P. L. & Moulton, H. M. (2007). Cell-penetrating peptides as transporters for morpholino oligomers: effects of amino acid composition on intracellular delivery and cytotoxicity. *Nucleic Acids Res* **35**, 5182-5191.

Xia, H., Mao, Q., Eliason, S. L., Harper, S. Q., Martins, I. H., Orr, H. T., Paulson, H. L., Yang, L., Kotin, R. M. & Davidson, B. L. (2004). RNAi suppresses polyglutamine-induced neurodegeneration in a model of spinocerebellar ataxia. *Nat Med* **10**, 816-820.

Yaffe, D. & Saxel, O. (1977). Serial passaging and differentiation of myogenic cells isolated from dystrophic mouse muscle. *Nature* **270**, 725-727.

Yang, W., Zhang, Y., Li, Y., Wu, Z. & Zhu, D. (2007). Myostatin induces cyclin D1 degradation to cause cell cycle arrest through a phosphatidylinositol 3-kinase/AKT/GSK-3 beta pathway and is antagonized by insulin-like growth factor 1. *J Biol Chem* **282**, 3799-3808.

Yankaskas, J. R., Marshall, B. C., Sufian, B., Simon, R. H. & Rodman, D. (2004). Cystic fibrosis adult care: consensus conference report. *Chest* **125**, 1S-39S.

Yin, H., Moulton, H. M., Betts, C., Merritt, T., Seow, Y., Ashraf, S., Wang, Q., Boutilier, J. & Wood, M. J. (2010). Functional rescue of dystrophin-deficient mdx mice by a chimeric peptide-PMO. *Mol Ther* **18**, 1822-1829.

Yin, H., Moulton, H. M., Betts, C., Seow, Y., Boutilier, J., Iverson, P. L. & Wood, M. J. (2009). A fusion peptide directs enhanced systemic dystrophin exon skipping and functional restoration in dystrophin-deficient mdx mice. *Hum Mol Genet* **18**, 4405-4414.

Yin, H., Moulton, H. M., Seow, Y., Boyd, C., Boutilier, J., Iverson, P. & Wood, M. J. (2008). Cell-penetrating peptide-conjugated antisense oligonucleotides restore systemic muscle and cardiac dystrophin expression and function. *Hum Mol Genet* **17**, 3909-3918.

Yokota, T., Lu, Q. L., Partridge, T., Kobayashi, M., Nakamura, A., Takeda, S. & Hoffman, E. (2009). Efficacy of systemic morpholino exon-skipping in Duchenne dystrophy dogs. *Ann Neurol* **65**, 667-676.

Yoshida, N., Yoshida, S., Koishi, K., Masuda, K. & Nabeshima, Y. (1998). Cell heterogeneity upon myogenic differentiation: down-regulation of MyoD and Myf-5 generates 'reserve cells'. *J Cell Sci* **111 (Pt 6)**, 769-779.

Yuan, J., Stein, D. A., Lim, T., Qiu, D., Coughlin, S., Liu, Z., Wang, Y., Blouch, R., Moulton, H. M., Iversen, P. L. & Yang, D. (2006). Inhibition of coxsackievirus B3 in cell cultures and in mice by peptide-conjugated morpholino oligomers targeting the internal ribosome entry site. *J Virol* **80**, 11510-11519.

Zaccagnini, G., Martelli, F., Magenta, A., Cencioni, C., Fasanaro, P., Nicoletti, C., Biglioli, P., Pelicci, P. G. & Capogrossi, M. C. (2007). p66(ShcA) and oxidative stress modulate myogenic differentiation and skeletal muscle regeneration after hind limb ischemia. *J Biol Chem* **282**, 31453-31459.

Zamecnik, P. C. & Stephenson, M. L. (1978). Inhibition of Rous sarcoma virus replication and cell transformation by a specific oligodeoxynucleotide. *Proc Natl Acad Sci U S A* **75**, 280-284.

Zamore, P. D., Tuschl, T., Sharp, P. A. & Bartel, D. P. (2000). RNAi: double-stranded RNA directs the ATP-dependent cleavage of mRNA at 21 to 23 nucleotide intervals. *Cell* **101**, 25-33.

Zhang, X. H. & Chasin, L. A. (2004). Computational definition of sequence motifs governing constitutive exon splicing. *Genes Dev* **18**, 1241-1250.

Zheng, B., Cao, B., Crisan, M., Sun, B., Li, G., Logar, A., Yap, S., Pollett, J. B., Drowley, L., Cassino, T., Gharaibeh, B., Deasy, B. M., Huard, J. & Peault, B. (2007). Prospective identification of myogenic endothelial cells in human skeletal muscle. *Nat Biotechnol* **25**, 1025-1034.

Zhu, X., Hadhazy, M., Wehling, M., Tidball, J. G. & McNally, E. M. (2000). Dominant negative myostatin produces hypertrophy without hyperplasia in muscle. *FEBS Lett* **474**, 71-75.

Zimmers, T. A., Davies, M. V., Koniaris, L. G., Haynes, P., Esquela, A. F., Tomkinson, K. N., McPherron, A. C., Wolfman, N. M. & Lee, S. J. (2002). Induction of cachexia in mice by systemically administered myostatin. *Science* **296**, 1486-1488.

Zitzmann, M. & Nieschlag, E. (2000). Hormone substitution in male hypogonadism. *Mol Cell Endocrinol* **161**, 73-88.